Fast finite difference numerical techniques for the time and frequency domain solution of electromagnetic problems

Piotr Przybyszewski

Ph.D. Thesis

Technical University of Gdańsk

Supervisor: Prof. Michał Mrozowski

Gdańsk 2001

To my wife Daniela

Contents

Symbols used in this thesis

General symbols

$\mathbf{L}$	—	operator
u	—	function
α	—	scalar parameter
$\underline{\underline{A}}$	—	matrix
$\underline{a}$	—	vector of parameters
$\vec{A}$	—	vector function
$\vec{A}_t$	—	transverse component of a vector function
A_z	—	longitudinal component of a vector function
A_x	—	x component of a vector function in Cartesian coordinates
A_y	—	y component of a vector function in Cartesian coordinates
$\bar{\bar{\alpha}}$	—	tensor
$\bar{\bar{\alpha}}_{tt}$	—	transverse component of a tensor
α_{zz}	—	longitudinal component of a tensor
z	—	longitudinal direction
j	—	imaginary unit
$\underline{\underline{I}}$	—	unit matrix
$\vec{\imath}_z$	—	unit vector in longitudinal direction
$\vec{n}$	—	unit vector normal to a surface
$\Re(.)$	—	real part
$\Im(.)$	—	imaginary part
$(.)^*$	—	complex conjugation
$(.)^{-1}$	—	inverse of an operator
$(.)^T$	—	transpose of an operator
$(.)^H$	—	Hermitian transpose of an operator
$< ., . >$	—	inner product
$< ., . >_p$	—	pseudo-inner product
$(.) \times (.)$	—	vector product of two vectors
$(.) \cdot (.)$	—	scalar product of two vectors

Physical quantities

$\vec{D}$	—	electric flux density
$\vec{B}$	—	magnetic flux density
$\vec{E}$	—	electric field intensity
$\vec{H}$	—	magnetic field intensity
$\bar{\bar{\epsilon}}$	—	permittivity tensor of the medium
$\bar{\bar{\mu}}$	—	permeability tensor of the medium

ϵ_r — relative permittivity of the medium
μ_r — relative permeability of the medium
ϵ_0 — permittivity of the vacuum
μ_0 — permeability of the vacuum
c — speed of light in the vacuum
ω — angular frequency
f — frequency
β_z — propagation constant

Operators

$\nabla \times (.)$ — rotation operator
$\nabla \cdot (.)$ — divergence operator
$\nabla(.)$ — gradient operator
$\nabla_t \cdot (.)$ — transverse divergence operator
$\nabla_t(.)$ — transverse gradient operator

Functions

$\delta(k,l)$ — Kronecker symbol ($\delta(k,l) = 0$ for $k \neq 1$, and $\delta(k,k) = 1$)
$J_i(r)$ — Bessel function of order i
$N_i(r)$ — Neumann function of order i

Chapter 1

Preface

1.1 Motivation and background

Many fundamental laws of physics are described by partial differential equations. In order to understand and predict the behavior of nature, one has to have means to resolve these equations for various boundary conditions. To this end many techniques have been devised in the last century. In the modern world, in which a computer became a commodity, the most popular approach is to take advantage of their data processing speed to perform all the calculations. With the constant progress in performance of personal computers the numerical modeling of various processes is gaining importance and momentum.

One of the simplest methods of the computational approach to differential equations in general, whose origins go back way before the computer age[1], involves replacing the continuous domain with a discrete one and evaluate the derivatives with approximate formulae based on the Taylor series. In other words, one writes down the equations representing laws of physics in a finite number of space points. The derivatives are represented by a simple linear combination of field values defined at neighboring points. Usually the points are arranged in a form of a structured mesh. For elliptic partial differential equations, this approach results in a system of linear equations which are then solved by means of standard linear algebra methods. For parabolic and hyperbolic systems one gets implicit or explicit iterative schemes which describe the evolution of field with respect to a selected variable.

The approach described above is at the heart of the family of various numerical techniques which are known as finite-difference methods [3, 48, 86]. Along with the finite-element methods [36, 86] they form the core of the majority of general purpose numerical solvers which are designed to solve partial differential equations. One obvious corollary is that assuming an infinite precision of computations, the accuracy of the solution in the finite-difference method depends primarily on the density of the mesh points. In the basic algorithm the local error of evaluation the derivative is proportional to h or h^2, where h is the distance between points in the mesh. The simplest way on increasing the accuracy is to refine the mesh. However, this technique increases the both the memory requirements and the solutions time, regardless of the type of partial differential equation being solved. Over last five decades considerable efforts have been made to improve the accuracy and performance of the finite-difference methods in various applications. One of the areas where a remarkable progress can be noted is computational electromagnetics.

[1] Ames [3] notes that Euler used this approach as early as in 1768.

Understanding the behavior of electromagnetic fields in complex environment is crucial for the development of modern civil and military communication systems including the Internet, mobile telephony, satellite TV. The physics of electric and magnetic fields is described by Maxwell's equations which, from the mathematical point of view, form a set of six partial differential equations in a four dimensional space-time continuum. Accordingly, finite-difference methods are a natural candidate for the numerical analysis of electromagnetic phenomena. Historically, the finite-difference techniques were first applied to static problems in which the electric or magnetic field can be described by a single scalar potential. In this case the boundary value problem becomes a classical Laplace equation:

$$\nabla^2 U = 0 \tag{1.1.1}$$

where U is a scalar potential. Solving this equation for various boundary conditions yields not only field distribution but also allows one to calculate the capacitance or inductance of a system under consideration.

The static analysis is sufficient for microwave transmission lines supporting TEM or quasi-TEM modes. To analyze waveguides supporting purely TE or TM waves the harmonic steady state can be assumed. In this case, Maxwell's equation can be reduced to a 2D scalar Helmholtz equation in the form

$$\nabla^2 U - k_0^2 U = 0 \tag{1.1.2}$$

where k is the wavenumber of a plane wave in an isotropic medium. Here, the application of the finite-difference technique leads to a standard matrix eigenvalue problem with a sparse five diagonal matrix [3, 48, 68]. The solution of this problem gives one the cutoff frequencies and field distribution for modes supported by the waveguide. A similar 3D equations can be formulated for isotropic resonant cavities. Obviously, both Laplace and Helmholtz equations can be analyzed with the right hand side source terms, in which case one gets the response of a system to a given excitation. In context of electromagentics this yields such parameters as monostatic and bistatic radar cross-section, scattering matrix etc.

For scalar fields the application of the finite difference technique is straightforward, at least for the interior problems. The finite difference analysis of simple waveguides and resonators was developed in the 70 [18, 32]. However, when scalar potential alone cannot be used and more than one field component enter into the equations, new problems arise. One of these problems concern the choice of the discretization points. Should all the field components be defined in the same points or should there be a separate mesh for each components? The answer to this question has lead to development of one of the most important numerical techniques in computational electromagnetics. In 1966 while investigating the finite-difference formulation of Maxwell's equations in time domain (initial value problem), Yee [90] suggested a discretization scheme (fig.1.1.1b) in which **two** interleaved meshes are used. The crucial point in the discretization scheme is that both electric and magnetic fields are represented. Each electric field component is surrounded by four magnetic field components which form a rectangular cell in a perpendicular plane. The same is true for each magnetic field which is circulated by four perpendicular electric fields. Due to this arrangement it is very easy to write down the discrete version of the Faraday and Ampère laws and express the coupling between electric and magnetic field underlying Maxwell's equations. This idea of two interleaved meshes and discretization of both electric and magnetic field components is a remarkable departure form a rather natural tendency to simplify the numerical solution of the problem at hand by eliminating

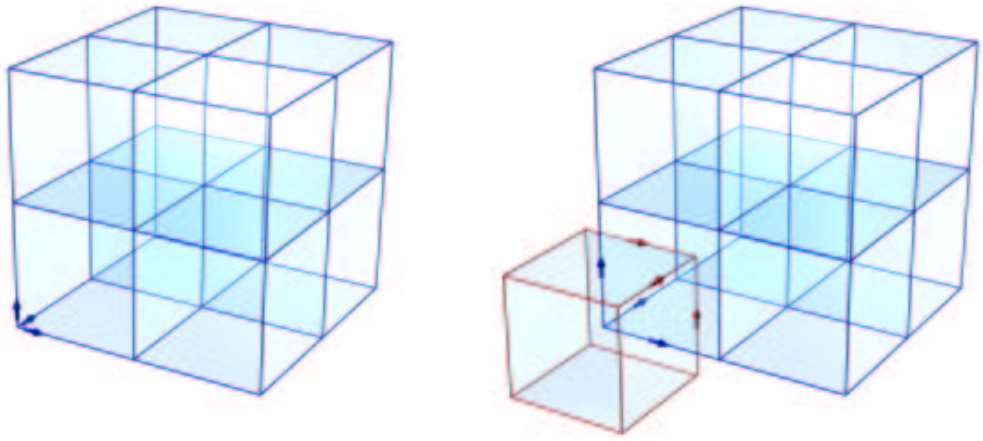

(a) (b)

Figure 1.1.1: *Single mesh (a) – all components are defined in the same mesh points, and Yee's mash (b) – two interleaved grids with different components defined on different points.*

quantities linked by analytical relations. In the case of Maxwell's equations, one can readily convert them to a wave equation. In the process, the electric or magnetic field is eliminated and the number of unknowns is halved. If this is done **before** discretization, only a single grid can be applied and this version of the finite-difference approach is still used by some authors [1, 8, 24, 70, 71].

Yee used a dual mesh approach to develop a marching-in-time explicit update algorithm for the analysis of transient phenomena. Since both electric and magnetic fields are involved, the field update proceeds in a leap-frog manner. This is to say that only one field (electric or magnetic) is calculated in a given iteration. Once this field has been calculated for the particular moment in time, the complementary field can be advanced by half-time step. Although extremely simple in implementation, the technique of Yee requires considerable computer resources. For a simplest problem it requires at least three times as many memory cells as the formulation using the scalar wave equations. This may explain why the dual mesh approach did not seem to be very appealing until mid seventies when Taflove and Brodwin [81,82] noted that the technique of Yee is advantageous for the problems for which Green's function is unknown such as the absorption of electromagnetic wave in complex inhomogeneous biological tissues. The method was extended to three dimensions and applied to both the sinusoidal steady-state and transient problems. In the 1980 the method received its present name the Finite-Difference Time Domain method (FD-TD) [78]. Through the eighties the FD-TD was advanced by Gwarek, Hoeffer, Taflove and Mur [12, 14, 15, 27–30, 41, 54, 55, 78–80, 84] and applied to the analysis of wave scattering, near and far fields, microwave cavities, planar and axisymmetrical circuits [29, 30, 84]. In the last decade the interest in the FD-TD method has exploded. As of September 10th, 2000 the Internet bibliographical database `www.fdtd.org` has recorded 3671 entries including 1978 journal papers, 150 PhD theses and 6 books [35, 45, 77, 79, 80, 83] devoted to the FD-TD methods. Currently at least 7 commercial codes are on the market that use this technique and problems such as nonlinear elements [11], soliton propagation [26, 39, 40, 91], dispersive media [25, 75], antenna design [49] have been successfully analyzed using Yee's discretization scheme combined with explicit leap-frog update technique.

FD-TD is in fact an explicit finite-difference leap-frog scheme for initial value problem

defined Maxwell's equations formulated in time domain. However, one is often interested in calculating the steady state solution for time harmonic excitation. In other words the fields are calculated for a fixed frequency. This is achieved by solving the frequency domain version of Maxwell's equations. Again, the finite-difference approach can be used to this end. By the way of analogy to the FD-TD this approach may be called the finite-difference frequency domain technique or FD-FD for short. However, while the FD-TD method is currently almost synonymous with Yee's mesh, the meshing in FD-FD frequently implies only a single mesh. This is because in frequency domain one usually works with wave equations i.e. formulations which use electric or magnetic field alone. As noted earlier this equation is derived from Maxwell's equations by means of simple differential operations. If the finite-difference scheme is applied **after** these operations have been carried out, Yee's meshing can not be applied. Weiland [88, 89] was the first to note that in fact Yee's mesh is of use also in frequency domain provided that the discretization is applied at the very early stage, that it to say the full set of Maxwell equations, and one of the fields is eliminated by applying the discrete version of operation $\nabla \times (.)$ to one of the equations. Since two interleaved meshes are used, separate discrete operators $\nabla \times (.)$ have been defined on each grid. The Maxwell equations defined on the continuum are transformed on grid equations with operators replaced by simple matrices. Weiland demonstrated that matrices associated with discrete operators on one grid are the transposes of the matrices defining analogous operators on the dual grid. When the operators are defined is such a manner the discrete equation preserve the basic properties of continuous ones. In particular, the following operator identities are satisfied:

$$\nabla \times \nabla(.) = 0 \tag{1.1.3}$$

$$\nabla \cdot \nabla \times (.) = 0 \tag{1.1.4}$$

With basic operators defined, it is easy to manipulate Maxwell's equations in order to derive the discrete equivalents of partial differential equations arising in electromagnetics and valid for the sinusoidal steady state. As a result one gets the system of linear equations in which the system matrix is defined by simple multiplication of a few sparse matrices representing appropriate continuous operators. These equations are solved by means of iterative techniques such as conjugate gradients, successive overrelaxation or more recently by Krylov space based iterative techniques such as GMRES or implicitly restarted Arnoldi method [4, 20, 21, 67, 76].

Formalism[2] introduced by Weiland is a very powerful tool and makes it very easy to investigate basic properties of grid equations. Moreover, one can easily prove that they have the same properties as their continuous counterpart. In particular such properties as energy conservation or nondivergent character of both electric and magnetic fields are readily seen [17]. Although Weiland developed matrix formalism originally only for frequency domain analysis, the discrete operators involve only space relations and, obviously, FD-TD may also be presented in the matrix form using the same double set of discrete operators. Needless to say, there is no need to form matrices explicitly while implementing the update algorithms.

In its basic form, the FD-TD (FD-FD) method has a purely numerical character. In principle, the accuracy improvement can be achieved by increasing the mesh density. This approach however has several drawbacks. First of all is that the number of unknowns

[2]Weiland uses the acronym FIT – for finite integration technique. For time domain and regular mesh FIT becomes FD-TD

increases by the factor of eight each time the discretization step h is halved. Additionally as in all explicit update schemes the maximum time step in the FD-TD is bounded above by the time required by the electromagnetic wave to propagate from one cell point to another. For FD-FD, which involves the solution of system of equations by means of iterative technique, increasing the mesh density implies increasing the spectral radius of the matrix, and this in turn slows down the convergence of the iterative solver [67]. As a result, the denser the mesh, the longer it takes to reach the steady state (for FD-TD) or to converge for (FD-FD). These two factors alone explain why extensive research effort is underway which would allow one to achieve high accuracy of FD-TD[3] method while keeping the solution time low. Among most promising developments to this end are the incorporation of the knowledge of the underlying physics into the method and finding better field representation. One example of using field theory is the problem of representation of various boundary conditions in the situation where the boundaries do not conform to the grid lines. Gwarek [28] showed that it is possible to deform the cell near boundary and use quasi-static expressions to evaluate the flux density. Another successful application of analytical techniques is subcell modeling[4] of dielectric and metal wedges [5, 6, 23, 31, 33, 46, 47, 55, 56, 60–62, 64, 72–74], thin wires [19] and thin gaps [87]. These techniques require certain preprocessing of a geometry and allow one to maintain the accuracy of the method for systems with complex boundary conditions without increasing the number of unknowns. In the case of subcell modeling, the changes essentially involve a modification of the expressions defining the derivatives (rotation, gradients) or integrals (circulations and fluxes) for selected cells in the mesh. These changes have local character. Apart from these localized modifications, where fields remain defined at grid points but the finite-difference formulae that link E and H field take into account the deformation of the field due to the presence of a material within a cell, new approaches have been proposed which involve entirely different field representation within entire subregions or even the whole domain of the problem. These methods often rely on the projection technique known as a method of moments and represent the field with finite series using different basis functions. One can mention here the explicit time domain algorithms such as partial eigenfunction expansion (PEE) [2, 43, 51] or multiresolution time domain method which decomposes field into wavelets [44].

As can be seen from the above, there is a great wealth of knowledge and concepts that have been proposed for the finite difference methods based on Yee's mesh, but it appears that so far only one theory exists, namely that of Weiland. While Weiland's formulation works well for regular meshes and homogeneous media it has never been applied to the newer concepts such as subcell modeling or hybrid method. The purpose of the work is to reflect upon the nature of the finite difference techniques in time and frequency domain and try to develop a unified framework alternative to that of Weiland, that could also be applicable to all types of equations which can be derived both directly from Maxwell's equations and from field theory based models. Another goal is to investigate basic properties of the modified equations, analyze sources of errors and propose a new formulation controlling these errors and, at the same time, preserving the consistency of the discrete equation with the continuous ones. A final goal is to develop hybrid

[3]Despite the fact that both FD-TD and FD-FD can be formally expressed using identical discrete operators defined on Yee's mesh, most of the developments regarding Yee's mesh have been reported in context of the FD-TD.

[4]By subcell modeling one understands accounting for the presence of a geometrically small feature within a cell which significantly perturbs the field causing the increase of local error in a regular finite-difference scheme.

techniques which link method of functional analysis with the finite differences with the ultimate goal of creating faster algorithms for the analysis of electromagnetic fields in time and frequency domain without compromising the accuracy.

1.2 Goal, claim and scope of this work

In the context of the previous section, the overall goal of this thesis is to develop a framework for creating new algorithms for faster finite-difference time and frequency domain analysis of microwave structures that do not compromise the accuracy of the results and self-consistency of the Maxwell's equations. We make the following claims:

- It is possible to develop new local schemes for modeling of arbitrarily located metal walls, dielectric boundaries or conductive wedges, which do not affect the self-consistency and the spectral radius of the operators associated with the standard Yee's mesh, and yet reduce the error to the level that is comparable with the numerical dispersion.

- In certain configurations, the computations may be significantly accelerated by combining of the standard finite difference methods with the method of moments.

In order to prove the validity of the above claims, the following major steps will be undertaken:

- Common framework will be created for the analysis of the finite-difference schemes in the time and frequency domain and the relation between the results provided by them will be established.

- Electromagnetic problems will be classified in the form of operator equations expressed in terms of a few basic operators. Methods of discretization of the basic operators will be presented, giving a common approach to the discretisation of every electromagnetic problem.

- New algorithms will be developed for modeling arbitrarily located metal walls, dielectric boundaries and conductive wedges. The spectral properties and consistency with Maxwell's equations will be thoroughly examined to show that new schemes do not spoil the properties of the standard mesh.

- New hybrid techniques combining the standard methods with the method of expansion of the field in the series of functions in 3D will be proposed.

- The standard finite-difference method will be combined with eigenfunction expansion techniques in 2D. The new approach will speed up the calculations when the same structure is analyzed for many frequency or propagation constant points.

- A series of tests demonstrating the efficiency and error reduction capabilities of the new schemes will be carried out.

1.3 Chapter outline

At the beginning, in chapter 2, the standard finite-difference schemes are presented. We present a series of the explicit-update schemes which, when written for the domain of time, form the Finite-Difference Time-Domain method. We also present the Finite-Difference Frequency-Domain method. In the same chapter, we analyze the numerical dispersion error. This error is strictly associated with the finite-difference schemes.

In chapter 3, we introduce a new concept of a symbolic space. This is a common framework for continuous and discrete equations. The operators defined in the symbolic space possess the same general properties in the continuous and discrete space. After introducing the new concept we write Maxwell's equations for 3D and 2D problems using the new notation. Maxwell's equations are expressed in terms of a few basic operators. Discretization of these operators instead of whole equations gives a common approach for various formulations of electromagnetic problems. Further on, we classify various problems in the form of operator equations in terms of the basic operators. Then, we show how to discretize the basic operators. We also give a note on the stability of the explicit update scheme arisen from the discretized equations.

In chapter 4, we present local schemes for modeling of metal walls, boundaries between dielectrics and conductive wedges. All the new algorithms are expressed in a form of modification of a few basic matrices.

Chapter 5 presents hybrid algorithms with space domain decomposition. These algorithms decompose the analyzed domain in space into a series of subdomains. The method may be combined with the standard finite-difference approach. We present the hybrid algorithms for modeling of subdomains uniform in one direction (eg. sections of waveguides) and for general 3D subdomains.

In chapter 6, we present eigenfunction expansion techniques for analysis of waveguides. These methods are based on method of moments and speed up the calculations when a waveguide is analyzed for many frequencies or propagation constants.

Chapter 7 presents numerical results of the tests performed to validate the algorithms presented in the previous chapters.

Chapter 2

Standard finite difference schemes

2.1 Preliminaries

In this chapter, we recall the standard description of finite difference methods for solving of electromagnetic problems. We start by presenting the problems by introducing the general taxonomy.

In the mathematical terms, the electromagnetic problems may be presented as different types of boundary value problems. They may be classified in various ways. When sources are present in the analyzed domain, these problems are called deterministic and may be written in the following general operator form:

$$\mathbf{L}u = g \tag{2.1.1}$$

where $\mathbf{L}$ is an operator derived from Maxwell's equations, u usually represents some or all components of the electromagnetic field, and g represents sources. On the other hand, we have nondeterministic problems, which involve free oscillations. They may be described by eq. (2.1.1) with $g = 0$:

$$\mathbf{L}u = 0 \tag{2.1.2}$$

Another classification category concerns the domain of functions appearing in the equations. The equations may be written for the domain of space and time as well as for the domain of space and frequency. For shortness, we call them the time domain and frequency domain formulations. Obviously, different solution methods have to be used for each formulations. The time domain equations may be solved using so called the explicit update techniques. Deterministic problems (i.e. problems of the form (2.1.1)) written in frequency domain lead to a system of linear equations while nondeterministic frequency domain formulations may be presented in the form of e.g. the following eigenvalue problem:

$$\mathbf{M}u = \lambda \mathbf{N}u \tag{2.1.3}$$

where $\mathbf{M}$ and $\mathbf{N}$ are again operators derived from Maxwell's equations, u represents the field, and λ is the eigenvalue with the physical interpretation associated with the frequency.

Very often, an advantage is taken of symmetries or other properties of the solution space. For instance, if the domain is uniform in one direction, or mathematically speaking it shows translational invariance in a distinguished direction, the analysis may be radically simplified provided the original problems are reformulated. One situation, very frequently occurring in computational electromagnetics, is uniformity (translational invariance) of

the structure along a particular coordinate. For instance assuming z is the distinguished direction, one can express the spatial variation of fields in the following form:

$$u(z) = ue^{-j\beta_z z} \tag{2.1.4}$$

where β_z is called the propagation constant. Note, that the first derivative with respect to z may be now substituted by $-j\beta_z$:

$$\frac{\partial}{\partial z}(.) \leftrightarrow -j\beta_z \tag{2.1.5}$$

Using this fact one get the formulations formally similar to (2.1.1), (2.1.2) or (2.1.3) but with different meaning of some of the parameters. For instance, in the case of formulation (2.1.3), λ may have physical interpretation associated with the propagation constant rather than with oscillation frequency.

The electromagnetic problems presented above may be solved in different ways. In this work we are concerned mainly with the finite-difference techniques. Depending on the formulation, this approach may lead to a system of linear equations (deterministic problems in the frequency domain), matrix eigenproblems (nondeterministic formulations in the frequency domain or in the domain of propagation constant), or the explicit update scheme (the time domain formulations). The algorithms based on the frequency domain formulations are called the Finite-Difference Frequency-Domain methods. The explicit update schemes in the domain of time are called the Finite-Difference Time-Domain methods.

In this chapter we present the classical description of both methods.

2.2 Finite difference methods

All the finite difference methods considered in this chapter are based on the technique named the central difference scheme which approximates first and second order derivatives by differences with a second order accuracy. We present this technique in sec. 2.2.1. Subsequently, we show how to apply the finite difference scheme to the solution of the first and second order initial value problems and how these solutions are related to the eigenvalues of the underlying operators. Fundamental issues related to the explicit update schemes such as stability are addressed in sections 2.2.3.

Having outlined the basic issues, we proceed with the introduction of the FD-TD (sec. 2.2.3.7) and FD-FD (sec. 2.2.4) in their classical forms.

2.2.1 Central differences

Discretization using the central difference scheme is based on expansion of functions into the Taylor series. This series around h_0 are given by the following equations:

$$f(h_0 + \frac{\Delta h}{2}) = \left[f(h) + \frac{\partial f(h)}{\partial h}\frac{\Delta h}{2} + \frac{\partial^2 f(h)}{\partial h^2}\frac{\Delta h^2}{8} + \frac{\partial^3 f(h)}{\partial h^3}\frac{\Delta h^3}{24} + ... \right]_{h=h_0} \tag{2.2.1}$$

$$f(h_0 - \frac{\Delta h}{2}) = \left[f(h) - \frac{\partial f(h)}{\partial h}\frac{\Delta h}{2} + \frac{\partial^2 f(h)}{\partial h^2}\frac{\Delta h^2}{8} - \frac{\partial^3 f(h)}{\partial h^3}\frac{\Delta h^3}{24} + ... \right]_{h=h_0} \tag{2.2.2}$$

$$f(h_0 + \Delta h) = \left[f(h) + \frac{\partial f(h)}{\partial h}\Delta h + \frac{\partial^2 f(h)}{\partial h^2}\frac{\Delta h^2}{2} + \frac{\partial^3 f(h)}{\partial h^3}\frac{\Delta h^3}{6} \right.$$

$$+ \quad \frac{\partial^4 f(h)}{\partial h^4}\frac{\Delta h^4}{24} + ...\Big]_{h=h_0} \tag{2.2.3}$$

$$f(h_0 - \Delta h) = \Big[f(h) - \frac{\partial f(h)}{\partial h}\Delta h + \frac{\partial^2 f(h)}{\partial h^2}\frac{\Delta h^2}{2} - \frac{\partial^3 f(h)}{\partial h^3}\frac{\Delta h^3}{6}$$

$$+ \quad \frac{\partial^4 f(h)}{\partial h^4}\frac{\Delta h^4}{24} - ...\Big]_{h=h_0} \tag{2.2.4}$$

Central interpolation From eqs. (2.2.1) and (2.2.2) we derive the central interpolation scheme:

$$\begin{aligned} f(h_0) &\approx \frac{f(h_0 + \frac{\Delta h}{2}) + f(h_0 - \frac{\Delta h}{2})}{2} \\ &= f(h_0) + \frac{\partial^2 f(h)}{\partial h^2}\frac{\Delta h^2}{8}\Big|_{h=h_0} + \mathcal{O}(\Delta h^4) \end{aligned} \tag{2.2.5}$$

Eq. (2.2.5) shows that the error in this approach may be approximated by the following expression:

$$\text{err} \approx \frac{\partial^2 f(h)}{\partial h^2}\frac{\Delta h^2}{8}\Big|_{h=h_0} \tag{2.2.6}$$

1st order central difference The same equations lead to the central difference approximation of a first order derivative:

$$\begin{aligned} f'(h_0) &\approx \frac{f(h_0 + \frac{\Delta h}{2}) - f(h_0 - \frac{\Delta h}{2})}{\Delta h} \\ &= \Big[\frac{\partial f(h)}{\partial h} + \frac{\partial^3 f(h)}{\partial h^3}\frac{\Delta h^2}{12}\Big]_{h=h_0} + \mathcal{O}(\Delta h^4) \end{aligned} \tag{2.2.7}$$

The error in this case may be approximated as follows:

$$\text{err} \approx \frac{\partial^3 f(h)}{\partial h^3}\frac{\Delta h^2}{12}\Big|_{h=h_0} \tag{2.2.8}$$

2nd order central difference From eqs. (2.2.3) and (2.2.4) we get the central difference approximation of a second order derivative:

$$\begin{aligned} f''(h_0) &\approx \frac{f(h_0 + \Delta h) - 2f(h_0) + f(h_0 - \Delta h)}{\Delta h} \\ &= \Big[\frac{\partial^2 f(h)}{\partial h^2} + \frac{\partial^4 f(h)}{\partial h^4}\frac{\Delta h^2}{12}\Big]_{h=h_0} + \mathcal{O}(\Delta h^4) \end{aligned} \tag{2.2.9}$$

with the error approximated by the equation:

$$\text{err} \approx \frac{\partial^4 f(h)}{\partial h^4}\frac{\Delta h^2}{12}\Big|_{h=h_0} \tag{2.2.10}$$

2.2.2 Integral interpretation

Let us now consider the following equation

$$\frac{1}{L}\int_A^B \frac{\partial}{\partial\tau} f(\tau)d\tau = \frac{f(B)-f(A)}{L} \tag{2.2.11}$$

This describes the mean value of the first derivative in the direction of integration between two points A and B over the integration line of length L (see fig. 2.2.1). One may note

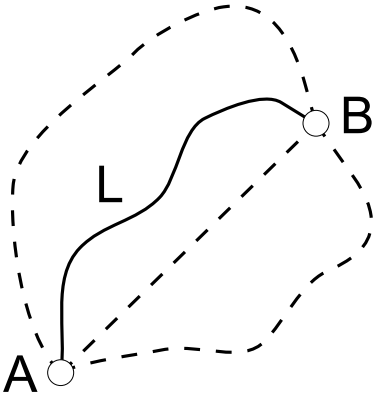

Figure 2.2.1: *Integral interpretation of the finite difference scheme.*

that this equation corresponds directly to eq. (2.2.7) when integrating over a straight line of length Δh. However, eq. (2.2.11) is more general than the central difference scheme described by (2.2.7) since it allows for arbitrary integration paths.

2.2.3 Explicit update schemes

Having briefly introduced the concept of central-differences, we can now show the applications of this concept to the solution of a simple initial value problems by means of an explicit update scheme.

We present an explicit update algorithm for the first order differential equation (sec. 2.2.3.1), for the second order differential equations (secs. 2.2.3.2 and 2.2.3.3), and the leap-frog schemes (secs. 2.2.3.4, 2.2.3.5). Whenever possible, the conditions of the stability of the solution procedure are given. The discussion of the accuracy of the method is postponed until sec. 2.3. Finally, in sec. 2.2.3.7, we introduce the Finite-Difference Time-Domain method which is a special case of the explicit update algorithms related to electromagnetics.

2.2.3.1 1st order central difference explicit update scheme

First order central difference explicit update algorithm arises from a first order differential equation of the following form:

$$\frac{\partial}{\partial\tau}u = j\mathbf{L}u \tag{2.2.12}$$

Discretization of eq. (2.2.12) in time using the central difference approach leads to the following equation:

$$u^{i+1} - u^{i-1} = 2j\Delta\tau\mathbf{L}u^i \tag{2.2.13}$$

Rearranging the terms in (2.2.13) we get the first order central difference explicit update procedure:

$$u^{i+1} = 2j\Delta\tau\mathbf{L}u^i + u^{i-1} \tag{2.2.14}$$

Eq. (2.2.14) may be written in a matrix form as follows:

$$\begin{bmatrix} u^{i+1} \\ u^i \end{bmatrix} = \begin{bmatrix} 2j\Delta\tau\mathbf{L} & 1 \\ 1 & 0 \end{bmatrix} \begin{bmatrix} u^i \\ u^{i-1} \end{bmatrix} \tag{2.2.15}$$

Stability condition Iterative methods may be used in practice only if they are stable. In order to derive the stability condition let us consider the following eigenproblem related to eq. (2.2.12):

$$\alpha_k u_k = \mathbf{L}u_k \tag{2.2.16}$$

Writing scheme (2.2.15) for the $k-th$ eigenvector u_k, we have:

$$\begin{bmatrix} u_k^{i+1} \\ u_k^i \end{bmatrix} = \begin{bmatrix} 2j\Delta\tau\mathbf{L} & 1 \\ 1 & 0 \end{bmatrix} \begin{bmatrix} u_k^i \\ u_k^{i-1} \end{bmatrix} \tag{2.2.17}$$

From eq. (2.2.16), it follows that we may now replace operator $\mathbf{L}$ by its eigenvalue α_k corresponding to eigenvectors u_k We get:

$$\begin{bmatrix} u_k^{i+1} \\ u_k^i \end{bmatrix} = \begin{bmatrix} 2j\Delta\tau\alpha_k & 1 \\ 1 & 0 \end{bmatrix} \begin{bmatrix} u_k^i \\ u_k^{i-1} \end{bmatrix} \tag{2.2.18}$$

Let us now convert the above equation to the following form

$$\begin{bmatrix} u_k^{i+1} \\ u_k^i \end{bmatrix} = \gamma_k \begin{bmatrix} u_k^i \\ u_k^{i-1} \end{bmatrix} \tag{2.2.19}$$

where γ_k is a parameter showing how the corresponding eigenvector changes in one explicit update step. We immediately see that if the scheme is to be stable then magnitude of γ_k should be less or equal to one for all eigenpairs of operator $\mathbf{L}$. The only question is how to find γ_k. To this end we simply put $u_k^{i+1} = \gamma_k u_k^i$ and $u_k^i = \gamma_k u_k^{i-1}$ and substitute this for the left hand side in (2.2.18). Subtracting the resulting vector form both sides gives

$$\begin{bmatrix} 0 \\ 0 \end{bmatrix} = \begin{bmatrix} 2j\Delta\tau\alpha_k - \gamma_k & 1 \\ 1 & -\gamma_k \end{bmatrix} \begin{bmatrix} u_k^i \\ u_k^{i-1} \end{bmatrix} \tag{2.2.20}$$

The determinant has to be equal zero, or

$$\gamma_k^2 - 2j\Delta\tau\alpha_k\gamma_k - 1 = 0 \tag{2.2.21}$$

The roots of this quadratic equation,in general complex, can be readily found using Vieta formulae. We have

$$\gamma_{k1}\gamma_{k2} = -1 \quad \text{and} \quad \gamma_{k1} + \gamma_{k2} = 2j\Delta\tau\alpha_k \tag{2.2.22}$$

From the first equation it is seen that γ_{k1}, γ_{k2} may be assumed in the following form:

$$\gamma_{k1,2} = \pm e^{\pm j\Delta\tau\alpha_{ek}} \tag{2.2.23}$$

where α_{ek} is a parameter which can be determined form the second Vieta identity. Using (2.2.23) we get:

$$\gamma_{k1} + \gamma_{k2} = 2j\sin(\Delta\tau\alpha_{ek}) = 2j\Delta\tau\alpha_k \tag{2.2.24}$$

From (2.2.24) we calculate α_{ek}:

$$\alpha_{ek} = \frac{\arcsin(\Delta\tau\alpha_k)}{\Delta\tau} \tag{2.2.25}$$

As noted above, for the explicit update algorithm defined by eq. (2.2.14) to be stable, the magnitude of γ_k cannot be greater than one for every eigenvalue α_k. This implies that α_{ek} must be real and from (2.2.25) we get the following stability condition for this algorithm:

$$\alpha_k \in \mathcal{R}, \qquad \Delta\tau \leq \frac{1}{\alpha_{k\max}} \tag{2.2.26}$$

2.2.3.2 Basic 2nd order central difference explicit update scheme

We shall now pass to the basic second order explicit update procedure which may be derived from a second order differential equation of the form:

$$\frac{\partial^2}{\partial\tau^2}u = -\mathbf{L}u \tag{2.2.27}$$

Discretizing of eq. (2.2.27) using the central difference scheme, we get:

$$u^{i+1} - 2u^i + u^{i-1} = -\Delta\tau^2\mathbf{L}u^i \tag{2.2.28}$$

The explicit update algorithm may be derived from (2.2.28) by rearranging the terms:

$$u^{i+1} = (2 - \Delta\tau^2\mathbf{L})u^i - u^{i-1} \tag{2.2.29}$$

We may write eq. (2.2.29) in a matrix form:

$$\begin{bmatrix} u^{i+1} \\ u^i \end{bmatrix} = \begin{bmatrix} 2 - \Delta\tau^2\mathbf{L} & -1 \\ 1 & 0 \end{bmatrix} \begin{bmatrix} u^i \\ u^{i-1} \end{bmatrix} \tag{2.2.30}$$

Stability analysis As in the previous case we shall perform the stability analysis by considering the eigenproblem given by the following equation:

$$\alpha_k^2 u_k = \mathbf{L}u_k \tag{2.2.31}$$

Since equation (2.2.30) must be valid for all eigenvectors of $\mathbf{L}$, we get:

$$\begin{bmatrix} u_k^{i+1} \\ u_k^i \end{bmatrix} = \begin{bmatrix} 2 - \Delta\tau^2\alpha_k & -1 \\ 1 & 0 \end{bmatrix} \begin{bmatrix} u_k^i \\ u_k^{i-1} \end{bmatrix} \tag{2.2.32}$$

Again we transform the above equation to the form given by (2.2.19). This gives the following characteristic equation:

$$\gamma_k^2 - (2 - \Delta\tau^2\alpha_k^2)\gamma_k + 1 = 0 \tag{2.2.33}$$

To solve this equation we note that

$$\gamma_{k1}\gamma_{k2} = 1 \quad \text{and} \quad \gamma_{k1} + \gamma_{k2} = -(2 - \Delta\tau^2\alpha_k^2) \tag{2.2.34}$$

The first equation implies that the roots can be assumed in the form

$$\gamma_{k1,2} = e^{\pm j\Delta\tau\alpha_{ek}} \tag{2.2.35}$$

Consequently we get

$$\gamma_{k1} + \gamma_{k2} = 2\cos(\Delta\tau\alpha_{ek}) = 2 - \Delta\tau^2\alpha_k^2 \tag{2.2.36}$$

This gives the following expression for α_{ek}

$$\alpha_{ek} = \frac{\arccos(1 - \frac{\Delta\tau^2\alpha_k^2}{2})}{\Delta\tau} \tag{2.2.37}$$

This equation leads to the stability condition. Since the magnitude of γ_k cannot be greater than one, the algorithm defined by eq. (2.2.29) is stable only if α_e is real for all eigenvalues α_k of operator $\mathbf{L}$. Form (2.2.37) we see that this is satisfied if

$$\alpha_k \in \mathcal{R}, \qquad \Delta\tau \leq \frac{2}{\alpha_{k\max}} \tag{2.2.38}$$

This constitutes the stability condition for the algorithm at hand.

2.2.3.3 General 2nd order central difference explicit update scheme

In this section, we develop a more general second order explicit update algorithm based on the differential equation of the following form:

$$-\frac{\partial^2}{\partial\tau^2}u - \frac{\partial}{\partial\tau}\mathbf{K}u = \mathbf{L}u \tag{2.2.39}$$

We discretize eq. (2.2.39) using the central difference scheme and get:

$$-\frac{1}{\Delta\tau^2}(u^{i+1} - 2u^i + u^{i-1}) - \frac{1}{2\Delta\tau}\mathbf{K}(u^{i+1} - u^{i-1}) = \mathbf{L}u^i \tag{2.2.40}$$

From (2.2.40), we get the equation describing the general second order explicit update procedure:

$$(1 + \frac{\Delta\tau}{2}\mathbf{K})u^{i+1} = (2 - \Delta\tau^2\mathbf{L})u^i - (1 - \frac{\Delta\tau}{2}\mathbf{K})u^{i-1} \tag{2.2.41}$$

Eq. (2.2.41) may be written in a matrix form as follows:

$$\begin{bmatrix} u^{i+1} \\ u^i \end{bmatrix} = \begin{bmatrix} (1 + \frac{\Delta\tau}{2}\mathbf{K}) & 0 \\ 0 & 1 \end{bmatrix}^{-1} \begin{bmatrix} 2 - \Delta\tau^2\mathbf{L} & -1 \\ 1 & 0 \end{bmatrix} \begin{bmatrix} 1 & 0 \\ 0 & (1 - \frac{\Delta\tau}{2}\mathbf{K}) \end{bmatrix} \begin{bmatrix} u^i \\ u^{i-1} \end{bmatrix} \tag{2.2.42}$$

Stability condition Derivation of the stability condition for the problem at hand requires more sophisticated procedure than those presented in the previous sections for the basic first and second order schemes. Here, we present only the final result. The details of the derivation may be found for instance in [69]. It is shown there, that the algorithm defined by eq. (2.2.41) is stable when the following conditions are satisfied:

$$\lambda_{\mathrm{K}} \in \mathcal{R}, \qquad \lambda_{\mathrm{K}} \geq 0, \qquad \mathbf{L} = \mathbf{L}^H, \qquad \mathbf{L} \geq 0, \qquad \Delta\tau \leq \frac{2}{\sqrt{||\mathbf{L}||}} \tag{2.2.43}$$

for every λ_{K}, where λ_{K} are eigenvalues of $\mathbf{K}$.

2.2.3.4 Basic leap-frog scheme

We now proceed to derivation of the basic leap-frog explicit update scheme which is used when two coupled first order equations are to be solved. Let us consider the following set of differential equations:

$$\frac{\partial}{\partial\tau}u = \mathbf{M}v \tag{2.2.44}$$
$$\frac{\partial}{\partial\tau}v = \mathbf{N}u \tag{2.2.45}$$

Both equations may be discretized in time with the central difference approach. We get:

$$\frac{1}{\Delta\tau}(u^{i+1}-u^i) = \mathbf{M}v^{i+0.5} \tag{2.2.46}$$
$$\frac{1}{\Delta\tau}(v^{i+0.5}-v^{i-0.5}) = \mathbf{N}u^i \tag{2.2.47}$$

This leads to the following update algorithm:

$$u^{i+1} = \Delta\tau\mathbf{M}v^{i+0.5}+u^i \tag{2.2.48}$$
$$v^{i+0.5} = \Delta\tau\mathbf{N}u^i+v^{i-0.5} \tag{2.2.49}$$

Note, that the calculation indeed proceeds in a leap-frog manner. The update equation for u involves v calculated half a time step earlier.

By manipulating the equations we see that the approach defined by eqs. (2.2.48) and (2.2.49) is equivalent to the following scheme:

$$u^{i+1} = (2+\Delta\tau^2\mathbf{MN})u^i-u^{i-1} \tag{2.2.50}$$
$$v^{i+0.5} = (2+\Delta\tau^2\mathbf{NM})v^{i-0.5}-v^{i-1.5} \tag{2.2.51}$$

The same expressions would arise from discretization of the following differential equations using the approach introduced in sec. 2.2.3.2:

$$\frac{\partial^2}{\partial\tau^2}u = \mathbf{MN}u \tag{2.2.52}$$
$$\frac{\partial^2}{\partial\tau^2}v = \mathbf{NM}v \tag{2.2.53}$$

Therefore, the analysis performed in sec. 2.2.3.2 is valid also in this case.

Stability condition Based on the discussion from sec. 2.2.3.2, eqs. (2.2.38), (2.2.52) and (2.2.53), we get the stability condition for the problem at hand:

$$\lambda_{\mathrm{L}}\in\mathcal{R},\qquad \lambda_{\mathrm{L}}\geq 0,\qquad \Delta\tau\leq\frac{2}{\sqrt{\lambda_{\mathrm{Lmax}}}} \tag{2.2.54}$$

for every λ_{L}, where λ_{L} are eigenvalues of $\mathbf{L}_u=-\mathbf{MN}$ or $\mathbf{L}_v=-\mathbf{NM}$ (they are the same).

2.2.3.5 General leap-frog scheme

The basic leap-frog scheme can be generalized to handle the following set of differential equations:

$$\frac{\partial}{\partial\tau}u = \mathbf{M}v + \mathbf{P}u \tag{2.2.55}$$

$$\frac{\partial}{\partial\tau}v = \mathbf{N}u + \mathbf{R}v \tag{2.2.56}$$

Discretization of (2.2.55) and (2.2.56) gives:

$$\frac{1}{\Delta\tau}(u^{i+1} - u^i) = \mathbf{M}v^{i+0.5} + \frac{1}{2}\mathbf{P}(u^{i+1} + u^i) \tag{2.2.57}$$

$$\frac{1}{\Delta\tau}(v^{i+0.5} - v^{i-0.5}) = \mathbf{N}u^i + \frac{1}{2}\mathbf{R}(v^{i+0.5} + v^{i-0.5}) \tag{2.2.58}$$

Eqs. (2.2.57) and (2.2.58) lead to the following update procedure:

$$u^{i+1} = \Delta\tau\left(1 - \frac{\Delta\tau}{2}\mathbf{P}\right)^{-1}\mathbf{M}v^{i+0.5} + \left(1 - \frac{\Delta\tau}{2}\mathbf{P}\right)^{-1}\left(1 + \frac{\Delta\tau}{2}\mathbf{P}\right)u^i \tag{2.2.59}$$

$$v^{i+0.5} = \Delta\tau\left(1 - \frac{\Delta\tau}{2}\mathbf{R}\right)^{-1}\mathbf{N}u^i + \left(1 - \frac{\Delta\tau}{2}\mathbf{R}\right)^{-1}\left(1 + \frac{\Delta\tau}{2}\mathbf{R}\right)v^{i-0.5} \tag{2.2.60}$$

Stability condition Eqs. (2.2.59), (2.2.60) are equivalent to the following algorithms.

$$\begin{aligned} u^{i+1} &= \left(1 - \frac{\Delta\tau}{2}\mathbf{P}\right)^{-1}\left(1 - \frac{\Delta\tau}{2}\mathbf{M}\mathbf{R}\mathbf{M}^{-1}\right)^{-1}\left[2 + \Delta\tau^2\left(\mathbf{M}\mathbf{N} - \frac{1}{2}\mathbf{M}\mathbf{R}\mathbf{M}^{-1}\mathbf{P}\right)\right]u^i \\ &- \left(1 - \frac{\Delta\tau}{2}\mathbf{P}\right)^{-1}\left(1 + \frac{\Delta\tau}{2}\mathbf{P}\right)u^{i-1} \end{aligned} \tag{2.2.61}$$

$$\begin{aligned} v^{i+0.5} &= \left(1 - \frac{\Delta\tau}{2}\mathbf{R}\right)^{-1}\left(1 - \frac{\Delta\tau}{2}\mathbf{N}\mathbf{P}\mathbf{N}^{-1}\right)^{-1}\left[2 + \Delta\tau^2\left(\mathbf{N}\mathbf{M} - \frac{1}{2}\mathbf{N}\mathbf{P}\mathbf{N}^{-1}\mathbf{R}\right)\right]v^{i-0.5} \\ &- \left(1 - \frac{\Delta\tau}{2}\mathbf{R}\right)^{-1}\left(1 + \frac{\Delta\tau}{2}\mathbf{R}\right)v^{i-1.5} \end{aligned} \tag{2.2.62}$$

It is hard to derive a general stability condition for algorithms (2.2.61) and (2.2.62). However, it may be shown (see [69] for details), that the scheme is stable in the following special cases:

$$\mathbf{P} = 0, \quad \lambda_{\mathrm{R}} \in \mathcal{R}, \quad \lambda_{\mathrm{R}} \leq 0, \quad \mathbf{M}\mathbf{N} = (\mathbf{M}\mathbf{N})^H, \quad \mathbf{M}\mathbf{N} \leq 0, \quad \Delta\tau \leq \frac{2}{\sqrt{||\mathbf{M}\mathbf{N}||}} \tag{2.2.63}$$

or

$$\mathbf{R} = 0, \quad \lambda_{\mathrm{P}} \in \mathcal{R}, \quad \lambda_{\mathrm{P}} \leq 0, \quad \mathbf{M}\mathbf{N} = (\mathbf{M}\mathbf{N})^H, \quad \mathbf{M}\mathbf{N} \leq 0, \quad \Delta\tau \leq \frac{2}{\sqrt{||\mathbf{M}\mathbf{N}||}} \tag{2.2.64}$$

for every λ_{P}, λ_{R}, where λ_{P}, λ_{R} are eigenvalues of, respectively, $\mathbf{P}$ and $\mathbf{R}$.

2.2.3.6 Remarks regarding stability

Having introduced basic explicit update schemes which can be used to solve a large class of initial value problems it is possible to make a general remark regarding the stability of the iterative procedures. From conditions (2.2.26), (2.2.38), (2.2.43), (2.2.54) and (2.2.64) it is readily seen that each scheme imposes certain conditions on the maximum time step allowed. This can be usually satisfied by a suitable choice of $\Delta\tau$. It has however to be born in mind that there are additional conditions which impose restrictions on properties of the operators involved. In particular, the semi-definiteness and symmetry are often needed.

2.2.3.7 Finite-Difference Time-Domain method

As indicated in the introduction, in the field of computational electromagnetics the finite difference explicit update scheme are traditionally called the Finite-Difference Time-Domain method. These algorithms may have various forms depending on the formulation from which they arise. As an example, we present a classical formulation of the Finite-Difference Time-Domain method for analysis of a three-dimensional lossy structure. In this case, Maxwell's equations in the Cartesian coordinates may be written as follows:

$$\begin{aligned}\begin{bmatrix} 0 & -\frac{\partial}{\partial z}(.) & \frac{\partial}{\partial y}(.) \\ \frac{\partial}{\partial z}(.) & 0 & -\frac{\partial}{\partial x}(.) \\ -\frac{\partial}{\partial y}(.) & \frac{\partial}{\partial x}(.) & 0 \end{bmatrix} \begin{bmatrix} H_x(x,y,z,t) \\ H_y(x,y,z,t) \\ H_z(x,y,z,t) \end{bmatrix} &= \frac{\partial}{\partial t}\epsilon(x,y,z) \begin{bmatrix} E_x(x,y,z,t) \\ E_y(x,y,z,t) \\ E_z(x,y,z,t) \end{bmatrix} \\ &+ \sigma(x,y,z) \begin{bmatrix} E_x(x,y,z,t) \\ E_y(x,y,z,t) \\ E_z(x,y,z,t) \end{bmatrix} \end{aligned} \tag{2.2.65}$$

$$\begin{bmatrix} 0 & -\frac{\partial}{\partial z}(.) & \frac{\partial}{\partial y}(.) \\ \frac{\partial}{\partial z}(.) & 0 & -\frac{\partial}{\partial x}(.) \\ -\frac{\partial}{\partial y}(.) & \frac{\partial}{\partial x}(.) & 0 \end{bmatrix} \begin{bmatrix} E_x(x,y,z,t) \\ E_y(x,y,z,t) \\ E_z(x,y,z,t) \end{bmatrix} = -\frac{\partial}{\partial t}\mu(x,y,z) \begin{bmatrix} H_x(x,y,z,t) \\ H_y(x,y,z,t) \\ H_z(x,y,z,t) \end{bmatrix} \tag{2.2.66}$$

Field components are discretized in space and time as follows:

$$f^{i_t}(i_x,i_y,i_z) = F(x_0+i_x\Delta x, y_0+i_y\Delta y, z_0+i_z\Delta z, t_0+i_t\Delta t) \tag{2.2.67}$$

Functions describing media properties are discretized in space:

$$\psi(i_x,i_y,i_z) = \Psi(x_0+i_x\Delta x, y_0+i_y\Delta y, z_0+i_z\Delta z) \tag{2.2.68}$$

f and ψ are the discrete functions associated with physical quantities, respectively, F and Ψ; i_x, i_y, i_z, i_t are integers, x_0, y_0, z_0 are coordinates of a reference grid point, Δx, Δy, Δz are grid steps in directions x, y and z respectively, t_0 is a reference time, and Δt is the time step.

Using Yee's dual mesh to discretize electric and magnetic field one can write the following update equations for the electric field [45, 79]:

$$\begin{aligned} e_x^{i_t+1}\left(i_x+\frac{1}{2},i_y,i_z\right) &= \frac{2\epsilon_{xx}(i_x+\frac{1}{2},i_y,i_z)-\Delta t\sigma_{xx}(i_x+\frac{1}{2},i_y,i_z)}{2\epsilon_{xx}(i_x+\frac{1}{2},i_y,i_z)+\Delta t\sigma_{xx}(i_x+\frac{1}{2},i_y,i_z)} \cdot e_x^{i_t}\left(i_x+\frac{1}{2},i_y,i_z\right) \\ &+ \frac{2\Delta t}{2\epsilon_{xx}(i_x+\frac{1}{2},i_y,i_z)+\Delta t\sigma_{xx}(i_x+\frac{1}{2},i_y,i_z)} \cdot \end{aligned}$$

$$\cdot \quad \left[\frac{1}{\Delta y}\left[h_z^{i_t+\frac{1}{2}}\left(i_x+\frac{1}{2},i_y+\frac{1}{2},i_z\right)-h_z^{i_t+\frac{1}{2}}\left(i_x+\frac{1}{2},i_y-\frac{1}{2},i_z\right)\right]\right.$$
$$-\quad \left.\frac{1}{\Delta z}\left[h_y^{i_t+\frac{1}{2}}\left(i_x+\frac{1}{2},i_y,i_z+\frac{1}{2}\right)-h_y^{i_t+\frac{1}{2}}\left(i_x+\frac{1}{2},i_y,i_z-\frac{1}{2}\right)\right]\right] \tag{2.2.69}$$

$$e_y^{i_t+1}\left(i_x,i_y+\frac{1}{2},i_z\right) = \frac{2\epsilon_{yy}(i_x,i_y+\frac{1}{2},i_z)-\Delta t\sigma_{yy}(i_x,i_y+\frac{1}{2},i_z)}{2\epsilon_{yy}(i_x,i_y+\frac{1}{2},i_z)+\Delta t\sigma_{yy}(i_x,i_y+\frac{1}{2},i_z)}\cdot e_y^{i_t}\left(i_x,i_y+\frac{1}{2},i_z\right)$$
$$+\quad \frac{2\Delta t}{2\epsilon_{yy}(i_x,i_y+\frac{1}{2},i_z)+\Delta t\sigma_{yy}(i_x,i_y+\frac{1}{2},i_z)}\cdot$$
$$\cdot \quad \left[\frac{1}{\Delta z}\left[h_x^{i_t+\frac{1}{2}}\left(i_x,i_y+\frac{1}{2},i_z+\frac{1}{2}\right)-h_x^{i_t+\frac{1}{2}}\left(i_x,i_y+\frac{1}{2},i_z-\frac{1}{2}\right)\right]\right.$$
$$-\quad \left.\frac{1}{\Delta x}\left[h_z^{i_t+\frac{1}{2}}\left(i_x+\frac{1}{2},i_y+\frac{1}{2},i_z\right)-h_z^{i_t+\frac{1}{2}}\left(i_x-\frac{1}{2},i_y+\frac{1}{2},i_z\right)\right]\right] \tag{2.2.70}$$

$$e_z^{i_t+1}\left(i_x,i_y,i_z+\frac{1}{2}\right) = \frac{2\epsilon_{zz}(i_x,i_y,i_z+\frac{1}{2})-\Delta t\sigma_{zz}(i_x,i_y,i_z+\frac{1}{2})}{2\epsilon_{zz}(i_x,i_y,i_z+\frac{1}{2})+\Delta t\sigma_{zz}(i_x,i_y,i_z+\frac{1}{2})}\cdot e_z^{i_t}\left(i_x,i_y,i_z+\frac{1}{2}\right)$$
$$+\quad \frac{2\Delta t}{2\epsilon_{zz}(i_x,i_y,i_z+\frac{1}{2})+\Delta t\sigma_{zz}(i_x,i_y,i_z+\frac{1}{2})}\cdot$$
$$\cdot \quad \left[\frac{1}{\Delta x}\left[h_y^{i_t+\frac{1}{2}}\left(i_x+\frac{1}{2},i_y,i_z+\frac{1}{2}\right)-h_y^{i_t+\frac{1}{2}}\left(i_x-\frac{1}{2},i_y,i_z-\frac{1}{2}\right)\right]\right.$$
$$-\quad \left.\frac{1}{\Delta y}\left[h_x^{i_t+\frac{1}{2}}\left(i_x,i_y+\frac{1}{2},i_z+\frac{1}{2}\right)-h_x^{i_t+\frac{1}{2}}\left(i_x,i_y-\frac{1}{2},i_z+\frac{1}{2}\right)\right]\right] \tag{2.2.71}$$

Magnetic field components are updated using the following formulas [45, 79]:

$$h_x^{i_t+\frac{1}{2}}\left(i_x,i_y+\frac{1}{2},i_z+\frac{1}{2}\right) = h_x^{i_t-\frac{1}{2}}\left(i_x,i_y+\frac{1}{2},i_z+\frac{1}{2}\right)+\frac{\Delta t}{\mu_{xx}(i_x,i_y+\frac{1}{2},i_z+\frac{1}{2})}\cdot$$
$$\cdot \quad \left[\frac{1}{\Delta z}\left[e_y^{i_t}\left(i_x,i_y+\frac{1}{2},i_z+1\right)-e_y^{i_t}\left(i_x,i_y+\frac{1}{2},i_z\right)\right]\right.$$
$$-\quad \left.\frac{1}{\Delta y}\left[e_z^{i_t}\left(i_x,i_y+1,i_z+\frac{1}{2}\right)-e_z^{i_t}\left(i_x,i_y,i_z+\frac{1}{2}\right)\right]\right] \tag{2.2.72}$$

$$h_y^{i_t+\frac{1}{2}}\left(i_x+\frac{1}{2},i_y,i_z+\frac{1}{2}\right) = h_y^{i_t-\frac{1}{2}}\left(i_x+\frac{1}{2},i_y,i_z+\frac{1}{2}\right)+\frac{\Delta t}{\mu_{yy}(i_x+\frac{1}{2},i_y,i_z+\frac{1}{2})}\cdot$$
$$\cdot \quad \left[\frac{1}{\Delta x}\left[e_z^{i_t}\left(i_x+1,i_y,i_z+\frac{1}{2}\right)-e_z^{i_t}\left(i_x,i_y,i_z+\frac{1}{2}\right)\right]\right.$$
$$-\quad \left.\frac{1}{\Delta z}\left[e_x^{i_t}\left(i_x+\frac{1}{2},i_y,i_z+1\right)-e_x^{i_t}\left(i_x+\frac{1}{2},i_y,i_z\right)\right]\right] \tag{2.2.73}$$

$$h_z^{i_t+\frac{1}{2}}\left(i_x+\frac{1}{2},i_y+\frac{1}{2},i_z\right) = h_z^{i_t-\frac{1}{2}}\left(i_x+\frac{1}{2},i_y+\frac{1}{2},i_z\right)+\frac{\Delta t}{\mu_{zz}(i_x+\frac{1}{2},i_y+\frac{1}{2},i_z)}\cdot$$
$$\cdot \quad \left[\frac{1}{\Delta y}\left[e_x^{i_t}\left(i_x+\frac{1}{2},i_y+1,i_z\right)-e_x^{i_t}\left(i_x+\frac{1}{2},i_y,i_z\right)\right]\right.$$
$$-\quad \left.\frac{1}{\Delta x}\left[e_y^{i_t}\left(i_x+1,i_y+\frac{1}{2},i_z\right)-e_y^{i_t}\left(i_x,i_y+\frac{1}{2},i_z\right)\right]\right]$$

(2.2.74)

Boundary conditions At this stage of discussion, we assume that the domain is surrounded by perfectly conducting metal planes coincident with nodes of tangential electric field components. In order to satisfy the boundary conditions, the field samples defined at these nodes should be set to zero. Further on in this thesis, more sophisticated methods modeling arbitrarily located metal planes and different boundary conditions will be presented.

Matrix form One may note, that the algorithm presented above is a special case of the general leap-frog scheme introduced in sec. 2.2.3.5 with the following substitutions:

$$\tau \longleftarrow t \tag{2.2.75}$$

$$u \overset{\text{discr}}{\longleftarrow} \vec{E} \tag{2.2.76}$$

$$v \overset{\text{discr}}{\longleftarrow} \vec{H} \tag{2.2.77}$$

$$\mathbf{M} \overset{\text{discr}}{\longleftarrow} \frac{1}{\epsilon}\nabla \times (.) \tag{2.2.78}$$

$$\mathbf{N} \overset{\text{discr}}{\longleftarrow} -\frac{1}{\mu}\nabla \times (.) \tag{2.2.79}$$

$$\mathbf{P} \overset{\text{discr}}{\longleftarrow} -\frac{\sigma}{\epsilon} \tag{2.2.80}$$

$$\mathbf{R} \overset{\text{discr}}{\longleftarrow} 0 \tag{2.2.81}$$

where symbol $\overset{\text{discr}}{\longleftarrow}$ denotes discretization. Note, that u, v are vectors, and operators $\mathbf{M}$, $\mathbf{N}$, $\mathbf{P}$ and $\mathbf{R}$ are matrices. Matrices $\mathbf{M}$ and $\mathbf{N}$ are sparse and $\mathbf{P}$ is diagonal. The set of matrix equations of the form (2.2.59), (2.2.60) is equivalent to the algorithm defined by eqs. (2.2.69)–(2.2.74).

Stability condition The above observation allows us to apply directly the results of the analysis performed in sec. 2.2.3.5. In particular, we may write the stability condition for the algorithm at hand. Starting from (2.2.64) we get the first condition:

$$\frac{\sigma}{\epsilon} \geq 0 \tag{2.2.82}$$

In order to derive the second condition, we should estimate the norm of the operator $\mathbf{MN}$. More detailed discussion of this problem performed further on, in sec. 3.9, will show that we may use the following relation:

$$||\mathbf{MN}|| \leq 4v_{\min}^2 \left(\frac{1}{\Delta x^2} + \frac{1}{\Delta y^2} + \frac{1}{\Delta z^2} \right) \tag{2.2.83}$$

where $v_{\min}$ is the minimum speed of the wave in the analyzed domain. This and eq. (2.2.64) give the second stability condition:

$$\Delta t \leq \frac{1}{v_{\min}\sqrt{\frac{1}{\Delta x^2} + \frac{1}{\Delta y^2} + \frac{1}{\Delta z^2}}} \tag{2.2.84}$$

In the above inequality we recognize the well known CFL (Courant-Freidrich-Lewy) condition [45, 79].

Although operator **MN** is not symmetric and, hence, does not satisfy condition (2.2.63), we may symmetrize it by constructing an equivalent algorithm with functions $u \overset{\text{discr}}{\longleftarrow} \sqrt{\epsilon}\vec{E}$ and $v \overset{\text{discr}}{\longleftarrow} \sqrt{\epsilon}\vec{H}$. In this case, symmetry of **MN**, and its negative semdefiniteness – both follow form $\mathbf{N} = -\mathbf{M}^T$ which is true for Yee's mesh.

2.2.4 Finite-Difference Frequency-Domain methods

So far, we have considered only the finite difference equations resulting from the initial value problems. As noted, in computational electromagnetics one also is interested in the boundary value problems specified for the sinusoidal steady state. Such problems occur when Maxwell's equations are written in the frequency domain. In this section, we shall present the classical technique known as the Finite-Difference Frequency-Domain method. The central difference techniques introduced in the previous sections are used for this task. Depending on the form of the differential equation this method leads to two important classes. When there are no sources in the analyzed domain, Maxwell's equations may be written in the form of eq. (2.1.2). In this case, the FD-FD method results in a matrix eigenproblem. This version is introduced in sec. 2.2.4.1. On the other hand, if sources are present (eq. (2.1.1)), the method leads to a system of linear equations. This algorithm is presented in sec. 2.2.4.2.

2.2.4.1 Nondeterministic problems

As noted earlier in this text, discretization of the frequency domain version of partial differential equations which is of interest in electromagnetics, often leads, for nondeterministic problems, to a matrix eigenproblem. In terms of physical interpretation, the problems may have one of the following meaning:

- Finding resonant frequencies and associated modes of a resonator. The eigenvalues are resonant frequencies ω or ω^2.
- Finding dispersion characteristics of a waveguide. The eigenvalues are propagation constants β_z or β_z^2 for various frequencies ω.
- Finding inverse dispersion characteristics of a waveguide. The eigenvalues are frequencies ω or ω^2 for various propagation constants β_z.
- Finding waveguide modes at cutoff. The eigenvalues are cutoff frequencies ω or ω^2 for $\beta_z = 0$.
- Finding static modes of a waveguide — the eigenvalues: β_z or β_z^2 for $\omega = 0$.

In every case the eigenvectors represent the field distribution of the associated modes.

To introduce the method, in this section we restrict our considerations to the algorithm arising from discretization of Maxwell's equations written in the Cartesian coordinates for a three-dimensional structure, i.e. the problem of finding resonant frequencies and modes of a 3D resonator. We assume that the electric and magnetic fields are harmonic functions of time defined as follows:

$$\vec{E}(x,y,z,t) = \vec{E}(x,y,z)\sin(\omega t) \tag{2.2.85}$$

$$\vec{H}(x,y,z,t) = \vec{H}(x,y,z)\cos(\omega t) \tag{2.2.86}$$

Maxwell's equations take up the form:

$$\begin{bmatrix} 0 & -\frac{\partial}{\partial z}(.) & \frac{\partial}{\partial y}(.) \\ \frac{\partial}{\partial z}(.) & 0 & -\frac{\partial}{\partial x}(.) \\ -\frac{\partial}{\partial y}(.) & \frac{\partial}{\partial x}(.) & 0 \end{bmatrix} \begin{bmatrix} H_x(x,y,z) \\ H_y(x,y,z) \\ H_z(x,y,z) \end{bmatrix} = \omega\epsilon(x,y,z) \begin{bmatrix} E_x(x,y,z) \\ E_y(x,y,z) \\ E_z(x,y,z) \end{bmatrix} \quad (2.2.87)$$

$$\begin{bmatrix} 0 & -\frac{\partial}{\partial z}(.) & \frac{\partial}{\partial y}(.) \\ \frac{\partial}{\partial z}(.) & 0 & -\frac{\partial}{\partial x}(.) \\ -\frac{\partial}{\partial y}(.) & \frac{\partial}{\partial x}(.) & 0 \end{bmatrix} \begin{bmatrix} E_x(x,y,z) \\ E_y(x,y,z) \\ E_z(x,y,z) \end{bmatrix} = \omega\mu(x,y,z) \begin{bmatrix} H_x(x,y,z) \\ H_y(x,y,z) \\ H_z(x,y,z) \end{bmatrix} \quad (2.2.88)$$

We now proceed to discretization of the above equations using the same approach as in the case of the FD-TD method, This is to say that Yee's mesh is used and field components and functions describing the properties material are discretized in space as follows:

$$f(i_x, i_y, i_z) = F(x_0 + i_x\Delta x, y_0 + i_y\Delta y, z_0 + i_z\Delta z) \quad (2.2.89)$$

where f is a discrete function associated with physical quantity F; i_x, i_y, i_z are integers, x_0, y_0, z_0 are coordinates of a reference grid point, and Δx, Δy, Δz are grid steps in directions x, y and z respectively. For Yee's mesh, discrete equivalent of eq. (2.2.87) takes up the form:

$$\begin{aligned} \omega e_x\left(i_x + \frac{1}{2}, i_y, i_z\right) &= \frac{1}{\epsilon_{xx}(i_x + \frac{1}{2}, i_y, i_z)} \cdot \\ &\cdot \left[\frac{1}{\Delta y}\left[h_z\left(i_x + \frac{1}{2}, i_y + \frac{1}{2}, i_z\right) - h_z\left(i_x + \frac{1}{2}, i_y - \frac{1}{2}, i_z\right)\right]\right. \\ &- \left.\frac{1}{\Delta z}\left[h_y\left(i_x + \frac{1}{2}, i_y, i_z + \frac{1}{2}\right) - h_y\left(i_x + \frac{1}{2}, i_y, i_z - \frac{1}{2}\right)\right]\right] \end{aligned} \quad (2.2.90)$$

$$\begin{aligned} \omega e_y\left(i_x, i_y + \frac{1}{2}, i_z\right) &= \frac{1}{\epsilon_{yy}(i_x, i_y + \frac{1}{2}, i_z)} \cdot \\ &\cdot \left[\frac{1}{\Delta z}\left[h_x\left(i_x, i_y + \frac{1}{2}, i_z + \frac{1}{2}\right) - h_x\left(i_x, i_y + \frac{1}{2}, i_z - \frac{1}{2}\right)\right]\right. \\ &- \left.\frac{1}{\Delta x}\left[h_z\left(i_x + \frac{1}{2}, i_y + \frac{1}{2}, i_z\right) - h_z\left(i_x - \frac{1}{2}, i_y + \frac{1}{2}, i_z\right)\right]\right] \end{aligned} \quad (2.2.91)$$

$$\begin{aligned} \omega e_z\left(i_x, i_y, i_z + \frac{1}{2}\right) &= \frac{1}{\epsilon_{zz}(i_x, i_y, i_z + \frac{1}{2})} \cdot \\ &\cdot \left[\frac{1}{\Delta x}\left[h_y\left(i_x + \frac{1}{2}, i_y, i_z + \frac{1}{2}\right) - h_y\left(i_x - \frac{1}{2}, i_y, i_z - \frac{1}{2}\right)\right]\right. \\ &- \left.\frac{1}{\Delta y}\left[h_x\left(i_x, i_y + \frac{1}{2}, i_z + \frac{1}{2}\right) - h_x\left(i_x, i_y - \frac{1}{2}, i_z + \frac{1}{2}\right)\right]\right] \end{aligned} \quad (2.2.92)$$

Discrete form of eq. (2.2.88) is given by the following equations:

$$\begin{aligned} \omega h_x\left(i_x, i_y + \frac{1}{2}, i_z + \frac{1}{2}\right) &= \frac{1}{\mu_{xx}(i_x, i_y + \frac{1}{2}, i_z + \frac{1}{2})} \cdot \\ &\cdot \left[\frac{1}{\Delta z}\left[e_y\left(i_x, i_y + \frac{1}{2}, i_z + 1\right) - e_y\left(i_x, i_y + \frac{1}{2}, i_z\right)\right]\right. \end{aligned}$$

$$- \quad \frac{1}{\Delta y}\left[e_z\left(i_x, i_y+1, i_z+\frac{1}{2}\right) - e_z\left(i_x, i_y, i_z+\frac{1}{2}\right)\right]\Bigg] \tag{2.2.93}$$

$$\begin{aligned}\omega h_y\left(i_x+\frac{1}{2}, i_y, i_z+\frac{1}{2}\right) &= \frac{1}{\mu_{yy}(i_x+\frac{1}{2}, i_y, i_z+\frac{1}{2})}\cdot \\ &\cdot \quad \left[\frac{1}{\Delta x}\left[e_z\left(i_x+1, i_y, i_z+\frac{1}{2}\right) - e_z\left(i_x, i_y, i_z+\frac{1}{2}\right)\right]\right. \\ &- \quad \left.\frac{1}{\Delta z}\left[e_x\left(i_x+\frac{1}{2}, i_y, i_z+1\right) - e_x\left(i_x+\frac{1}{2}, i_y, i_z\right)\right]\right]\end{aligned} \tag{2.2.94}$$

$$\begin{aligned}\omega h_z\left(i_x+\frac{1}{2}, i_y+\frac{1}{2}, i_z\right) &= \frac{1}{\mu_{zz}(i_x+\frac{1}{2}, i_y+\frac{1}{2}, i_z)}\cdot \\ &\cdot \quad \left[\frac{1}{\Delta y}\left[e_x\left(i_x+\frac{1}{2}, i_y+1, i_z\right) - e_x\left(i_x+\frac{1}{2}, i_y, i_z\right)\right]\right. \\ &- \quad \left.\frac{1}{\Delta x}\left[e_y\left(i_x+1, i_y+\frac{1}{2}, i_z\right) - e_y\left(i_x, i_y+\frac{1}{2}, i_z\right)\right]\right]\end{aligned} \tag{2.2.95}$$

Boundary conditions Again, for simplicity it is assumed the the domain is bounded by a perfect electric conductor coinciding with the nodes corresponding to the tangential electric field components.

Matrix eigenproblems Eqs. (2.2.90)–(2.2.95) may be written in the form of a matrix eigenproblem with eigenvalues ω and eigenvectors $\begin{bmatrix} \underline{e} \\ \underline{h} \end{bmatrix}$:

$$\omega \begin{bmatrix} \underline{e} \\ \underline{h} \end{bmatrix} = \begin{bmatrix} 0 & \underline{\underline{L}}_{eh} \\ \underline{\underline{L}}_{he} & 0 \end{bmatrix} \begin{bmatrix} \underline{e} \\ \underline{h} \end{bmatrix} \tag{2.2.96}$$

where $\underline{e}$, $\underline{h}$ are vectors of, respectively, electric and magnetic discrete field components. Simple modification leads to the following eigenproblems:

$$\omega^2 \underline{e} = \underline{\underline{L}}_{eh}\underline{\underline{L}}_{he}\underline{e} \tag{2.2.97}$$

$$\omega^2 \underline{h} = \underline{\underline{L}}_{he}\underline{\underline{L}}_{eh}\underline{h} \tag{2.2.98}$$

with eigenvalues ω^2 and eigenvectors, respectively, $\underline{e}$ and $\underline{h}$.

2.2.4.2 Deterministic problems

In a similar manner, we may derive a matrix equation associated with deterministic problems, i.e. when sources are present in the analyzed domain. Restricting the considerations to 3D problems, this equation takes up the following form:

$$\begin{bmatrix} \omega\underline{\underline{I}}_{ee} & -\underline{\underline{L}}_{eh} \\ -\underline{\underline{L}}_{he} & \omega\underline{\underline{I}}_{hh} \end{bmatrix} \begin{bmatrix} \underline{e} \\ \underline{h} \end{bmatrix} = \begin{bmatrix} \underline{j}_e(\omega) \\ \underline{j}_m(\omega) \end{bmatrix} \tag{2.2.99}$$

where $\underline{\underline{I}}_{ee}$ and $\underline{\underline{I}}_{hh}$ are the unit matrices and $\underline{j}_e(\omega)$, $\underline{j}_m(\omega)$ represent, respectively, electric and magnetic source currents. Eq. 2.2.99 is a system of linear equations which may be solved for every given frequency using a numerical solver.

2.3 Accuracy of finite difference methods

With basic finite difference schemes established we may now turn to the question of error introduced by the discretization. Before examining this matter in greater detail, let us make an observation that will facilitate the discussion. As noted in sec. 2.2.3.4, the leap frog scheme can be related to the basic second order algorithm discussed in sec. 2.2.3.2. This relation was found useful in deriving the stability condition. Let us look at the FD-TD method from this perspective to relate it to the FD-FD technique. Assuming $\sigma = 0$, FD-TD is reduced to one of the equivalent forms (2.2.50) or (2.2.51). Comparing these equivalent forms to the equations (2.2.97) and (2.2.98) derived for the FD-FD we may note that they are very similar. In fact substituting

$$\frac{\partial^2}{\partial \tau^2} = -\omega^2 \tag{2.3.1}$$

$$u \overset{\text{discr}}{\longleftarrow} \vec{E} \tag{2.3.2}$$

$$v \overset{\text{discr}}{\longleftarrow} \vec{H} \tag{2.3.3}$$

$$\mathbf{M} = -\underline{\underline{L}}_{he} \tag{2.3.4}$$

$$\mathbf{N} = \underline{\underline{L}}_{eh} \tag{2.3.5}$$

we pass from (2.2.50) to (2.2.97) and from (2.2.51) to (2.2.98). This indicates that we can analyze together properties of FD-TD and FD-FD, if a relation between results provided by one algorithm and the other is established.

To this end, let us consider the accuracy of the second order finite-difference algorithm for the equation:

$$-\frac{\partial^2}{\partial \tau^2} f(\tau) = \alpha^2 f(\tau) \tag{2.3.6}$$

This equation has two general solutions: $\sin(\alpha\tau)$ and $\cos(\alpha\tau)$. Discretizing it for the first of these solutions, we get:

$$-\frac{1}{\Delta\tau}\left[\sin(\alpha\tau + \alpha\Delta\tau) - 2\sin(\alpha\tau) + \sin(\alpha\tau + \alpha\Delta\tau)\right] = \tilde{\alpha}^2 \sin(\alpha\tau) \tag{2.3.7}$$

Since the left hand side only approximates the second order derivative, it was necessary to replace α^2 with and approximate value $\tilde{\alpha}^2$. We shall now find the relation between $\tilde{\alpha}^2$ and the true value α^2. Applying simple trigonometric transformations to the above equation, we get:

$$\begin{aligned} -\frac{1}{\Delta\tau}\left[\sin(\alpha\tau)\cos(\alpha\Delta\tau) + \cos(\alpha\tau)\sin(\alpha\Delta\tau)\right. &- \\ 2\sin(\alpha\tau) &+ \\ \left.\sin(\alpha\tau)\cos(\alpha\Delta\tau) - \cos(\alpha\tau)\sin(\alpha\Delta\tau)\right] &= \\ -\frac{2}{\Delta\tau}\sin(\alpha\tau)\left[\cos(\alpha\Delta\tau) - 1\right] &= \tilde{\alpha}^2 \sin(\alpha\tau) \end{aligned} \tag{2.3.8}$$

from which we get:

$$\tilde{\alpha}^2 = -\frac{2\cos(\alpha\Delta\tau) - 2}{\Delta\tau^2} \tag{2.3.9}$$

This equation may be solved for α yielding

$$\alpha = \frac{\arccos(1 - \frac{\Delta\tau^2\tilde{\alpha}^2}{2})}{\Delta\tau} \tag{2.3.10}$$

The above equations have important implications both for establishing the relation between the FD-TD and FD-FD and the analysis of error in the finite difference schemes involving second order differential operators. Let us say a few words about the first one. Substituting ω^2 for α^2 gives the formulas which allow one to calculate the FD-TD results corresponding to any particular frequency from FD-FD results or vice-versa (provided the space discretization operators are the same). Let us note that equation (2.3.10) is identical to equation (2.2.37) which was used to derive the stability condition of the explicit update scheme.

In the same manner, we may use equation (2.2.25) to perform the analysis of an analogous error involved in the first order differential operator:

$$\alpha = \frac{\arcsin(\Delta\tau\tilde{\alpha})}{\Delta\tau} \tag{2.3.11}$$

2.3.1 Numerical dispersion

Inaccuracy which is described by relations such as (2.3.9) is called the numerical dispersion. This type of error is associated with numerical dispersion. It depends on the finite difference formula used to approximate a differential operator and decreases with decreased discretization step. Figs. 2.3.1 and 2.3.2 show the result of dispersion for the first and second order operators approximated via central difference formulas.

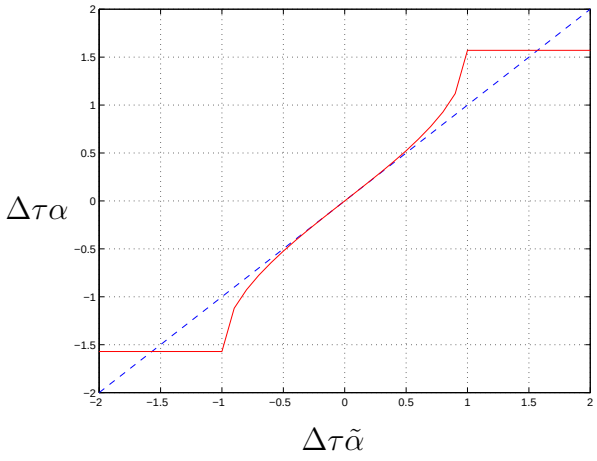

Figure 2.3.1: *Dispersion error associated with the finite difference approximation to a first order differential operator. The stability condition in explicit update algorithms is* $|\Delta\tau\alpha| \leq 1$.

From the figures, it is seen that the error level depends both on $\Delta\tau$ and α. In computational electromagnetics α has often the meaning of a wavenumber. Hence, the product of $\Delta\tau\alpha$ is inversely proportional to the number of discretization points per wavelength.

In this section, we shall analyze the bounds for the error associated with various discretization schemes for ordinary and partial differential equations which are of interests from the viewpoint of computational electromagnetics. Only algorithms involving second order operators will be discussed. In sec. 2.3.1.1, we derive the error bounds for two sample algorithms. In sec. 2.3.1.2, we point out the final results for the rest of the algorithms of interest.

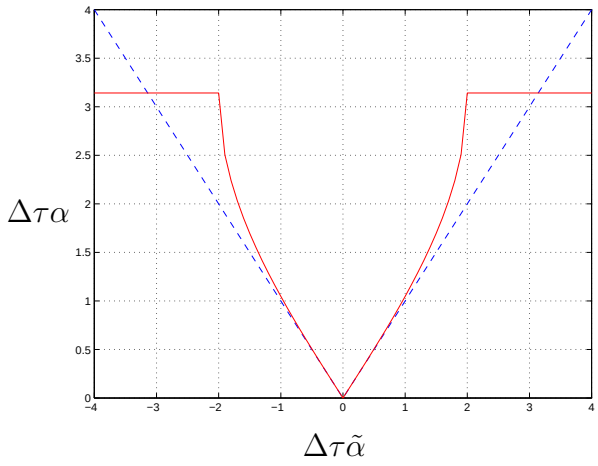

Figure 2.3.2: *Dispersion error associated with the central finite difference approximation to a second order differential operator. The stability condition in explicit update algorithms is* $|\Delta\tau\alpha| \leq 2$.

2.3.1.1 Analysis of the dispersion error

We start with the derivation of the magnitude of the dispersion error for a central finite difference approximation to a canonical second order differential operator. To this end, we use eq. (2.3.9). Assuming that $\Delta\tau\alpha$ is small enough, we may simplify this equation by substituting cosine function with the first three terms of its Taylor series expansion about 0:

$$\tilde{\alpha}^2 \simeq -\frac{2(1-\frac{\alpha^2\Delta\tau^2}{2}+\frac{\alpha^4\Delta\tau^4}{24})-2}{\Delta\tau^2} \tag{2.3.12}$$

and finally we get:

$$\tilde{\alpha}^2 \simeq \alpha^2\left(1-\frac{\alpha^2\Delta\tau^2}{12}\right) \tag{2.3.13}$$

The above formula implies that the solution of the eigenvalue problem using the discretization scheme for the second order derivative results in eigenvalues which are lower than the analytical ones. The error has a constant sign and its relative value is expressed by the following relation:

$$\mathrm{err}_{\alpha^2} \simeq -\frac{\alpha^2\Delta\tau^2}{12} \tag{2.3.14}$$

Relative error for α Note, that err_{α^2} is the relative error for α^2. Let us find more practical parameter err_α which is the relative error for α, i.e. it satisfies the following definition:

$$\tilde{\alpha} = \alpha(1+\mathrm{err}_\alpha) \tag{2.3.15}$$

Squaring both sides of this equation gives:

$$\tilde{\alpha}^2 = \alpha^2(1+2\mathrm{err}_\alpha+\mathrm{err}_\alpha^2) \tag{2.3.16}$$

We may now compare this equation with the equation defining err_{α^2}:

$$\tilde{\alpha}^2 = \alpha^2(1+\mathrm{err}_{\alpha^2}) \tag{2.3.17}$$

This gives:

$$\mathrm{err}_{\alpha^2} = 2\mathrm{err}_\alpha + \mathrm{err}_\alpha^2 \tag{2.3.18}$$

Since only relatively small errors are of practical interest, we may skip the last term in this equation. This leads to:

$$\mathrm{err}_\alpha \simeq 0.5\mathrm{err}_{\alpha^2} \tag{2.3.19}$$

From this and (2.3.14), we finally get:

$$\mathrm{err}_\alpha \simeq -\frac{\alpha^2 \Delta\tau^2}{24} \tag{2.3.20}$$

Wave equation In the next step of the analysis of the numerical dispersion we pass to the operators emerging in the computational electromagnetics. To this end, we consider the wave equation[1] which, for a wave propagating in a homogeneous medium, may be represented by the following operator:

$$-\mu\epsilon\frac{\partial^2}{\partial t^2}(.) = -\frac{\partial^2}{\partial x^2}(.) - \frac{\partial^2}{\partial y^2}(.) - \frac{\partial^2}{\partial z^2}(.) \tag{2.3.21}$$

From the separation condition we get the following analytic dispersion relation:

$$\mu\epsilon\omega^2 = \beta_x^2 + \beta_y^2 + \beta_z^2 \tag{2.3.22}$$

where ω is an angular frequency and β_x, β_y, β_z are propagation constants in direction x, y, z respectively. We may now note, that the discretization of the domain with respect to a variable leads to the substitution of the corresponding derivative in (2.3.21) by the second order central difference. According to the analysis performed above, this leads to the error in the corresponding eigenvalue in the characteristic equation (2.3.22). The corresponding variable is therefore affected by the relative error defined in eq. (2.3.14). Depending on the variables which are discretized in a particular finite difference method, we may expect different numerical dispersion errors. We consider the following cases:

1. Frequency domain formulation, two spatial derivative operators are discretized, the third one is evaluated analytically, the unknown is ω (i.e. a 2D problem of finding ω vs. e.g. β_z)

2. Frequency domain formulation, two spatial derivative operators are discretized, the propagation constant in the third direction is regarded as the unknown (i.e. a 2D problem of finding e.g. β_z vs ω)

3. Time domain formulation, two spatial and time derivative operators are discretized, the third spatial derivative is evaluated analytically, the unknown is ω (i.e. a 2D problem of finding ω vs. e.g. β_z by means of an explicit update algorithm in time domain)

4. Frequency domain formulation, three spatial derivative operators are discretized, the propagation constant in one direction is regarded as the unknown (i.e. a 2D problem of finding e.g. β_z vs ω by means of an explicit update algorithm in the space domain)

[1]The solution of Maxwell's equations also satisfies the wave equation

5. Frequency domain formulation, three spatial derivative operators are discretized, ω is regarded as the unknown (i.e. a 3D problem of finding ω)

6. Time domain formulation, three spatial derivative operators are discretized, ω is regarded as the unknown (i.e. a 3D problem of finding ω by means of the explicit update algorithm in time domain)

Analysis of sample algorithm As an example, let us analyze in detail the first algorithm from the above list, that is to say a 2D problem discretized in space and solved in frequency domain. The corresponding discrete dispersion equation becomes:

$$\mu\epsilon\tilde{\omega}^2 = \tilde{\beta}_x^2 + \tilde{\beta}_y^2 + \beta_z^2 \tag{2.3.23}$$

or in terms of the exact values and the relative errors:

$$\mu\epsilon\omega^2(1+\mathrm{err}_{\omega^2}) = \beta_x^2(1+\mathrm{err}_{\beta_x^2}) + \beta_y^2(1+\mathrm{err}_{\beta_y^2}) + \beta_z^2 \tag{2.3.24}$$

This leads to the equation:

$$\mu\epsilon\omega^2 + \mu\epsilon\omega^2\mathrm{err}_{\omega^2} = \beta_x^2 + \beta_y^2 + \beta_z^2 + \beta_x^2\mathrm{err}_{\beta_x^2} + \beta_y^2\mathrm{err}_{\beta_y^2} \tag{2.3.25}$$

Subtracting eq. (2.3.22) from this equation, we get:

$$\mu\epsilon\omega^2\mathrm{err}_{\omega^2} = \beta_x^2\mathrm{err}_{\beta_x^2} + \beta_y^2\mathrm{err}_{\beta_y^2} \tag{2.3.26}$$

This gives the following formulae for err_{ω^2}:

$$\mathrm{err}_{\omega^2} = -\frac{1}{12\mu\epsilon\omega^2}(\beta_x^4\Delta x^2 + \beta_y^4\Delta y^2) \tag{2.3.27}$$

It is obvious that this error depends on the direction of propagation. In order to find this relation, we express β_x and β_y as follows:

$$\beta_x = \beta_0\cos\phi \tag{2.3.28}$$
$$\beta_y = \beta_0\sin\phi \tag{2.3.29}$$

where ϕ denotes the angle of the direction of propagation with respect to axis x, and β_0 satisfies the following equation:

$$\beta_0^2 = \beta_x^2 + \beta_y^2 = \mu\epsilon\omega^2 - \beta_z^2 \tag{2.3.30}$$

Putting (2.3.28), (2.3.29) into (2.3.27), we get:

$$\mathrm{err}_{\omega^2} = -\frac{\beta_0^4}{12\mu\epsilon\omega^2}(\Delta x^2\cos^4\phi + \Delta y^2\sin^4\phi) \tag{2.3.31}$$

Let us now find the smallest and the largest values of this error. To this end, let us find zero of the first derivative with respect to ϕ of eq. (2.3.31). This gives:

$$\sin\phi\cos\phi(\Delta x^2\cos^2\phi - \Delta y^2\sin^2\phi) = 0 \tag{2.3.32}$$

Eq. (2.3.32) has the following solutions:

$$\phi \in \{0^o, 90^o, 180^o, 270^o\} \qquad \vee \qquad |\tan\phi| = \frac{\Delta x}{\Delta y} \tag{2.3.33}$$

Putting (2.3.33) into (2.3.31), we find the smallest and the largest level of the numerical dispersion error:

$$\mathrm{err}_{\omega^2\mathrm{min}} = -\frac{(\mu\epsilon\omega^2 - \beta_z^2)^2}{\mu\epsilon\omega^2} \cdot \frac{1}{12(\frac{1}{\Delta x^2} + \frac{1}{\Delta y^2})} \tag{2.3.34}$$

$$\mathrm{err}_{\omega^2\mathrm{max}} = -\frac{(\mu\epsilon\omega^2 - \beta_z^2)^2}{\mu\epsilon\omega^2} \cdot \frac{\max(\Delta x^2, \Delta y^2)}{12} \tag{2.3.35}$$

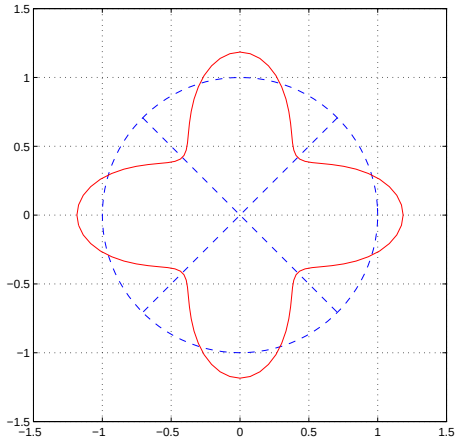

Figure 2.3.3: *Magnitude of the relative numerical dispersion error [%] as a function of the direction of propagation in 2D.* $\beta_z = 0, f = 18\mathrm{GHz}, v = c, \Delta x = \Delta y = 1\mathrm{mm}$.

Relative error versus direction of propagation The above analysis shows that the numerical dispersion error depends on the direction of propagation. It may be shown also in the case of other finite difference algorithms of interest that the magnitude of this error is the largest for the direction corresponding to the axis with the largest grid step and it takes up its smallest value for the direction corresponding to the diagonal of the finite difference cell in 2D or cube in 3D. As an example, we present the magnitude of the relative numerical dispersion error as a function of the direction of propagation in 2D grid in fig. 2.3.3. The data were calculated for propagation constant $\beta_z = 0$ at frequency $f = 18\mathrm{GHz}$ in the vacuum ($v = c$) using a rectangular grid with the grid step $\Delta x = \Delta y = 1\mathrm{mm}$. In this case, the ratio between the grid step and the wave length is equal $\Delta x/\lambda = 0.06$. The numbers at the axes denote the error in percents. In our case, the range of the error is about 0.6–1.2%.

2.3.1.2 Level of error for various algorithms

In the previous section, we analyzed in detail the numerical dispersion error for a sample 2D problem defined and solved in frequency domain deriving the error bounds of the dispersion error. In this section, we give results for the remaining algorithms given on the list. The detailed derivation is omitted as it proceeds along the same lines as in the case already covered. Accordingly, here we present only the final equations for minimum and maximum relative errors and the plots. For completeness, we include also already described case.

2D eigenproblems in frequency domain As discussed in the preceding section, operators $\frac{\partial^2}{\partial x^2}(.)$ and $\frac{\partial^2}{\partial y^2}(.)$ are discretized. The discrete dispersion equation takes up, in this case, the following form:

$$\mu\epsilon\tilde{\omega}^2 = \beta_x^2\left(1 - \frac{\beta_x^2\Delta x^2}{12}\right) + \beta_y^2\left(1 - \frac{\beta_y^2\Delta y^2}{12}\right) + \beta_z^2 \tag{2.3.36}$$

The analysis of this equation yields the following minimum and maximum relative errors of ω^2:

$$\mathrm{err}_{\omega^2}\mathrm{min} = -\frac{(\mu\epsilon\omega^2 - \beta_z^2)^2}{\mu\epsilon\omega^2} \cdot \frac{1}{12(\frac{1}{\Delta x^2} + \frac{1}{\Delta y^2})} \tag{2.3.37}$$

$$\mathrm{err}_{\omega^2}\mathrm{max} = -\frac{(\mu\epsilon\omega^2 - \beta_z^2)^2}{\mu\epsilon\omega^2} \cdot \frac{\max(\Delta x^2, \Delta y^2)}{12} \tag{2.3.38}$$

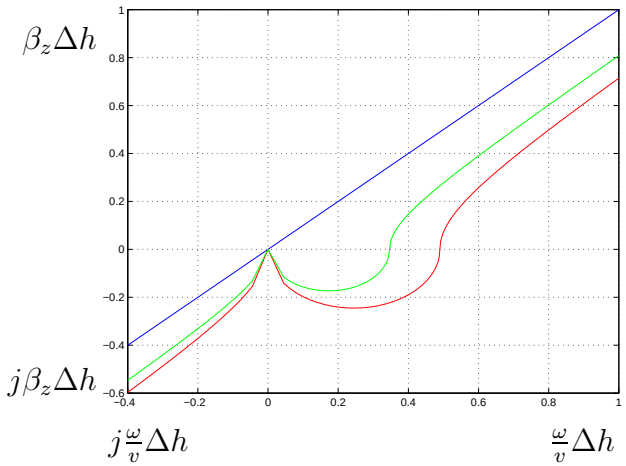

Figure 2.3.4: *Relative numerical dispersion error for 2D eigenproblems in frequency domain.* $\Delta x = \Delta y$, $\mathrm{Err}_\omega = 0.5\%, 1\%$. *See the explanations in the text.*

In fig. 2.3.4, we present the dispersion characteristics versus frequency in a normalized chart. We assume that the grid is rectangular, i.e. $\Delta x = \Delta y = \Delta h$. The figure shows the range of β_z for a given frequency when the maximum level of the relative error of frequency is assumed to be $\mathrm{Err}_\omega = 0.5\%$ and 1%. As an example, let us consider a wave in the vacuum at frequency 10GHz analyzed using a rectangular grid of size $\Delta h = 3$mm. This gives $\frac{\omega}{v}\Delta h \simeq 0.63$. We find at the chart the useful range of $\beta_z\Delta h$. For $\mathrm{Err}_\omega = 0.5\%$, we get $\beta_z\Delta h \simeq 0.4$–$0.6$ which gives $\beta_z \simeq 133$–$200\frac{\mathrm{rad}}{\mathrm{m}}$ and for $\mathrm{Err}_\omega = 1\%$: $\beta_z\Delta h \simeq 0.3$–$0.6$ and $\beta_z \simeq 100$–$200\frac{\mathrm{rad}}{\mathrm{m}}$.

Frequency domain formulation of 2D problems solved for propagation constant. In this case, two spatial differential operators are discretized and β_z is sought. The discrete dispersion equation may be written as follows:

$$\tilde{\beta}_z^2 = \mu\epsilon\omega^2 - \beta_x^2\left(1 - \frac{\beta_x^2\Delta x^2}{12}\right) - \beta_y^2\left(1 - \frac{\beta_y^2\Delta y^2}{12}\right) \tag{2.3.39}$$

from which we get the following minimum and maximum relative errors of β_z^2:

$$\mathrm{err}_{\beta_z^2\mathrm{min}} = \frac{(\mu\epsilon\omega^2 - \beta_z^2)^2}{\beta_z^2} \cdot \frac{1}{12(\frac{1}{\Delta x^2} + \frac{1}{\Delta y^2})} \tag{2.3.40}$$

$$\mathrm{err}_{\beta_z^2\mathrm{max}} = \frac{(\mu\epsilon\omega^2 - \beta_z^2)^2}{\beta_z^2} \cdot \frac{\max(\Delta x^2, \Delta y^2)}{12} \tag{2.3.41}$$

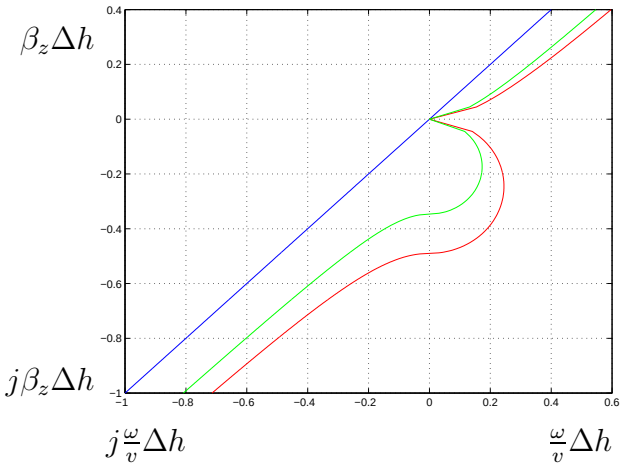

Figure 2.3.5: *Relative numerical dispersion error for 2D problems solved in the space domain.* $\Delta x = \Delta y$, $\mathrm{Err}_{\beta_z} = 0.5\%, 1\%$.

Fig. 2.3.5 presents the dispersion characteristics versus propagation constant in a normalized chart for $\Delta x = \Delta y = \Delta h$. giving the range of frequency for a given propagation constant and the maximum level of the relative error $\mathrm{Err}_{\beta_z} = 0.5\%$ and 1%

2D explicit update scheme in time domain In this case operators $\frac{\partial^2}{\partial t^2}(.)$, $\frac{\partial^2}{\partial x^2}(.)$ and $\frac{\partial^2}{\partial y^2}(.)$ are discretized and ω is evaluated by means of an explicit update scheme in time domain. The discrete dispersion equation has the form:

$$\mu\epsilon\tilde{\omega}^2\left(1 - \frac{\tilde{\omega}^2\Delta t^2}{12}\right) = \beta_x^2\left(1 - \frac{\beta_x^2\Delta x^2}{12}\right) + \beta_y^2\left(1 - \frac{\beta_y^2\Delta y^2}{12}\right) + \beta_z^2 \tag{2.3.42}$$

The minimum and maximum relative errors of ω^2 are:

$$\mathrm{err}_{\omega^2\mathrm{min}} = \frac{\Delta t^2\tilde{\omega}^2}{12 - \Delta t^2\tilde{\omega}^2} - \frac{(\mu\epsilon\omega^2 - \beta_z^2)^2}{\mu\epsilon\omega^2} \cdot \frac{1}{(12 - \Delta t^2\tilde{\omega}^2)(\frac{1}{\Delta x^2} + \frac{1}{\Delta y^2})} \tag{2.3.43}$$

$$\mathrm{err}_{\omega^2\mathrm{max}} = \frac{\Delta t^2\tilde{\omega}^2}{12 - \Delta t^2\tilde{\omega}^2} - \frac{(\mu\epsilon\omega^2 - \beta_z^2)^2}{\mu\epsilon\omega^2} \cdot \frac{\max(\Delta x^2, \Delta y^2)}{12 - \Delta t^2\tilde{\omega}^2} \tag{2.3.44}$$

Frequency domain formulation, 2D explicit update scheme in the space domain used to find the propagation constant For this algorithm, $\frac{\partial^2}{\partial x^2}(.)$, $\frac{\partial^2}{\partial y^2}(.)$ and $\frac{\partial^2}{\partial z^2}(.)$ are discretized and β_z is evaluated by means of an explicit update scheme in space domain. The discrete dispersion equation takes up the form:

$$\tilde{\beta}_z^2\left(1 - \frac{\tilde{\beta}_z^2\Delta z^2}{12}\right) = \mu\epsilon\omega^2 - \beta_x^2\left(1 - \frac{\beta_x^2\Delta x^2}{12}\right) - \beta_y^2\left(1 - \frac{\beta_y^2\Delta y^2}{12}\right) \tag{2.3.45}$$

with the following relative errors of β_z:

$$\mathrm{err}_{\beta_z^2\mathrm{min}} = \frac{\Delta z^2\tilde{\beta}_z^2}{12-\Delta z^2\tilde{\beta}_z^2} + \frac{(\mu\epsilon\omega^2-\beta_z^2)^2}{\beta_z^2}\cdot\frac{1}{(12-\Delta z^2\tilde{\beta}_z^2)(\frac{1}{\Delta x^2}+\frac{1}{\Delta y^2})} \quad (2.3.46)$$

$$\mathrm{err}_{\beta_z^2\mathrm{max}} = \frac{\Delta z^2\tilde{\beta}_z^2}{12-\Delta z^2\tilde{\beta}_z^2} + \frac{(\mu\epsilon\omega^2-\beta_z^2)^2}{\beta_z^2}\cdot\frac{\max(\Delta x^2,\Delta y^2)}{12-\Delta z^2\tilde{\beta}_z^2} \quad (2.3.47)$$

3D problems (frequency domain) Three spatial derivative operators are discretized and ω is evaluated. The discrete dispersion equation may be written as:

$$\mu\epsilon\tilde{\omega}^2 = \beta_x^2\left(1-\frac{\beta_x^2\Delta x^2}{12}\right)+\beta_y^2\left(1-\frac{\beta_y^2\Delta y^2}{12}\right)+\beta_z^2\left(1-\frac{\beta_z^2\Delta z^2}{12}\right) \quad (2.3.48)$$

The relative errors in this case are:

$$\mathrm{err}_{\omega^2\mathrm{min}} = -\mu\epsilon\omega^2\cdot\frac{1}{12(\frac{1}{\Delta x^2}+\frac{1}{\Delta y^2}+\frac{1}{\Delta z^2})} \quad (2.3.49)$$

$$\mathrm{err}_{\omega^2\mathrm{max}} = -\mu\epsilon\omega^2\cdot\frac{\max(\Delta x^2,\Delta y^2,\Delta z^2)}{12} \quad (2.3.50)$$

The maximum level of the relative error of frequency for a rectangular grid (i.e. $\Delta x = \Delta y = \Delta z = \Delta h$) is given in a normalized chart in fig. 2.3.6.

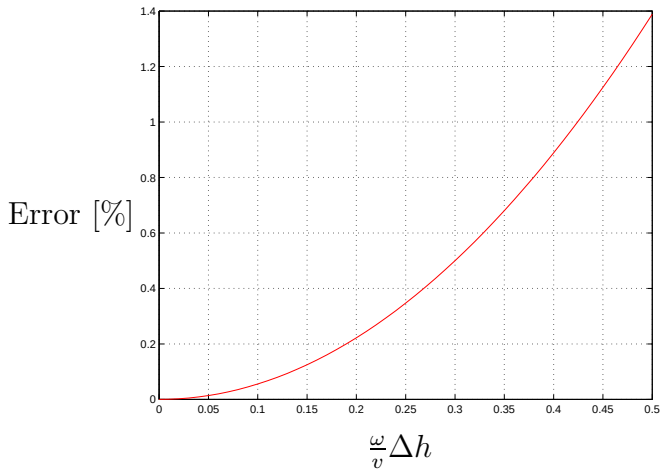

Figure 2.3.6: *Maximum level of the relative numerical dispersion error in frequency for 3D eigenproblems in frequency domain versus normalized frequency. ($\Delta x = \Delta y = \Delta z = \Delta h$)*

3D explicit update scheme (time domain) Here, all four operators (three with respect to space and one with respect to time) are discretized and ω is evaluated by means of an explicit update scheme in time domain. The discrete dispersion equation is the following:

$$\mu\epsilon\tilde{\omega}^2\left(1-\frac{\tilde{\omega}^2\Delta t^2}{12}\right) = \beta_x^2\left(1-\frac{\beta_x^2\Delta x^2}{12}\right)+\beta_y^2\left(1-\frac{\beta_y^2\Delta y^2}{12}\right)+\beta_z^2\left(1-\frac{\beta_z^2\Delta z^2}{12}\right) \quad (2.3.51)$$

with the relative errors:

$$\mathrm{err}_{\omega^2\mathrm{min}} = \frac{\Delta t^2\tilde{\omega}^2}{12-\Delta t^2\tilde{\omega}^2} - \mu\epsilon\omega^2 \cdot \frac{1}{(12-\Delta t^2\tilde{\omega}^2)(\frac{1}{\Delta x^2}+\frac{1}{\Delta y^2}+\frac{1}{\Delta z^2})} \tag{2.3.52}$$

$$\mathrm{err}_{\omega^2\mathrm{max}} = \frac{\Delta t^2\tilde{\omega}^2}{12-\Delta t^2\tilde{\omega}^2} - \mu\epsilon\omega^2 \cdot \frac{\max(\Delta x^2, \Delta y^2, \Delta z^2)}{12-\Delta t^2\tilde{\omega}^2} \tag{2.3.53}$$

Practical note The expressions for minimum and maximum relative errors presented above include the exact values of, depending on the algorithm, ω or β_z, which are unknown a priori. They should be substituted by their approximations $\tilde{\omega}$ or $\tilde{\beta}_z$ respectively. Such an approach is valid when the relative errors are small, which is the case in practice.

Correction of the numerical dispersion error The knowledge of the error bounds for any particular algorithm is very useful as this allows one to minimize the average error in the case where the propagation direction is not known. It was shown that the calculated value $\tilde{\alpha}^2$ is placed between $\alpha^2(1+\mathrm{err}_{\alpha^2\mathrm{min}})$ and $\alpha^2(1+\mathrm{err}_{\alpha^2\mathrm{max}})$, where α^2 is the exact solution (either ω^2 or β_z^2 depending on the algorithm). In order to minimize the mean value of the relative error, the following relation should be satisfied:

$$\mathrm{err}_{\alpha^2\mathrm{min}} = -\mathrm{err}_{\alpha^2\mathrm{max}} \tag{2.3.54}$$

However, the analysis of the algorithms of interest shows, that this condition is not satisfied in a general case. Therefore, the calculated values should be multiplied by the following correction factor:

$$\mathrm{corr}_{\alpha^2} = \frac{2}{2+\mathrm{err}_{\alpha^2\mathrm{min}}+\mathrm{err}_{\alpha^2\mathrm{max}}} \tag{2.3.55}$$

The corrected value will be then:

$$\tilde{\alpha}^2_{\mathrm{corr}} = \mathrm{corr}_{\alpha^2} \cdot \tilde{\alpha}^2 \tag{2.3.56}$$

The new corrected value $\tilde{\alpha}^2_{\mathrm{corr}}$ is now placed between $\alpha^2(1-0.5\Delta\mathrm{err}_{\alpha^2})$ and $\alpha^2(1+0.5\Delta\mathrm{err}_{\alpha^2})$ where $\Delta\mathrm{err}_{\alpha^2}$ is defined as follows:

$$\Delta\mathrm{err}_{\alpha^2} = |\mathrm{err}_{\alpha^2\mathrm{max}} - \mathrm{err}_{\alpha^2\mathrm{min}}| \tag{2.3.57}$$

and the mean value of the relative error is equal zero. The above analysis and eq. (2.3.19) show, that the maximum level of the relative error with respect to α after correction is equal:

$$\mathrm{Err}_{\alpha} \simeq 0.25\Delta\mathrm{err}_{\alpha^2} \tag{2.3.58}$$

2.3.2 Other sources of errors

In the preceding sections we have established the upper and the lower bounds for the numerical dispersion errors in several variants of finite difference methods. It is obvious, that the numerical dispersion is caused by the discretization of the domain and cannot be avoided. As the derived expression indicate, this error decreases with decreasing grid size. In addition to the numerical dispersion there are also other factors related to discretization which affects the accuracy of the final solution. In electromagnetics, the most important

additional factors which have to be considered are the location of interfaces between media and boundaries and the presence of singularities of the field.

While these factors contribute to the overall accuracy, magnitude of the errors can be reduced either by the grid size reduction or an application of the field theory. The second approach is by far more appealing because, if the additional errors are brought below the numerical dispersion error without decreasing the grid size, the algorithm will have the greatest accuracy which is theoretically possible.

In the following sections, we shortly describe the nature of errors other than the numerical dispersion. Further in this work, new algorithms based on the field theoretical analysis reducing these errors will be presented.

2.3.2.1 Boundary conditions

In practical simulations, one often encounters a situation when surfaces at which Dirichlet or Neumann boundary conditions are specified do not coincide with the finite difference grid. This introduces the error which often exceeds the level of the error due to the numerical dispersion. Therefore, there is a need to locally change the standard finite difference algorithm near boundaries. The algorithms reducing this kind of errors to the order of the numerical dispersion are based on the integral form of Maxwell's equations and are derived in secs. 4.4, 4.5.

2.3.2.2 Interfaces between media

Boundaries between different media may also introduce an error whose magnitude is significantly larger than the error due to numerical dispersion. Also in this case, algorithms based on the properties of the electromagnetic fields at the media interfaces can be derived reducing this error to the level of the numerical dispersion error. These algorithms are described in sec. 4.2 (for 2D) and in sec. 4.3 (for 3D).

2.3.2.3 Field singularities

Electromagnetic field changes very rapidly in the vicinity of wedges and thin wires. Accordingly, the assumption regarding the linear change of field within a cell is far from being satisfied. In can be shown, that in the case of central finite differences, the local truncation error in Taylor's expansion is unbounded near singularities of the field introduced by e.g. edges of metal laminas. This local error often significantly affects the global accuracy of the computations. Therefore, if elements such as wedges, convex corners or thin wires are present in the analyzed domain, the standard expressions for the finite-difference operators should be modified in order to account for a particular type of singularity. A modified algorithm dealing with this problem is presented in secs. 4.6, 4.7.

Chapter 3

Symbolic space

3.1 Introduction

It was noted that time domain formulation (as some frequency domain ones) may be solved by means of the explicit update algorithms. In order for these algorithms to be stable the operators involved have to possess certain properties which, in the most general case, are expressed by conditions (2.2.63) or (2.2.64). It has been proven [85] that these conditions are satisfied for 3D Maxwell's grid equations or in other words for a basic discretization scheme in 3D using Yee's mesh. It can be also easily proven that except for the boundedness also continuous operators defined on appropriate domains satisfy these conditions. However, in many cases, one is interested in 2D problems. Such problems usually arise in the analysis of waveguides and lead to different operators for which these properties have not been investigated. It was also pointed out that the basic discretization scheme may result in an error which exceeds the level of the error due to the numerical dispersion. The only reasonable way of controlling this type of error is via the local modification of the operators. Obviously, in order to be useful, such local modifications cannot change the properties of the entire operator. If this is not the case, then the scheme becomes unstable or, at best, if only the spectral radius is increased as a result of the modification, one may have to reduce the time step. Previous chapter showed the equivalence of the time and frequency domain formulations. Obviously, if an explicit update scheme is not used, the system of linear equations is solved and the problem of stability does not come into play. One has to bear in mind, that the rate of convergence of the iterative solvers depends on the properties of the underlying matrix, such as for instance the spectral radius. As a result, changes introduced by local schemes to the global operator are of importance both for frequency (FD-FD) and time domain methods (FD-TD).

Intuitively, one may expect that a correctly constructed discrete operator, which either incorporates local modifications or not, should guarantee that the laws of physics are preserved. Since these laws are related to the properties of the operators in the continuous space there is a need of finding a common framework for construction of operator equations in continuous and discretized space. To this end, we introduce a new concept of symbolic space. The symbolic space is the space where operators are expected to possess the same general properties in the continuous space and the discrete one. (With the exception of boundedness – continuous operators are unbounded as they operate in infinite dimensional spaces, discrete ones are bounded). Using the concept of symbolic space we shall derive operator equations for 3D and 2D. These equations will be used for

verifying the consistency of local subcell models which will be derived in the next chapter.

To derive the operators in the symbolic space for 2D and 3D cases it is enough to consider only the eigenvalue problems that describe either the free oscillation (3D) or guided wave propagation (2D). In general the second case refers to waveguides which are structures uniform in one direction. This fact radically simplifies the analysis. The solution provides the field distribution as a function of transverse coordinates, and a propagation constant as a function of frequency (or the other way round). For waveguides, Maxwell's equations can be converted to an eigenvalue problem but there are several possibilities discussed in sec. 3.5.3.

3.2 Formulation of a problem in 3D

In order to define operators required for the 3D analysis using the symbolic space we have to consider the continuous space first. Let us write Maxwell's equations in the continuous space for a 3D problem:

$$-\sigma\vec{E} + \nabla \times \vec{H} = j\omega\bar{\bar{\epsilon}} \cdot \vec{E} + \vec{J} \tag{3.2.1}$$

$$\nabla \times \vec{E} = -j\omega\bar{\bar{\mu}} \cdot \vec{H} \tag{3.2.2}$$

These equations may also be written in terms of flux density fields:

$$-\sigma\bar{\bar{\epsilon}}^{-1} \cdot \vec{D} + \nabla \times \bar{\bar{\mu}}^{-1} \cdot \vec{B} = j\omega\vec{D} + \vec{J} \tag{3.2.3}$$

$$\nabla \times \bar{\bar{\epsilon}}^{-1} \cdot \vec{D} = -j\omega\vec{B} \tag{3.2.4}$$

Let us also write Maxwell's divergence equations:

$$\nabla \cdot \vec{D} = \rho \tag{3.2.5}$$

$$\nabla \cdot \vec{B} = 0 \tag{3.2.6}$$

3.3 Formulation of a problem in 2D

For the 2D problems we restrict the analysis to waveguides uniform in the z direction. We assume that all materials in the analyzed structures are lossless. In order to simplify analysis further, the fields are decomposed into transverse (denoted with subscript $_t$) and longitudinal (denoted with $_z$) parts. The propagation constant and the angular frequency are denoted with β_z and ω, respectively. With these conventions, Maxwell's equations in terms of the intensity fields take up the form:

$$\begin{bmatrix} -j\beta_z\vec{i}_z \times (.) & -\vec{i}_z \times \nabla_t(.) \\ -\nabla_t \cdot \vec{i}_z \times (.) & 0 \end{bmatrix} \begin{bmatrix} \vec{H}_t \\ H_z \end{bmatrix} = j\omega \begin{bmatrix} \bar{\bar{\epsilon}}_{tt} & \bar{\epsilon}_{tz} \\ \bar{\epsilon}_{zt} & \epsilon_{zz} \end{bmatrix} \begin{bmatrix} \vec{E}_t \\ E_z \end{bmatrix} \tag{3.3.1}$$

$$\begin{bmatrix} -j\beta_z\vec{i}_z \times (.) & -\vec{i}_z \times \nabla_t(.) \\ -\nabla_t \cdot \vec{i}_z \times (.) & 0 \end{bmatrix} \begin{bmatrix} \vec{E}_t \\ E_z \end{bmatrix} = -j\omega \begin{bmatrix} \bar{\bar{\mu}}_{tt} & \bar{\mu}_{tz} \\ \bar{\mu}_{zt} & \mu_{zz} \end{bmatrix} \begin{bmatrix} \vec{H}_t \\ H_z \end{bmatrix} \tag{3.3.2}$$

Similarly, in terms of the flux density fields, we get:

$$\begin{bmatrix} -j\beta_z\vec{i}_z \times (.) & -\vec{i}_z \times \nabla_t(.) \\ -\nabla_t \cdot \vec{i}_z \times (.) & 0 \end{bmatrix} \begin{bmatrix} \bar{\bar{\nu}}_{tt} & \bar{\nu}_{tz} \\ \bar{\nu}_{zt} & \nu_{zz} \end{bmatrix} \begin{bmatrix} \vec{B}_t \\ B_z \end{bmatrix} = j\omega \begin{bmatrix} \vec{D}_t \\ D_z \end{bmatrix} \tag{3.3.3}$$

$$\begin{bmatrix} -j\beta_z\vec{i}_z \times (.) & -\vec{i}_z \times \nabla_t(.) \\ -\nabla_t \cdot \vec{i}_z \times (.) & 0 \end{bmatrix} \begin{bmatrix} \bar{\bar{\chi}}_{tt} & \bar{\chi}_{tz} \\ \bar{\chi}_{zt} & \chi_{zz} \end{bmatrix} \begin{bmatrix} \vec{D}_t \\ D_z \end{bmatrix} = -j\omega \begin{bmatrix} \vec{B}_t \\ B_z \end{bmatrix} \tag{3.3.4}$$

In the forgoing analysis, we also use Maxwell's divergence equations, which for decomposed fields take up the following form:

$$\nabla_t \cdot \vec{D}_t - j\beta_z D_z = 0 \tag{3.3.5}$$
$$\nabla_t \cdot \vec{B}_t - j\beta_z B_z = 0 \tag{3.3.6}$$

Since we consider only lossless materials, the following conditions are satisfied [13, 53]:

$$\begin{bmatrix} \bar{\bar{\epsilon}}^H_{tt} & \bar{\epsilon}^H_{zt} \\ \bar{\epsilon}^H_{tz} & \epsilon^*_{zz} \end{bmatrix} = \begin{bmatrix} \bar{\bar{\epsilon}}_{tt} & \bar{\epsilon}_{tz} \\ \bar{\epsilon}_{zt} & \epsilon_{zz} \end{bmatrix} \tag{3.3.7}$$
$$\begin{bmatrix} \bar{\bar{\mu}}^H_{tt} & \bar{\mu}^H_{zt} \\ \bar{\mu}^H_{tz} & \mu^*_{zz} \end{bmatrix} = \begin{bmatrix} \bar{\bar{\mu}}_{tt} & \bar{\mu}_{tz} \\ \bar{\mu}_{zt} & \mu_{zz} \end{bmatrix} \tag{3.3.8}$$

Analogous relations are valid for tensors $\bar{\bar{\chi}}$ and $\bar{\bar{\nu}}$.

3.4 Symbolic space for 3D problems

We may now introduce operators in the symbolic space for the 3D case. In this space, we use common symbols for continuous and discrete basic operators, functions and scalars which occur in the 3D problem. As the same continuous operators may be defined for different boundary conditions, such an approach is only possible if we introduce the boundary conditions of a particular operator domain to the symbols[1]. The new symbols are given together with the continuous and discrete operators in tab. 3.4. Note that each differential operator is defined twice. One for the boundary conditions satisfied by function $\vec{E}$ or $\vec{D}$ and for the second time for boundary conditions of function $\vec{H}$ or $\vec{B}$. We may now rewrite eqs. (3.2.1)–(3.2.4) for the symbolic space:

$$-\mathbf{S}e + \mathbf{R_m}h = j\omega\mathbf{E}e + i \tag{3.4.1}$$
$$\mathbf{R_e}e = -j\omega\mathbf{M}h \tag{3.4.2}$$

and

$$-\mathbf{S}\mathbf{E}^{-1}d + \mathbf{R_m}\mathbf{M}^{-1}b = j\omega d + i \tag{3.4.3}$$
$$\mathbf{R_e}\mathbf{E}^{-1}d = -j\omega b \tag{3.4.4}$$

Eqs. (3.2.5), (3.2.6) take up the following form:

$$\mathbf{D_e}d = r \tag{3.4.5}$$
$$\mathbf{D_m}b = 0 \tag{3.4.6}$$

[1]Care has to be taken when applying such operators to functions. Such operators can be applied only to functions belonging to their domain.

Table 3.4.1: *Symbols of basic operators and functions in symbolic, continuous and discrete spaces. Subscript $_e$ denotes boundary conditions of function $\vec{E}$ or $\vec{D}$ depending on the operator, and subscript $_m$ denotes boundary conditions of function $\vec{H}$ or $\vec{B}$ (see the text for explanation).*

Symbol	Continuous space	Discrete space
$\mathbf{R_e}$	$\nabla \times (.)_e$	$\underline{\underline{R}}_e$
$\mathbf{R_m}$	$\nabla \times (.)_m$	$\underline{\underline{R}}_m$
$\mathbf{D_e}$	$\nabla \cdot (.)_e$	$\underline{\underline{D}}_e$
$\mathbf{D_m}$	$\nabla \cdot (.)_m$	$\underline{\underline{D}}_m$
$\mathbf{G_e}$	$\nabla (.)_e$	$\underline{\underline{G}}_e$
$\mathbf{G_m}$	$\nabla (.)_m$	$\underline{\underline{G}}_m$
$\mathbf{E}$	$\bar{\bar{\epsilon}}$	$\underline{\underline{E}}$
$\mathbf{M}$	$\bar{\bar{\mu}}$	$\underline{\underline{M}}$
$\mathbf{S}$	σ	$\underline{\underline{S}}$
e	$\vec{E}$	$\underline{e}$
h	$\vec{H}$	$\underline{h}$
d	$\vec{D}$	$\underline{d}$
b	$\vec{B}$	$\underline{b}$
i	$\vec{J}$	$\underline{i}$
r	ρ	$\underline{r}$
$< u, v >$	$\iiint_V \vec{U} \cdot \vec{V} dv$	$\Delta x \Delta y \Delta z \sum_i u_i v_i$

3.4.1 Properties of basic operators

We now derive properties of the 3D basic operators.

Rotation operator Let us start from the following property of the continuous rotation operator:

$$\nabla \cdot (\vec{U} \times \vec{V}) = \vec{V} \cdot \nabla \times \vec{U} - \vec{U} \cdot \nabla \times \vec{V} \tag{3.4.7}$$

This may be written in the integral form as follows:

$$\iiint_V \vec{V} \cdot \nabla \times \vec{U} dv = \iiint_V \vec{U} \cdot \nabla \times \vec{V} dv + \iiint_V \nabla \cdot (\vec{U} \times \vec{V}) dv \tag{3.4.8}$$

From the Gauss law, we have:

$$\iiint_V \nabla \cdot (\vec{U} \times \vec{V}) dv = \iint_{\delta V} (\vec{U} \times \vec{V}) \cdot \vec{n} ds \tag{3.4.9}$$

where δV is the boundary of the domain V. If we substitute for fields $\vec{E}$, $\vec{H}$, respectively, vectors $\vec{U}$, $\vec{V}$ and assume that the domain is surrounded by the electric and/or magnetic walls, the integral on the right hand side vanishes:

$$\iint_{\delta V} (\vec{E} \times \vec{H}) \cdot \vec{n} ds = 0 \tag{3.4.10}$$

This gives the following property in the symbolic space:

$$\mathbf{R_e} = \mathbf{R_m^T} \tag{3.4.11}$$

Divergence and gradient operators We may note, that gradient operator does not appear in the formulation of a problem in 3D in sec. 3.2. However, for completeness, we introduce without a proof the following property of gradient and divergence operators:

$$\nabla \cdot (.) = -[\nabla(.)]^T \tag{3.4.12}$$

and extend it to the symbolic space as follows:

$$\mathbf{D_e} = -\mathbf{G_e}^T \tag{3.4.13}$$
$$\mathbf{D_m} = -\mathbf{G_m}^T \tag{3.4.14}$$

Operators corresponding to material tensors For lossless materials, the following properties hold:

$$\mathbf{E} = \mathbf{E}^H \tag{3.4.15}$$
$$\mathbf{M} = \mathbf{M}^H \tag{3.4.16}$$

Other properties The following property is well known in the continuous space:

$$\nabla \cdot \nabla \times (.) = 0 \tag{3.4.17}$$
$$\nabla \times \nabla(.) = 0 \tag{3.4.18}$$

We expand these equations to the symbolic space. From (3.4.17), we get the following two equations:

$$\mathbf{D_e R_m} = 0 \tag{3.4.19}$$
$$\mathbf{D_m R_e} = 0 \tag{3.4.20}$$

Analogously, (3.4.18) leads to:

$$\mathbf{R_e G_e} = 0 \tag{3.4.21}$$
$$\mathbf{R_m G_m} = 0 \tag{3.4.22}$$

3.4.2 3D problems

Deterministic problems Maxwell's equations written in the form (3.4.1), (3.4.2) or (3.4.3), (3.4.4) with nonzero current i describe deterministic problems with i representing sources. We may formulate such problems in a single equation. Combining eqs. (3.4.1), (3.4.2) into a matrix-operator form we get the following 6-component formula:

$$\begin{bmatrix} -\mathbf{E}^{-1}\mathbf{S} & \mathbf{E}^{-1}\mathbf{R_m} \\ -\mathbf{M}^{-1}\mathbf{R_e} & 0 \end{bmatrix} \begin{bmatrix} e \\ h \end{bmatrix} = j\omega \begin{bmatrix} e \\ h \end{bmatrix} + \begin{bmatrix} \mathbf{E}^{-1} i \\ 0 \end{bmatrix} \tag{3.4.23}$$

Analogously, combination of (3.4.3) and (3.4.4) gives:

$$\begin{bmatrix} -\mathbf{S}\mathbf{E}^{-1} & \mathbf{R_m}\mathbf{M}^{-1} \\ -\mathbf{R_e}\mathbf{E}^{-1} & 0 \end{bmatrix} \begin{bmatrix} d \\ b \end{bmatrix} = j\omega \begin{bmatrix} d \\ b \end{bmatrix} + \begin{bmatrix} i \\ 0 \end{bmatrix} \tag{3.4.24}$$

Magnetic fields may be eliminated from the above equations. This way, we get 3-component formulations:

$$\mathbf{E}^{-1}\mathbf{R_m}\mathbf{M}^{-1}\mathbf{R_e} e = \omega^2 e - j\omega \mathbf{E}^{-1}\mathbf{S} e - j\omega \mathbf{E}^{-1} i \tag{3.4.25}$$
$$\mathbf{R_m}\mathbf{M}^{-1}\mathbf{R_e}\mathbf{E}^{-1} d = \omega^2 d - j\omega \mathbf{S}\mathbf{E}^{-1} d - j\omega i \tag{3.4.26}$$

Nondeterministic problems With the absence of sources (i.e. for $i = 0$), the problem becomes nondeterministic and the corresponding equations formulate an eigenproblem. For instance, from (3.4.27), we get:

$$\begin{bmatrix} -\mathbf{E}^{-1}\mathbf{S} & \mathbf{E}^{-1}\mathbf{R_m} \\ -\mathbf{M}^{-1}\mathbf{R_e} & 0 \end{bmatrix} \begin{bmatrix} e \\ h \end{bmatrix} = j\omega \begin{bmatrix} e \\ h \end{bmatrix} \tag{3.4.27}$$

This equation represents an eigenproblem with eigenvalues $j\omega$ and eigenvectors $\begin{bmatrix} e \\ h \end{bmatrix}$.

Nondeterministic problems for lossless structures Equations may be further simplified if the medium is lossless. In this case $\mathbf{S} = 0$, and operators $\mathbf{E}$, $\mathbf{M}$ are hermitian. From (3.4.25) and (3.4.26), we get:

$$\mathbf{E}^{-1}\mathbf{R_m}\mathbf{M}^{-1}\mathbf{R_e}e = \omega^2 e \tag{3.4.28}$$
$$\mathbf{R_m}\mathbf{M}^{-1}\mathbf{R_e}\mathbf{E}^{-1}d = \omega^2 d \tag{3.4.29}$$

Analogously, we may now eliminate the electric field components from eqs. (3.4.23) and (3.4.24). In this case, we get the following 3-component eigenproblems:

$$\mathbf{M}^{-1}\mathbf{R_e}\mathbf{E}^{-1}\mathbf{R_m}h = \omega^2 h \tag{3.4.30}$$
$$\mathbf{R_e}\mathbf{E}^{-1}\mathbf{R_m}\mathbf{M}^{-1}b = \omega^2 b \tag{3.4.31}$$

The pairs of eigenproblems (3.4.28), (3.4.29), and (3.4.30), (3.4.31) are transposed to each other. For lossless structures without sources, eqs. (3.4.23), (3.4.24) formulate eigenproblems, which are also transposed to each other.

3.4.3 Static solutions

It is easy to verify, that about one third of solutions of the problems defined in sec. 3.4.2 are static modes (i.e. solutions corresponding to $\omega = 0$). These solutions do not satisfy Maxwell's divergence equations (3.4.5) and (3.4.6):

$$\mathbf{D_e}d \neq r \tag{3.4.32}$$
$$\mathbf{D_m}b \neq 0 \tag{3.4.33}$$

They may be written in the form:

$$e = \mathbf{G_e}u_e \tag{3.4.34}$$
$$h = \mathbf{G_m}u_m \tag{3.4.35}$$

where u_e, u_m are scalar fields. The static solutions may cause a problem when solving a nondeterministic problem with some solvers, because it may be difficult to separate the lowest order modes of interest. Note, that this is not a problem in the case of the FD-TD method, since we may use sources without static excitation. In order to solve the problem, we may shift zero eigenvalues, corresponding to the static solutions, in frequency. To this end, we should modify the operators by adding new terms. These new terms cannot have influence on the actual dynamic solutions. In addition to this condition, we will assure that the part of the result operator corresponding to the actual dynamic modes will not have influence on the shifted static solutions. Limiting our discussion to the case

of the nondeterministic problems for lossless structures, we get the following new forms of eqs. (3.4.28), (3.4.29), (3.4.30) and (3.4.31):

$$\mathbf{E}^{-1}\mathbf{R_m}\mathbf{M}^{-1}\mathbf{R_e}e + \mathbf{G_e}\mathbf{A_e}\mathbf{D_e}\mathbf{E}e = \omega^2 e \tag{3.4.36}$$

$$\mathbf{R_m}\mathbf{M}^{-1}\mathbf{R_e}\mathbf{E}^{-1}d + \mathbf{E}\mathbf{G_e}\mathbf{A_e}\mathbf{D_e}d = \omega^2 d \tag{3.4.37}$$

$$\mathbf{M}^{-1}\mathbf{R_e}\mathbf{E}^{-1}\mathbf{R_m}h + \mathbf{G_m}\mathbf{A_m}\mathbf{D_m}\mathbf{M}h = \omega^2 h \tag{3.4.38}$$

$$\mathbf{R_e}\mathbf{E}^{-1}\mathbf{R_m}\mathbf{M}^{-1}b + \mathbf{M}\mathbf{G_m}\mathbf{A_m}\mathbf{D_m}b = \omega^2 b \tag{3.4.39}$$

where $\mathbf{A_e}$, $\mathbf{A_m}$ are arbitrary positive and symmetric operators defined in appropriate spaces. If these operators are symmetric, the eigenproblems are in the same relations with their transposals as before. It is easy to verify, that for $\mathbf{A_e} = \frac{v^2}{\epsilon}$ and $\mathbf{A_m} = \frac{v^2}{\mu}$, the new term in each equation is positive and its spectral radius is approximately equal to the spectral radius of the dynamic part of the global operator. Therefore, positiveness and the norm of the global operator do not change. Solutions of the new equations contain now spurious modes. In order to test if a solution is spurious (static) or dynamic we should substitute it to one of the equations (3.4.28), (3.4.29), (3.4.30) or (3.4.31).

Similar approach to the static solutions, but with another form of operators $\mathbf{A_e}$, $\mathbf{A_m}$, may be found in [7, 16].

3.5 Symbolic space for 2D problems

Despite fewer dimensions it is necessary to consider more elementary operators in 2D than in 3D. We introduce symbols of all the operators required in 2D in Tab. 3.5. Again, subscript $_e$ denotes boundary conditions of function $\vec{E}_t$ or D_z depending on the operator. Analogously, subscript $_m$ denotes boundary conditions of function $\vec{H}_t$ or B_z. For instance, $\mathbf{D_{te}}$ corresponds to a transverse divergence operator acting on functions that fulfill the boundary conditions for an appropriate components of the transverse electric flux density field. Symbol $\mathbf{G_{te}}$ denotes a transverse gradient operator which acts on functions fulfilling the boundary conditions for the longitudinal electric intensity field component. Similarly, symbol $\mathbf{G_{tm}}$ denotes a transverse gradient operator corresponding to the magnetic field.

Let us now rewrite the equations presented in sec. 3.3 in the symbolic space. Eqs. (3.3.1) and (3.3.2) become:

$$\begin{bmatrix} -j\beta_z\mathbf{Z_m} & -\mathbf{Z_m}\mathbf{G_{tm}} \\ -\mathbf{D_{te}}\mathbf{Z_m} & 0 \end{bmatrix} \begin{bmatrix} h_t \\ h_z \end{bmatrix} = j\omega \begin{bmatrix} \mathbf{E_{tt}} & \mathbf{E_{tz}} \\ \mathbf{E_{zt}} & \mathbf{E_{zz}} \end{bmatrix} \begin{bmatrix} e_t \\ e_z \end{bmatrix} \tag{3.5.1}$$

$$\begin{bmatrix} -j\beta_z\mathbf{Z_e} & -\mathbf{Z_e}\mathbf{G_{te}} \\ -\mathbf{D_{tm}}\mathbf{Z_e} & 0 \end{bmatrix} \begin{bmatrix} e_t \\ e_z \end{bmatrix} = -j\omega \begin{bmatrix} \mathbf{M_{tt}} & \mathbf{M_{tz}} \\ \mathbf{M_{zt}} & \mathbf{M_{zz}} \end{bmatrix} \begin{bmatrix} h_t \\ h_z \end{bmatrix} \tag{3.5.2}$$

Eqs. (3.3.3), (3.3.4) take up the form:

$$\begin{bmatrix} -j\beta_z\mathbf{Z_m} & -\mathbf{Z_m}\mathbf{G_{tm}} \\ -\mathbf{D_{te}}\mathbf{Z_m} & 0 \end{bmatrix} \begin{bmatrix} \mathbf{N_{tt}} & \mathbf{N_{tz}} \\ \mathbf{N_{zt}} & \mathbf{N_{zz}} \end{bmatrix} \begin{bmatrix} b_t \\ b_z \end{bmatrix} = j\omega \begin{bmatrix} d_t \\ d_z \end{bmatrix} \tag{3.5.3}$$

$$\begin{bmatrix} -j\beta_z\mathbf{Z_e} & -\mathbf{Z_e}\mathbf{G_{te}} \\ -\mathbf{D_{tm}}\mathbf{Z_e} & 0 \end{bmatrix} \begin{bmatrix} \mathbf{F_{tt}} & \mathbf{F_{tz}} \\ \mathbf{F_{zt}} & \mathbf{F_{zz}} \end{bmatrix} \begin{bmatrix} d_t \\ d_z \end{bmatrix} = -j\omega \begin{bmatrix} b_t \\ b_z \end{bmatrix} \tag{3.5.4}$$

From (3.3.5), (3.3.6), we get:

$$\mathbf{D_{te}}d_t - j\beta_z d_z = 0 \tag{3.5.5}$$

$$\mathbf{D_{tm}}b_t - j\beta_z b_z = 0 \tag{3.5.6}$$

Table 3.5.1: *Symbols of basic operators and functions in symbolic, continuous and discrete spaces. Subscript $_e$ denotes boundary conditions of function $\vec{E}_t$ or D_z depending on the operator, and subscript $_m$ denotes boundary conditions of function $\vec{H}_t$ or B_z (see the text for explanation).*

Symbolic space	Continuous space	Discrete space
$\mathbf{D_{te}}$	$\nabla_t \cdot (.)_e$	$\underline{\underline{D}}_{te}$
$\mathbf{D_{tm}}$	$\nabla_t \cdot (.)_m$	$\underline{\underline{D}}_{tm}$
$\mathbf{G_{te}}$	$\nabla_t (.)_e$	$\underline{\underline{G}}_{te}$
$\mathbf{G_{tm}}$	$\nabla_t (.)_m$	$\underline{\underline{G}}_{tm}$
$\mathbf{Z_e}$	$\vec{i}_z \times (.)_e$	$\underline{\underline{Z}}_{e}$
$\mathbf{Z_m}$	$\vec{i}_z \times (.)_m$	$\underline{\underline{Z}}_{m}$
$\mathbf{E_{tt}}$	$\bar{\bar{\epsilon}}_{tt}$	$\underline{\underline{E}}_{tt}$
$\mathbf{E_{tz}}$	$\bar{\epsilon}_{tz}$	$\underline{\underline{E}}_{tz}$
$\mathbf{E_{zt}}$	$\bar{\epsilon}_{zt}$	$\underline{\underline{E}}_{zt}$
$\mathbf{E_{zz}}$	ϵ_{zz}	$\underline{\underline{E}}_{zz}$
$\mathbf{M_{tt}}$	$\bar{\bar{\mu}}_{tt}$	$\underline{\underline{M}}_{tt}$
$\mathbf{M_{tz}}$	$\bar{\mu}_{tz}$	$\underline{\underline{M}}_{tz}$
$\mathbf{M_{zt}}$	$\bar{\mu}_{zt}$	$\underline{\underline{M}}_{zt}$
$\mathbf{M_{zz}}$	μ_{zz}	$\underline{\underline{M}}_{zz}$
$\mathbf{F_{tt}}$	$\bar{\bar{\chi}}_{tt}$	$\underline{\underline{F}}_{tt}$
$\mathbf{F_{tz}}$	$\bar{\chi}_{tz}$	$\underline{\underline{F}}_{tz}$
$\mathbf{F_{zt}}$	$\bar{\chi}_{zt}$	$\underline{\underline{F}}_{zt}$
$\mathbf{F_{zz}}$	χ_{zz}	$\underline{\underline{F}}_{zz}$
$\mathbf{N_{tt}}$	$\bar{\bar{\nu}}_{tt}$	$\underline{\underline{N}}_{tt}$
$\mathbf{N_{tz}}$	$\bar{\nu}_{tz}$	$\underline{\underline{N}}_{tz}$
$\mathbf{N_{zt}}$	$\bar{\nu}_{zt}$	$\underline{\underline{N}}_{zt}$
$\mathbf{N_{zz}}$	ν_{zz}	$\underline{\underline{N}}_{zz}$
e_t	$\vec{E}_t$	$\underline{e}_t$
e_z	E_z	$\underline{e}_z$
h_t	$\vec{H}_t$	$\underline{h}_t$
h_z	H_z	$\underline{h}_z$
d_t	$\vec{D}_t$	$\underline{d}_t$
d_z	D_z	$\underline{d}_z$
b_t	$\vec{B}_t$	$\underline{b}_t$
b_z	B_z	$\underline{b}_z$
$< u, v >$	$\iint_S \vec{U} \cdot \vec{V} ds$	$\Delta x \Delta y \sum_i u_i v_i$

It should be emphasized, that the equations introduced above are more general than those presented in sec. 3.3. Here we extended the properties valid in the continuous space, in such a way that they are also valid in the discretized domain. Note, that up to this time, we have not made any assumption regarding the method of discretization.

3.5.1 Properties of basic operators

In this section, we derive the properties of the basic operators defined above. Further on, these properties will help us to transform operator equations and provide conditions for constructing discretized operators.

Transverse divergence and transverse gradient operators Here, we establish conditions under which the following property of the operators $\nabla_t \cdot (.)$, $\nabla_t(.)$ is satisfied:

$$[\nabla_t \cdot (.)]^T = -\nabla_t(.) \tag{3.5.7}$$

Eq. (3.5.7) implies, that for an arbitrary pair of scalar functions f and vector functions $\vec{U}$ the following statement is true:

$$\left\langle f, \nabla_t \cdot \vec{U} \right\rangle_p = -\left\langle \nabla_t f, \vec{U} \right\rangle_p \tag{3.5.8}$$

Operation $< ., . >_p$ in the above equation denotes the pseudo-inner product [53]. We use the following property of operator $\nabla_t \cdot (.)$:

$$\nabla_t \cdot (f\vec{U}) = f\nabla_t \cdot \vec{U} + \vec{U} \cdot \nabla_t f \tag{3.5.9}$$

The pseudo-inner product (3.5.8) takes up the form:

$$\iint_S f\nabla_t \cdot \vec{U} ds = -\iint_S \vec{U} \cdot \nabla_t f ds + \iint_S \nabla_t \cdot (f\vec{U}) ds \tag{3.5.10}$$

In order to prove (3.5.7) we should show that the last integral in (3.5.10) vanishes. From the Gauss law we have:

$$\iint_S \nabla_t \cdot (f\vec{U}) ds = \int_{\delta S} f\vec{U} \cdot \vec{n} dl \tag{3.5.11}$$

where δS is the boundary of domain S and $\vec{n}$ is a unit vector normal to δS. The integral vanishes if for every point on δS one of the statements is true:

$$f = 0 \quad \text{or} \quad \vec{U} \cdot \vec{n} = 0 \tag{3.5.12}$$

Eq. (3.5.12) defines the space of the pairs $(f, \vec{U})$. If the pair $(f, \vec{U})$ belongs to one of the spaces: $(H_z, \vec{B}_t)$, $(H_z, \vec{\imath}_z \times \vec{E}_t)$, $(E_z, \vec{\imath}_z \times \vec{H}_t)$, $(E_z, \vec{D}_t)$, then for a combination of electric and magnetic wall boundaries, condition (3.5.12) is satisfied. Therefore, the following equations are true:

$$\mathbf{D_{te}} = -\mathbf{G_{te}^T} \tag{3.5.13}$$

$$\mathbf{D_{tm}} = -\mathbf{G_{tm}^T} \tag{3.5.14}$$

Operator $\vec{i}_z \times (.)$ It is well known, that the following property of operator $\vec{i}_z \times (.)$ takes place:

$$\vec{i}_z \times (.) = -[\vec{i}_z \times (.)]^T \tag{3.5.15}$$

We extend this relation to the symbolic space as follows:

$$\mathbf{Z_e} = -\mathbf{Z_m^T} \tag{3.5.16}$$

This equation also ensures that for real values of β_z, the global rotation operators in eqs. (3.5.1) and (3.5.2) (or (3.5.3) and (3.5.4)) are hermitian transposed to each other:

$$\begin{bmatrix} -j\beta_z\mathbf{Z_m} & -\mathbf{Z_m}\mathbf{G_{tm}} \\ -\mathbf{D_{te}}\mathbf{Z_m} & 0 \end{bmatrix}^H = \begin{bmatrix} -j\beta_z^*\mathbf{Z_e} & -\mathbf{Z_e}\mathbf{G_{te}} \\ -\mathbf{D_{tm}}\mathbf{Z_e} & 0 \end{bmatrix} \tag{3.5.17}$$

Furthermore, we may note that operator $\vec{i}_z \times (.)$ is unitary, which means that its inversion is equivalent to the transposition:

$$[\vec{i}_z \times (.)]^{-1} = [\vec{i}_z \times (.)]^T \tag{3.5.18}$$

This and eq. (3.5.16) give:

$$\mathbf{Z_e^{-1}} = -\mathbf{Z_m} \tag{3.5.19}$$

Operators corresponding to material tensors We assumed, that we deal with lossless materials. This implied properties (3.3.7) and (3.3.8). Both equations may be written in the symbolic space as follows:

$$\begin{bmatrix} \mathbf{E}_{\mathbf{tt}}^H & \mathbf{E}_{\mathbf{tz}}^H \\ \mathbf{E}_{\mathbf{zt}}^H & \mathbf{E}_{\mathbf{zz}}^H \end{bmatrix} = \begin{bmatrix} \mathbf{E_{tt}} & \mathbf{E_{zt}} \\ \mathbf{E_{tz}} & \mathbf{E_{zz}} \end{bmatrix} \tag{3.5.20}$$

$$\begin{bmatrix} \mathbf{M}_{\mathbf{tt}}^H & \mathbf{M}_{\mathbf{tz}}^H \\ \mathbf{M}_{\mathbf{zt}}^H & \mathbf{M}_{\mathbf{zz}}^H \end{bmatrix} = \begin{bmatrix} \mathbf{M_{tt}} & \mathbf{M_{zt}} \\ \mathbf{M_{tz}} & \mathbf{M_{zz}} \end{bmatrix} \tag{3.5.21}$$

This also gives:

$$\begin{bmatrix} \mathbf{F}_{\mathbf{tt}}^H & \mathbf{F}_{\mathbf{tz}}^H \\ \mathbf{F}_{\mathbf{zt}}^H & \mathbf{F}_{\mathbf{zz}}^H \end{bmatrix} = \begin{bmatrix} \mathbf{F_{tt}} & \mathbf{F_{zt}} \\ \mathbf{F_{tz}} & \mathbf{F_{zz}} \end{bmatrix} \tag{3.5.22}$$

$$\begin{bmatrix} \mathbf{N}_{\mathbf{tt}}^H & \mathbf{N}_{\mathbf{tz}}^H \\ \mathbf{N}_{\mathbf{zt}}^H & \mathbf{N}_{\mathbf{zz}}^H \end{bmatrix} = \begin{bmatrix} \mathbf{N_{tt}} & \mathbf{N_{zt}} \\ \mathbf{N_{tz}} & \mathbf{N_{zz}} \end{bmatrix} \tag{3.5.23}$$

Other properties One of the basic properties of differential operators is

$$\nabla_t \cdot \vec{i}_z \times \nabla_t(.) = 0 \tag{3.5.24}$$

Expanding the above formula to the symbolic space, we get the following properties:

$$\mathbf{D_{tm}}\mathbf{Z_e}\mathbf{G_{te}} = 0 \tag{3.5.25}$$

$$\mathbf{D_{te}}\mathbf{Z_m}\mathbf{G_{tm}} = 0 \tag{3.5.26}$$

Properties valid for homogeneous isotropic media If the medium is isotropic and homogeneous, we may write the following relation:

$$\mathbf{E}_{\mathbf{tt}}^{-1}\mathbf{Z}_{\mathbf{m}}\mathbf{M}_{\mathbf{tt}}^{-1}\mathbf{Z}_{\mathbf{e}} = v^2\mathbf{I}_{\mathbf{tt}} \tag{3.5.27}$$

where v denotes the wave speed and $\mathbf{I_{tt}}$ is the identity operator defined on the transverse fields. This condition is based on the formulations presented in sec. 3.5.3 and guarantees that the propagation constant and the frequency are related to each other by the following equation:

$$\omega^2 - \omega_0^2 = v^2\beta_z^2 \tag{3.5.28}$$

where ω_0 is the cutoff angular frequency of the corresponding mode.

Final comment All the properties presented above may be seen as constraints on the construction of discrete operators. However, as will be shown in the next sections, all these properties will be satisfied, in a natural way, as a consequence of the field behavior, Maxwell's equations and Yee's grid.

3.5.2 Construction of real operators

Equations presented at the beginning of sec. 3.5 may, in general, lead to formulations with complex operators. This will be the case, for instance, when real value of β_z is treated as a parameter. This situation will further lead to matrix equations with complex matrices. Solving of complex equations requires more computation time and computer memory than in the case of equations with real matrices. Therefore, it is useful to reformulate our equations in such a way that they will lead to equations with real operators. It is obvious, that such reconstruction is not possible in a general case (for instance complex value of parameters β_z or ω, complex operators arise from material tensors). However, it is possible in the most common situations. Such situations include problems with a real or imaginary parameter β_z or a real or imaginary parameter ω. An appropriate character of the operators arisen from the material tensors is also required in these cases. Let us derive the new equations.

It is easy to verify, that eqs. (3.5.1) and (3.5.2) may be written in the following manner:

$$\begin{bmatrix} -jm\beta_z\mathbf{Z}_{\mathbf{m}} & -\mathbf{Z}_{\mathbf{m}}\mathbf{G}_{\mathbf{tm}} \\ -\mathbf{D}_{\mathbf{te}}\mathbf{Z}_{\mathbf{m}} & 0 \end{bmatrix} \begin{bmatrix} nh_t \\ mnh_z \end{bmatrix} = jn\omega \begin{bmatrix} \mathbf{E}_{\mathbf{tt}} & m\mathbf{E}_{\mathbf{tz}} \\ m^*\mathbf{E}_{\mathbf{zt}} & \mathbf{E}_{\mathbf{zz}} \end{bmatrix} \begin{bmatrix} me_t \\ e_z \end{bmatrix} \tag{3.5.29}$$

$$\begin{bmatrix} -jm^*\beta_z\mathbf{Z}_{\mathbf{e}} & -\mathbf{Z}_{\mathbf{e}}\mathbf{G}_{\mathbf{te}} \\ -\mathbf{D}_{\mathbf{tm}}\mathbf{Z}_{\mathbf{e}} & 0 \end{bmatrix} \begin{bmatrix} me_t \\ e_z \end{bmatrix} = -jn^*\omega \begin{bmatrix} \mathbf{M}_{\mathbf{tt}} & m^*\mathbf{M}_{\mathbf{tz}} \\ m\mathbf{M}_{\mathbf{zt}} & \mathbf{M}_{\mathbf{zz}} \end{bmatrix} \begin{bmatrix} nh_t \\ mnh_z \end{bmatrix} \tag{3.5.30}$$

where m, n are parameters taking values ± 1 or $\pm j$. In the same way we may rewrite eqs. (3.5.3) and (3.5.4):

$$\begin{bmatrix} -jm\beta_z\mathbf{Z}_{\mathbf{m}} & -\mathbf{Z}_{\mathbf{m}}\mathbf{G}_{\mathbf{tm}} \\ -\mathbf{D}_{\mathbf{te}}\mathbf{Z}_{\mathbf{m}} & 0 \end{bmatrix} \begin{bmatrix} \mathbf{N}_{\mathbf{tt}} & m^*\mathbf{N}_{\mathbf{tz}} \\ m\mathbf{N}_{\mathbf{zt}} & \mathbf{N}_{\mathbf{zz}} \end{bmatrix} \begin{bmatrix} nb_t \\ mnb_z \end{bmatrix} = jn\omega \begin{bmatrix} md_t \\ d_z \end{bmatrix} \tag{3.5.31}$$

$$\begin{bmatrix} -jm^*\beta_z\mathbf{Z}_{\mathbf{e}} & -\mathbf{Z}_{\mathbf{e}}\mathbf{G}_{\mathbf{te}} \\ -\mathbf{D}_{\mathbf{tm}}\mathbf{Z}_{\mathbf{e}} & 0 \end{bmatrix} \begin{bmatrix} \mathbf{F}_{\mathbf{tt}} & m\mathbf{F}_{\mathbf{tz}} \\ m^*\mathbf{F}_{\mathbf{zt}} & \mathbf{F}_{\mathbf{zz}} \end{bmatrix} \begin{bmatrix} md_t \\ d_z \end{bmatrix} = -jn^*\omega \begin{bmatrix} nb_t \\ mnb_z \end{bmatrix} \tag{3.5.32}$$

Eqs. (3.5.5), (3.5.6) take up the form:

$$\mathbf{D}_{\mathbf{te}}md_t - jm\beta_z d_z = 0 \tag{3.5.33}$$

$$\mathbf{D}_{\mathbf{tm}}nb_t - jm^*\beta_z mnb_z = 0 \tag{3.5.34}$$

Table 3.5.2: *Values of parameters m, n and the corresponding character of β_z, ω and operators corresponding to material tensors in the formulations with real operators. The rest of the basic matrices must be real.*

m	n	β_z	ω	$\mathbf{E_{tz}}, \mathbf{E_{zt}}, \mathbf{M_{tz}}, \mathbf{M_{zt}}$
± 1	± 1	imag.	imag.	real
± 1	$\pm j$	imag.	real	real
$\pm j$	± 1	real	imag.	imag.
$\pm j$	$\pm j$	real	real	imag.

Table 3.5.2 shows the values of parameters m and n and the corresponding character of β_z, ω and operators arisen from material tensors. Assuming that the rest of the basic operators are real, the choice of the parameters according to this table will lead to formulations with real operators.

Example As an example, let us rewrite eqs. (3.5.29), (3.5.30) for real values of β_z and ω. We substitute m and n by j and get:

$$\begin{bmatrix} \beta_z \mathbf{Z_m} & -\mathbf{Z_m G_{tm}} \\ -\mathbf{D_{te} Z_m} & 0 \end{bmatrix} \begin{bmatrix} jh_t \\ -h_z \end{bmatrix} = -\omega \begin{bmatrix} \mathbf{E_{tt}} & j\mathbf{E_{tz}} \\ -j\mathbf{E_{zt}} & \mathbf{E_{zz}} \end{bmatrix} \begin{bmatrix} je_t \\ e_z \end{bmatrix} \tag{3.5.35}$$

$$\begin{bmatrix} -\beta_z \mathbf{Z_e} & -\mathbf{Z_e G_{te}} \\ -\mathbf{D_{tm} Z_e} & 0 \end{bmatrix} \begin{bmatrix} je_t \\ e_z \end{bmatrix} = -\omega \begin{bmatrix} \mathbf{M_{tt}} & -j\mathbf{M_{tz}} \\ j\mathbf{M_{zt}} & \mathbf{M_{zz}} \end{bmatrix} \begin{bmatrix} jh_t \\ -h_z \end{bmatrix} \tag{3.5.36}$$

In this case, operators $\mathbf{E_{tz}}, \mathbf{E_{zt}}, \mathbf{M_{tz}}, \mathbf{M_{zt}}$ must by strictly imaginary[2] and the rest of the basic operators must be real. Note, that also eqs. (3.5.1), (3.5.2) lead to formulations with real operators, if β_z, ω are both imaginary and all the basic matrices are real.

3.5.3 Eigenproblems

The operators defined in the symbolic space render the manipulations of Maxwell's equations much easier. In this section we shall present a whole class of eigenproblems which can be derived from Maxwell's equations. (The derivation may be found in app. A).

The eigenproblems presented here are based on the approach proposed in sec. 3.5.2 with parameters m and n. Such an approach enables one to construct equations with real matrices in the most common cases. In order to make our discussion more clear when referring to the equations, we assume that β_z and ω are real. In other words, we assume that parameters m and n are both set to j (according to tab. 3.5.2).

The simplest form are the most general six field component formulations presented in tab. 3.5.3. If β_z is treated as a parameter, the eigenvalues are ω and the right eigenvectors are vectors containing all the intensity field components. The left eigenvectors, or eigenvectors of the transposed eigenproblem, are vectors containing all the flux density field components. If ω is a parameter, the eigenvalues are β_z, the right eigenvectors are the same as in the previous case, but the left eigenvectors are different and contain only the transverse field components of the intensity fields.

The solutions of the problems with six field components contain static modes which do not satisfy conditions (3.5.5), (3.5.6). These solutions may be removed by eliminating the

[2]This includes the case of strictly bidirectional structures, where these operators vanish.

Table 3.5.3: *6 field component ω and β_z formulations for general anisotropic waveguides. Fields with subscript $_{k*}$ correspond to $\omega = \omega_k^*$, $\beta_z = \beta_{zk}^*$ (such substitution must be performed for both, parameter and eigenvalue).*

Eigenproblem	Parameter	Eigenvalue	Eigenvector	
			right	left
$[\mathbf{L_0} + (jn^*\omega)\mathbf{L}_\omega + (jm^*\beta_z)\mathbf{L}_\beta]u = 0$	$jm^*\beta_z$	$jn^*\omega_k$	$\begin{bmatrix} me_{tk} \\ e_{zk} \\ nh_{tk} \\ mnh_{zk} \end{bmatrix}$	$\begin{bmatrix} md_{tk*} \\ d_{zk*} \\ nb_{tk*} \\ mnb_{zk*} \end{bmatrix}$
	$jn^*\omega$	$jm^*\beta_{zk}$	$\begin{bmatrix} me_{tk} \\ e_{zk} \\ nh_{tk} \\ mnh_{zk} \end{bmatrix}$	$\begin{bmatrix} -\mathbf{Z_m}n^*h_{tk*} \\ 0 \\ \mathbf{Z_e}m^*e_{tk*} \\ 0 \end{bmatrix}$

$$\mathbf{L_0} = \begin{bmatrix} 0 & -\mathbf{Z_e}\mathbf{G_{te}} & 0 & 0 \\ -\mathbf{D_{tm}}\mathbf{Z_e} & 0 & 0 & 0 \\ 0 & 0 & 0 & \mathbf{Z_m}\mathbf{G_{tm}} \\ 0 & 0 & \mathbf{D_{te}}\mathbf{Z_m} & 0 \end{bmatrix}$$

$$\mathbf{L}_\omega = \begin{bmatrix} 0 & 0 & \mathbf{M_{tt}} & m^*\mathbf{M_{tz}} \\ 0 & 0 & m\mathbf{M_{zt}} & \mathbf{M_{zz}} \\ n^2\mathbf{E_{tt}} & n^2m\mathbf{E_{tz}} & 0 & 0 \\ n^2m^*\mathbf{E_{zt}} & n^2\mathbf{E_{zz}} & 0 & 0 \end{bmatrix}$$

$$\mathbf{L}_\beta = \begin{bmatrix} -\mathbf{Z_e} & 0 & 0 & 0 \\ 0 & 0 & 0 & 0 \\ 0 & 0 & m^2\mathbf{Z_m} & 0 \\ 0 & 0 & 0 & 0 \end{bmatrix}$$

longitudinal field components from the most general eigenproblems. This leads to four field component formulations. The formulation presented in tab. 3.5.4 has parameter β_z and eigenvalues ω^2. The eigenvectors contain the transverse flux density field components. In the formulation from tab. 3.5.5, the parameter is ω, the eigenvalues are β_z^2 and the eigenvectors contain the transverse intensity fields. If β_z is a parameter, we may further reduce the number of field components. This produces two eigenproblems with two field components (see tab. 3.5.4). The eigenvalues in these cases are ω^2 and the eigenvectors are the transverse electric or transverse magnetic flux density fields.

Elimination of electric or magnetic fields from the general formulation with six fields leads to the formulations with three field components (tab. 3.5.6). However, these formulations also contain static solutions. The parameter in these case is β_z and the eigenvalues are ω^2. The eigenvectors are all three components of the electric or magnetic fields.

Table 3.5.4: *4 and 2 field component ω and ω^2 formulations for general anisotropic waveguides.*

Eigenproblem	Parameter	Eigenvalue	Eigenvector	
			right	left
$\begin{bmatrix} 0 & \mathbf{L_{db}} \\ \mathbf{L_{bd}} & 0 \end{bmatrix} \begin{bmatrix} md_t \\ nb_t \\ md_t \\ nb_t \end{bmatrix} = (jn^*\omega_k) \begin{bmatrix} md_t \\ nb_t \\ md_t \\ nb_t \end{bmatrix}$	$jm^*\beta_z$	$jn^*\omega_k$	$\begin{bmatrix} md_{tk} \\ nb_{tk} \end{bmatrix}$	$\begin{bmatrix} \mathbf{Z_m} n^* b_{tk*} \\ -\mathbf{Z_e} m^* d_{tk*} \end{bmatrix}$
$-n^2\mathbf{L_{db}}\mathbf{L_{bd}}d_t = \omega^2 d_t$	$jm^*\beta_z$	ω_k^2	d_{tk}	$\mathbf{Z_m} b_{tk*}$
$-n^2\mathbf{L_{bd}}\mathbf{L_{db}}b_t = \omega^2 b_t$	$jm^*\beta_z$	ω_k^2	b_{tk}	$\mathbf{Z_e} d_{tk*}$

$$
\begin{aligned}
\mathbf{L_{db}} &= -m^2 n^2 \mathbf{Z_m} m^* \mathbf{N_{tz}} \mathbf{D_{tm}} \\
&- n^2 \mathbf{Z_m} \mathbf{G_{tm}} m \mathbf{N_{zt}} \\
&- \tfrac{1}{jm^*\beta_z} n^2 \mathbf{Z_m} \mathbf{G_{tm}} \mathbf{N_{zz}} \mathbf{D_{tm}} \\
&- jm\beta_z n^2 \mathbf{Z_m} \mathbf{N_{tt}} \\
\mathbf{L_{bd}} &= m^2 \mathbf{Z_e} m \mathbf{F_{tz}} \mathbf{D_{te}} \\
&+ \mathbf{Z_e} \mathbf{G_{te}} m^* \mathbf{F_{zt}} \\
&+ \tfrac{1}{jm\beta_z} \mathbf{Z_e} \mathbf{G_{te}} \mathbf{F_{zz}} \mathbf{D_{te}} \\
&+ jm^*\beta_z \mathbf{Z_e} \mathbf{F_{tt}}
\end{aligned}
$$

Table 3.5.5: *4 field component β_z formulation for general anisotropic waveguides.*

Eigenproblem	Parameter	Eigenvalue	Eigenvector	
			right	left
$\begin{bmatrix} \mathbf{L_{ee}} & \mathbf{L_{eh}} \\ \mathbf{L_{he}} & \mathbf{L_{hh}} \end{bmatrix} \begin{bmatrix} me_t \\ nh_t \\ me_t \\ nh_t \end{bmatrix} = (jm^*\beta_z) \begin{bmatrix} me_t \\ nh_t \\ me_t \\ nh_t \end{bmatrix}$	$jn^*\omega$	$jm^*\beta_{zk}$	$\begin{bmatrix} me_{tk} \\ nh_{tk} \end{bmatrix}$	$\begin{bmatrix} \mathbf{Z_m} n^* h_{tk*} \\ -\mathbf{Z_e} m^* e_{tk*} \end{bmatrix}$

$$
\begin{aligned}
\mathbf{L_{ee}} &= \mathbf{G_{te}} \mathbf{E_{zz}^{-1}} m^* \mathbf{E_{zt}} \\
&- \mathbf{Z_m} m^* \mathbf{M_{tz}} \mathbf{M_{zz}^{-1}} \mathbf{D_{tm}} \mathbf{Z_e} \\
\mathbf{L_{eh}} &= \tfrac{1}{jn\omega} \mathbf{G_{te}} \mathbf{E_{zz}^{-1}} \mathbf{D_{te}} \mathbf{Z_m} \\
&- jn^*\omega \mathbf{Z_m} \mathbf{M_{tt}} \\
&+ jn^*\omega \mathbf{Z_m} m^* \mathbf{M_{tz}} \mathbf{M_{zz}^{-1}} m \mathbf{M_{zt}} \\
\mathbf{L_{he}} &= -\tfrac{1}{jn^*\omega} m^2 \mathbf{G_{tm}} \mathbf{M_{zz}^{-1}} \mathbf{D_{tm}} \mathbf{Z_e} \\
&+ jn\omega m^2 \mathbf{Z_e} \mathbf{E_{tt}} \\
&- jn\omega m^2 \mathbf{Z_e} m \mathbf{E_{tz}} \mathbf{E_{zz}^{-1}} m^* \mathbf{E_{zt}} \\
\mathbf{L_{hh}} &= m^2 \mathbf{G_{tm}} \mathbf{M_{zz}^{-1}} m \mathbf{M_{zt}} \\
&- m^2 \mathbf{Z_e} m \mathbf{E_{tz}} \mathbf{E_{zz}^{-1}} \mathbf{D_{te}} \mathbf{Z_m}
\end{aligned}
$$

Table 3.5.6: *3 field component ω^2 formulations for general anisotropic waveguides.*

Eigenproblem	Parameter	Eigenvalue	Eigenvector	
			right	left
$\mathbf{FR_m NR_e}e = \omega^2 e$	$jm^*\beta_z$	ω_k^2	$\begin{bmatrix} me_{tk} \\ e_{zk} \end{bmatrix}$	$\begin{bmatrix} md_{tk*} \\ d_{zk*} \end{bmatrix}$
$\mathbf{NR_e FR_m}h = \omega^2 h$	$jm^*\beta_z$	ω_k^2	$\begin{bmatrix} h_{tk} \\ mh_{zk} \end{bmatrix}$	$\begin{bmatrix} b_{tk*} \\ mb_{zk*} \end{bmatrix}$
$\mathbf{R_m} = \begin{bmatrix} -jm\beta_z\mathbf{Z_m} & -\mathbf{Z_m G_{tm}} \\ -\mathbf{D_{te}Z_m} & 0 \end{bmatrix}$			$\mathbf{F} = \begin{bmatrix} \mathbf{F_{tt}} & \mathbf{F_{tz}} \\ \mathbf{F_{zt}} & \mathbf{F_{zz}} \end{bmatrix}$	
$\mathbf{R_e} = \begin{bmatrix} -jm^*\beta_z\mathbf{Z_e} & -\mathbf{Z_e G_{te}} \\ -\mathbf{D_{tm}Z_e} & 0 \end{bmatrix}$			$\mathbf{N} = \begin{bmatrix} \mathbf{N_{tt}} & \mathbf{N_{tz}} \\ \mathbf{N_{zt}} & \mathbf{N_{zz}} \end{bmatrix}$	

Table 3.5.7: *4 field component $\omega\beta_z$ and ω^2 formulations for strictly bidirectional waveguides.*

Eigenproblem	Parameter	Eigenvalue	Eigenvector	
			right	left
$(\omega^2\mathbf{L_{\omega^2}} + \mathbf{L_0})\begin{bmatrix} me_t \\ nh_t \end{bmatrix} =$	ω^2	$m^*n^*\omega_k\beta_{zk}$	$\begin{bmatrix} me_{tk} \\ nh_{tk} \end{bmatrix}$	$\begin{bmatrix} \mathbf{Z_m}n^*h_{tk*} \\ -\mathbf{Z_e}m^*e_{tk*} \end{bmatrix}$
$m^*n^*\omega\beta_z\begin{bmatrix} me_t \\ nh_t \end{bmatrix}$	$m^*n^*\omega\beta_z$	ω_k^2	$\begin{bmatrix} me_{tk} \\ nh_{tk} \end{bmatrix}$	$\begin{bmatrix} md_{tk*} \\ nb_{tk*} \end{bmatrix}$
$\mathbf{L_{\omega^2}} = \begin{bmatrix} 0 & -n^2\mathbf{Z_m M_{tt}} \\ m^2\mathbf{Z_e E_{tt}} & 0 \end{bmatrix}$				
$\mathbf{L_0} = \begin{bmatrix} 0 & -n^2\mathbf{G_{te}E_{zz}^{-1}D_{te}Z_m} \\ m^2\mathbf{G_{tm}M_{zz}^{-1}D_{tm}Z_e} & 0 \end{bmatrix}$				

Table 3.5.8: *4 field component $\omega\beta_z$ and β_z^2 formulations for strictly bidirectional waveguides.*

Eigenproblem	Parameter	Eigenvalue	Eigenvector	
			right	left
$(\beta_z^2\mathbf{L_{\beta^2}} + \mathbf{L_0})\begin{bmatrix} md_t \\ nb_t \end{bmatrix} =$	β_z^2	$m^*n^*\omega_k\beta_{zk}$	$\begin{bmatrix} md_{tk} \\ nb_{tk} \end{bmatrix}$	$\begin{bmatrix} \mathbf{Z_m}n^*b_{tk*} \\ -\mathbf{Z_e}m^*d_{tk*} \end{bmatrix}$
$m^*n^*\omega\beta_z\begin{bmatrix} md_t \\ nb_t \end{bmatrix}$	$m^*n^*\omega\beta_z$	β_{zk}^2	$\begin{bmatrix} md_{tk} \\ nb_{tk} \end{bmatrix}$	$\begin{bmatrix} me_{tk*} \\ nh_{tk*} \end{bmatrix}$
$\mathbf{L_{\beta^2}} = \begin{bmatrix} 0 & -n^2\mathbf{Z_m M_{tt}^{-1}} \\ m^2\mathbf{Z_e E_{tt}^{-1}} & 0 \end{bmatrix}$				
$\mathbf{L_0} = \begin{bmatrix} 0 & n^2\mathbf{Z_m G_{tm} M_{zz}^{-1} D_{tm}} \\ -m^2\mathbf{Z_e G_{te} E_{zz}^{-1} D_{te}} & 0 \end{bmatrix}$				

The equations may be simplified if the structure is strictly bidirectional. Four field component formulations produce in this case eigenproblems presented in tabs. 3.5.7 and 3.5.8. One may note, that quantity $\omega\beta_z$ appears as a parameter or eigenvalues in these formulations. If it is a parameter, the solution of the eigenproblem will produce the dispersion characteristics in another coordinate system.

In strictly bidirectional waveguides, the number of field components may further be reduced. Tab. 3.5.9 presents the formulations with only two field components.

In two special cases, i.e. at cutoff and in the static case, the equations may be reduced to the scalar eigenproblems. These formulations are presented in tab. 3.5.10.

Table 3.5.9: *2 field component ω^2 and β_z^2 formulations for strictly bidirectional waveguides.*

Eigenproblem	Parameter	Eigenvalue	Eigenvector	
			right	left
$\mathbf{L_{dd}}d_t = \omega^2 d_t$	β_z^2	ω_k^2	d_{tk}	$\mathbf{Z_m}b_{tk*}$
$\mathbf{L_{bb}}b_t = \omega^2 b_t$	β_z^2	ω_k^2	b_{tk}	$\mathbf{Z_e}d_{tk*}$
$\mathbf{L_{ee}}e_t = \beta_z^2 e_t$	ω^2	β_{zk}^2	e_{tk}	$\mathbf{Z_m}h_{tk*}$
$\mathbf{L_{hh}}h_t = \beta_z^2 h_t$	ω^2	β_{zk}^2	h_{tk}	$\mathbf{Z_e}e_{tk*}$

$$
\begin{aligned}
\mathbf{L_{dd}} &= -\beta_z^2 \mathbf{Z_m M_{tt}^{-1} Z_e E_{tt}^{-1}} \\
&+ \mathbf{Z_m G_{tm} M_{zz}^{-1} D_{tm} Z_e E_{tt}^{-1}} \\
&+ \mathbf{Z_m M_{tt}^{-1} Z_e G_{te} E_{zz}^{-1} D_{te}} \\
\mathbf{L_{bb}} &= -\beta_z^2 \mathbf{Z_e E_{tt}^{-1} Z_m M_{tt}^{-1}} \\
&+ \mathbf{Z_e G_{te} E_{zz}^{-1} D_{te} Z_m M_{tt}^{-1}} \\
&+ \mathbf{Z_e E_{tt}^{-1} Z_m G_{tm} M_{zz}^{-1} D_{tm}} \\
\mathbf{L_{ee}} &= -\omega^2 \mathbf{Z_m M_{tt} Z_e E_{tt}} \\
&- \mathbf{Z_m M_{tt} G_{tm} M_{zz}^{-1} D_{tm} Z_e} \\
&+ \mathbf{G_{te} E_{zz}^{-1} D_{te} E_{tt}} \\
\mathbf{L_{hh}} &= -\omega^2 \mathbf{Z_e E_{tt} Z_m M_{tt}} \\
&- \mathbf{Z_e E_{tt} G_{te} E_{zz}^{-1} D_{te} Z_m} \\
&+ \mathbf{G_{tm} M_{zz}^{-1} D_{tm} M_{tt}}
\end{aligned}
$$

Table 3.5.10: *Scalar ω^2 cutoff and β_z^2 static formulations for strictly bidirectional waveguides.*

Eigenproblem	Parameter	Eigenvalue	Eigenvector	
			right	left
$\mathbf{E_{zz}^{-1} D_{te} Z_m M_{tt}^{-1} Z_e G_{te}} e_z = \omega^2 e_z$	$\beta_z^2 = 0$	ω_k^2	e_{zk}	d_{zk}
$\mathbf{M_{zz}^{-1} D_{tm} Z_e E_{tt}^{-1} Z_m G_{tm}} h_z = \omega^2 h_z$	$\beta_z^2 = 0$	ω_k^2	h_{zk}	b_{zk}
$\mathbf{E_{zz}^{-1} D_{te} E_{tt} G_{te}} e_z = \beta_z^2 e_z$	$\omega^2 = 0$	β_{zk}^2	e_{zk}	d_{zk}
$\mathbf{M_{zz}^{-1} D_{tm} M_{tt} G_{tm}} h_z = \beta_z^2 h_z$	$\omega^2 = 0$	β_{zk}^2	h_{zk}	b_{zk}

3.6 Discretization of 2D basic operators

In sec. 3.5.3, we developed different eigenproblems based on Maxwell's equations which are suitable for the analysis of waveguides. All these equations are defined in terms of a few basic operators. Since we extended the definition of the basic operators by introducing the symbolic space, all these equations are valid in continuous space as well as in the discrete space. However, up to this time, nothing has been said about the construction of the discrete basic operators. We discuss it here for all operators defined in Tab. 3.5, using the properties derived in sec. 3.5.1. In this section, we present the form of discrete matrices in the homogeneous parts of the domain. Inhomogeneities are discussed in chapter 4.

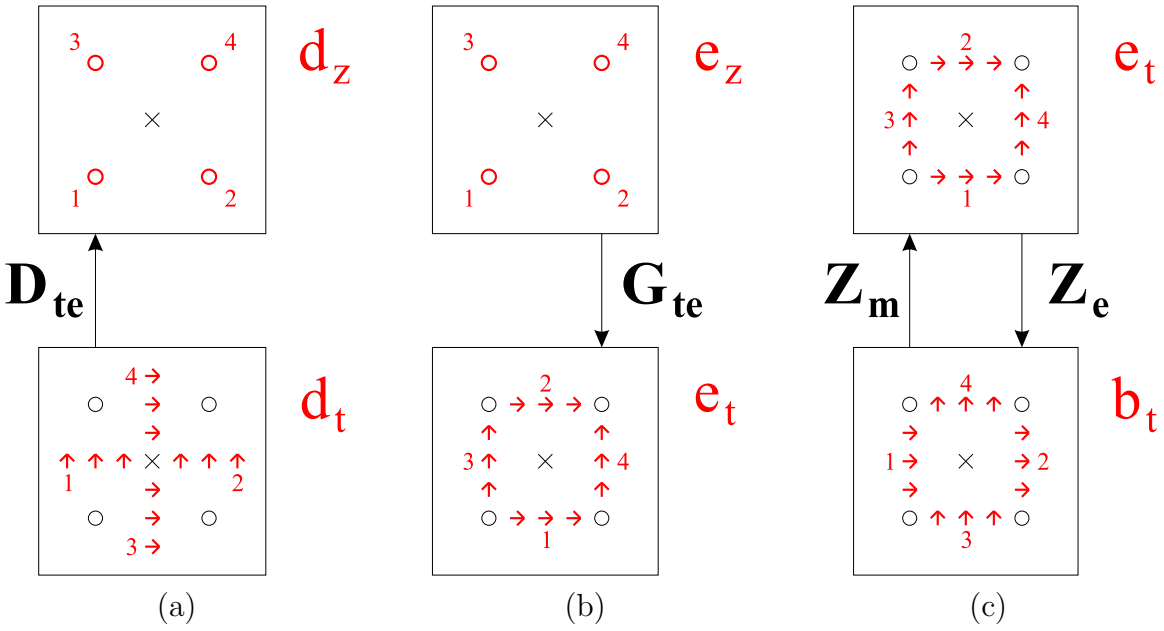

Figure 3.6.1: *Fragments of 2D Yee's grid corresponding to the domains and ranges of matrices* $\underline{\underline{D}}_{te}$ *(a)* $\underline{\underline{G}}_{te}$ *(b) and* $\underline{\underline{Z}}_{e}$, $\underline{\underline{Z}}_{m}$ *(c). Numbers in the figures denote position of vector elements associated with the nodes in the corresponding vectors.*

Discretization of functions The form of the discrete operators depends on the approach used for the discretization of the fields. The fields are discretized to form Yee's mesh. This means that if the relation between two fields is expressed by the first order differential operator, the grids corresponding to these fields are shifted with respect to each other by half a cell size. This enables one to use the central difference scheme when discretizing the differential operators. Moreover, the grids corresponding to different fields differ by the integration paths in the integral interpretation of the grid equations[3]. For instance, vectors $\underline{d}_t$ (discretized transverse electric flux density) and $\underline{d}_z$ (discretized longitudinal electric flux density) are related to each other by the discretized version of eq. (3.5.5):

$$j\beta_z \underline{d}_z = \underline{\underline{D}}_{te} \underline{d}_t \tag{3.6.1}$$

[3]See sec. 2.2.2.

Since we use the central difference scheme to discretize the electric transverse divergence operator, nodes[4] d_z are shifted by a half of the cell size with respect to nodes d_t. Moreover, the integration paths corresponding to nodes d_t go through the points with the equal distance from the closest nodes d_z. This situation is presented in fig. 3.6.1(a). The domain (d_t) and the range (d_z) of operator $\underline{\underline{D}}_{te}$ are denoted with red color. The arrows denote direction of the vectors.

Let us now consider the case of the discrete electric intensity fields e_t, e_z and discrete electric transverse gradient $\underline{\underline{G}}_{te}$ (fig. 3.6.1(b)). The relation between both fields may be formulated in the static case as follows

$$\underline{e}_t = -\frac{1}{j\beta_z}\underline{\underline{G}}_{te}\underline{e}_z \tag{3.6.2}$$

The central difference procedures require in this case that nodes e_t are shifted by a half of the cell size with respect to grid e_z. From the integral interpretation of the grid equations it follows that the integration paths of field e_t go through points between two closest elements e_z. One may note, that in general this has not to be the straight lines. This fact will be used when presenting the local schemes (chapter 4) where some of the cells will be deformed. In the homogeneous parts of the domain, however, there is no reason to use the integration paths different than the straight lines.

If we now look at the example of operators $\underline{\underline{Z}}_e$, $\underline{\underline{Z}}_m$, we may note that they only change the direction of the vectors. This means, that the grids and the integration paths are the same in the domains and ranges of these operators (see example in fig. 3.6.1(c)).

Fig. 3.6.2 presents the grids for all the discrete fields together with the basic operators with denoted domains and ranges. Different integration paths for the transverse fields may be seen in this figure. In particular, one may note the difference between the integration paths of the flux density and intensity fields. This implies, that the material matrices are simple diagonal operators with the elements being the material constants only if the field variation within a single cell is close to linear. Otherwise, these matrices may have more complicated, even nondiagonal forms. We present such cases in chapter 4.

Discretization of operators In order to derive the basic operators let us consider the case of the electric transverse gradient. Let us use the continuous form of eq. (3.6.2) written for component E_x

$$E_x = -\frac{1}{j\beta_z}\frac{\partial}{\partial x}E_z \tag{3.6.3}$$

We discretize this equation using the central difference approach and write it for node 1 of the transverse electric field from fig. 3.6.1(b)

$$E_{t1} = -\frac{1}{j\beta_z}\frac{1}{\Delta x}(E_{z2} - E_{z1}) \tag{3.6.4}$$

This equation defines the row of matrix $\underline{\underline{G}}_{te}$ corresponding to node E_{t1}. The part of matrix $\underline{\underline{G}}_{te}$ corresponding to all nodes from fig. 3.6.1(b) has the following form:

$$\underline{\underline{G}}_{te} = \begin{bmatrix} -\Delta x^{-1} & \Delta x^{-1} & 0 & 0 \\ 0 & 0 & -\Delta x^{-1} & \Delta x^{-1} \\ -\Delta y^{-1} & 0 & \Delta y^{-1} & 0 \\ 0 & -\Delta y^{-1} & 0 & \Delta y^{-1} \end{bmatrix} \tag{3.6.5}$$

[4]We use term *nodes* for the differential interpretation of the grid equations. Each node has a corresponding integration path or area associated with the integral interpretation.

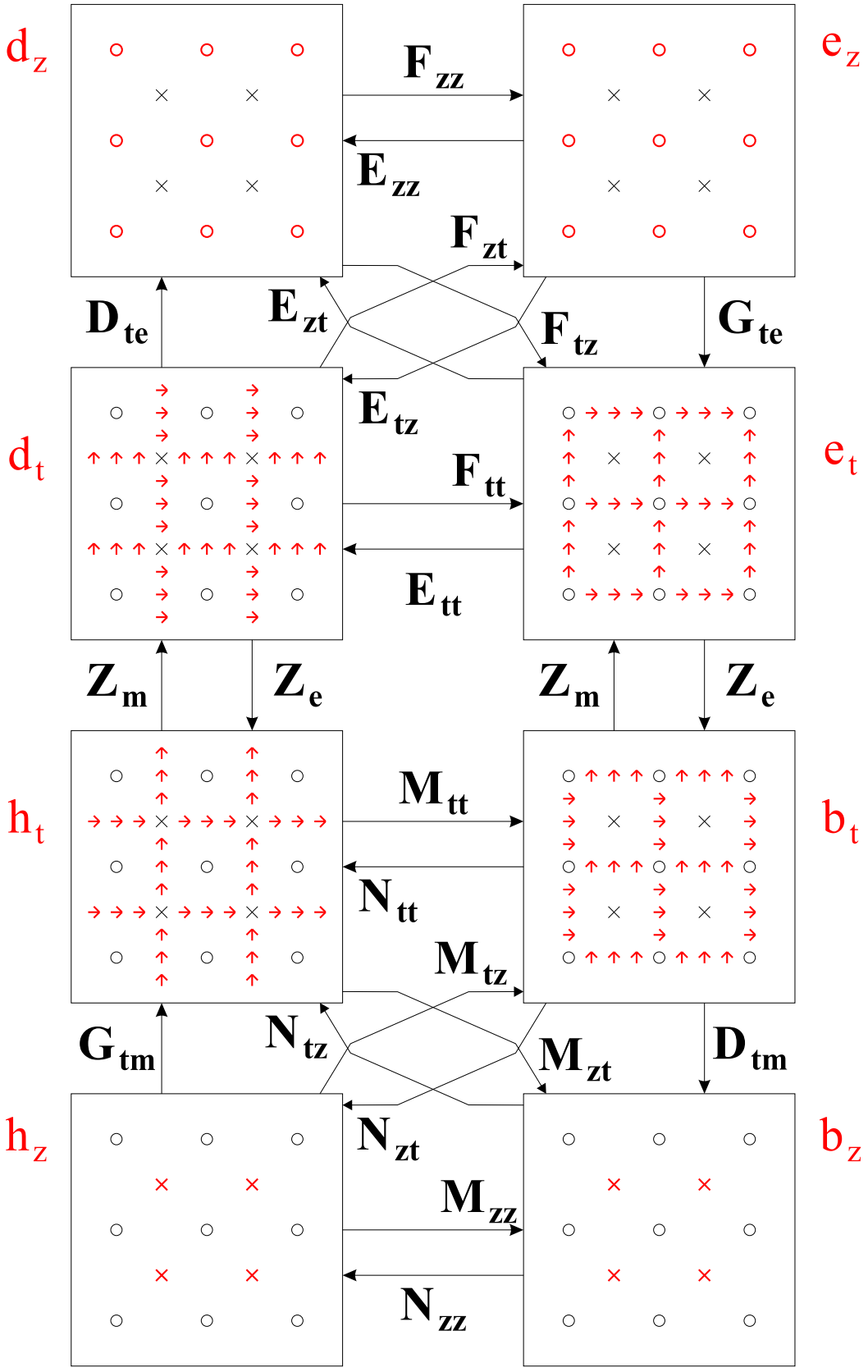

Figure 3.6.2: *Discrete fields and operators in the finite difference method for 2D structures.*

One may note that every row of this matrix contains all the nonzero elements of the global operator. Location of these elements in the global matrix depends on the numbering of the nodes. In general, if node E_x has number m in vector $\underline{e}_t$ and node E_z has number n in vector $\underline{e}_z$, the element of matrix $\underline{\underline{G}}_{te}$ corresponding to the interaction between these nodes will be located in m-th row and n-th column. In the same way we derive discrete magnetic transverse gradient $\underline{\underline{G}}_{tm}$.

An analogous procedure may be performed in order to define matrices $\underline{\underline{D}}_{te}$, $\underline{\underline{D}}_{tm}$. We get operators of the form $\underline{\underline{D}}_{te} = -\underline{\underline{G}}_{te}^T$ and $\underline{\underline{D}}_{tm} = -\underline{\underline{G}}_{tm}^T$, satisfying conditions (3.5.13) and (3.5.14).

In a similar manner, we may derive matrices $\underline{\underline{Z}}_e$ and $\underline{\underline{Z}}_m$. The fragments of these matrices corresponding to the nodes from fig. 3.6.1(c) have the following form

$$\underline{\underline{Z}}_e = \begin{bmatrix} 0 & 0 & 1 & 0 \\ 0 & 0 & 0 & 1 \\ -1 & 0 & 0 & 0 \\ 0 & -1 & 0 & 0 \end{bmatrix} \qquad \underline{\underline{Z}}_m = \begin{bmatrix} 0 & 0 & 1 & 0 \\ 0 & 0 & 0 & 1 \\ -1 & 0 & 0 & 0 \\ 0 & -1 & 0 & 0 \end{bmatrix} \tag{3.6.6}$$

Material matrices which correspond to the material tensors are, in the homogeneous parts of the domain, diagonal with elements being the material constants at the corresponding point.

3.7 Discretization of 3D basic operators

Analogously, we may discretize basic operators in 3D.

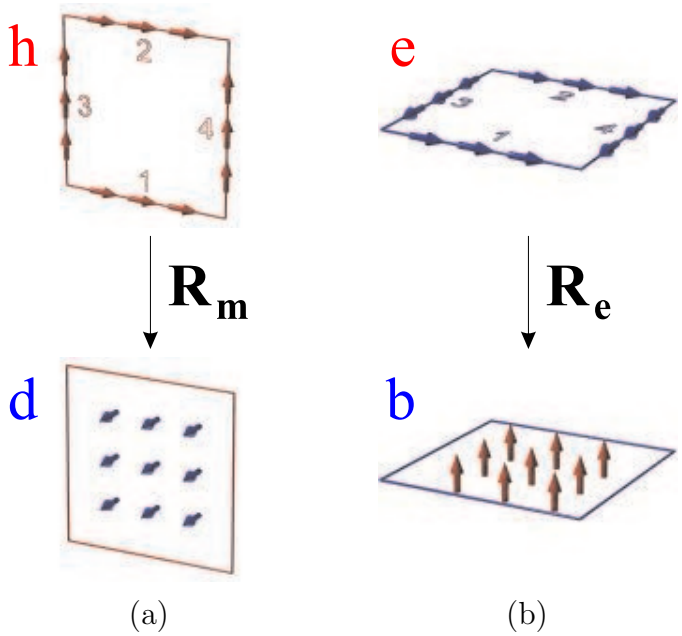

(a) (b)

Figure 3.7.1: *Fragments of 3D Yee's grid corresponding to the domains and ranges of matrices* $\underline{\underline{R}}_m$ *(a) and* $\underline{\underline{R}}_e$ *(b).*

Discretization of functions The fields are discretized to form 3D Yee's mesh. As in the 2D case, the discretized fields differ by position of nodes and by the areas of

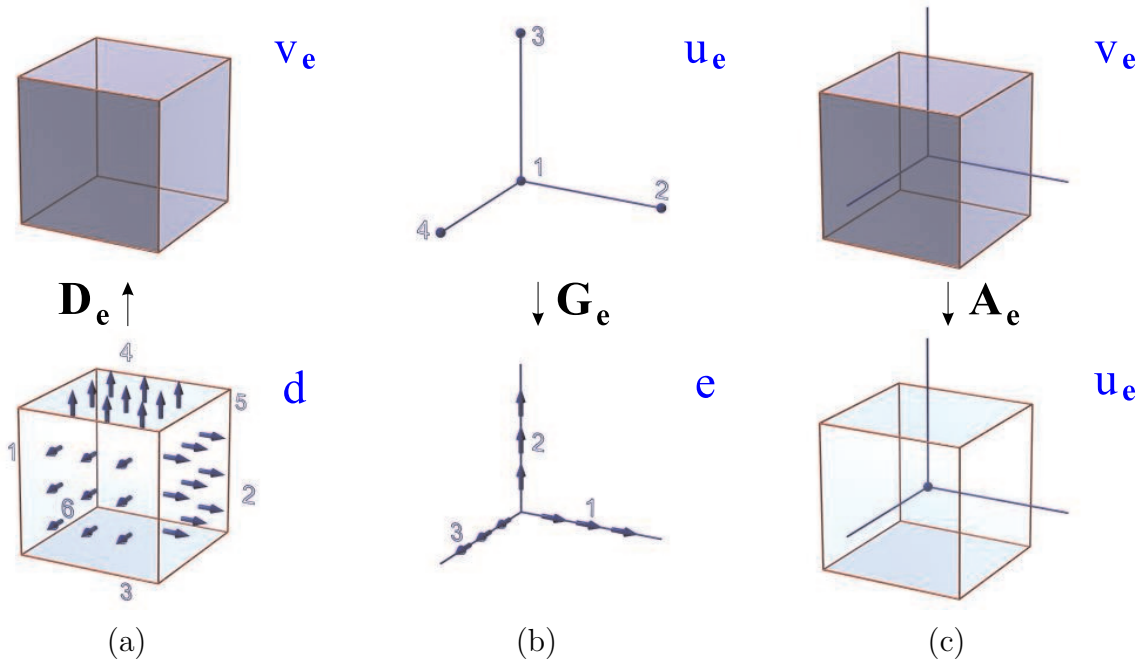

Figure 3.7.2: *Fragments of 3D Yee's grid corresponding to the domains and ranges of matrices* $\underline{\underline{D}}_e$ *(a),* $\underline{\underline{G}}_e$ *(b) and* $\underline{\underline{A}}_e$ *(c).*

integration. For instance, relation between vectors $\underline{b}$ (discretized magnetic flux density) and $\underline{e}$ (discretized electric intensity) may be written as follows.

$$-j\omega\underline{b} = \underline{\underline{R}}_e\underline{e} \tag{3.7.1}$$

The electric rotation operator is discretized using the central difference scheme. Therefore, nodes b must be shifted in space versus the corresponding nodes e. In particular, nodes b_z are shifted by a half of the cell size with respect to nodes e_x, e_y. The same is true for nodes b_x with respect to e_y, e_z and for b_y with respect to e_x, e_z. Moreover, the integration paths of nodes e determine the integration surface of the corresponding node b in the integral interpretation of the grid equations. This may be seen in fig. 3.7.1(b). Four integration lines of four nodes e determine the integration area of cell b.

In order to get discrete representations of operators $\mathbf{D_e}$, $\mathbf{D_m}$, we also need to define their ranges. These are spaces of scalar functions, respectively, v_e and v_m defined as follows[5]:

$$v_e = \mathbf{D_e}d \tag{3.7.2}$$
$$v_m = \mathbf{D_m}b \tag{3.7.3}$$

The domains of operators $\mathbf{D_e}$, $\mathbf{D_m}$ are, respectively, spaces $\{d\}$ and $\{b\}$. Analogously, we define domains of operators $\mathbf{G_e}$, $\mathbf{G_m}$ as spaces of scalar functions u_e, u_m:

$$e \longleftarrow \mathbf{G_e}u_e \tag{3.7.4}$$
$$h \longleftarrow \mathbf{G_m}u_m \tag{3.7.5}$$

The ranges of these operators[6] are, respectively, spaces $\{e\}$ and $\{h\}$. Since operators, $\mathbf{D_e}$ and $\mathbf{G_e}$ will be discretized using the central difference scheme, discrete scalar nodes u_e,

[5]We use these functions to define the spaces. Note, that the equations are equivalent to (3.4.5), (3.4.6).
[6]Note, that expressions (3.7.4), (3.7.5) define the static solutions according to eqs. (3.4.34) and (3.4.35).

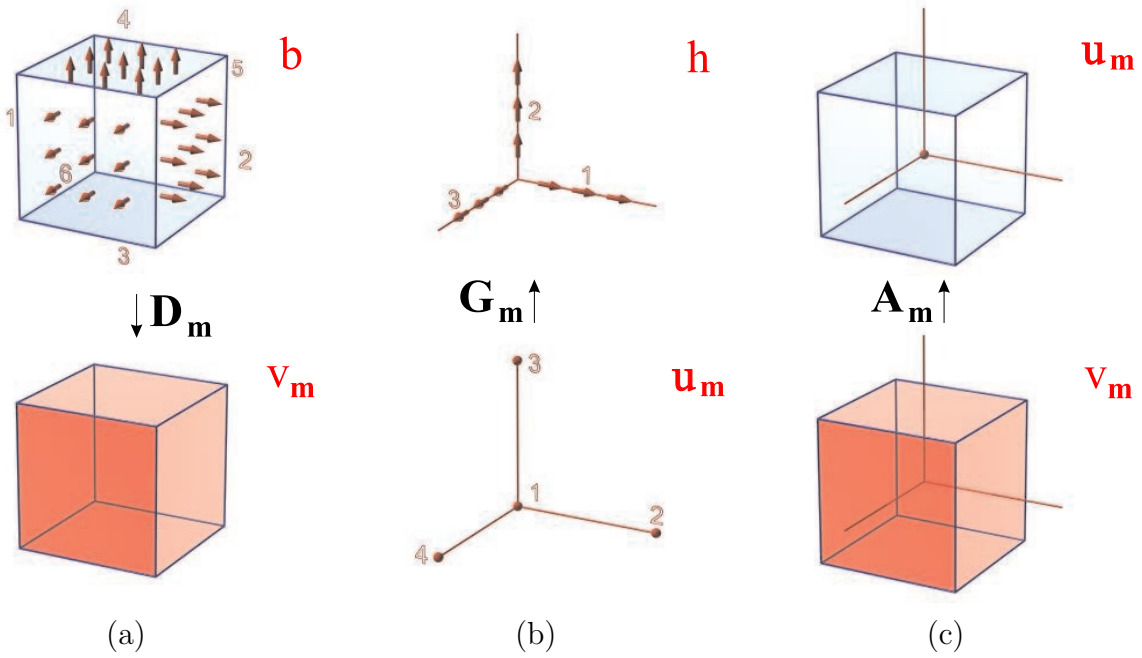

Figure 3.7.3: *Fragments of 3D Yee's grid corresponding to the domains and ranges of matrices* $\underline{\underline{D}}_m$ *(a),* $\underline{\underline{G}}_m$ *(b) and* $\underline{\underline{A}}_m$ *(c).*

v_e are shifted in space by a half of the cell size with respect to the neighbor pairs of nodes e_x, e_y, e_z (or d_x, d_y, d_z) This is shown in fig. 3.7.2(a) and (b). The figure also shows the integration areas corresponding to the nodes in the integral interpretation of the grid equations. Note, that the integration surfaces corresponding to nodes d_x, d_y, d_z define the integration volume corresponding to nodes v_e as shown in fig. 3.7.2(a). Fig. 3.7.2(c) presents domain and range of matrix $\underline{\underline{A}}_e$ being a discretized version of operator $\mathbf{A_e}$ defined in sec. 3.4.3.

Analogously, we may define grid of discrete nodes u_m and v_m with a half of the cell size shift with respect to nodes h_x, h_y, h_z (or b_x, b_y, b_z) as shown in fig. 3.7.3.

Fig. 3.7.4 presents the grids corresponding to all of the discrete 3D fields. The figure also shows the discrete operators with their domains and ranges. As in the 2D case, differences between integration areas may be seen. In particular, we may note differences between the integration areas for the flux density (surfaces) and intensity fields (lines).

Discretization of operators Let us write eq. (3.7.1) for node B_y in the continuous space:

$$-j\omega B_y = \frac{\partial}{\partial z}E_x - \frac{\partial}{\partial x}E_z \tag{3.7.6}$$

This equation may be discretized using the central difference scheme:

$$-j\omega b_y = \left(\frac{1}{\Delta z}(e_{x2} - e_{x1}) - \frac{1}{\Delta x}(e_{z3} - e_{z4})\right) \tag{3.7.7}$$

where the nodes correspond to fig. 3.7.1(b). From the above equation, we get all nonzero elements of sparse matrix $\underline{\underline{R}}_e$ corresponding to node b_y from the figure.

$$\underline{\underline{R}}_e = \left[\begin{array}{cccc} -\Delta z^{-1} & \Delta z^{-1} & -\Delta x^{-1} & \Delta x^{-1} \end{array}\right] \tag{3.7.8}$$

The rows of matrix $\underline{\underline{R}}_e$ correspond to nodes b and the columns correspond to nodes e. Analogously, we may define nonzero elements of matrix $\underline{\underline{R}}_m$ corresponding to the nodes from fig. 3.7.1(a):

$$\underline{\underline{R}}_m = \left[\begin{array}{cccc} \Delta y^{-1} & -\Delta y^{-1} & \Delta x^{-1} & -\Delta x^{-1} \end{array} \right] \tag{3.7.9}$$

In the same manner, we derive matrices $\underline{\underline{D}}_e$ and $\underline{\underline{G}}_e$. Nonzero elements of these matrices corresponding to the nodes from figs. 3.7.2(a) and (b) are:

$$\underline{\underline{D}}_e = \left[\begin{array}{cccccc} -\Delta x^{-1} & \Delta x^{-1} & -\Delta y^{-1} & \Delta y^{-1} & -\Delta z^{-1} & \Delta z^{-1} \end{array} \right] \tag{3.7.10}$$

$$\underline{\underline{G}}_e = \left[\begin{array}{cccc} -\Delta x^{-1} & \Delta x^{-1} & 0 & 0 \\ -\Delta y^{-1} & 0 & \Delta y^{-1} & 0 \\ -\Delta z^{-1} & 0 & 0 & \Delta z^{-1} \end{array} \right] \tag{3.7.11}$$

Nonzero elements of operators $\underline{\underline{D}}_m$ and $\underline{\underline{G}}_m$ corresponding to the nodes from figs. 3.7.3(a) and (b) look in the same manner.

Like in the case of 2D basic operators, the material matrices in the homogeneous parts of the domain are diagonal. The elements of these matrices are simply the values of the appropriate material constant at the corresponding point.

One may easily verify, that the basic operators defined this way satisfy all the conditions derived in sec. 3.4.1.

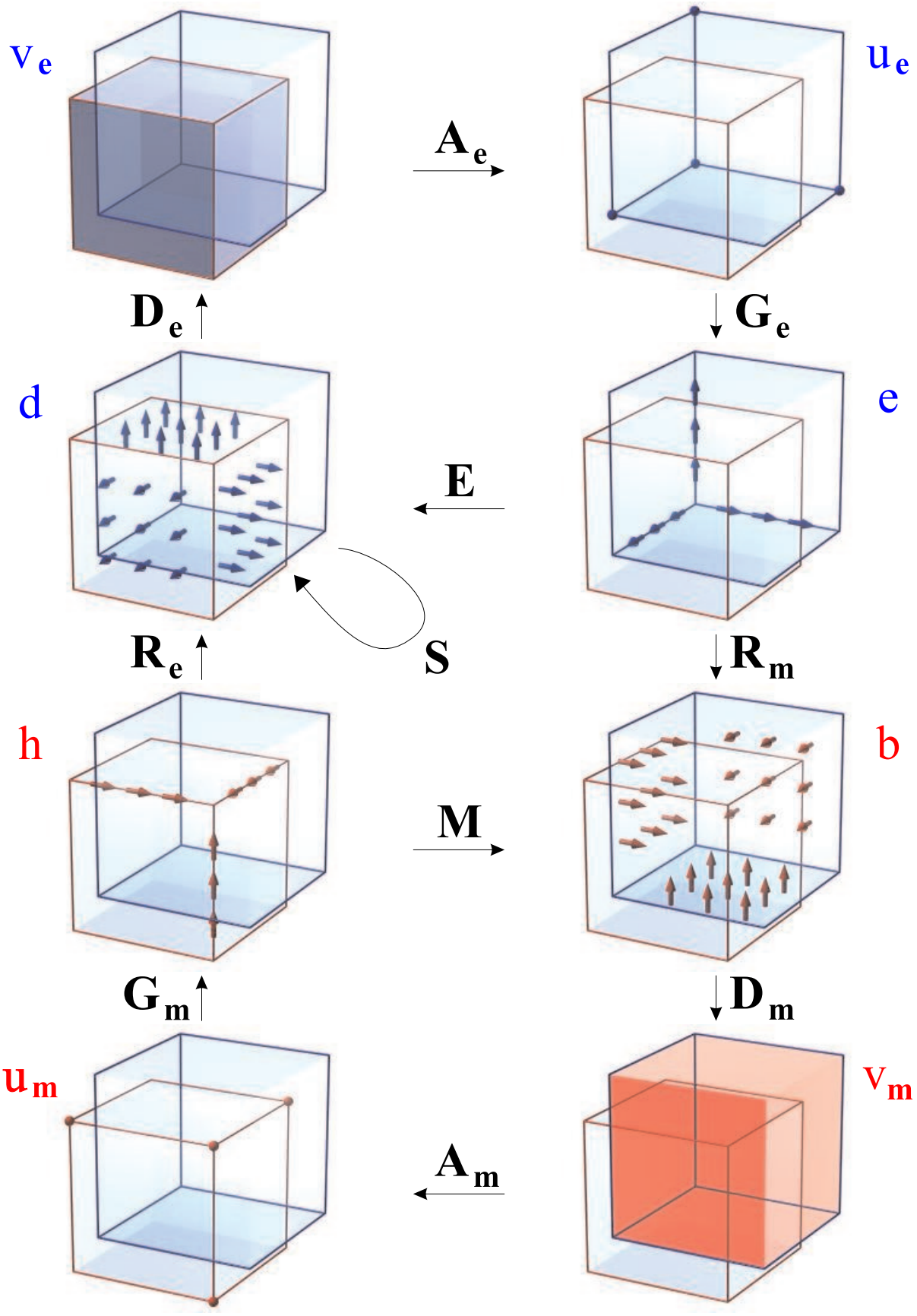

Figure 3.7.4: *Discrete fields and operators in the finite difference method for 3D structures.*

3.8 Stability of 2D explicit update schemes

As shown in sec. 2.2.3, every eigenproblem has its potential counterpart in the form of an explicit update scheme. In particular, all formulations presented in sec. 3.5.3 may be expressed in this form. It should be emphasized, however, that although these formulations are defined in the more general symbolic space, the explicit update algorithms are meaningful only in the case of the discretized equations. This is due to the fact, that, as shown in sec. 2.2.3, the stability conditions of these algorithms require limited spectrum of the operator in the corresponding eigenproblems, while the operators in the continuous space are unbounded. Moreover, discretization is the only way to convert an operator equation into the form of a numerical algorithm[7].

Although every eigenproblem from sec. 3.5.3 may be converted to an explicit update algorithm, not all of the obtained schemes will satisfy the stability conditions. In particular, in most practical cases, the stability conditions are not satisfied, if the scheme arise from the formulations with eigenvalues β_z or β_z^2. Stability conditions (2.2.26) and (2.2.38) require in these cases, that all solutions β_z of the corresponding eigenproblem are real[8]. In other words, all modes should propagate. This condition is satisfied for the frequencies larger than the cutoff frequency of the highest order mode. It is obvious, that this frequency range does not include the range, where the numerical dispersion error is small and the modes of interest are easy to separate.

Estimation of the time step in the explicit update schemes In order to find the maximum time step of the explicit update schemes, we need to estimate the norm of the operator in the corresponding eigenproblem (according to the discussion from sec. 2.2.3). We may use the fact that the nonzero[9] eigenvalues of every eigenproblem derived in sec. 3.5.3 correspond to the same values of ω. Therefore, it is sufficient to test the norm of one general operator. The result may be then used for other operators. We limit our discussion to strictly bidirectional waveguides. Further on, we base the analysis on ω^2 2-component formulations found in tab. 3.5.9. These eigenproblems may be written in the following manner:

$$(\beta_z^2\mathbf{L}_{\mathbf{dt}\beta^2} + \mathbf{L}_{\mathbf{dtH}} + \mathbf{L}_{\mathbf{dtE}})d_t = \omega^2 d_t \tag{3.8.1}$$

$$(\beta_z^2\mathbf{L}_{\mathbf{bt}\beta^2} + \mathbf{L}_{\mathbf{btH}} + \mathbf{L}_{\mathbf{btE}})b_t = \omega^2 b_t \tag{3.8.2}$$

where the suboperators are defined as follows:

$$\mathbf{L}_{\mathbf{dt}\beta^2} = -\mathbf{Z_m}\mathbf{M}_{\mathbf{tt}}^{-1}\mathbf{Z_e}\mathbf{E}_{\mathbf{tt}}^{-1} \tag{3.8.3}$$

$$\mathbf{L}_{\mathbf{dtH}} = \mathbf{Z_m}\mathbf{G_{tm}}\mathbf{M}_{\mathbf{zz}}^{-1}\mathbf{D_{tm}}\mathbf{Z_e}\mathbf{E}_{\mathbf{tt}}^{-1} \tag{3.8.4}$$

$$\mathbf{L}_{\mathbf{dtE}} = \mathbf{Z_m}\mathbf{M}_{\mathbf{tt}}^{-1}\mathbf{Z_e}\mathbf{G_{te}}\mathbf{E}_{\mathbf{zz}}^{-1}\mathbf{D_{te}} \tag{3.8.5}$$

$$\mathbf{L}_{\mathbf{bt}\beta^2} = -\mathbf{Z_e}\mathbf{E}_{\mathbf{tt}}^{-1}\mathbf{Z_m}\mathbf{M}_{\mathbf{tt}}^{-1} \tag{3.8.6}$$

$$\mathbf{L}_{\mathbf{btE}} = \mathbf{Z_e}\mathbf{G_{te}}\mathbf{E}_{\mathbf{zz}}^{-1}\mathbf{D_{te}}\mathbf{Z_m}\mathbf{M}_{\mathbf{tt}}^{-1} \tag{3.8.7}$$

$$\mathbf{L}_{\mathbf{btH}} = \mathbf{Z_e}\mathbf{E}_{\mathbf{tt}}^{-1}\mathbf{Z_m}\mathbf{G_{tm}}\mathbf{M}_{\mathbf{zz}}^{-1}\mathbf{D_{tm}} \tag{3.8.8}$$

[7]However, this discretization may have form other than the finite difference technique presented in this chapter. Such methods as FEM, SDA and others are also based on a discretization of an operator equation.

[8]This also implies that all solutions β_z^2 must be real and positive.

[9]Some of the eigenproblems contain static solutions, and hence, have a number of multiply degenerated zero eigenvalues.

It is easy to verify, that the following relations are satisfied:

$$\mathbf{L_{bt\beta^2}} = -\mathbf{Z_m}\mathbf{L}^H_{\mathbf{db\beta^2}}\mathbf{Z_m} \quad (3.8.9)$$

$$\mathbf{L_{btE}} = -\mathbf{Z_m}\mathbf{L}^H_{\mathbf{dbE}}\mathbf{Z_m} \quad (3.8.10)$$

$$\mathbf{L_{btH}} = -\mathbf{Z_m}\mathbf{L}^H_{\mathbf{dbH}}\mathbf{Z_m} \quad (3.8.11)$$

It is obvious that $\mathbf{L_{bt\beta^2}}$ has the same eigenvalues as $\mathbf{L_{dt\beta^2}}$ and the same is true for pairs of operators $\mathbf{L_{btE}}$, $\mathbf{L_{dbE}}$ and $\mathbf{L_{btH}}$, $\mathbf{L_{dbH}}$.

Let us use the following estimation:

$$||\mathbf{L_{dt}}|| \leq ||\mathbf{L_{dt}}||_{\beta_z=0} + ||\beta_z^2\mathbf{L_{dt\beta^2}}|| \quad (3.8.12)$$

We may estimate the norm of operator $\mathbf{L_{dt\beta^2}}$ as follows:

$$||\mathbf{L_{dt\beta^2}}|| \leq v^2_{\max} \quad (3.8.13)$$

$||\mathbf{L_{dt}}||_{\beta_z=0}$ is the norm of the operator $\mathbf{L_{dt}}$ at cutoff.

In order to find this norm, let us calculate fields d_{tH} and b_{tE} corresponding to, respectively, modes H and E at cutoff:

$$d_{tH} = -\frac{1}{j\omega_H}\mathbf{Z_m}\mathbf{G_{tm}}h_z \quad (3.8.14)$$

$$b_{tE} = \frac{1}{j\omega_E}\mathbf{Z_e}\mathbf{G_{te}}e_z \quad (3.8.15)$$

According to properties (3.5.25) and (3.5.26), we get:

$$\mathbf{L_{dtE}}d_{tH} = 0 \quad (3.8.16)$$

$$\mathbf{L_{btH}}b_{tE} = 0 \quad (3.8.17)$$

This means, that, at cutoff, eigenproblems (3.8.1), (3.8.2) reduce to the following eigeproblems for modes E and H:

$$\mathbf{L_{dtH}}d_{tH} = \omega^2 d_{tH} \quad (3.8.18)$$

$$\mathbf{L_{btE}}b_{tE} = \omega^2 b_{tE} \quad (3.8.19)$$

The eigenvalues of these equations being the squares of cutoff frequencies for, respectively, modes E and H are the same as the eigenvalues of the following two scalar eigenproblems:

$$\mathbf{L_{ezE}}e_{zE} = \omega^2 e_{zE} \quad (3.8.20)$$

$$\mathbf{L_{hzH}}h_{zE} = \omega^2 h_{zH} \quad (3.8.21)$$

where operators $\mathbf{L_{ezE}}$, $\mathbf{L_{hzH}}$ are defined as follows:

$$\mathbf{L_{ezE}} = \mathbf{E}^{-1}_{\mathbf{zz}}\mathbf{D_{te}}\mathbf{Z_m}\mathbf{M}^{-1}_{\mathbf{tt}}\mathbf{Z_e}\mathbf{G_{te}} \quad (3.8.22)$$

$$\mathbf{L_{hzH}} = \mathbf{M}^{-1}_{\mathbf{zz}}\mathbf{D_{tm}}\mathbf{Z_e}\mathbf{E}^{-1}_{\mathbf{tt}}\mathbf{Z_m}\mathbf{G_{tm}} \quad (3.8.23)$$

The above analysis gives the following formula for the norm of operators $\mathbf{L_{bt}}$, $\mathbf{L_{dt}}$ for $\beta_z = 0$:

$$||\mathbf{L_{bt}}||_{\beta_z=0} = ||\mathbf{L_{dt}}||_{\beta_z=0} = \max(||\mathbf{L_{dtE}}||, ||\mathbf{L_{dtH}}||) = \max(||\mathbf{L_{ezE}}||, ||\mathbf{L_{hzH}}||) \quad (3.8.24)$$

Table 3.8.1: *Estimation of the norm maximum of operators* $\mathbf{L_{ezE}}$ *and* $\mathbf{L_{hzH}}$. *Analysis of nonzero elements in row i.* ϵ, μ *are associated with nodes, respectively,* e_z, h_z *corresponding to row i.* μ_{x+}, μ_{x-}, μ_{y+}, μ_{y-} *and* ϵ_{x+}, ϵ_{x-}, ϵ_{y+}, ϵ_{y-} *correspond to, respectively, nodes* h_x, h_y *in the neighborhood of node* e_z *and* e_x, e_y *in the neighborhood of node* h_z.

	$\mathbf{L_{ezE}}$	$\mathbf{L_{hzH}}$
a_{ii}	$\frac{1}{\epsilon\mu_{x+}\Delta x^2}+\frac{1}{\epsilon\mu_{x-}\Delta x^2}+$ $\frac{1}{\epsilon\mu_{y+}\Delta y^2}+\frac{1}{\epsilon\mu_{y-}\Delta y^2}$	$\frac{1}{\mu\epsilon_{x+}\Delta x^2}+\frac{1}{\mu\epsilon_{x-}\Delta x^2}+$ $\frac{1}{\mu\epsilon_{y+}\Delta y^2}+\frac{1}{\mu\epsilon_{y-}\Delta y^2}$
$a_{ij}(i\neq j)$	$-\frac{1}{\epsilon\mu_{x+}\Delta x^2}$ $-\frac{1}{\epsilon\mu_{x-}\Delta x^2}$ $-\frac{1}{\epsilon\mu_{y+}\Delta y^2}$ $-\frac{1}{\epsilon\mu_{y-}\Delta y^2}$	$-\frac{1}{\mu\epsilon_{x+}\Delta x^2}$ $-\frac{1}{\mu\epsilon_{x-}\Delta x^2}$ $-\frac{1}{\mu\epsilon_{y+}\Delta y^2}$ $-\frac{1}{\mu\epsilon_{y-}\Delta y^2}$
$\sum_j \lvert a_{ij}\rvert$	$\frac{2}{\epsilon\mu_{x+}\Delta x^2}+\frac{2}{\epsilon\mu_{x-}\Delta x^2}+$ $\frac{2}{\epsilon\mu_{y+}\Delta y^2}+\frac{2}{\epsilon\mu_{y-}\Delta y^2}$	$\frac{2}{\mu\epsilon_{x+}\Delta x^2}+\frac{2}{\mu\epsilon_{x-}\Delta x^2}+$ $\frac{2}{\mu\epsilon_{y+}\Delta y^2}+\frac{2}{\mu\epsilon_{y-}\Delta y^2}$
$\lVert\underline{\underline{A}}\rVert_{\max}$	$v_{\max}^2(\frac{4}{\Delta x^2}+\frac{4}{\Delta y^2})$	$v_{\max}^2(\frac{4}{\Delta x^2}+\frac{4}{\Delta y^2})$

Now, we have to estimate the norm of operators $\mathbf{L_{ezE}}$, $\mathbf{L_{hzH}}$. We use the following property:

$$\lVert\underline{\underline{A}}\rVert \leq \lVert\underline{\underline{A}}\rVert_{\max} = \max_i \sum_j |a_{ij}| \tag{3.8.25}$$

The above equation shows that we may estimate the norm of an operator via analysis of its nonzero elements. Tab. 3.8.1 shows the nonzero elements of operators $\mathbf{L_{ezE}}$, $\mathbf{L_{hzH}}$ and presents the estimation of their norm maximum. Substituting the results of the analysis from the table and eq. (3.8.13) into (3.8.12), we get:

$$\lVert\mathbf{L_{dt}}\rVert \leq v_{\max}^2\left(\frac{4}{\Delta x^2}+\frac{4}{\Delta y^2}+\beta_z^2\right) \tag{3.8.26}$$

Substituting the above estimation of the norm into (2.2.38), we get the well known stability condition [50]:

$$\Delta t \leq \frac{1}{v_{\max}\sqrt{\frac{1}{\Delta x^2}+\frac{1}{\Delta y^2}+\frac{\beta_z^2}{4}}} \tag{3.8.27}$$

In addition to (3.8.27), β_z must satisfy the following condition:

$$\beta_z^2 \in \mathcal{R} \qquad \wedge \qquad \beta_z^2 \geq 0 \tag{3.8.28}$$

In other words, β_z must be real.

Positiveness of operators in eqs. (3.8.1) and (3.8.2), also required for the stability, is obvious, since each of the terms given by eqs. (3.8.3)–(3.8.8) may be presented as a product of two positive and symmetric operators. Note, that this is always true when the conditions derived in sec. 3.5.1 are satisfied.

3.9 Stability of 3D explicit update schemes

Analogously to the discussion from the previous section, we derive stability conditions for explicit update algorithms written for 3D problems. When testing the norms, we use property (3.8.25) and the norm maximum. We test the norm maximum of operators in eigenproblems (3.4.36), (3.4.37), (3.4.38) and (3.4.39) with $\mathbf{A_e} = \frac{v^2}{\epsilon}$ and $\mathbf{A_m} = \frac{v^2}{\mu}$. As it was said in sec. 3.4.3, these norms maximum are the same as in the case of eigenproblems with unshifted static solutions (eqs. (3.4.28), (3.4.29), (3.4.30) and (3.4.31)). Now, we use the fact that for the highest order modes, the field is concentrated in the area where the wave can propagate at the highest speed (in the unbounded medium) or, in other words, of the maximum value of $1/(\mu\epsilon)$. Therefore, when using expression (3.8.25), we may analyze nonzero elements of the operator only in rows corresponding to this area. The norm maximum, hence, corresponds to a suboperator consisting only of these rows. This radically simplifies the analysis. Tab. 3.9.1 presents the nonzero elements of the operators (they are the same for each matrix). Using these elements, we calculate the norm maximum. From the table and eq. (2.2.38), we get the well known CFL (Courant-Freidrich-Lewy) stability condition [45, 79]:

$$\Delta t \leq \frac{1}{v_{\max}\sqrt{\frac{1}{\Delta x^2} + \frac{1}{\Delta y^2} + \frac{1}{\Delta z^2}}} \tag{3.9.1}$$

As in the 2D case, positiveness of operators in eqs. (3.4.36), (3.4.37), (3.4.38), (3.4.39) is obvious because, as follows from the properties derived in sec. 3.4.1, each of the terms may be expressed as a product of two positive and symmetric operators.

When the domain is lossy, we deal with the explicit update scheme described in sec. 2.2.3.3. In this case, the algorithm must satisfy condition (2.2.43) in order to be stable. We note that operator $\mathbf{L}$ must be symmetric. Although the operators in eqs. (3.4.36), (3.4.37), (3.4.38), (3.4.39) are not symmetric, we may easily symmetrize them by writing equivalent equations. For instance, for eq. (3.4.36) or (3.4.37) upgraded with a term corresponding to losses, we get:

$$\begin{aligned} \mathbf{E}^{-1/2}\mathbf{R_m}\mathbf{M}^{-1}\mathbf{R_e}\mathbf{E}^{-1/2}(\mathbf{E}^{1/2}e) \; &+ \\ \mathbf{E}^{1/2}\mathbf{G_e}\mathbf{A_e}\mathbf{D_e}\mathbf{E}^{1/2}(\mathbf{E}^{1/2}e) \; &= \; \omega^2(\mathbf{E}^{1/2}e) - j\omega\mathbf{E}^{-1/2}\mathbf{S}\mathbf{E}^{-1/2}(\mathbf{E}^{1/2}e) \end{aligned} \tag{3.9.2}$$

Note, that since operator $\mathbf{E}$ is hermitian and positive, operator $\mathbf{E}^{1/2}$ is also hermitian. Now, the operator on the left hand side of the equation is hermitian. The eigenfunctions of (3.9.2) are fields $\mathbf{E}^{1/2}e$. Eqs. (3.4.38) and (3.4.39) may be symmetrized in the same manner, with the eigenfunctions $\mathbf{M}^{1/2}h$. From eq. (3.9.2) it follows, that according to eq. (3.4.36), in order to get a stable algorithm, Δt must satisfy condition (3.9.1) and operators $\mathbf{E}$, $\mathbf{S}$ must have the following property:

$$\mathbf{E}^{-1/2}\mathbf{S}\mathbf{E}^{-1/2} \geq 0 \tag{3.9.3}$$

This means, that both operators, $\mathbf{E}$ and $\mathbf{S}$, must be positive. This is the case in practice, since $\mathbf{E} = \bar{\bar{\epsilon}}$ and $\mathbf{S} = \sigma$.

Table 3.9.1: *Estimation of the norm maximum of 3D operators in eigenproblems with eigenvalues ω^2. Analysis of nonzero elements in row i in the region of the highest value of the speed of wave $v_{\max}$.*

a_{ii}	$v_{\max}^2\left(\frac{2}{\Delta x^2}+\frac{2}{\Delta y^2}+\frac{2}{\Delta z^2}\right)$
$a_{ij}(i\neq j)$	$-v_{\max}^2/\Delta x^2$ $-v_{\max}^2/\Delta x^2$ $-v_{\max}^2/\Delta y^2$ $-v_{\max}^2/\Delta y^2$ $-v_{\max}^2/\Delta z^2$ $-v_{\max}^2/\Delta z^2$
$\sum_j \lvert a_{ij}\rvert$	$v_{\max}^2\left(\frac{4}{\Delta x^2}+\frac{4}{\Delta y^2}+\frac{4}{\Delta z^2}\right)$
$\lvert\lvert\underline{\underline{A}}\rvert\rvert_{\max}$	$4v_{\max}^2\left(\frac{1}{\Delta x^2}+\frac{1}{\Delta y^2}+\frac{1}{\Delta z^2}\right)$

Chapter 4

Local schemes

4.1 Introduction

In secs. 3.6, 3.7 we presented the form of the basic operators in the homogeneous parts of the domain. These forms are valid, when the field variation within the cell is close to linear and the medium does not change within the cell. If this is not the case, the standard expressions have to be modified so as not to introduce the error. In most cases the fundamental assumptions are not fulfilled only for some cells. For these cells one may derive special expressions called local schemes. The local schemes introduce the corrections that are needed to give a more accurate description of Maxwell's equation on a discrete grid. It has to be noted that the grid equations involve a number of basic operators which are applied consecutively. The local schemes can modify some or all operators but this changes should be introduced in such a manner as not to affect the constraints imposed on them, expressed by the properties discussed in the previous chapter. Since the sequence of basic operators defines an appropriate problem, while devising the local scheme one may arbitrarily select one or more operators. In this thesis we propose to base local schemes on the modification of the operators describing the media parameters. This means that the operators corresponding to integral or differential operators are unchanged, i.e. they have the same form as for the regular cells and linear field variations. The modifications are localized in the basic matrices corresponding to material tensors. This implies that for some cells these operators are no longer simply diagonal matrices containing appropriate material constants at the corresponding points. Material matrices have to be modified in order to correctly represent the field behavior in the grid equations with using standard finite-difference operators. A similar technique has been proposed by Gwarek [27, 29] to account for the presence of electric and magnetic walls that do not coincide with mesh points and by Celuch-Marcysiak and Gwarek [10] to handle cells loaded with different media. In this chapter, we derive alternative local schemes for arbitrarily located dielectric boundaries (secs. 4.2, 4.3) and electric walls (secs. 4.4, 4.5). In these cases, the modification of the grid operators corresponding to media are relatively simple. More complicated case, such as modeling of field singularity in the vicinity of conductive wedges is treated in secs. 4.6, 4.7.

4.2 Modeling of interfaces between media in 2D

The first problem which requires an appropriate local scheme is the situation presented in fig. 4.2.1, which depicts a dielectric boundary crossing Yee's cell. Here, it is obvious

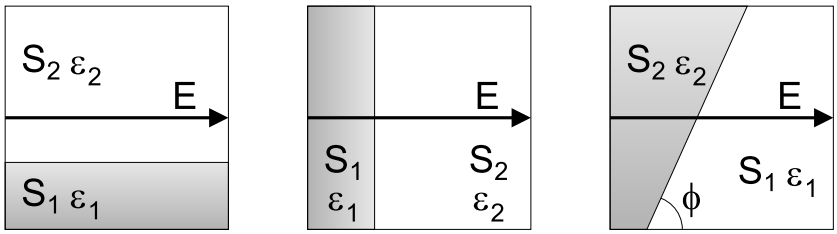

Figure 4.2.1: *Electric field at 2D Yee's cell: parallel (a), normal (b) and at an arbitrary angle with respect to the dielectric boundary (c).*

that the operators which have to be modified have to do with the media properties. This can be accomplished by deriving the effective permittivity for this cell which should be selected in such a way that e.g. the field discontinuities are accounted for. We split the analysis into three parts associated with different location of the boundary with respect to Yee's cell and presented in figs. 4.2.1(a), (b) and (c), namely for boundary parallel, normal and at an arbitrary angle with respect to the vector[1].

Vector parallel to the boundary In order to derive the effective permittivity for the electric fields parallel to the dielectric boundary (fig. 4.2.1(a)), we start from the following definition:

$$\epsilon_{||} = \frac{\tilde{D}_{||}}{\tilde{E}_{||}} \tag{4.2.1}$$

where $\tilde{D}_{||}$ and $\tilde{E}_{||}$ are the mean values of, respectively, electric flux density and intensity fields. Both symbols may be expressed in the integral form. We get:

$$\epsilon_{||} = \frac{\frac{1}{S}\left[\iint_{S_1} \epsilon_1 E_{||} ds + \iint_{S_2} \epsilon_2 E_{||} ds\right]}{\frac{1}{S}\iint_S E_{||} ds} \tag{4.2.2}$$

Since the intensity fields parallel to the boundary are continuous, we may assume that $E_{||}$ is constant in the entire cell:

$$E_{||} = \text{const} \tag{4.2.3}$$

This simplifies eq. (4.2.2), and finally, we get:

$$\epsilon_{||} = \frac{\epsilon_1 S_1 + \epsilon_2 S_2}{S} \tag{4.2.4}$$

This equation defines the effective permittivity for the parallel electric field. Note, that in 2D this is also the effective permittivity for z electric field component, since it is always parallel to the boundary.

[1]It has to be noted that the results of the vectors parallel and normal to the boundary have been earlier obtained by other authors [9, 42]. Their derivation is included here for completeness. Also, some researchers published formulas for oblique interfaces [9, 42], but for that case the approach was different from that presented in this thesis and the final expressions obtained here are different from those published elsewhere.

Vector normal to the boundary Analogously, we derive the effective permittivity for the normal fields (fig. 4.2.1(b)). This time, we start from the following integral formulation:

$$\epsilon_\perp = \frac{\tilde{D}_\perp}{\tilde{E}_\perp} = \frac{\frac{1}{S}\iint_S D_\perp ds}{\frac{1}{S}\left[\iint_{S_1}\frac{1}{\epsilon_1}D_\perp ds + \iint_{S_2}\frac{1}{\epsilon_2}D_\perp ds\right]} \tag{4.2.5}$$

The flux density fields normal to the boundary are continuous. Therefore, we may assume that $D_\perp$ is constant over the entire cell:

$$D_\perp = \text{const} \tag{4.2.6}$$

Putting (4.2.6) into (4.2.5), we get the effective permittivity for the normal electric fields:

$$\epsilon_\perp = \frac{S}{\frac{S_1}{\epsilon_1} + \frac{S_2}{\epsilon_2}} \tag{4.2.7}$$

Vector at an arbitrary angle with respect to the boundary More general case, with the electric vector at an arbitrary angle with respect to the boundary (fig. 4.2.1(c)), requires more sophisticated treatment. We split the normal and parallel fields into x and y components:

$$E_\perp = E_x \sin\phi + E_y \cos\phi \tag{4.2.8}$$
$$E_{||} = -E_x \cos\phi + E_y \sin\phi \tag{4.2.9}$$
$$D_\perp = D_x \sin\phi + D_y \cos\phi \tag{4.2.10}$$
$$D_{||} = -D_x \cos\phi + D_y \sin\phi \tag{4.2.11}$$

And ϕ is the angle between the boundary and x field component. The flux density and intensity fields are related to each other by the following formulae:

$$D_\perp = \epsilon_\perp E_\perp \tag{4.2.12}$$
$$D_{||} = \epsilon_{||} E_{||} \tag{4.2.13}$$

where $\epsilon_\perp$, $\epsilon_{||}$ are defined by eqs. (4.2.7) and (4.2.4) respectively. Putting (4.2.8), (4.2.9), (4.2.10), and (4.2.11) into (4.2.12) and (4.2.13), we get:

$$D_x \cos\phi + D_y \sin\phi = \epsilon_\perp E_x \cos\phi + \epsilon_\perp E_y \sin\phi \tag{4.2.14}$$
$$-D_x \sin\phi + D_y \cos\phi = -\epsilon_{||} E_x \sin\phi + \epsilon_{||} E_y \cos\phi \tag{4.2.15}$$

Relation between the flux density and intensity fields defines the effective permittivity in the form of the following tensor:

$$\begin{aligned}\bar{\bar{\epsilon}}_{tt\,eff} &= \begin{bmatrix}\cos\phi & -\sin\phi \\ \sin\phi & \cos\phi\end{bmatrix}\begin{bmatrix}\epsilon_\perp & 0 \\ 0 & \epsilon_{||}\end{bmatrix}\begin{bmatrix}\cos\phi & \sin\phi \\ -\sin\phi & \cos\phi\end{bmatrix} \\ &= \begin{bmatrix}\epsilon_\perp\cos^2\phi + \epsilon_{||}\sin^2\phi & (\epsilon_\perp - \epsilon_{||})\sin\phi\cos\phi \\ (\epsilon_\perp - \epsilon_{||})\sin\phi\cos\phi & \epsilon_\perp\sin^2\phi + \epsilon_{||}\cos^2\phi\end{bmatrix}\end{aligned} \tag{4.2.16}$$

We may radically simplify the algorithm by ignoring non-diagonal elements of this tensor. This leads to the following effective permittivity for the field component from fig. 4.2.1(c):

$$\epsilon_{eff} = \epsilon_\perp \sin^2\phi + \epsilon_{||}\cos^2\phi \tag{4.2.17}$$

Boundary between magnetics In a similar manner we may calculate the effective permeability:

$$\mu_{eff} = \mu_{\perp} \sin^2 \phi + \mu_{||} \cos^2 \phi \tag{4.2.18}$$

where the effective parallel and normal permeabilities are defined as follows:

$$\mu_{||} = \frac{\mu_1 S_1 + \mu_2 S_2}{S} \tag{4.2.19}$$

$$\mu_{\perp} = \frac{S}{\frac{S_1}{\mu_1} + \frac{S_2}{\mu_2}} \tag{4.2.20}$$

Modification of operators Calculated effective permittivities ϵ_{eff} appear as diagonal elements of matrices $\underline{\underline{E}}_{tt}$ (nodes E_x, E_y) or $\underline{\underline{E}}_{zz}$ (nodes E_z) at the positions corresponding to the modified nodes. Analogously, effective permeabilities μ_{eff} are diagonal elements of matrices $\underline{\underline{M}}_{tt}$ or $\underline{\underline{M}}_{zz}$.

Stability condition of the explicit update schemes We may note that the effective permittivity or permeability derived in this section is always larger than the smallest one. Therefore, the new algorithm does not change the stability condition of the explicit update procedures.

4.3 Modeling of interfaces between media in 3D

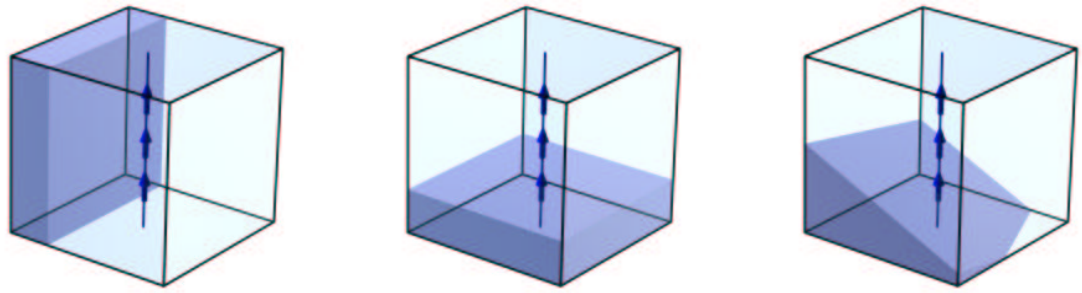

(a) (b) (c)

Figure 4.3.1: *Electric field at 3D Yee's cell: parallel (a), normal (b) and at an arbitrary angle ϕ with respect to the dielectric boundary (c).*

Analogously to the 2D case presented in sec. 4.2, we may derive the effective permittivities and permeabilities for the cells crossed by a boundary between two media. For the fields parallel to the boundary (fig. 4.3.1(a)), we have:

$$\epsilon_{eff||} = \frac{\epsilon_1 V_1 + \epsilon_2 V_2}{V} \tag{4.3.1}$$

$$\mu_{eff||} = \frac{\mu_1 V_1 + \mu_2 V_2}{V} \tag{4.3.2}$$

where V_1, V_2 are volumes of the regions corresponding to medium, respectively, 1 and 2 in the cell. For the fields perpendicular to the boundary (fig. 4.3.1(b)), we have:

$$\epsilon_{eff\perp} = \frac{V}{\frac{V_1}{\epsilon_1} + \frac{V_2}{\epsilon_2}} \tag{4.3.3}$$

$$\mu_{eff\perp} = \frac{V}{\frac{V_1}{\mu_1} + \frac{V_2}{\mu_2}} \tag{4.3.4}$$

In a general case (fig. 4.3.1(c)), the effective material constants may be expressed in terms of two previous pairs of equations:

$$\epsilon_{eff} = \epsilon_{eff||} \cos^2 \phi + \epsilon_{eff\perp} \sin^2 \phi \tag{4.3.5}$$
$$\mu_{eff} = \mu_{eff||} \cos^2 \phi + \mu_{eff\perp} \sin^2 \phi \tag{4.3.6}$$

where ϕ is an angle between the boundary and the direction of the field. The effective material constants calculated this way should be set at the appropriate diagonal positions of matrices $\underline{\underline{E}}$ (for the effective permittivity ϵ_{eff}) and $\underline{\underline{M}}_{tt}$ (for the effective permeability μ_{eff}).

4.4 Modeling of metal boundaries in 2D

In this section, we introduce a technique for a less straightforward problem of accounting for the presence of metal planes that do not coincide with Yee's grid by a suitable local modification of media properties.

Tangential components of the electric intensity field vanish at electric walls. Therefore, if the electric nodes in Yee's mesh coincide with the wall, the modeling of the boundary is reduced to removal of these nodes from the basic operators. This corresponds to setting the appropriate fields to zero. However, in practice the electric wall may be arbitrarily located with respect to the grid. In order to correctly model such a general case, Yee's nodes should be deformed in the vicinity of the boundary, moving the integration paths of the tangential components of the electric intensity field to the wall.

The algorithm presented in this section is similar to the approaches proposed by Gwarek [27] and Railton [63, 65]. Although these methods may be expressed in terms of modification of the basic matrices, they do not satisfy the postulates derived in sec. 3.5.1.

4.4.1 Simple cells

Let us consider the case of a fragment of 2D Yee's grid presented in fig. 4.4.1. Maxwell's grid equations in the integral form for standard node H_z in fig. 4.4.1(a) may be written as follows

$$-j\omega\Delta x\Delta y\mu H_z = \Delta x(E_{x2} - E_{x1}) - \Delta y(E_{y2} - E_{y1}) \tag{4.4.1}$$

Let us now consider the modified node in the neighborhood of the electric wall shown in fig. 4.4.1(b). Note, that nodes E_{x2} and E_{z01}, E_{z11} were moved to the boundary, and hence vanish, since the tangential electric intensity field vanishes at electric wall. Maxwell's grid equations for modified node H_z take up the form

$$-j\omega S_{hz}\mu H_z = \Delta x(0 - E_{x1}) + (\Delta y + a)E_{y1} - (\Delta y + b)E_{y2} \tag{4.4.2}$$

This may be rewritten as follows

$$-j\omega\Delta x\Delta y\left(\mu\frac{S_{hz}}{\Delta x\Delta y}\right)H_z = \Delta x(0 - E_{x1}) - \Delta y(E'_{y2} - E'_{y1}) \tag{4.4.3}$$

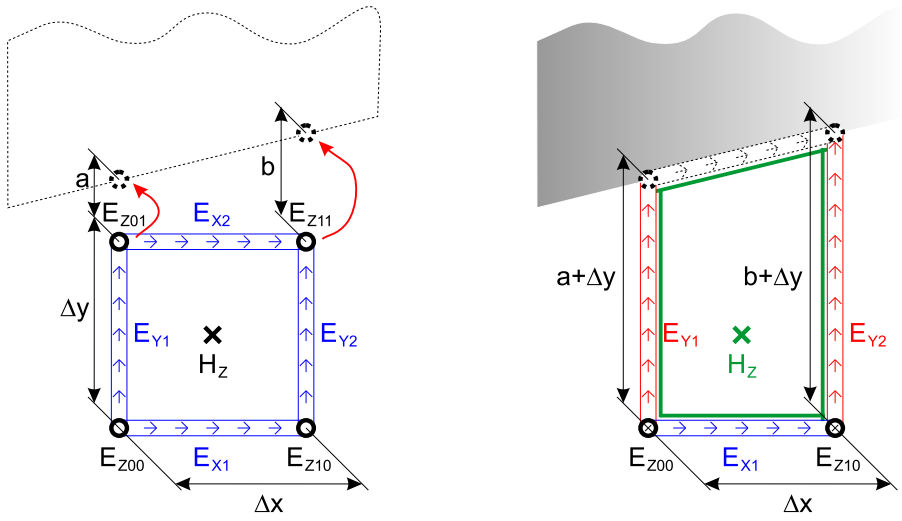

Figure 4.4.1: *Nodes E_x and E_y in the vicinity of an electric wall in the finite difference algorithm before (a) and after (b) modification.*

where fields E'_{y1}, E'_{y2} are related to E_{y1}, E_{y2} by the following formulae

$$E'_{y1} = \frac{\Delta y + a}{\Delta y} E_{y1} = \left(\frac{1}{\epsilon}\frac{\Delta y + a}{\Delta y}\right) D_{y1} \tag{4.4.4}$$

$$E'_{y2} = \frac{\Delta y + b}{\Delta y} E_{y2} = \left(\frac{1}{\epsilon}\frac{\Delta y + b}{\Delta y}\right) D_{y2} \tag{4.4.5}$$

Let us note, that introducing quantities E'_{y1}, E'_{y2} instead of E_{y1}, E_{y2} to vector $\underline{e}_t$, we do not modify matrices $\underline{\underline{D}}_{te}$, $\underline{\underline{G}}_{te}$. We modify only the corresponding diagonal elements of matrix $\underline{\underline{E}}_{tt}$. Comparing eq. (4.4.3) with (4.4.1) we see that the deformation of node H_z may be realized by introducing effective permeability at this node and effective permittivities at the corresponding nodes E_{y1} and E_{y2}. The effective permeability is given by the following equation

$$\mu_{zzeff} = \mu \frac{S_{hz}}{\Delta x \Delta y} \tag{4.4.6}$$

and this value should be set at the corresponding diagonal element in matrix $\underline{\underline{M}}_{zz}$. From eqs. (4.4.4) and (4.4.5) it follows that the effective permittivities corresponding to nodes E_{y1} and E_{y2} have the form

$$\epsilon_{yyeff1} = \epsilon \frac{\Delta y}{\Delta y + a} \tag{4.4.7}$$

$$\epsilon_{yyeff2} = \epsilon \frac{\Delta y}{\Delta y + b} \tag{4.4.8}$$

These values will appear at appropriate places at the main diagonal of matrix $\underline{\underline{E}}_{tt}$.

As shown in sec. 3.6 the integration paths for fields E_y and B_x in the integral interpretation of the grid equations are the same (see fig. 4.4.2). Therefore, we also need to modify the equations for the transverse magnetic fields. By introducing quantity B'_x instead of B_x into vector $\underline{b}_t$, we guarantee that operators $\underline{\underline{D}}_{tm}$, $\underline{\underline{G}}_{tm}$ have the standard form. B'_x is

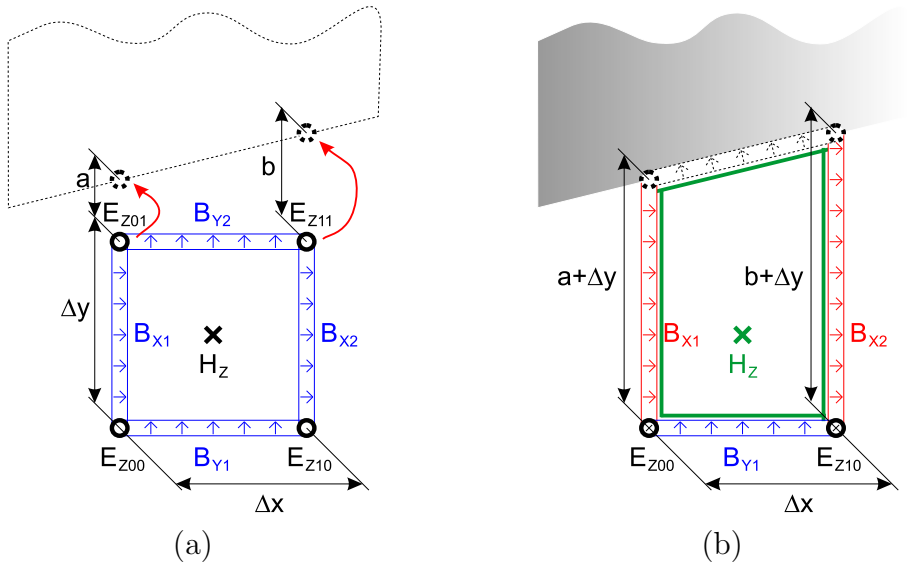

Figure 4.4.2: *Nodes B_x and B_y in the vicinity of an electric wall in the finite difference algorithm before (a) and after (b) modification. Compare with fig. 4.4.1.*

related to B_x as follows

$$B'_x = \frac{\Delta y + a}{\Delta y} B_x = \left(\mu \frac{\Delta y + a}{\Delta y} \right) H_x \tag{4.4.9}$$

This leads to the following effective permeability at node B_{x1}

$$\mu_{xxeff1} = \mu \frac{\Delta y + a}{\Delta y} \tag{4.4.10}$$

Analogously for node B_{x2} we have:

$$\mu_{xxeff2} = \mu \frac{\Delta y + b}{\Delta y} \tag{4.4.11}$$

These effective permeabilities are appropriate diagonal elements of matrix $\underline{\underline{M}}_{tt}$.

4.4.2 General cells

In the previous section, we presented a simple cell in the vicinity of the boundary. However, definition of such cell does not cover all possible situations. Figs. 4.4.3 and 4.4.4 present a more general case. Here, we have node H_{z22} but the other H field (H_{z12}) required for updating field E_{y12} does not exist. Therefore, we should modify the algorithm. As shown in fig. 4.4.3(a), instead of node E_{y12}, we introduce virtual node E_v. Let us write discretized Maxwell's equations for electric flux density nodes D_{y11}, D_v, D_{x21}:

$$j\omega \Delta x D_{y11} = -(H_{z21} - H_{z11}) \tag{4.4.12}$$

$$j\omega S_v D_v = -(H_{z22} - H_{z12}) \tag{4.4.13}$$

$$j\omega \Delta y D_{x21} = (H_{z22} - H_{z21}) \tag{4.4.14}$$

Node H_{z12} appearing in (4.4.13) does not exist. We assume that the magnetic field is constant over the new larger cell H_{z11} and copy H_{z11} to H_{z12}:

$$H_{z12} = H_{z11} \tag{4.4.15}$$

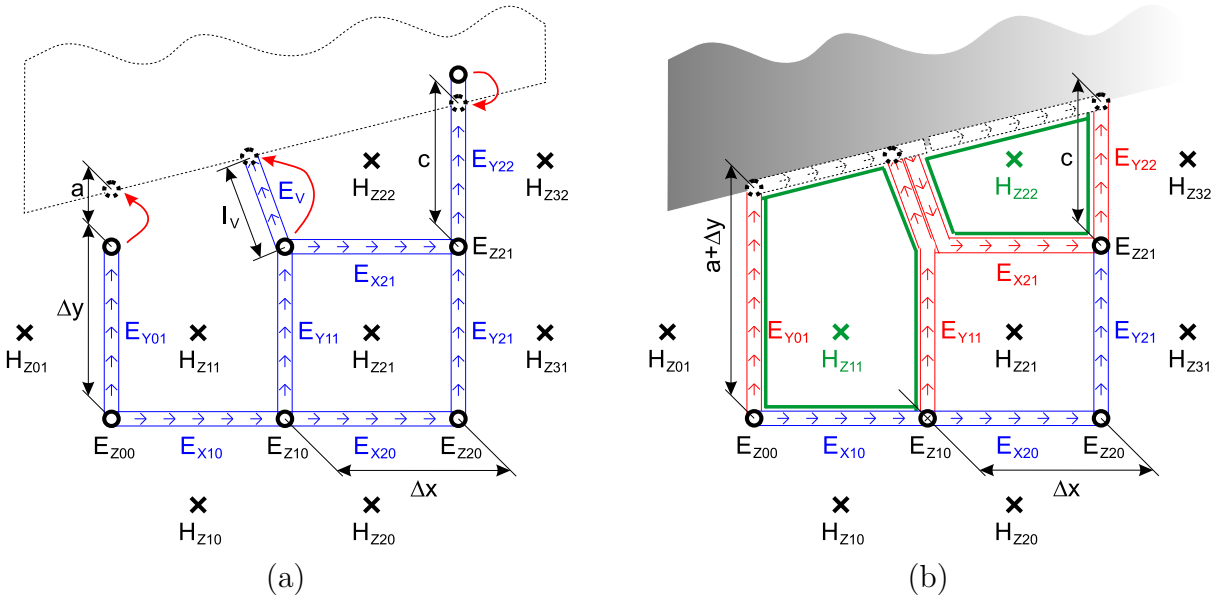

Figure 4.4.3: *Nodes E_x and E_y in the vicinity of an electric wall in the finite difference algorithm before (a) and after (b) modification.*

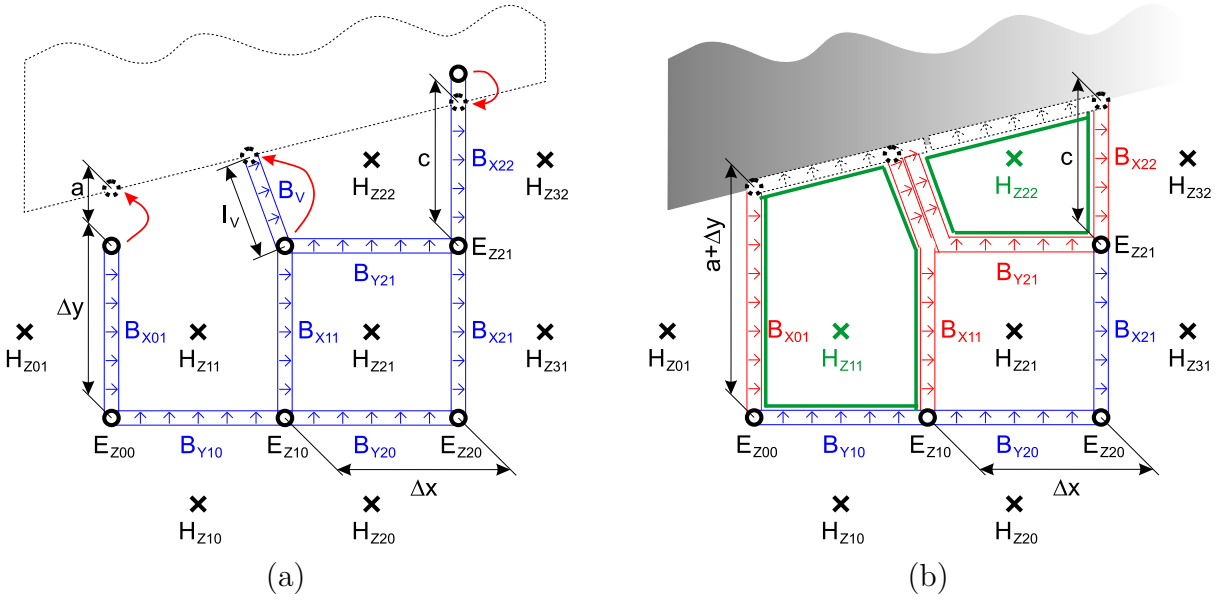

Figure 4.4.4: *Nodes B_x and B_y in the vicinity of an electric wall in the finite difference algorithm before (a) and after (b) modification. Compare with fig. 4.4.3.*

Eq. (4.4.13) takes up the form:

$$j\omega S_v D_v = -(H_{z22} - H_{z11}) \tag{4.4.16}$$

As fig. 4.4.3(b) shows, we want to remove node E_v (D_v). The information about field D_v will not be lost, however, since we may calculate it from (4.4.12) and (4.4.14):

$$\begin{aligned} j\omega S_v D_v &= -(H_{z22} - H_{z21}) - (H_{z21} - H_{z11}) \\ &= -j\omega\Delta y D_{x21} + j\omega\Delta x D_{y11} \end{aligned} \tag{4.4.17}$$

Dividing both sides by $j\omega S_v$, we get:

$$D_v = \frac{\Delta x}{S_v} D_{y11} - \frac{\Delta y}{S_v} D_{x21} \tag{4.4.18}$$

Let us write discretized Maxwell's equations for nodes H_{z11}, H_{z21}, H_{z22} for the situation from fig. 4.4.3(b):

$$-j\omega\mu_{zz11} S_{hz11} H_{z11} = \Delta y E_{y11} + l_v E_v - (\Delta y + a) E_{y01} + \Delta x E_{x10} \tag{4.4.19}$$

$$-j\omega\mu_{zz21}\Delta x\Delta y H_{z21} = \Delta y E_{y21} - \Delta x E_{x21} - \Delta y E_{y11} + \Delta x E_{x20} \tag{4.4.20}$$

$$-j\omega\mu_{zz22} S_{hz22} H_{z22} = c E_{y22} - l_v E_v + \Delta x E'_{x21} \tag{4.4.21}$$

The equations above use modified integration paths. We may also write these equations with the standard integration paths. The modification will be then introduced into effective material constants. The standard equations may be written as follows:

$$-j\omega\mu'_{zz11}\Delta x\Delta y H_{z11} = \Delta y E'_{y11} - \Delta y E'_{y01} + \Delta x E_{x10} \tag{4.4.22}$$

$$-j\omega\mu_{zz21}\Delta x\Delta y H_{z21} = \Delta y E_{y21} - \Delta x E'_{x21} - \Delta y E'_{y11} + \Delta x E_{x20} \tag{4.4.23}$$

$$-j\omega\mu'_{zz22}\Delta x\Delta y H_{z22} = \Delta y E'_{y22} + \Delta x E'_{x21} \tag{4.4.24}$$

Comparing (4.4.19)–(4.4.21) with (4.4.22)–(4.4.24), we get a set of new quantities:

$$\mu'_{zz11} = \mu_{zz11} \frac{S_{hz11}}{\Delta x\Delta y} \tag{4.4.25}$$

$$\mu'_{zz22} = \mu_{zz22} \frac{S_{hz22}}{\Delta x\Delta y} \tag{4.4.26}$$

and

$$E'_{y01} = \frac{\Delta y + a}{\Delta y} E_{y01} \tag{4.4.27}$$

$$E'_{y22} = \frac{c}{\Delta y} E_{y22} \tag{4.4.28}$$

According to the discussion from sec. 4.4.1, eqs. (4.4.27), (4.4.28) lead to the following effective permittivieties for nodes E_{y01} E_{y22}:

$$\epsilon'_{yy01} = \epsilon_{yy01} \frac{\Delta y}{\Delta y + a} \tag{4.4.29}$$

$$\epsilon'_{yy22} = \epsilon_{yy22} \frac{\Delta y}{c} \tag{4.4.30}$$

Moreover, from (4.4.19)–(4.4.24), we get:

$$E'_{y11} = E_{y11} + \frac{l_v}{\Delta y} E_v \tag{4.4.31}$$

$$E'_{x21} = E_{x21} - \frac{l_v}{\Delta x} E_v \tag{4.4.32}$$

$$\Delta x E'_{x21} + \Delta y E'_{y11} = \Delta x E_{x21} + \Delta y E_{y11} \tag{4.4.33}$$

It is clearly seen that quantities E'_{y11} and E'_{x21} defined by eqs. (4.4.31) and (4.4.32) satisfy also eq. (4.4.33). Expressing the right hand side of eq. (4.4.31) in terms of the flux density fields, we get:

$$E'_{y11} = \frac{1}{\epsilon_{yy11}} D_{y11} + \frac{l_v}{\Delta y} \frac{1}{\epsilon_v} D_v \tag{4.4.34}$$

Using (4.4.18), we get:

$$\begin{aligned} E'_{y11} &= \frac{1}{\epsilon_{yy11}} D_{y11} + \frac{l_v}{\Delta y} \frac{1}{\epsilon_v} \left(\frac{\Delta x}{S_v} D_{y11} - \frac{\Delta y}{S_v} D_{x21} \right) \\ &= \left(\frac{1}{\epsilon_{yy11}} + \frac{\Delta x}{\Delta y} \frac{l_v}{S_v} \frac{1}{\epsilon_v} \right) D_{y11} - \frac{l_v}{S_v} \frac{1}{\epsilon_v} D_{x21} \end{aligned} \tag{4.4.35}$$

In a similar manner we develop an expression for E'_{x21} starting from (4.4.32) and using (4.4.13) and (4.4.18):

$$\begin{aligned} E'_{x21} &= \frac{1}{\epsilon_{xx21}} D_{x21} - \frac{l_v}{\Delta x} \frac{1}{\epsilon_v} D_v \\ &= \frac{1}{\epsilon_{xx21}} D_{x21} - \frac{l_v}{\Delta x} \frac{1}{\epsilon_v} \left(\frac{\Delta x}{S_v} D_{y11} - \frac{\Delta y}{S_v} D_{x21} \right) \\ &= \left(\frac{1}{\epsilon_{xx21}} + \frac{\Delta y}{\Delta x} \frac{l_v}{S_v} \frac{1}{\epsilon_v} \right) D_{x21} - \frac{l_v}{S_v} \frac{1}{\epsilon_v} D_{y11} \end{aligned} \tag{4.4.36}$$

Eqs. (4.4.35), (4.4.36) may be expressed in a matrix form as follows:

$$\begin{bmatrix} E'_{x21} \\ E'_{y11} \end{bmatrix} = \begin{bmatrix} \frac{1}{\epsilon_{xx21}} + \frac{\Delta y}{\Delta x} \frac{l_v}{S_v} \frac{1}{\epsilon_v} & -\frac{l_v}{S_v} \frac{1}{\epsilon_v} \\ -\frac{l_v}{S_v} \frac{1}{\epsilon_v} & \frac{1}{\epsilon_{yy11}} + \frac{\Delta x}{\Delta y} \frac{l_v}{S_v} \frac{1}{\epsilon_v} \end{bmatrix} \begin{bmatrix} D_{x21} \\ D_{y11} \end{bmatrix} \tag{4.4.37}$$

Matrix in (4.4.37) defines a part of matrix $\underline{\underline{E}}_{tt}$ (or $\underline{\underline{E}}_{tt}^{-1}$) corresponding to nodes D_{x21}, D_{y11}. Note that the matrix is nondiagonal, but it is symmetric and, hence, satisfies postulates (3.5.20), (3.5.22).

Local anisotropy associated with nondiagonal elements of matrix $\underline{\underline{E}}_{tt}^{-1}$ complicates inversion of this matrix. Note, that for a diagonal matrix, the inversion is equivalent to inversion of its diagonal elements. However, we may exclude 2×2 submatrices[2] of the form from eq. (4.4.37) from the global operator. Inversion of operator[3] $\underline{\underline{E}}_{tt}^{-1}$ requires, hence, inversion of all submatrices associated with the general cells. This is a simple operation of a low numerical cost, since the submatrices are small[4].

[2] In sec. 4.4.3, we deal with corner cells which lead to 3×3 submatrices.

[3] and, analogously, operator $\underline{\underline{M}}_{tt}$.

[4] An analogous discussion may be performed for calculation of operator $\underline{\underline{E}}_{tt}^{1/2}$ ($\underline{\underline{M}}_{tt}^{1/2}$) which may be required for a symmetrization of some problems in a manner analogous to eq. (3.9.2) written for 3D.

We may perform an analogous analysis for fields B_{x11}, B_{y21} from fig. 4.4.4. All the equations will be dual to the equations presented above according to the duality relations developed in app. A.3.1. Finally, we get the following relation between fields B'_{x11}, B'_{y21} and H_{x11}, H_{y21}:

$$\begin{bmatrix} B'_{x11} \\ B'_{y21} \end{bmatrix} = \begin{bmatrix} \mu_{xx11} + \frac{\Delta x}{\Delta y}\frac{l_v}{S_v}\mu_v & \frac{l_v}{S_v}\mu_v \\ \frac{l_v}{S_v}\mu_v & \mu_{yy21} + \frac{\Delta y}{\Delta x}\frac{l_v}{S_v}\mu_v \end{bmatrix} \begin{bmatrix} H_{x11} \\ H_{y21} \end{bmatrix} \tag{4.4.38}$$

We may now write a relation between all flux density and intensity fields from figs. 4.4.3 and 4.4.4 in a form of matrix equations. We assume that the domain is homogeneous.

$$\begin{bmatrix} E_{x10} \\ E_{x20} \\ E'_{x21} \\ E'_{y01} \\ E'_{y11} \\ E_{y21} \\ E'_{y22} \end{bmatrix} = \frac{1}{\epsilon} \begin{bmatrix} 1 & 0 & 0 & 0 & 0 & 0 & 0 \\ 0 & 1 & 0 & 0 & 0 & 0 & 0 \\ 0 & 0 & 1 + \frac{\Delta y}{\Delta x}\frac{l_v}{S_v} & 0 & -\frac{l_v}{S_v} & 0 & 0 \\ 0 & 0 & 0 & \frac{\Delta y + a}{\Delta y} & 0 & 0 & 0 \\ 0 & 0 & -\frac{l_v}{S_v} & 0 & 1 + \frac{\Delta x}{\Delta y}\frac{l_v}{S_v} & 0 & 0 \\ 0 & 0 & 0 & 0 & 0 & 1 & 0 \\ 0 & 0 & 0 & 0 & 0 & 0 & \frac{c}{\Delta y} \end{bmatrix} \begin{bmatrix} D_{x10} \\ D_{x20} \\ D_{x21} \\ D_{y01} \\ D_{y11} \\ D_{y21} \\ D_{y22} \end{bmatrix} \tag{4.4.39}$$

$$\begin{bmatrix} B'_{x01} \\ B'_{x11} \\ B_{x21} \\ B'_{x22} \\ B_{y10} \\ B_{y20} \\ B'_{y21} \end{bmatrix} = \mu \begin{bmatrix} \frac{\Delta y + a}{\Delta y} & 0 & 0 & 0 & 0 & 0 & 0 \\ 0 & 1 + \frac{\Delta x}{\Delta y}\frac{l_v}{S_v} & 0 & 0 & 0 & 0 & \frac{l_v}{S_v} \\ 0 & 0 & 1 & 0 & 0 & 0 & 0 \\ 0 & 0 & 0 & \frac{c}{\Delta y} & 0 & 0 & 0 \\ 0 & 0 & 0 & 0 & 1 & 0 & 0 \\ 0 & 0 & 0 & 0 & 0 & 1 & 0 \\ 0 & \frac{l_v}{S_v} & 0 & 0 & 0 & 0 & 1 + \frac{\Delta y}{\Delta x}\frac{l_v}{S_v} \end{bmatrix} \begin{bmatrix} H_{x01} \\ H_{x11} \\ H_{x21} \\ H_{x22} \\ H_{y10} \\ H_{y20} \\ H_{y21} \end{bmatrix} \tag{4.4.40}$$

Operators in (4.4.39), (4.4.40) are parts of, respectively, global matrices $\underline{\underline{E}}^{-1}_{tt}$ and $\underline{\underline{M}}_{tt}$ corresponding to the nodes from the figure. It is clearly seen, that these operators satisfy condition (3.5.27) for homogeneous domains.

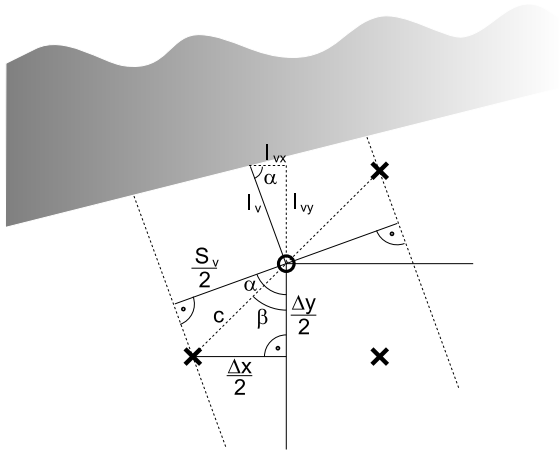

Figure 4.4.5: *Calculation of factor $\frac{l_v}{S_v}$. l_v is the shortest path from the removed e_z cell to the metal. Path S_v is perpendicular to l_v.*

Finding factor $\frac{l_v}{S_v}$ We have not said anything yet about the choice of parameters l_v and S_v. Fig. 4.4.5 will help us to find them. Parameter l_v should be the shortest path

from the removed e_z cell (in our case cell E_{z11}) to the metal. Parameter S_v should be the length of the line perpendicular to l_v connecting two lines parallel to l_v and crossing h_z cells used for update of D_v (in our case nodes H_{z11}, H_{z22} from fig. 4.4.3) as shown in fig. 4.4.5. Let us now find the actual value of factor $\frac{l_v}{S_v}$. Analyzing the figure, we get:

$$\begin{aligned} \frac{S_v}{2c} &= \cos(\alpha - \beta) \\ &= \cos\alpha\cos\beta + \sin\alpha\sin\beta \end{aligned} \tag{4.4.41}$$

We calculate sines and cosines also from the figure:

$$\cos\alpha = \frac{l_{vx}}{l_v} \tag{4.4.42}$$

$$\sin\alpha = \frac{l_{vy}}{l_v} \tag{4.4.43}$$

$$\cos\beta = \frac{\Delta y}{2c} \tag{4.4.44}$$

$$\sin\beta = \frac{\Delta x}{2c} \tag{4.4.45}$$

Putting the above equations into (4.4.41), we get:

$$\frac{S_v}{2c} = \frac{\Delta y l_{vx}}{2cl_v} + \frac{\Delta x l_{vy}}{2cl_v} \tag{4.4.46}$$

This leads to the following expression for $\frac{l_v}{S_v}$:

$$\frac{l_v}{S_v} = \frac{l_v^2}{\Delta y l_{vx} + \Delta x l_{vy}} \tag{4.4.47}$$

4.4.3 Corner cells

Analogously, we may derive a local scheme for a corner cell presented, before modification, in fig. 4.4.6 and, after modification, in fig. 4.4.7. We define submatrix $\underline{\underline{E}}_{tt}^{-1}$ using the following relation between three electric intensity cells and the corresponding flux density cells from fig. 4.4.7:

$$\begin{bmatrix} E'_{x21} \\ E'_{y11} \\ E'_{y21} \end{bmatrix} = \underline{\underline{E}}_{tt}^{-1} \begin{bmatrix} D_{x21} \\ D_{y11} \\ D_{y21} \end{bmatrix} \tag{4.4.48}$$

Submatrix $\underline{\underline{E}}_{tt}^{-1}$ is defined as follows:

$$\underline{\underline{E}}_{tt}^{-1} = \begin{bmatrix} \frac{1}{\epsilon_{xx21}} + \frac{\Delta y}{\Delta x}\left(\frac{l_{v1}}{S_{v1}}\frac{1}{\epsilon_{v1}} + \frac{l_{v2}}{S_{v2}}\frac{1}{\epsilon_{v2}}\right) & -\frac{l_{v1}}{S_{v1}}\frac{1}{\epsilon_{v1}} & \frac{l_{v2}}{S_{v2}}\frac{1}{\epsilon_{v2}} \\ -\frac{l_{v1}}{S_{v1}}\frac{1}{\epsilon_{v1}} & \frac{1}{\epsilon_{yy11}} + \frac{\Delta x}{\Delta y}\frac{l_{v1}}{S_{v1}}\frac{1}{\epsilon_{v1}} & 0 \\ \frac{l_{v2}}{S_{v2}}\frac{1}{\epsilon_{v2}} & 0 & \frac{1}{\epsilon_{yy21}} + \frac{\Delta x}{\Delta y}\frac{l_{v2}}{S_{v2}}\frac{1}{\epsilon_{v2}} \end{bmatrix} \tag{4.4.49}$$

Analogously, we define submatrix $\underline{\underline{M}}_{tt}$ (see figs. 4.4.8, 4.4.9):

$$\begin{bmatrix} B'_{x11} \\ B'_{x21} \\ B'_{y21} \end{bmatrix} = \underline{\underline{M}}_{tt} \begin{bmatrix} H_{x11} \\ H_{x21} \\ H_{y21} \end{bmatrix} \tag{4.4.50}$$

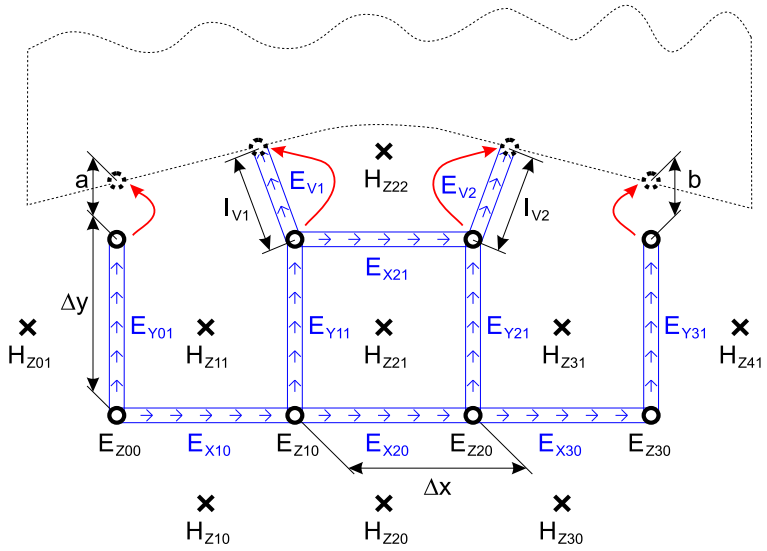

Figure 4.4.6: *Nodes E_x and E_y in the vicinity of an electric wall corner in the finite difference algorithm before modification.*

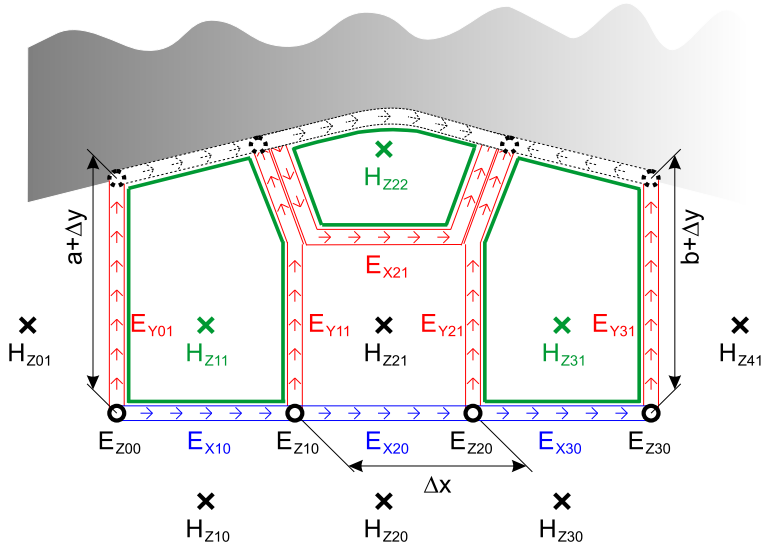

Figure 4.4.7: *Nodes E_x and E_y in the vicinity of an electric wall corner in the finite difference algorithm after modification.*

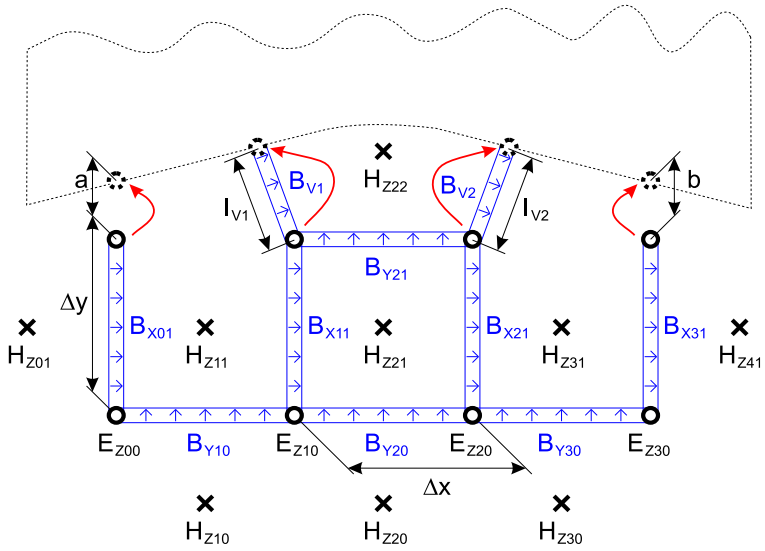

Figure 4.4.8: *Nodes B_x and B_y in the vicinity of an electric wall corner in the finite difference algorithm before modification.*

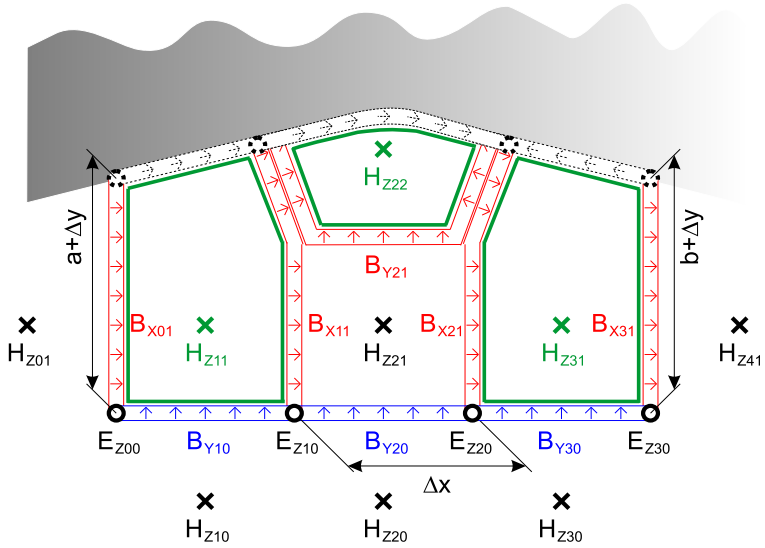

Figure 4.4.9: *Nodes B_x and B_y in the vicinity of an electric wall corner in the finite difference algorithm after modification.*

$\underline{\underline{M}}_{tt}$ may be written in the following way:

$$\underline{\underline{M}}_{tt} = \begin{bmatrix} \mu_{xx11} + \frac{\Delta x}{\Delta y}\frac{l_{v1}}{S_{v1}}\mu_{v1} & 0 & \frac{l_{v1}}{S_{v1}}\mu_{v1} \\ 0 & \mu_{xx21} + \frac{\Delta x}{\Delta y}\frac{l_{v2}}{S_{v2}}\mu_{v2} & -\frac{l_{v2}}{S_{v2}}\mu_{v2} \\ \frac{l_{v1}}{S_{v1}}\mu_{v1} & -\frac{l_{v2}}{S_{v2}}\mu_{v2} & \mu_{yy21} + \frac{\Delta y}{\Delta x}\left(\frac{l_{v1}}{S_{v1}}\mu_{v1} + \frac{l_{v2}}{S_{v2}}\mu_{v2}\right) \end{bmatrix} \tag{4.4.51}$$

4.4.4 Stability condition for the explicit update schemes

For an explicit update scheme to remain stable, the modification of the basic operators cannot change positiveness and norm maximum of the global matrix[5]. In sec. 3.8, we showed that it is enough to test properties of operators $\mathbf{L_{ezE}}$ and $\mathbf{L_{hzH}}$ defined by, respectively, eqs. (3.8.22) and (3.8.23), to get the stability condition. Let us construct these operators for the nodes from figs. 4.4.3, 4.4.4. They are expressed in terms of basic matrices, and hence, we have to define them. The basic matrices will operate on the following vectors:

$$\underline{e}_t = \begin{bmatrix} E_{x10} \\ E_{x20} \\ E_{x21} \\ E_{y01} \\ E_{y11} \\ E_{y21} \\ E_{y22} \end{bmatrix}, \quad \underline{e}_z = \begin{bmatrix} E_{z0-1} \\ E_{z1-1} \\ E_{z2-1} \\ E_{z-10} \\ \mathbf{E_{z00}} \\ \mathbf{E_{z10}} \\ \mathbf{E_{z20}} \\ E_{z30} \\ \mathbf{E_{z21}} \\ E_{z31} \end{bmatrix}, \quad \underline{h}_t = \begin{bmatrix} H_{x01} \\ H_{x11} \\ H_{x21} \\ H_{x22} \\ H_{y10} \\ H_{y20} \\ H_{y21} \end{bmatrix}, \quad \underline{h}_z = \begin{bmatrix} H_{z10} \\ H_{z20} \\ H_{z01} \\ \mathbf{H_{z11}} \\ \mathbf{H_{z21}} \\ H_{z31} \\ \mathbf{H_{z22}} \\ H_{z32} \end{bmatrix} \tag{4.4.52}$$

Operators $\underline{\underline{G}}_{tm}$, $\underline{\underline{D}}_{tm}$, $\underline{\underline{G}}_{te}$, $\underline{\underline{D}}_{te}$ may be written as follows:

$$\underline{\underline{G}}_{tm} = \begin{bmatrix} 0 & 0 & -x & x & 0 & 0 & 0 & 0 \\ 0 & 0 & 0 & -x & x & 0 & 0 & 0 \\ 0 & 0 & 0 & 0 & -x & x & 0 & 0 \\ 0 & 0 & 0 & 0 & 0 & 0 & -x & x \\ -y & 0 & 0 & y & 0 & 0 & 0 & 0 \\ 0 & -y & 0 & 0 & y & 0 & 0 & 0 \\ 0 & 0 & 0 & 0 & -y & 0 & y & 0 \end{bmatrix} \tag{4.4.53}$$

$$\underline{\underline{D}}_{tm} = \begin{bmatrix} -x & x & 0 & 0 & -y & 0 & 0 \\ 0 & -x & x & 0 & 0 & -y & y \\ 0 & 0 & 0 & x & 0 & 0 & -y \end{bmatrix} \tag{4.4.54}$$

[5]We assume, that conditions derived in sec. 3.5.1 concerning symmetry are satisfied. It is true in our case, since modified matrices $\underline{\underline{E}}_{tt}^{-1}$, $\underline{\underline{M}}_{tt}$ are symmetric.

$$\underline{\underline{G}}_{te} = \begin{bmatrix} x & 0 & 0 & 0 & -x & 0 & 0 & 0 & 0 & 0 \\ -x & x & 0 & 0 & 0 & 0 & 0 & 0 & 0 & 0 \\ 0 & -x & x & 0 & 0 & 0 & 0 & 0 & 0 & 0 \\ 0 & 0 & -x & 0 & 0 & 0 & 0 & 0 & x & 0 \\ 0 & 0 & 0 & x & 0 & 0 & 0 & 0 & 0 & 0 \\ 0 & 0 & 0 & -x & 0 & 0 & 0 & 0 & 0 & x \\ y & 0 & 0 & 0 & 0 & -y & 0 & 0 & 0 & 0 \\ 0 & y & 0 & 0 & 0 & 0 & -y & 0 & 0 & 0 \\ 0 & 0 & y & 0 & 0 & 0 & 0 & -y & 0 & 0 \\ -y & 0 & 0 & 0 & 0 & 0 & 0 & 0 & 0 & 0 \\ 0 & -y & 0 & 0 & 0 & 0 & 0 & 0 & 0 & 0 \\ 0 & 0 & -y & y & 0 & 0 & 0 & 0 & 0 & 0 \\ 0 & 0 & 0 & -y & 0 & 0 & 0 & 0 & 0 & 0 \end{bmatrix} \tag{4.4.55}$$

$$\underline{\underline{D}}_{te} = \begin{bmatrix} -x & x & 0 & 0 & 0 & 0 & -y & 0 & 0 & y & 0 & 0 & 0 \\ 0 & -x & x & 0 & 0 & 0 & 0 & -y & 0 & 0 & y & 0 & 0 \\ 0 & 0 & -x & x & 0 & 0 & 0 & 0 & -y & 0 & 0 & y & 0 \\ 0 & 0 & 0 & 0 & -x & x & 0 & 0 & 0 & 0 & 0 & -y & y \end{bmatrix} \tag{4.4.56}$$

where $x = 1/\Delta x$, $y = 1/\Delta y$. Matrices $\underline{\underline{Z}}_e$, $\underline{\underline{Z}}_m$ have the following form:

$$\underline{\underline{Z}}_e = \begin{bmatrix} 0 & 0 & 0 & -1 & 0 & 0 & 0 \\ 0 & 0 & 0 & 0 & -1 & 0 & 0 \\ 0 & 0 & 0 & 0 & 0 & -1 & 0 \\ 0 & 0 & 0 & 0 & 0 & 0 & -1 \\ 0 & 0 & 0 & 0 & 0 & 0 & 0 \\ 1 & 0 & 0 & 0 & 0 & 0 & 0 \\ 0 & 1 & 0 & 0 & 0 & 0 & 0 \\ 0 & 0 & 1 & 0 & 0 & 0 & 0 \end{bmatrix}, \quad \underline{\underline{Z}}_m = \begin{bmatrix} 0 & 0 & 0 & 0 & -1 & 0 & 0 \\ 0 & 0 & 0 & 0 & 0 & -1 & 0 \\ 0 & 0 & 0 & 0 & 0 & 0 & -1 \\ 0 & 0 & 0 & 0 & 0 & 0 & 0 \\ 1 & 0 & 0 & 0 & 0 & 0 & 0 \\ 0 & 1 & 0 & 0 & 0 & 0 & 0 \\ 0 & 0 & 1 & 0 & 0 & 0 & 0 \\ 0 & 0 & 0 & 1 & 0 & 0 & 0 \end{bmatrix} \tag{4.4.57}$$

Using eqs. (3.8.22), (3.8.23) and the basic matrices defined above, we construct operators $\mathbf{L_{ezE}}$ and $\mathbf{L_{hzH}}$. Analogously to the discussion from sec. 3.8, we estimate the norm maximum of these operators and test their definiteness. The results of the analysis are shown in tab. 4.4.1 for operator $\mathbf{L_{hzH}}$ and in tab 4.4.2 for operator $\mathbf{L_{ezE}}$. By comparing the norm maximum of the operators from tabs. 4.4.1, 4.4.2 with the norm from tab. 3.8.1 we can see that stability condition (3.8.27) will not change if the following conditions are satisfied:

$$\frac{1}{\mu\epsilon}\frac{\Delta x\Delta y}{S_{hz11}}\left[\frac{2}{\Delta y^2}+\frac{2}{\Delta x^2}\left(2+\frac{a}{\Delta y}+\frac{\Delta x}{\Delta y}\frac{l_v}{S_v}\right)\right] \leq \frac{4}{\mu\epsilon}\left(\frac{1}{\Delta x^2}+\frac{1}{\Delta y^2}\right) \tag{4.4.58}$$

$$\frac{1}{\mu\epsilon}\frac{\Delta x\Delta y}{S_{hz22}}\left[\frac{2}{\Delta x^2}\left(\frac{c}{\Delta y}+\frac{\Delta x}{\Delta y}\frac{l_v}{S_v}\right)+\frac{2}{\Delta y^2}\right] \leq \frac{4}{\mu\epsilon}\left(\frac{1}{\Delta x^2}+\frac{1}{\Delta y^2}\right) \tag{4.4.59}$$

$$\frac{4}{\mu\epsilon\Delta x^2}+\frac{1}{\mu\epsilon\Delta x^2}\left(2+\frac{\Delta y}{\Delta y+a}\right) \leq \frac{4}{\mu\epsilon}\left(\frac{1}{\Delta x^2}+\frac{1}{\Delta y^2}\right) \tag{4.4.60}$$

$$\frac{4}{\mu\epsilon\Delta x^2}+\frac{2}{\mu\epsilon\Delta y^2}+\frac{1}{\mu\epsilon\Delta y^2}\frac{1+2\frac{\Delta y}{\Delta x}\frac{l_v}{S_v}}{1+(\frac{\Delta x}{\Delta y}+\frac{\Delta y}{\Delta x})\frac{l_v}{S_v}} \leq \frac{4}{\mu\epsilon}\left(\frac{1}{\Delta x^2}+\frac{1}{\Delta y^2}\right) \tag{4.4.61}$$

$$\frac{1}{\mu\epsilon\Delta x^2}\frac{1+2\frac{\Delta x}{\Delta y}\frac{l_v}{S_v}}{1+(\frac{\Delta x}{\Delta y}+\frac{\Delta y}{\Delta x})\frac{l_v}{S_v}}+\frac{2}{\mu\epsilon\Delta x^2}+\frac{2}{\mu\epsilon\Delta y^2} + \frac{1}{\mu\epsilon\Delta y^2}\frac{\Delta y}{c} \leq \frac{4}{\mu\epsilon}\left(\frac{1}{\Delta x^2}+\frac{1}{\Delta y^2}\right) \tag{4.4.62}$$

Table 4.4.1: *Estimation of norm maximum of operator* $\mathbf{L_{hzH}}$. *Analysis of nonzero elements in rows corresponding to nodes* H_{z11}, H_{z12} *and* H_{z22}.

	H_{z11}	H_{z12}	H_{z22}
a_{ii}	$\frac{1}{\mu\epsilon\Delta x^2}\left(1+\frac{a}{\Delta y}\right)+$ $\frac{1}{\mu\epsilon\Delta x^2}\left(1+\frac{\Delta x}{\Delta y}\frac{l_v}{S_v}\right)+$ $\frac{1}{\mu\epsilon\Delta y^2}$	$\frac{2}{\mu\epsilon\Delta x^2}+\frac{2}{\mu\epsilon\Delta y^2}$	$\frac{1}{\mu\epsilon\Delta x^2}\frac{c}{\Delta y}+$ $\frac{1}{\mu\epsilon\Delta y^2}\left(1+\frac{\Delta y}{\Delta x}\frac{l_v}{S_v}\right)$
$a_{ij}(i\neq j)$	$-\frac{1}{\mu\epsilon\Delta y^2}$ $-\frac{1}{\mu\epsilon\Delta x^2}\left(1+\frac{a}{\Delta y}\right)$ $-\frac{1}{\mu\epsilon\Delta x^2}$ $\frac{1}{\mu\epsilon\Delta x\Delta y}\frac{l_v}{S_v}$	$-\frac{1}{\mu\epsilon\Delta y^2}$ $-\frac{1}{\mu\epsilon\Delta x^2}$ $-\frac{1}{\mu\epsilon\Delta x^2}$ $-\frac{1}{\mu\epsilon\Delta y^2}$	$\frac{1}{\mu\epsilon\Delta x\Delta y}\frac{l_v}{S_v}$ $-\frac{1}{\mu\epsilon\Delta y^2}$ $-\frac{1}{\mu\epsilon\Delta x^2}\frac{c}{\Delta y}$
$\sum_j\lvert a_{ij}\rvert$	$\frac{1}{\mu\epsilon}\frac{\Delta x\Delta y}{S_{hz11}}\left[\frac{2}{\Delta y^2}+\right.$ $\left.\frac{2}{\Delta x^2}\left(2+\frac{a}{\Delta y}+\frac{\Delta x}{\Delta y}\frac{l_v}{S_v}\right)\right]$	$\frac{4}{\mu\epsilon}\left(\frac{1}{\Delta x^2}+\frac{1}{\Delta y^2}\right)$	$\frac{1}{\mu\epsilon}\frac{\Delta x\Delta y}{S_{hz22}}\left[\frac{2}{\Delta x^2}\right.$ $\left.\left(\frac{c}{\Delta y}+\frac{\Delta x}{\Delta y}\frac{l_v}{S_v}\right)+\frac{2}{\Delta y^2}\right]$

These conditions may be simplified, and finally we get the following set of conditions:

$$S_{hz11} \geq \frac{\Delta x\Delta y}{2} \tag{4.4.63}$$

$$S_{hz22} \geq \frac{\Delta x\Delta y}{2} \tag{4.4.64}$$

$$2+\frac{a}{\Delta y}+\frac{\Delta x}{\Delta y}\frac{l_v}{S_v} \leq 2\frac{S_{hz11}}{\Delta x\Delta y} \tag{4.4.65}$$

$$\frac{c}{\Delta y}+\frac{\Delta x}{\Delta y}\frac{l_v}{S_v} \leq 2\frac{S_{hz11}}{\Delta x\Delta y} \tag{4.4.66}$$

$$a \geq -\frac{\Delta y}{2} \tag{4.4.67}$$

$$c \geq \frac{\Delta y}{2} \tag{4.4.68}$$

$$\frac{l_v}{S_v} \geq 0 \tag{4.4.69}$$

Analogous analysis may be performed for the corner cells from sec. 4.4.3. This leads to the same conditions.

4.4.5 Example

Local schemes presented in secs. 4.4.1, 4.4.2, 4.4.3 and conditions (4.4.63)–(4.4.69) derived with the stability analysis performed in sec. 4.4.4 define an algorithm for treatment of an arbitrarily located electric wall in the finite-difference grid. Fig. 4.4.10 presents an example of Yee's mesh of cells E_x, E_y, E_z and H_z crossed by an electric wall. Nodes E_z in the vicinity of the wall are shifted to the wall and removed from the vector. All the cells which are removed are marked green. Fig. 4.4.11 presents the same mesh after modification. Modified cells E_x, E_y are marked red and modified cells H_z are marked green.

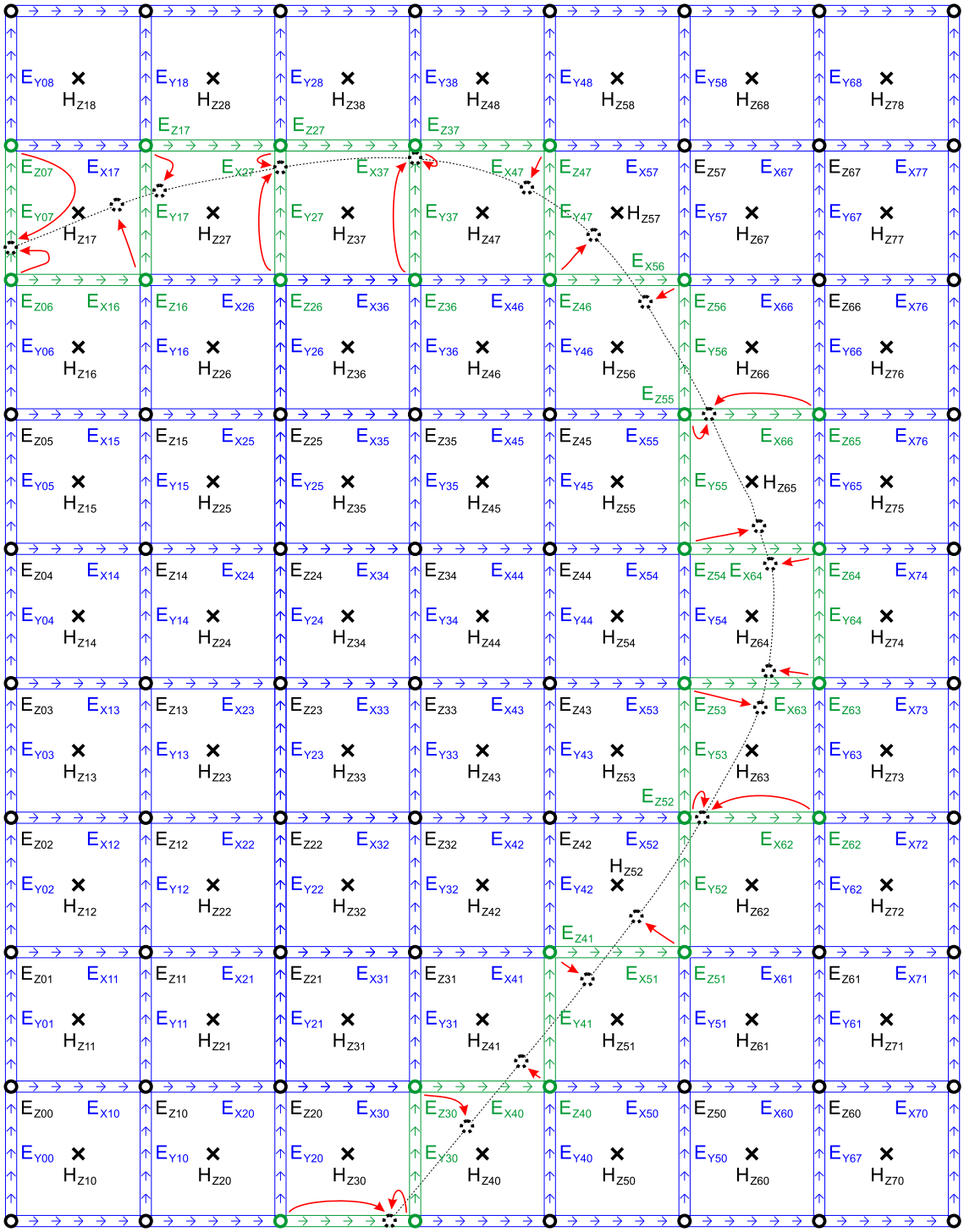

Figure 4.4.10: *Nodes E_x, E_y, E_z and H_z crossed by an electric wall in the finite difference algorithm before modification. Nodes E_z in the vicinity of the wall will be shifted to the wall and removed from the vector. Green cells will be removed.*

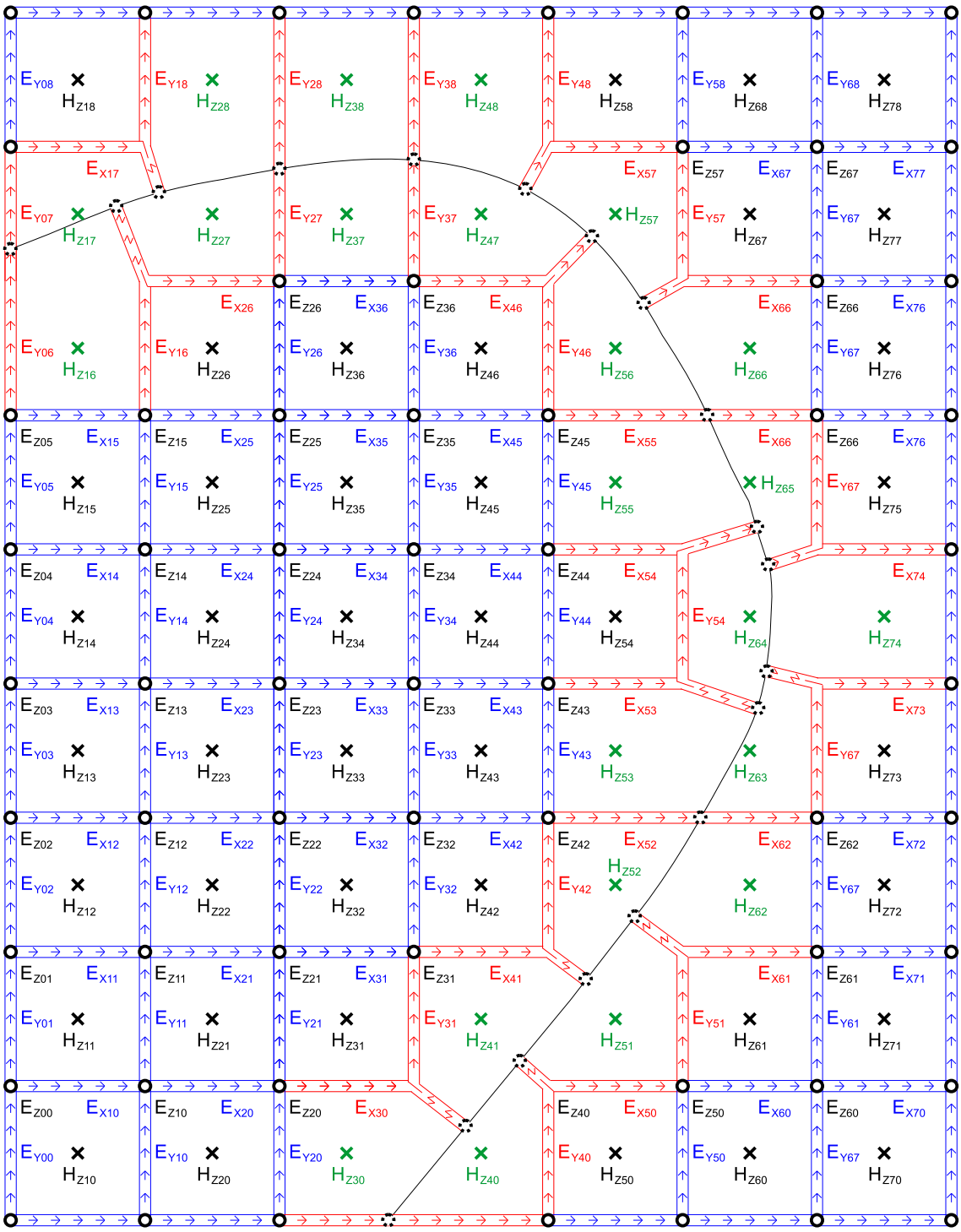

Figure 4.4.11: *Nodes E_x, E_y, E_z and H_z crossed by an electric wall in the finite difference algorithm after modification (compare with fig. 4.4.10). Modified cells E_x, E_y are red and modified cells H_z are green.*

Table 4.4.2: *Estimation of norm maximum of operator* $\mathbf{L_{ezE}}$. *Analysis of nonzero elements in rows corresponding to nodes* E_{z00}, E_{z10} *and* E_{z21}.

	E_{z00}	E_{z10}	E_{z21}
a_{ii}	$\frac{2}{\mu\epsilon\Delta x^2}+$ $\frac{1}{\mu\epsilon\Delta y^2}\left(1+\frac{\Delta y}{\Delta y+a}\right)$	$\frac{2}{\mu\epsilon\Delta x^2}+\frac{1}{\mu\epsilon\Delta y^2}+$ $\frac{1}{\mu\epsilon\Delta y^2}\frac{1+\frac{\Delta y}{\Delta x}\frac{l_v}{S_v}}{1+(\frac{\Delta x}{\Delta y}+\frac{\Delta y}{\Delta x})\frac{l_v}{S_v}}$	$\frac{2}{\mu\epsilon\Delta x^2}\frac{1+\frac{\Delta x}{\Delta y}\frac{l_v}{S_v}}{1+(\frac{\Delta x}{\Delta y}+\frac{\Delta y}{\Delta x})\frac{l_v}{S_v}}+$ $\frac{2}{\mu\epsilon\Delta x^2}+\frac{2}{\mu\epsilon\Delta y^2}\left(1+\frac{\Delta y}{c}\right)$
$a_{ij}(i\neq j)$	$-\frac{1}{\mu\epsilon\Delta x^2}$ $-\frac{1}{\mu\epsilon\Delta x^2}$ $-\frac{1}{\mu\epsilon\Delta y^2}$	$-\frac{1}{\mu\epsilon\Delta x^2}$ $-\frac{1}{\mu\epsilon\Delta x^2}$ $-\frac{1}{\mu\epsilon\Delta y^2}\frac{\frac{\Delta y}{\Delta x}\frac{l_v}{S_v}}{1+(\frac{\Delta x}{\Delta y}+\frac{\Delta y}{\Delta x})\frac{l_v}{S_v}}$ $-\frac{1}{\mu\epsilon\Delta y^2}$	$-\frac{1}{\mu\epsilon\Delta x^2}\frac{\frac{\Delta x}{\Delta y}\frac{l_v}{S_v}}{1+(\frac{\Delta x}{\Delta y}+\frac{\Delta y}{\Delta x})\frac{l_v}{S_v}}$ $-\frac{1}{\mu\epsilon\Delta x^2}$ $-\frac{1}{\mu\epsilon\Delta y^2}$
$\sum_j\lvert a_{ij}\rvert$	$\frac{4}{\mu\epsilon\Delta x^2}+$ $\frac{1}{\mu\epsilon\Delta x^2}\left(2+\frac{\Delta y}{\Delta y+a}\right)$	$\frac{4}{\mu\epsilon\Delta x^2}+\frac{2}{\mu\epsilon\Delta y^2}+$ $\frac{1}{\mu\epsilon\Delta y^2}\frac{1+2\frac{\Delta y}{\Delta x}\frac{l_v}{S_v}}{1+(\frac{\Delta x}{\Delta y}+\frac{\Delta y}{\Delta x})\frac{l_v}{S_v}}$	$\frac{1}{\mu\epsilon\Delta x^2}\frac{1+2\frac{\Delta x}{\Delta y}\frac{l_v}{S_v}}{1+(\frac{\Delta x}{\Delta y}+\frac{\Delta y}{\Delta x})\frac{l_v}{S_v}}+$ $\frac{2}{\mu\epsilon\Delta x^2}+\frac{2}{\mu\epsilon\Delta y^2}+$ $\frac{1}{\mu\epsilon\Delta y^2}\frac{\Delta y}{c}$

4.5 Modeling of metal boundaries in 3D

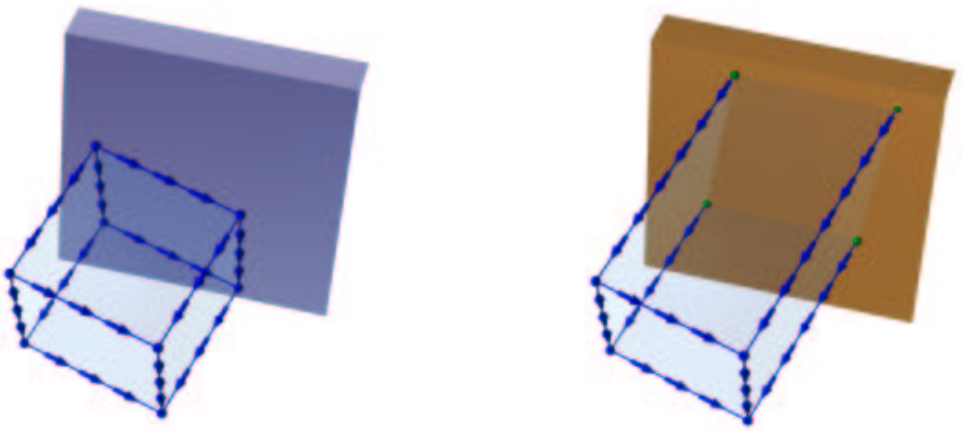

(a) (b)

Figure 4.5.1: *Nodes E in the vicinity of an electric wall in the 3D finite difference algorithm before (a) and after (b) modification.*

The definition of rotation operator is expressed in terms of line and surface integrals. Since Maxwell's equations are written with such operators, it is intuitively seen, that the finite difference local schemes derived for 2D equations may be easily generalized for 3D case. In particular, we may generalize the 2D algorithm presented in sec. 4.4 to get its 3D version. Fig. 4.5.1 presents a simple 3D cell in the vicinity of a metal plane. This figure corresponds to fig. 4.4.1 presenting the 2D version. Fig. 4.5.1(b) shows, that nodes u_e close to the boundary are moved to the metal wall. These elements should be removed from the vector. By examining the figure, we see, that as in the 2D case, we should modify the line integrals of the electric intensity field and the surface integrals of the magnetic flux density field in the grid equations. As before, this leads to modification of

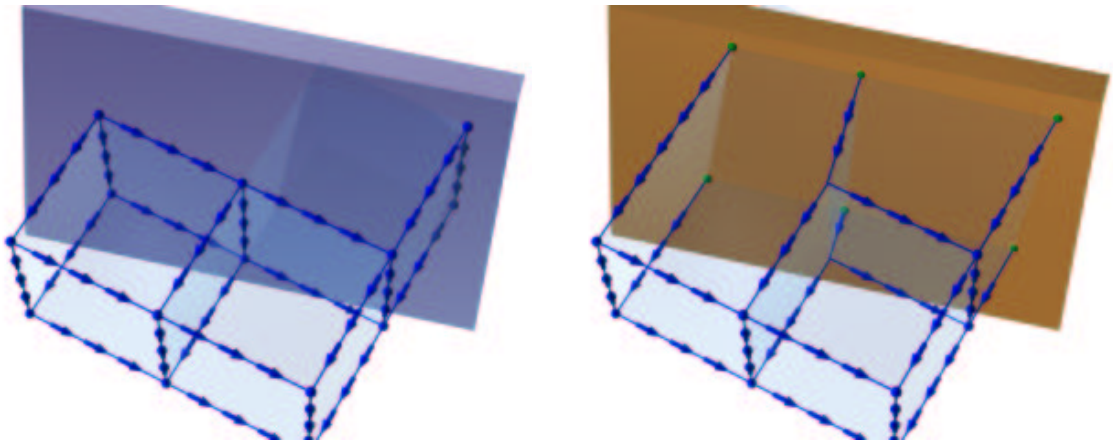

(a) (b)

Figure 4.5.2: *Nodes E in the vicinity of an electric wall in the 3D finite difference algorithm before (a) and after (b) modification.*

matrices corresponding to material properties, $\underline{\underline{E}}$ and $\underline{\underline{M}}$, with effective permittivities and permeabilities. Also note, that the volume corresponding to the scalar field v_m changes in the vicinity of the wall. This leads to modification of matrix $\underline{\underline{A}}_m$ if it is used.

Analogously, fig. 4.5.2, presenting a general location of a wall with respect to the grid, corresponds to fig. 4.4.3. As before, this general case leads to nondiagonal elements of matrices $\underline{\underline{E}}$, $\underline{\underline{M}}$.

4.6 Modeling of field singularities in 2D

We shall now derive an algorithm improving accuracy when the analyzed structure may lead to singularities of the electromagnetic field. Such singularities may appear for instance near conductive wedges. Because such elements are very common in practice (for instance in planar structures), improvement of the finite-difference methods to reduce the errors in these cases appears to be a very important problem. In a standard approach, knowledge of the field behavior in the vicinity of the singularity is used. There are many algorithms based on this approach in the literature [5,6,23,31,33,46,47,55,62,64,72–74]. All these methods stem from a technique called the method of Woods [86] adapted for Yee's mesh. One big disadvantage of the published techniques is that they may lead to relatively large local error if the structure moves with respect to the finite-difference grid. This are important limitations which make analysis of a particular structure difficult or even impossible because it requires the mesh which takes into account the location of the singular points. Moreover, most of the published methods require local homogeneity of the domain. In this section we shall develop a new algorithm which allows one to place the object introducing the field singularity at an arbitrary position with respect to the mesh in homogeneous and inhomogeneous domains [56, 60, 61]. This algorithm will match the concept of modification of basic matrices. A general idea is again to modify matrices $\underline{\underline{E}}_{tt}$, $\underline{\underline{M}}_{tt}$ so that the field behavior is correctly represented by the standard grid equations.

4.6.1 General investigations

Algorithm based on cutoff solutions We expand the longitudinal field components in the region of singularity into a series of functions:

$$e_z = \sum_i c_{ei} e_{zci} \tag{4.6.1}$$

$$h_z = \sum_i c_{hi} h_{zci} \tag{4.6.2}$$

where c_{ei}, c_{hi} are unknown coefficients. Functions e_{zci}, h_{zci} are the solutions of cutoff scalar equations for $\omega = 0$ in the vicinity of the singularity (see tab. 3.5.10):

$$\mathbf{D_{te} Z_m M_{tt}^{-1} Z_e G_{te}} e_{zci} = 0 \tag{4.6.3}$$

$$\mathbf{D_{tm} Z_e E_{tt}^{-1} Z_m G_{tm}} h_{zci} = 0 \tag{4.6.4}$$

We assume that these solutions are already known[6]. Let us concentrate on field e_z. Limiting the sum in (4.6.1) to the first few terms and writing it for a few grid points e_z we may present it in the following matrix form:

$$\underline{e}_z = \underline{\underline{B}}_{ec} \underline{c}_e \tag{4.6.5}$$

Further on, we assume, that the number of elements in the sum is equal to the number of grid points, and hence $\underline{\underline{B}}_{ec}$ is a square matrix. We also assume, that the location of these points does not lead to the singularity of the matrix. Element ij of matrix $\underline{\underline{B}}_{ec}$ is equal to the value of function e_{zci} of series (4.6.1) at grid point e_{zj}:

$$B_{ecij} = e_{zci}|_{e_{zj}} \tag{4.6.6}$$

Let us now write Maxwell's cutoff equation for field $\underline{b}_t$ in terms of field $\underline{e}_z$:

$$-j\omega \underline{b}_t = -\underline{\underline{Z}}_e \underline{\underline{G}}_{te} \underline{e}_z \tag{4.6.7}$$

Note, that here we use symbols $\underline{\underline{Z}}_e$, $\underline{\underline{G}}_{te}$ not for the global operators but only for their parts corresponding to nodes b_t and e_z in the vicinity of the singularity. In the same manner, we will use symbols $\underline{\underline{Z}}_m$, $\underline{\underline{G}}_{tm}$, $\underline{\underline{E}}_{tt}$ and $\underline{\underline{M}}_{tt}$, Putting eq. (4.6.5) to (4.6.7), we get the relation between field vector $\underline{b}_t$ and coefficient vector $\underline{c}_e$:

$$-j\omega \underline{b}_t = -\underline{\underline{Z}}_e \underline{\underline{G}}_{te} \underline{\underline{B}}_{ec} \underline{c}_e \tag{4.6.8}$$

This leads to:

$$\underline{c}_e = -j\omega \underline{\underline{B}}_{ec}^{-1} \underline{\underline{G}}_{te}^{I} \underline{\underline{Z}}_m \underline{b}_t \tag{4.6.9}$$

Operation $(.)^I$ is a quasi-inversion and will be discussed in one of the next paragraphs. At this stage of discussion, we may assume that it is equivalent to the inversion. Vector $\underline{h}_t$ may be expressed in terms of $\underline{c}_e$ as follows:

$$-j\omega \underline{h}_t = \underline{\underline{G}}_{tm} \underline{\underline{A}}_{ec} \underline{c}_e \tag{4.6.10}$$

Matrix $\underline{\underline{A}}_{ec}$ in this equation converts coefficients c_{ei} into indefinite integrals. Further on, matrix $\underline{\underline{G}}_{tm}$ converts it to the definite integrals. Element ij of matrix $\underline{\underline{A}}_{ec}$ is the value of appropriate indefinite integral of function e_{zci} at grid point h_{zj}:

$$A_{ecij} = \int \frac{1}{\mu} \frac{\partial}{\partial x} e_{zci} dy \Big|_{h_{zj}} = -\int \frac{1}{\mu} \frac{\partial}{\partial y} e_{zci} dx \Big|_{h_{zj}} \tag{4.6.11}$$

[6] In the next section, we deal with conductive wedges, where these solutions are expressed analytically.

Putting eq. (4.6.9) into (4.6.10), we get:

$$\underline{h}_t = \underline{\underline{G}}_{tm}\underline{\underline{A}}_{ec}\underline{\underline{B}}_{ec}^{-1}\underline{\underline{G}}_{te}^{I}\underline{\underline{Z}}_{m}\underline{b}_t \tag{4.6.12}$$

The above equation shows relation between fields $\underline{h}_t$ and $\underline{b}_t$. Since $\underline{h}_t = \underline{\underline{M}}_{tt}^{-1}\underline{b}_t$ this also defines operator $\underline{\underline{M}}_{tt}^{-1}$:

$$\underline{\underline{M}}_{tt}^{-1} = \underline{\underline{G}}_{tm}\underline{\underline{A}}_{ec}\underline{\underline{B}}_{ec}^{-1}\underline{\underline{G}}_{te}^{I}\underline{\underline{Z}}_{m} \tag{4.6.13}$$

In the same manner, we construct matrix $\underline{\underline{E}}_{tt}^{-1}$:

$$\underline{\underline{E}}_{tt}^{-1} = -\underline{\underline{G}}_{te}\underline{\underline{A}}_{hc}\underline{\underline{B}}_{hc}^{-1}\underline{\underline{G}}_{tm}^{I}\underline{\underline{Z}}_{e} \tag{4.6.14}$$

with matrices $\underline{\underline{B}}_{hc}$, $\underline{\underline{A}}_{hc}$ defined as follows:

$$B_{hcij} = h_{zci}|_{h_{zj}} \tag{4.6.15}$$

$$A_{hcij} = \int \frac{1}{\epsilon}\frac{\partial}{\partial x}h_{zci}dy\Big|_{e_{zj}} = -\int \frac{1}{\epsilon}\frac{\partial}{\partial y}h_{zci}dx\Big|_{e_{zj}} \tag{4.6.16}$$

We should note, that operators $\underline{\underline{M}}_{tt}^{-1}$, $\underline{\underline{E}}_{tt}^{-1}$ defined this way are not symmetric, and hence do not satisfy conditions derived in sec. 3.5.1. The symmetry problem will be solved in one of the next paragraphs.

Algorithm based on static solutions Analogous procedure may be performed when constructing the basis from static equations for $\beta_z = 0$:

$$\mathbf{D_{te}E_{tt}G_{te}}e_{zsi} = 0 \tag{4.6.17}$$
$$\mathbf{D_{tm}M_{tt}G_{tm}}h_{zsi} = 0 \tag{4.6.18}$$

This leads to the following definitions of matrices $\underline{\underline{E}}_{tt}$ and $\underline{\underline{M}}_{tt}$:

$$\underline{\underline{E}}_{tt} = \underline{\underline{Z}}_{m}\underline{\underline{G}}_{tm}\underline{\underline{A}}_{es}\underline{\underline{B}}_{es}^{-1}\underline{\underline{G}}_{te}^{I} \tag{4.6.19}$$
$$\underline{\underline{M}}_{tt} = -\underline{\underline{Z}}_{e}\underline{\underline{G}}_{te}\underline{\underline{A}}_{hs}\underline{\underline{B}}_{hs}^{-1}\underline{\underline{G}}_{tm}^{I} \tag{4.6.20}$$

Matrices $\underline{\underline{B}}_{es}$, $\underline{\underline{B}}_{hs}$, $\underline{\underline{A}}_{es}$, $\underline{\underline{A}}_{hs}$ in the above equations are defined as follows:

$$B_{esij} = e_{zsi}|_{e_{zj}} \tag{4.6.21}$$
$$B_{hsij} = h_{zsi}|_{h_{zj}} \tag{4.6.22}$$

$$A_{esij} = \int \epsilon\frac{\partial}{\partial x}e_{zsi}dy\Big|_{h_{zj}} = -\int \epsilon\frac{\partial}{\partial y}e_{zsi}dx\Big|_{h_{zj}} \tag{4.6.23}$$
$$A_{hsij} = \int \mu\frac{\partial}{\partial x}h_{zsi}dy\Big|_{e_{zj}} = -\int \mu\frac{\partial}{\partial y}h_{zsi}dx\Big|_{e_{zj}} \tag{4.6.24}$$

Equivalence of cutoff and static approach We may show that algorithms based on cutoff and static equations are equivalent. Assuming that the domain is isotropic, eqs. (4.6.3) and (4.6.18) may be written as follows:

$$\left[\frac{\partial}{\partial x}\frac{1}{\mu}\frac{\partial}{\partial x}(.)+\frac{\partial}{\partial y}\frac{1}{\mu}\frac{\partial}{\partial y}(.)\right]e_{zci} = 0 \tag{4.6.25}$$

$$\left[\frac{\partial}{\partial x}\mu\frac{\partial}{\partial x}(.)+\frac{\partial}{\partial y}\mu\frac{\partial}{\partial y}(.)\right]h_{zsi} = 0 \tag{4.6.26}$$

Applying double indefinite integral $\iint(.)dxdy$ to these equations, we get the following relations:

$$\int\frac{1}{\mu}\frac{\partial}{\partial x}e_{zci}dy = -\int\frac{1}{\mu}\frac{\partial}{\partial y}e_{zci}dx \tag{4.6.27}$$

$$\int\mu\frac{\partial}{\partial x}h_{zsi}dy = -\int\mu\frac{\partial}{\partial y}h_{zsi}dx \tag{4.6.28}$$

One may note, that the integrals in (4.6.27) are functions satisfying eq. (4.6.26). Analogously, integrals (4.6.28) are solutions of (4.6.25). Therefore, the relations between basis functions h_{zsi} and e_{zci} may be written with accuracy to the scaling factor in the following way:

$$h_{zsi} = \int\frac{1}{\mu}\frac{\partial}{\partial x}e_{zci}dy = -\int\frac{1}{\mu}\frac{\partial}{\partial y}e_{zci}dx \tag{4.6.29}$$

$$e_{zci} = \int\mu\frac{\partial}{\partial x}h_{zsi}dy = -\int\mu\frac{\partial}{\partial y}h_{zsi}dx \tag{4.6.30}$$

Analogously, we may write the relations between basis functions e_{zsi} and h_{zci}. This and the definitions of matrices $\underline{\underline{A}}_{**}$ and $\underline{\underline{B}}_{**}$ give the following relations.

$$\underline{\underline{B}}_{es} = \underline{\underline{A}}_{hc} \tag{4.6.31}$$

$$\underline{\underline{A}}_{es} = \underline{\underline{B}}_{hc} \tag{4.6.32}$$

$$\underline{\underline{B}}_{hs} = \underline{\underline{A}}_{ec} \tag{4.6.33}$$

$$\underline{\underline{A}}_{hs} = \underline{\underline{B}}_{ec} \tag{4.6.34}$$

We may now compare eqs. (4.6.19), (4.6.20) with (4.6.13), (4.6.14) and conclude, based on the above relations, that they are equivalent.

Properties of the algorithm in the homogeneous domain We may note, that in the homogeneous domain, the cutoff and static solutions form the same basis. This gives the following relations:

$$\underline{\underline{A}}_{ec} = \mu\underline{\underline{B}}_{hc} \tag{4.6.35}$$

$$\underline{\underline{A}}_{hc} = \epsilon\underline{\underline{B}}_{ec} \tag{4.6.36}$$

This and the definitions of matrices $\underline{\underline{E}}_{tt}$, $\underline{\underline{M}}_{tt}$ imply, that the algorithm presented above satisfies condition (3.5.27) written for the homogeneous domain.

Symmetrization of operators $\underline{\underline{E}}_{tt}$, $\underline{\underline{M}}_{tt}$ We should note, that operators $\underline{\underline{M}}_{tt}^{-1}$, $\underline{\underline{E}}_{tt}^{-1}$ (or $\underline{\underline{E}}_{tt}$, $\underline{\underline{M}}_{tt}$) defined above are not symmetric, and hence do not satisfy conditions (3.5.20), (3.5.21). Fortunately, the algorithm is not sensitive to small deformations of Yee's cells in the vicinity of the wedge. Therefore, we may choose the locations of the appropriate nodes in the way leading to symmetric operators. This may be also achieved in a simpler way, where we symmetrize nonsymmetric matrices as follows:

$$\underline{\underline{C}} \leftarrow 0.5(\underline{\underline{C}} + \underline{\underline{C}}^T) \tag{4.6.37}$$

where $\underline{\underline{C}}$, denotes the operator to be symmetrized. In order not to disturb condition (3.5.27) for homogeneous domains, we should symmetrize only one of the pairs $\underline{\underline{E}}_{tt}$, $\underline{\underline{M}}_{tt}^{-1}$ or $\underline{\underline{M}}_{tt}$, $\underline{\underline{E}}_{tt}^{-1}$.

Quasi-inversion of matrices $\underline{\underline{G}}_{te}$, $\underline{\underline{G}}_{tm}$ Expressions describing matrices $\underline{\underline{E}}_{tt}$, $\underline{\underline{M}}_{tt}$ include inversions of matrices $\underline{\underline{G}}_{te}$ and $\underline{\underline{G}}_{tm}$. Unfortunately, in many cases, these matrices cannot be inverted, because they are singular. Let us note, however, that zero eigenvalue of these operators correspond to one of the static modes $e_{zi} = \text{const}$ or $h_{zi} = \text{const}$. These modes do not have the transverse field components, and hence have no influence on matrices $\underline{\underline{E}}_{tt}$ and $\underline{\underline{M}}_{tt}$. Therefore, we may assume that these modes do not exist in the global field. In this case we may remove zero eigenvalue as follows:

$$\underline{\underline{G}}'_{tm} = \underline{\underline{G}}_{tm} + \underline{h}_{t0}\underline{h}_{z0}^T \tag{4.6.38}$$

where $\underline{h}_{z0}$ is nonzero eigenvector corresponding to zero eigenvalue, and $\underline{h}_{t0}$ is an arbitrary nonzero vector in space $\{\underline{h}_t\}$. Operator $\underline{\underline{G}}'_{tm}$ is not singular and may be inverted. We call operator $\underline{\underline{G}}_{tm}^{'-1}$ the quasi-inversion of $\underline{\underline{G}}_{tm}$ ($\underline{\underline{G}}_{tm}^{I} = \underline{\underline{G}}_{tm}^{'-1}$).

Stability of the explicit update schemes Stability condition of the explicit update schemes has not been established analiticaly, and will be the subject of the numerical tests performed in chapter 7.

4.6.2 Conductive wedges

When a conductive wedge is the source of singularity (fig. 4.6.1(a)), series (4.6.1), (4.6.2) take up the form [47]:

$$e_z = \sum_{i=1}^{\infty} \alpha_{ej} c_{ei} r^{\nu_i} \sin(\nu_i \phi) \tag{4.6.39}$$

$$h_z = \sum_{i=0}^{\infty} \alpha_{hj} c_{hi} r^{\nu_i} \cos(\nu_i \phi) \tag{4.6.40}$$

where α_{ej}, α_{hj}, ν_i have to be chosen in a way satisfying all boundary conditions.

Thin conductive strips at dielectric boundary Tab. (4.6.1) presents definition of basic operators for the conductive wedge placed symmetrically between two dielectrics (figs. 4.6.1(b,c)). One may note, that this includes a very common case of a thin metal strip placed on a dielectric boundary, which may be seen as a conductive wedge of angle $\alpha = 0$.

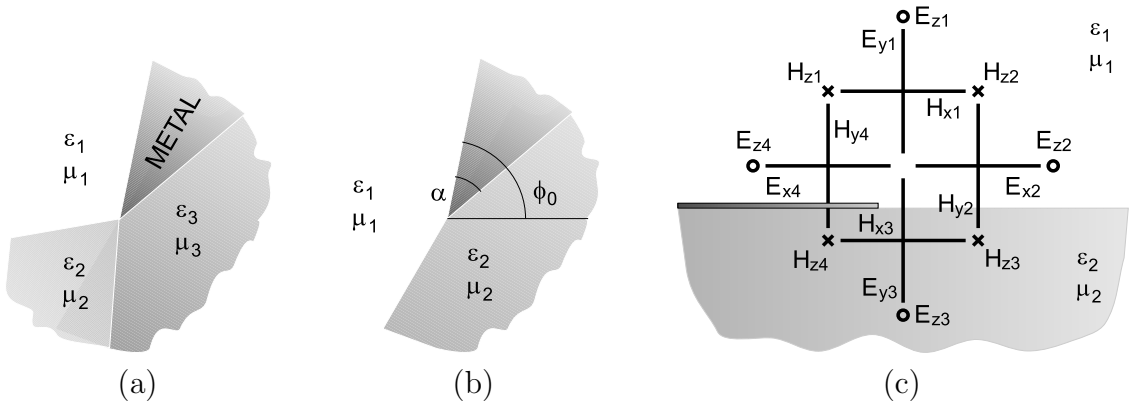

Figure 4.6.1: *Conductive wedge in an inhomogeneous domain: general case (a), wedge symmetrically placed between two dielectrics (b), nodes used in the correction algorithm for the wedge of angle $\alpha = 0$ at $\phi_0 = 180^o$ (c).*

4.6.3 Thin wires

Analogously, we may use the algorithm derived in sec. 4.6.1 to model a thin conductive wire of radius a. Assuming that the wire is placed in a homogeneous domain, series (4.6.1), (4.6.2) become:

$$e_z = \sum_{i=1}^{\infty} \left[a_{ei} J_i(r) + b_{ei} N_i(r)\right] \left[c_{esi} \sin(i\phi) + c_{eci} \cos(i\phi)\right] \tag{4.6.41}$$

$$h_z = \sum_{i=0}^{\infty} \left[a_{hi} J_i(r) + b_{hi} N_i(r)\right] \left[c_{hsi} \sin(i\phi) + c_{hci} \cos(i\phi)\right] \tag{4.6.42}$$

where $J_i(r)$, $N_i(r)$ are, respectively, Bessel and Neumann functions, and a_{ei}, b_{ei}, a_{hi}, b_{hi} are coefficients satisfying the following boundary conditions:

$$a_{ei} J_i(a) + b_{ei} N_i(a) = 0 \tag{4.6.43}$$

$$a_{hi} J_i'(a) + b_{hi} N_i'(a) = 0 \tag{4.6.44}$$

Coefficients c_{esi}, c_{eci} and c_{hsi}, c_{hci} in eqs. (4.6.41), (4.6.42) are elements of, respectively, vectors $\underline{c}_e$ (eq. (4.6.5)) and $\underline{c}_h$.

Table 4.6.1: *Definition of basic matrices for the conductive wedge placed symmetrically between two dielectrics.*

$$\underline{\underline{B}}_{ec} = \begin{bmatrix} 0 & s_{11} & s_{12} & s_{13} \\ 0 & s_{21} & (\mu/\mu_1)s_{22} & s_{23} \\ 0 & s_{31} & (\mu_2/\mu_1)s_{22} & s_{33} \\ 1 & 0 & 0 & 0 \end{bmatrix} \qquad \underline{\underline{A}}_{ec} = \frac{1}{\mu_1} \begin{bmatrix} 1 & c_{11} & c_{12} & c_{13} \\ 1 & c_{21} & c_{22} & c_{23} \\ 1 & (\mu_1/\mu_2)c_{31} & c_{32} & (\mu_1/\mu_2)c_{33} \\ 1 & (\mu_1/\mu_2)c_{41} & c_{42} & (\mu_1/\mu_2)c_{43} \end{bmatrix}$$

$$\underline{\underline{B}}_{hc} = \begin{bmatrix} 1 & c_{11} & c_{12} & c_{13} \\ 1 & c_{21} & c_{22} & c_{23} \\ 1 & (\epsilon_2/\epsilon_1)c_{31} & c_{32} & (\epsilon_2/\epsilon_1)c_{33} \\ 1 & (\epsilon_2/\epsilon_1)c_{41} & c_{42} & (\epsilon_2/\epsilon_1)c_{43} \end{bmatrix} \qquad \underline{\underline{A}}_{hc} = \frac{1}{\epsilon_1} \begin{bmatrix} 0 & s_{11} & s_{12} & s_{13} \\ 0 & s_{21} & (\epsilon_1/\epsilon)s_{22} & s_{23} \\ 0 & s_{31} & (\epsilon_1/\epsilon_2)s_{32} & s_{33} \\ 1 & 0 & 0 & 0 \end{bmatrix}$$

$$\underline{\underline{G}}_{tm} = \underline{\underline{H}}^{-1} \begin{bmatrix} -1 & 1 & 0 & 0 \\ 0 & 1 & -1 & 0 \\ 0 & 0 & 1 & -1 \\ 0 & 0 & 0 & 0 \end{bmatrix} \qquad \underline{\underline{G}}^{I}_{tm} = \begin{bmatrix} -0.75 & 0.5 & 0.25 & 0 \\ 0.25 & 0.5 & 0.25 & 0 \\ 0.25 & -0.5 & 0.25 & 0 \\ 0.25 & -0.5 & -0.75 & 0 \end{bmatrix} \underline{\underline{H}}$$

$$\underline{\underline{G}}_{te} = \underline{\underline{H}}^{-1} \begin{bmatrix} 1 & 0 & 0 & 0 \\ 0 & 1 & 0 & 0 \\ 0 & 0 & -1 & 0 \\ 0 & 0 & 0 & 0 \end{bmatrix} \qquad \underline{\underline{G}}^{I}_{te} = \begin{bmatrix} 1 & 0 & 0 & 0 \\ 0 & 1 & 0 & 0 \\ 0 & 0 & -1 & 0 \\ 0 & 0 & 0 & 0 \end{bmatrix} \underline{\underline{H}}$$

$$\underline{\underline{Z}}_{e} = \begin{bmatrix} 1 & 0 & 0 & 0 \\ 0 & -1 & 0 & 0 \\ 0 & 0 & 1 & 0 \\ 0 & 0 & 0 & -1 \end{bmatrix} \qquad \underline{\underline{Z}}_{m} = \begin{bmatrix} -1 & 0 & 0 & 0 \\ 0 & 1 & 0 & 0 \\ 0 & 0 & -1 & 0 \\ 0 & 0 & 0 & 1 \end{bmatrix}$$

$$\underline{\underline{H}} = \mathrm{diag}(\Delta x, \Delta y, \Delta x, \Delta y)$$

$$s_{ij} = r_i^{\nu_j} \sin \nu_j \phi_i$$
$$c_{ij} = r_i^{\nu_j} \cos \nu_j \phi_i$$
$$\nu_i = \frac{i\pi}{2\pi - \alpha}$$

4.7 Modeling of field singularities in 3D

Like in the case of metal boundaries, the 2D algorithm dealing with singularities, presented in sec. 4.6, may be easily generalized for 3D case. To this end, we use static solutions of wave equations in the region of the singularity:

$$\mathbf{R_m M^{-1} R_e} e_{si} = 0 \tag{4.7.1}$$
$$\mathbf{R_e E^{-1} R_m} h_{si} = 0 \tag{4.7.2}$$

These solutions may be written in the following form:

$$e_{si} = \mathbf{G_e} u_{esi} \tag{4.7.3}$$
$$h_{si} = \mathbf{G_m} u_{msi} \tag{4.7.4}$$

where u_{esi}, u_{msi} are scalar fields. We substitute eqs. (4.7.3), (4.7.4) into, respectively, (3.4.5) and (3.4.6), and get the following operator equations[7] for u_{esi}, u_{msi}:

$$\mathbf{D_e E G_e} u_{esi} = 0 \tag{4.7.5}$$
$$\mathbf{D_m M G_m} u_{msi} = 0 \tag{4.7.6}$$

Now, we expand potentials u_e, u_m into series of static solutions u_{esi} and u_{msi}:

$$u_e = \sum_i c_{ei} u_{esi} \tag{4.7.7}$$
$$u_m = \sum_i c_{mi} u_{msi} \tag{4.7.8}$$

Eq. (4.7.7) may be written for a few grid points points u_{ej}. Limiting the series to the first few terms, we may write this equation in the following matrix form:

$$\underline{u}_e = \underline{\underline{B}}_e \underline{c}_e \tag{4.7.9}$$

where the elements of matrix $\underline{\underline{B}}_e$ are defined as follows:

$$B_{eij} = u_{esi}|_{u_{ej}} \tag{4.7.10}$$

i.e. the element of matrix $\underline{\underline{B}}_e$ in row i and column j is the value of function u_{esi} at grid point u_{ej}. Like in the 2D case, we assume, that matrix $\underline{\underline{B}}_e$ is square and not singular. In the next step, we write eq. (4.7.3) for a few points e in the region of the singularity. This, again, may be presented in the matrix form:

$$\underline{e} = \underline{\underline{G}}_e \underline{u}_e \tag{4.7.11}$$

Substituting the above equation into (4.7.9) and inverting the matrices, we get a relation between vectors $\underline{c}_e$ and $\underline{e}$:

$$\underline{c}_e = \underline{\underline{B}}_e^{-1} \underline{\underline{G}}_e^I \underline{e} \tag{4.7.12}$$

where $(.)^I$ is the quasi-inversion already described in sec. 4.6.1. Let us now write equations for all three components of the electric flux density field in terms of the scalar field u_e.

[7] We assume, that $r = 0$.

From (4.7.3), we get:

$$D_x = \epsilon \frac{\partial}{\partial x} u_e \tag{4.7.13}$$

$$D_y = \epsilon \frac{\partial}{\partial y} u_e \tag{4.7.14}$$

$$D_z = \epsilon \frac{\partial}{\partial z} u_e \tag{4.7.15}$$

These quantities may be averaged over the integration surfaces corresponding to the nodes d_x, d_y, d_z:

$$d_x = \frac{1}{\Delta y \Delta z} \iint_{S_{yz}} \epsilon \frac{\partial}{\partial x} u_e dy dz \tag{4.7.16}$$

$$d_y = \frac{1}{\Delta x \Delta z} \iint_{S_{xz}} \epsilon \frac{\partial}{\partial y} u_e dx dz \tag{4.7.17}$$

$$d_z = \frac{1}{\Delta x \Delta y} \iint_{S_{xy}} \epsilon \frac{\partial}{\partial z} u_e dx dy \tag{4.7.18}$$

In order to calculate the above definite integrals, we should define indefinite integrals at appropriate grid points (nodes u_{mj}). Instead of functions u_e, we now use the elements of series (4.7.7) u_{esi}. We get:

$$A_{exij} = \iint \epsilon \frac{\partial}{\partial x} u_{esi} dy dz \Big|_{u_{mj}} \tag{4.7.19}$$

$$A_{eyij} = \iint \epsilon \frac{\partial}{\partial y} u_{esi} dx dz \Big|_{u_{mj}} \tag{4.7.20}$$

$$A_{ezij} = \iint \epsilon \frac{\partial}{\partial z} u_{esi} dx dy \Big|_{u_{mj}} \tag{4.7.21}$$

These elements define matrices $\underline{\underline{A}}_{ex}$, $\underline{\underline{A}}_{ey}$ and $\underline{\underline{A}}_{ez}$. The indefinite integrals may be now converted to the definite ones. For instance, for nodes d_x, we get:

$$\underline{\underline{C}}_{ex} \underline{d} = \underline{\underline{C}}_{ex} \underline{\underline{R}}_m \underline{\underline{G}}_m \underline{\underline{A}}_{ex} \underline{c}_e \tag{4.7.22}$$

where $\underline{\underline{C}}_{ex}$ is diagonal matrix with diagonal elements equal to 1, if the element corresponds to x field component, and 0 elsewhere. In the same manner, we may calculate y and z components of vector $\underline{d}$ defining analogous matrices $\underline{\underline{C}}_{ey}$ and $\underline{\underline{C}}_{ez}$. Combining these equations together and using (4.7.12), we get the following relation between fields $\underline{d}$ and $\underline{e}$:

$$\underline{d} = \left(\underline{\underline{C}}_{ex} \underline{\underline{R}}_m \underline{\underline{G}}_m \underline{\underline{A}}_{ex} + \underline{\underline{C}}_{ey} \underline{\underline{R}}_m \underline{\underline{G}}_m \underline{\underline{A}}_{ey} + \underline{\underline{C}}_{ez} \underline{\underline{R}}_m \underline{\underline{G}}_m \underline{\underline{A}}_{ez} \right) \underline{\underline{B}}_e^{-1} \underline{\underline{G}}_e^I \underline{e} \tag{4.7.23}$$

Since $\underline{d} = \underline{\underline{E}}\, \underline{e}$, the above equation defines matrix $\underline{\underline{E}}$:

$$\underline{\underline{E}} = \left(\underline{\underline{C}}_{ex} \underline{\underline{R}}_m \underline{\underline{G}}_m \underline{\underline{A}}_{ex} + \underline{\underline{C}}_{ey} \underline{\underline{R}}_m \underline{\underline{G}}_m \underline{\underline{A}}_{ey} + \underline{\underline{C}}_{ez} \underline{\underline{R}}_m \underline{\underline{G}}_m \underline{\underline{A}}_{ez} \right) \underline{\underline{B}}_e^{-1} \underline{\underline{G}}_e^I \tag{4.7.24}$$

In the same manner, we may calculate matrix $\underline{\underline{M}}$ using series (4.7.8):

$$\underline{\underline{M}} = \left(\underline{\underline{C}}_{mx} \underline{\underline{R}}_e \underline{\underline{G}}_e \underline{\underline{A}}_{mx} + \underline{\underline{C}}_{my} \underline{\underline{R}}_e \underline{\underline{G}}_e \underline{\underline{A}}_{my} + \underline{\underline{C}}_{mz} \underline{\underline{R}}_e \underline{\underline{G}}_e \underline{\underline{A}}_{mz} \right) \underline{\underline{B}}_m^{-1} \underline{\underline{G}}_e^I \tag{4.7.25}$$

with the elements of matrices $\underline{\underline{A}}_{mx}$, $\underline{\underline{A}}_{my}$, $\underline{\underline{A}}_{mz}$ defined as follows:

$$A_{mxij} = \iint \epsilon \frac{\partial}{\partial x} u_{msi} dydz \Big|_{u_{ej}} \tag{4.7.26}$$

$$A_{myij} = \iint \epsilon \frac{\partial}{\partial y} u_{msi} dxdz \Big|_{u_{ej}} \tag{4.7.27}$$

$$A_{mzij} = \iint \epsilon \frac{\partial}{\partial z} u_{msi} dxdy \Big|_{u_{ej}} \tag{4.7.28}$$

and analogous diagonal matrices $\underline{\underline{C}}_{mx}$, $\underline{\underline{C}}_{my}$, $\underline{\underline{C}}_{mz}$ with the unit elements corresponding to the appropriate field components.

Chapter 5

Schemes involving space decomposition

5.1 Introduction

In the previous chapter we discussed standard FD algorithms where the whole domain was covered with Yee's mesh. Local schemes were introduced to better approximate the field within a cell. In the derivation of local schemes the use was made of the analytical description of the electromagnetic fields. This concept can be extended further if one has a good analytical technique which is valid for regions spanning many cells. In this chapter, we introduce such algorithms. The general concept can be summarized as follows. Instead of covering the whole space with the mesh the analyzed domain is decomposed into a set of subdomains. As shown in fig. 5.1.1, the analyzed structure is divided into

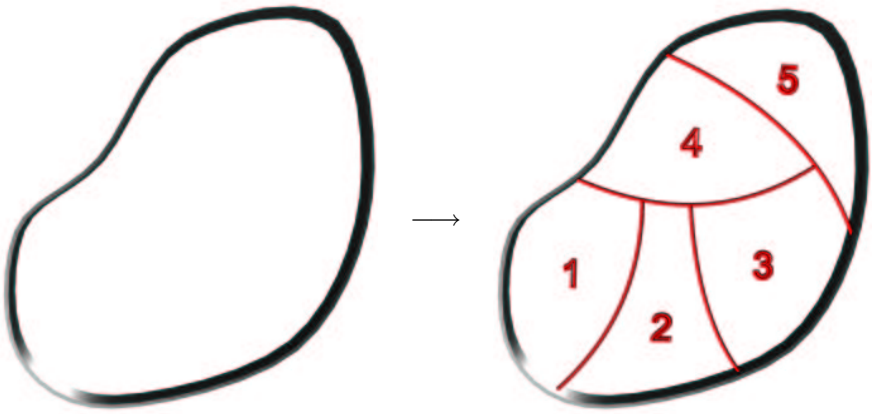

Figure 5.1.1: *Domain decomposition.*

smaller subregions. In general, each of these subregions may be analyzed using a different algorithm which does not to be based on finite difference approximations. One has to take care to satisfy the appropriate boundary conditions as well as the continuity conditions between the subdomains.

For the structure shown in fig. 5.1.2 divided into two subdomains with the common boundary $\delta\Omega$ the continuity condition given as follows:

$$\left.\begin{array}{rcl} E_{t1} & = & E_{t2} \\ H_{t1} & = & H_{t2} \end{array}\right\} \text{on } \delta\Omega \tag{5.1.1}$$

where subscript $_t$ denotes the field component tangential to the boundary and indices denote the subregions.

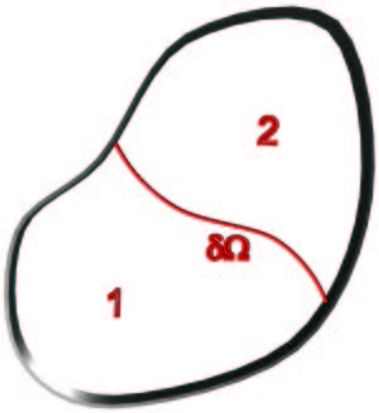

Figure 5.1.2: *Field matching concept. The tangential intensity field components on the boundary $\delta\Omega$ should match.*

In this chapter, we show how to use the eigenfunction expansion technique for modeling fields in some of the subdomains and how to impose the continuity conditions when different field representations are used in two adjacent subdomains.

We present two approaches depending on the type of the analyzed region. The first, less general approach, which extends the hybrid PEE-FDTD technique proposed in [51], deals with structures which involve subdomains uniform in one direction. In sec. 5.2, we introduce the algorithm which converts 3D problem in this subdomain into a series of 1D problems. From the technical point of view, the subdomain may be treated as a section of a waveguide and each of these 1D problems is related to a different mode of this guide.

Nonuniform structures require different treatment. Algorithm for modeling general 3D subdomains is presented in sec. 5.3. Also in this case, a 3D problem is converted into a series of 1D problems, and each of them is related to a resonance of the structure constructed from the subdomain with the appropriate boundary conditions.

Since in this thesis we deal with the finite difference methods, the most interesting for us is the interface between the eigenfunction expansion techniques modeling a given subdomain and FD-FD or FD-TD method used in its neighborhood. Because of the properties of the finite difference techniques, such an interface has to be realized based on two planes of Yee's grid. The area of these two planes is in fact a common region of the subdomains analyzed with the eigenfunction technique and the finite difference method. This is presented in fig. 5.1.3, where the interface planes are denoted with numbers 0 and 1. The field in plane 0 is calculated with the finite difference algorithm and is the source for the field in the subdomain analyzed with the eigenfunction expansion method. Analogously, the field in plane 1 is obtained from the eigenfunction expansion technique and acts as a source for the finite difference part of the algorithm.

The interfaces based on the scheme presented above are presented for the algorithms modeling subdomains uniform in one direction (sec. 5.2.3) and for a more general 3D technique (sec. 5.3.2).

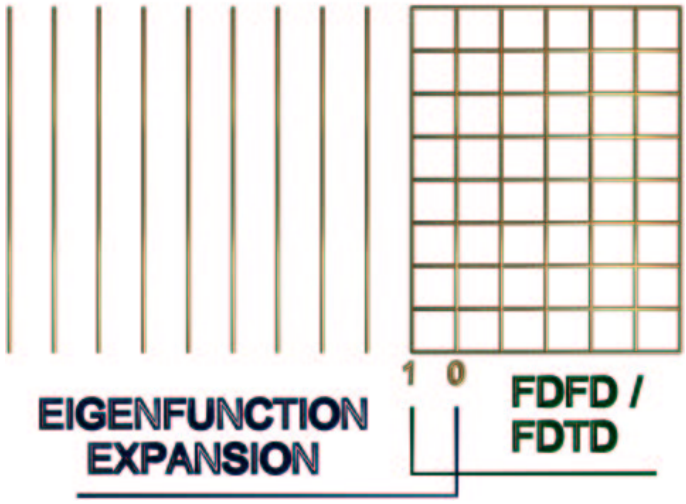

Figure 5.1.3: *Interface between the partial eigenfunction expansion technique and the finite difference approach.*

5.2 Subdomains uniform in one direction

The computation time in the finite difference methods may be significantly reduced in the regions where the analyzed structure is uniform in one direction. From the technical point of view, such structures may be treated as sections of waveguides. In fig. 5.2.1, we give four examples of homogeneous and inhomogeneous waveguides. The sections of all these structures may be modeled using the algorithms presented below. We introduce the modal expansion technique which converts a 3D electromagnetic problem in a section of waveguide into a much faster 1D finite difference model. In sec. 5.2.1, we deal with homogeneously loaded waveguides. We take advantage of the orthogonality relations between the electromagnetic field in such structures, and get a series of independent algorithms for modeling of each mode of the waveguide separately. Inhomogeneously loaded waveguides do not have this property and therefore require more sophisticated treatment. We present this approach in sec. 5.2.2. Finally, in sec. 5.2.3 we introduce the interface between the modal expansion techniques and the finite difference method.

5.2.1 Homogeneous waveguides

In waveguides that have uniform cross-section, each mode satisfies the following dispersion equation [37]:

$$\mu\epsilon(\omega^2 - \omega_k^2) f_k = \beta_z^2 f_k \tag{5.2.1}$$

where ω_k is the cutoff frequency of the k-th mode and f_k represents the corresponding field distribution across a waveguide. We assume that z represents the direction of uniformity of the waveguide. Eq. (5.2.1) may be written independently for each mode of the waveguide. In the domain of time and space it becomes:

$$\mu\epsilon \left[\frac{\partial^2}{\partial t^2} + \omega_k^2 \right] f_k = \frac{\partial^2}{\partial z^2} f_k \tag{5.2.2}$$

This leads to the following equation:

$$\frac{\partial^2}{\partial t^2} f_k = \frac{1}{\mu\epsilon} \frac{\partial^2}{\partial z^2} f_k - \omega_k^2 f_k \tag{5.2.3}$$

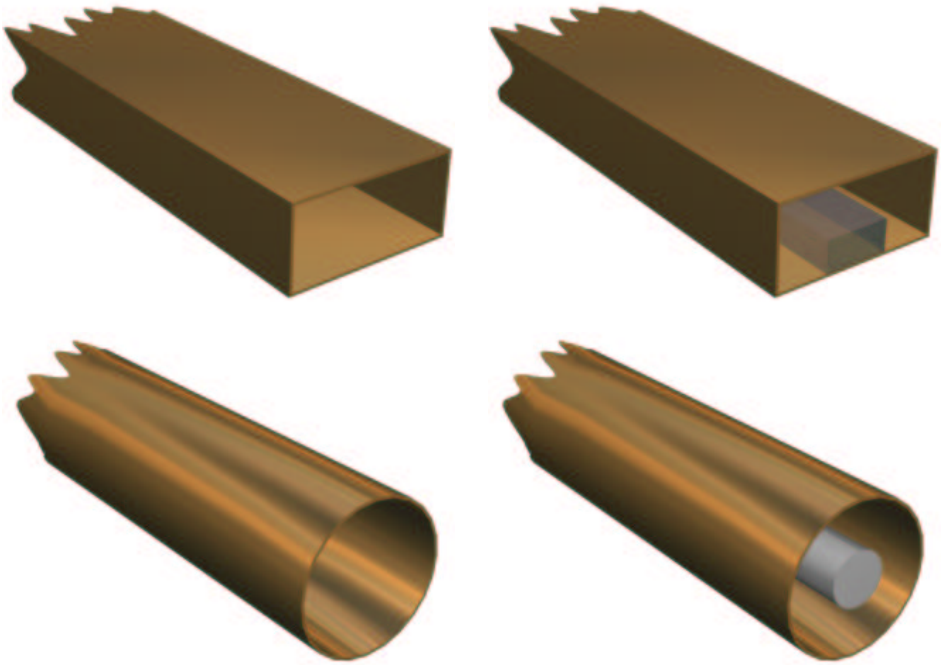

Figure 5.2.1: *Examples of homogeneous and inhomogeneous waveguides.*

We may discretize eq. (5.2.3) with respect to variable z using the central difference scheme to get the partial eigenfunction expansion scheme proposed in [51]

$$\frac{\partial^2}{\partial t^2} f_k(j_z) = -\left(\frac{2}{\mu\epsilon\Delta z^2} + \omega_k^2\right) f_k(j_z) + \frac{1}{\mu\epsilon\Delta z^2}\left[f_k(j_z - 1) + f_k(j_z + 1)\right] \tag{5.2.4}$$

$f_k(j_z)$ is a discretized field, and is a function of j_z which denotes a plane of the 1D grid with the constant grid step Δz. A sample grid placed in the rectangular waveguide from fig. 5.2.1 is shown in fig. 5.2.2.

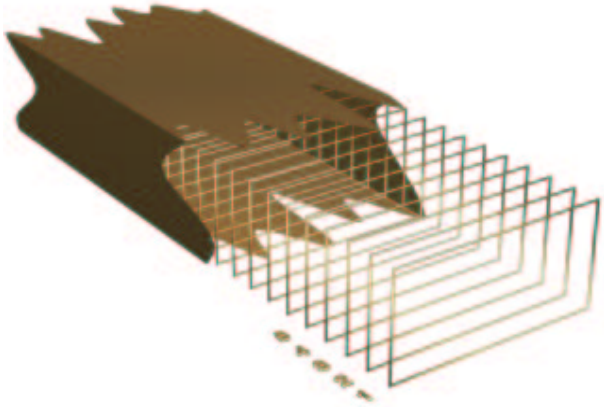

Figure 5.2.2: *A 1D grid of the partial eigenfunction expansion method in a homogeneous rectangular waveguide.*

In the frequency domain eq. (5.2.4) may be written in the following form:

$$\omega^2 \underline{f}_k = \underline{\underline{L}}\,\underline{f}_k \tag{5.2.5}$$

where $\underline{f}_k = [f_k(0), f_k(1), ...]^T$, and matrix $\underline{\underline{L}}$ is defined as follows:

$$\underline{\underline{L}} = \frac{1}{\mu\epsilon\Delta z^2}\begin{bmatrix} 2 & -1 & 0 & \cdots & 0 \\ -1 & 2 & -1 & & \vdots \\ 0 & -1 & 2 & \ddots & 0 \\ \vdots & & \ddots & \ddots & -1 \\ 0 & \cdots & 0 & -1 & 2 \end{bmatrix} + \omega_k^2 \underline{\underline{I}} \tag{5.2.6}$$

Note, that eq. (5.2.5) assumes appropriate boundary conditions at the first and last cross-planes of the grid. In practice, the eigenfunction expansion technique is used as a part of a hybrid procedure, being connected via an interface to another techniques modeling neighboring subdomains. Therefore, operator $\underline{\underline{L}}$ should be treated as a part of a larger global operator modeling the whole domain. The interface between the modal expansion and the finite difference approach is presented in sec. 5.2.3

According to the analysis performed in sec. 2.2.3.2, eq. (5.2.5) may also be written in the domain of time using the explicit update scheme.

Stability condition for the explicit update scheme We showed in sec. 2.2.3.2, that the stability condition depends on the norm of the operator of the corresponding matrix eigenproblem. This norm, for the problem at hand, may be estimated based on eq. (5.2.6) using the norm maximum. This gives:

$$||\underline{\underline{L}}|| = \omega_{\max}^2 \leq \frac{4}{\mu\epsilon\Delta z^2} + \omega_k^2 \tag{5.2.7}$$

The stability condition becomes:

$$\omega_k \in \mathcal{R}, \qquad \Delta t \leq \frac{1}{v\sqrt{\frac{1}{\Delta z^2} + (\frac{\omega_k}{2v})^2}} \tag{5.2.8}$$

where $v = (\mu\epsilon)^{-1/2}$ is the wave speed. In addition to the stability condition (5.2.8) matrix $\underline{\underline{L}}$ has to have real and positive spectrum. This condition is satisfied, since the operator is symmetric and diagonally dominant.

5.2.2 Inhomogeneously loaded waveguides

Since eq. (5.2.1) is satisfied only if the waveguide is homogeneous, inhomogeneously loaded waveguides require a different treatment [22]. This approach is based on the eigenfunction expansion algorithms developed for the fast analysis of dispersive properties of waveguides [57–59]. We assume that the dispersion equation has already been solved for the analyzed waveguide at a few discrete points, i.e. we know a few solutions of the form $(\vec{E}_{tk}, \vec{H}_{tk}, \omega_k, \beta_{zk})$ from the dispersion characteristics. A sample dispersion characteristics of a waveguide is shown in fig. 5.2.3. In the first step, we expand the fields in a section of this guide into a series of modes from our set of the known solutions:

$$\vec{E}_t = \sum_k a_k \vec{E}_{tk} \tag{5.2.9}$$

$$\vec{H}_t = \sum_k b_k \vec{H}_{tk} \tag{5.2.10}$$

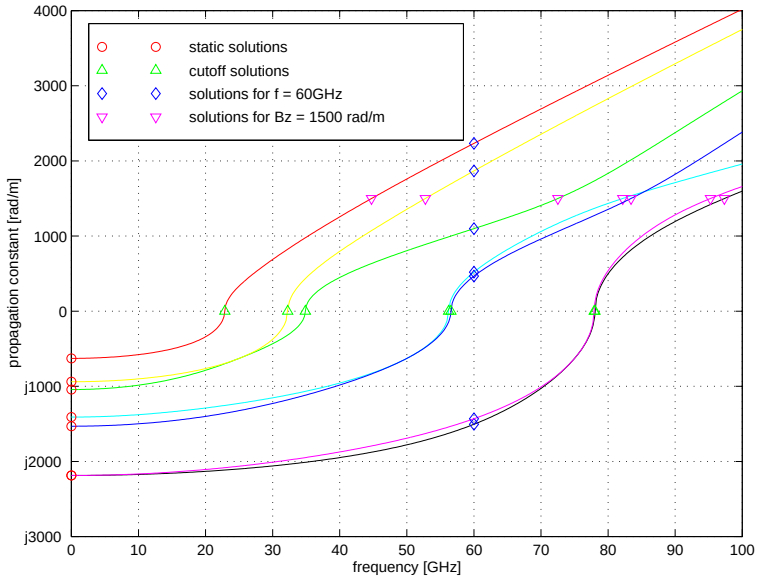

Figure 5.2.3: *Sample dispersion characteristics of a waveguide and various bases for the eigenfunction expansion technique: static solutions ($f = 0$), cutoff solutions ($\beta_z = 0$), solutions for f=60GHz, and for $\beta_z = 1500$ rad/m.*

The choice of the solutions from the characteristics may have large influence on the final results. A good choice are the points corresponding to lower order modes for $\beta_z^2 = \text{const}$ (eg. solutions at cutoff or for $\beta_z = 1500\text{rad/m}$ in fig. 5.2.3) or $\omega^2 = \text{const}$ (eg. static solutions or solutions for $f = 60\text{GHz}$ in the same figure). In these cases, the basis created by $\vec{E}_{tk}$, $\vec{H}_{tk}$ is strongly minimal[1] [38]. Further on, we assume that ω_k^2 and β_{zk}^2 are real. Based on these expansions, we may write the wave equation in the following form[2]:

$$\underline{\underline{G}}\,(\omega^2\underline{\underline{I}} - \underline{\underline{\Omega}}^{\,2})\underline{a} = \underline{\underline{S}}\,(\beta_z^2\underline{\underline{I}} - \underline{\underline{Z}}^{\,2})\underline{a} \tag{5.2.11}$$

where: $\underline{a} = [a_1, a_2, ...]^T$, $\underline{\underline{\Omega}}^{\,2} = \text{diag}(\omega_k^2)$, $\underline{\underline{Z}}^{\,2} = \text{diag}(\beta_{zk}^2)$, and the elements of matrices $\underline{\underline{G}}$ and $\underline{\underline{S}}$ are given by the equations:

$$G_{lk} = \iint_S \vec{D}_{tk} \cdot \vec{\imath}_z \times \vec{B}_{tl}^{\,*} ds \tag{5.2.12}$$

$$S_{lk} = \iint_S \vec{E}_{tk} \cdot \vec{\imath}_z \times \vec{H}_{tl}^{\,*} ds \tag{5.2.13}$$

Eq. (5.2.11) may be written in the domain of time and space. We get:

$$\underline{\underline{G}}\left(\underline{\underline{I}}\,\frac{\partial^2}{\partial t^2}(.) + \underline{\underline{\Omega}}^{\,2}\right)\underline{a} = \underline{\underline{S}}\left(\underline{\underline{I}}\,\frac{\partial^2}{\partial z^2}(.) + \underline{\underline{Z}}^{\,2}\right)\underline{a} \tag{5.2.14}$$

This gives:

$$\frac{\partial^2}{\partial t^2}\underline{a} = \left[\underline{\underline{G}}^{\,-1}\underline{\underline{S}}\left(\underline{\underline{I}}\,\frac{\partial^2}{\partial z^2}(.) + \underline{\underline{Z}}^{\,2}\right) - \underline{\underline{\Omega}}^{\,2}\right]\underline{a} \tag{5.2.15}$$

[1] see also chapter 6.

[2] We introduce this equation *a priori* without presenting details of eigenfunction expansion methods used to develop this formula. These methods are investigated in chapter 6. Derivation of eq. (5.2.11) is given in sec. 6.3.1.

We now use the central difference approach with respect to variable z. Eq. (5.2.15) becomes:

$$\frac{\partial^2}{\partial t^2}\underline{a}\,(j_z) = -\left[\underline{\underline{G}}^{-1}\underline{\underline{S}}\left(\frac{2}{\Delta z^2}\underline{\underline{I}} - \underline{\underline{Z}}^{\,2}\right) + \underline{\underline{\Omega}}^{\,2}\right]\underline{a}\,(j_z) + \frac{1}{\Delta z^2}\underline{\underline{G}}^{-1}\underline{\underline{S}}\,[\underline{a}\,(j_z-1) + \underline{a}\,(j_z+1)] \tag{5.2.16}$$

An analogous approach may be applied for the magnetic fields. This leads to the following equation:

$$\frac{\partial^2}{\partial t^2}\underline{b}\,(j_z) = -\left[\underline{\underline{G}}^{-H}\underline{\underline{S}}^{\,H}\left(\frac{2}{\Delta z^2}\underline{\underline{I}} - \underline{\underline{Z}}^{\,2}\right) + \underline{\underline{\Omega}}^{\,2}\right]\underline{b}\,(j_z) + \frac{1}{\Delta z^2}\underline{\underline{G}}^{-H}\underline{\underline{S}}^{\,H}\,[\underline{b}\,(j_z-1) + \underline{b}\,(j_z+1)] \tag{5.2.17}$$

where $\underline{b} = [b_1, b_2, ...]^T$. Like in the previous section, j_z identifies a slice in the 1D grid (see fig. 5.2.4).

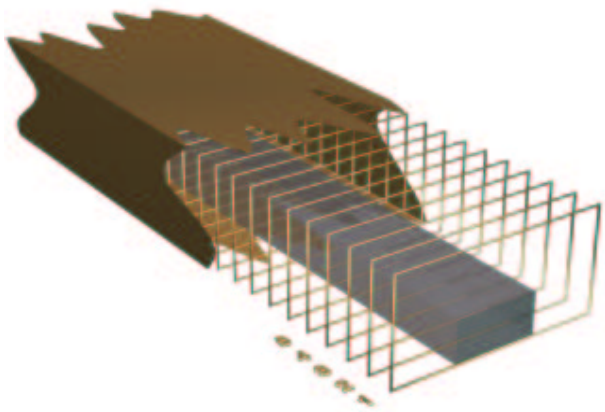

Figure 5.2.4: *A 1D grid of the eigenfunction expansion method in an inhomogeneously loaded rectangular waveguide.*

Note, that the PEE algorithm for modeling of homogeneous waveguides presented in sec. 5.2.1 is a special case of the technique presented here. When $\epsilon(x,y) = \epsilon$, $\mu(x,y) = \mu$ the matrices are defined as follows:

$$\underline{\underline{G}}^{-1}\underline{\underline{S}} = (\mu\epsilon)^{-1}\underline{\underline{I}} \tag{5.2.18}$$

$$\underline{\underline{\Omega}} = \mathrm{diag}(\omega_k) \tag{5.2.19}$$

$$\underline{\underline{Z}} = 0 \tag{5.2.20}$$

where ω_k are in this case the cutoff frequencies of the corresponding modes. Based on eq. (5.2.16) or (5.2.17), we may construct a matrix equation written in frequency domain. For instance, eq. (5.2.16) becomes:

$$\omega^2\underline{a}\,' = \underline{\underline{L}}\,\underline{a}\,' \tag{5.2.21}$$

where $\underline{a}\,' = [\underline{a}\,(0)^T, \underline{a}\,(1)^T, ...]^T$, and matrix $\underline{\underline{L}}$ has the following form:

$$\underline{\underline{L}} = \begin{bmatrix} \underline{\underline{X}} & \underline{\underline{Y}} & \underline{\underline{0}} & \cdots & \underline{\underline{0}} \\ \underline{\underline{Y}} & \underline{\underline{X}} & \underline{\underline{Y}} & & \vdots \\ \underline{\underline{0}} & \underline{\underline{Y}} & \underline{\underline{X}} & \ddots & \underline{\underline{0}} \\ \vdots & & \ddots & \ddots & \underline{\underline{Y}} \\ \underline{\underline{0}} & \cdots & \underline{\underline{0}} & \underline{\underline{Y}} & \underline{\underline{X}} \end{bmatrix} \tag{5.2.22}$$

with matrices $\underline{\underline{X}}$, $\underline{\underline{Y}}$ defined as:

$$\underline{\underline{X}} = \underline{\underline{G}}^{-1}\underline{\underline{S}}\left(\frac{2}{\Delta z^2}\underline{\underline{I}} - \underline{\underline{Z}}^2\right) + \underline{\underline{\Omega}}^2 \tag{5.2.23}$$

$$\underline{\underline{Y}} = -\frac{1}{\Delta z^2}\underline{\underline{G}}^{-1}\underline{\underline{S}} \tag{5.2.24}$$

Again, in practice, matrix $\underline{\underline{L}}$ is a part of global operator which models all subdomains using a hybrid approach (see the discussion in the previous section).

We may also write eqs. (5.2.16) or (5.2.17), in the form of an explicit update algorithm presented in sec. 2.2.3.2 in order to get the solution in the domain of time.

Stability condition of explicit update scheme In order to derive the stability condition for the explicit update algorithm, we should estimate the norm of operator $\underline{\underline{L}}$ defined by eq. (5.2.22). From the norm maximum, we get:

$$||\underline{\underline{L}}|| = \omega_{\max}^2 \leq \frac{4v_{\max}^2}{\Delta z^2} + \max_k(v_{\max}^2\beta_{zk}^2 + \omega_k^2) \tag{5.2.25}$$

According to sec. 2.2.3.2 and eq. (5.2.25) we get the following stability condition for the algorithm at hand:

$$\Delta t \leq \frac{1}{v_{\max}\sqrt{\frac{1}{\Delta z^2} + \frac{1}{4}\max_k\left(\beta_{zk}^2 + \frac{\omega_k^2}{v_{\max}^2}\right)}} \tag{5.2.26}$$

It should also be shown, that matrix $\underline{\underline{L}}$ has real and positive spectrum. In sec. 5.2.3, where we define the interface of the new approach with the classic finite difference algorithms, we limit the analysis to the case, when the expansion functions are calculated for a constant frequency (i.e. $\omega_k^2 = \text{const}$) or for $\beta_{zk}^2 = \text{const}$. It may be shown, that in these cases reality and positiveness of the spectrum of the operator results from the relations between the fields.

5.2.3 Interface with Finite-Difference methods

The classic finite difference algorithms can easily be combined with the eigenfunction expansion techniques introduced above. To this end, an interface between two algorithms has to be developed.

Since the algorithm presented in sec. 5.2.2 is a special case of the more general technique described in sec. 5.2.1, we define the interface with the standard finite difference algorithms only for the general case.

A sample interface between the modal expansion and finite difference techniques is shown in fig. 5.2.5. Two distinguished grid planes, 0 and 1, may be seen in this figure. The "finite difference" to "eigenfunction expansion" interface is defined at plane 0, and the "eigenfunction expansion" to "finite difference" interface is defined at plane 1. Both partial interfaces are described below.

"finite difference" to "eigenfunction expansion" interface We match the tangential electric field components at a selected plane (say plane $i_z = 0$ in fig. 5.2.5) in the following way:

$$\sum_i a_i(0)\vec{E}_{ti} = \vec{E}_t \tag{5.2.27}$$

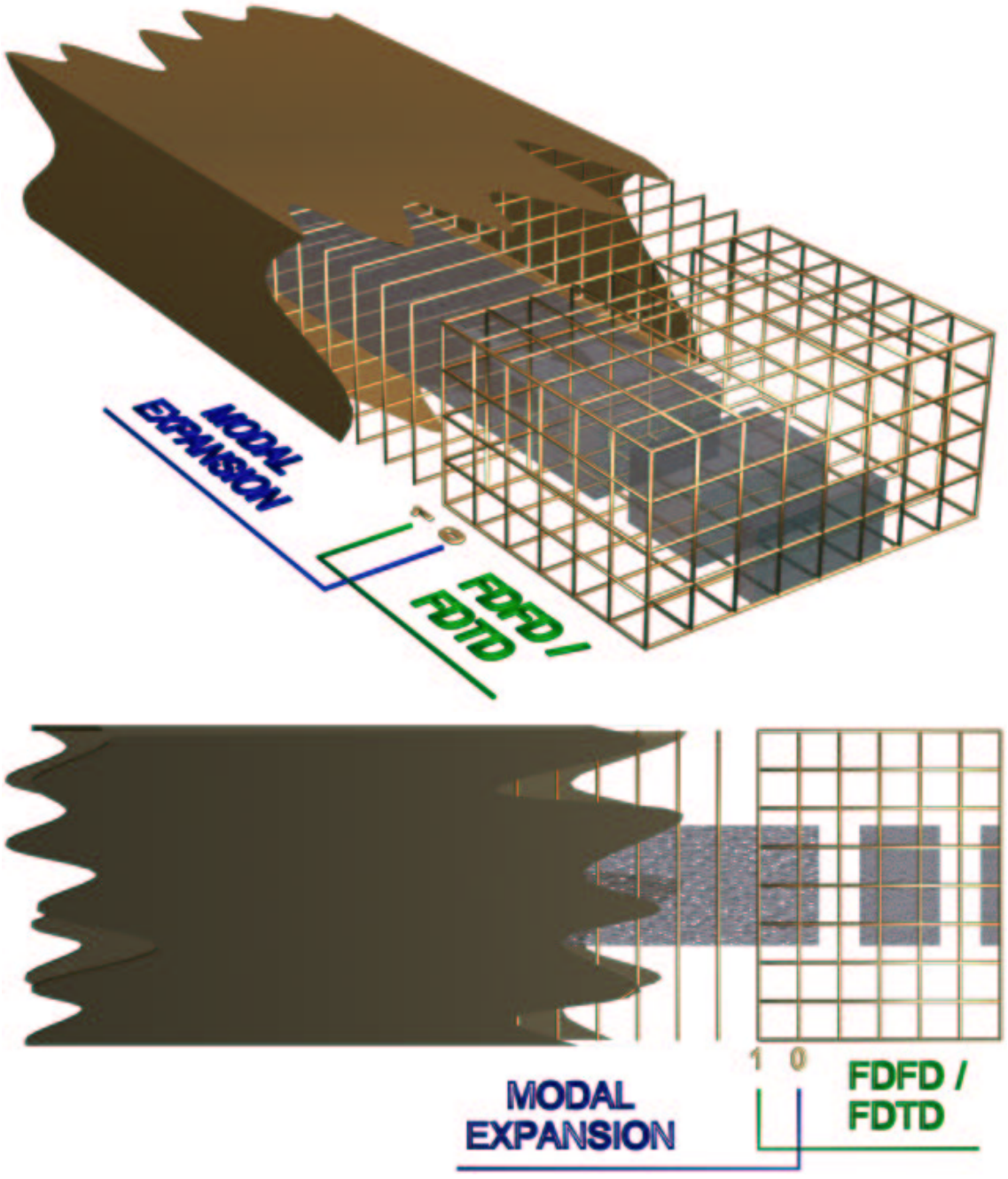

Figure 5.2.5: *Two views of interface between the modal expansion algorithm and the standard FD-FD/FD-TD technique.*

where the series on the left hand side arises from the eigenfunction expansion algorithm, and vector $\vec{E}_t$ represents the field calculated using the standard finite difference method. Assuming that the expansion functions are calculated for a constant frequency, i.e. $\omega_k^2 = \text{const} = \omega_0^2$ and hence

$$\underline{\underline{\Omega}}^{\,2} = \omega_0^2 \underline{\underline{I}} \tag{5.2.28}$$

we may make advantage of the orthogonality relations between intensity fields[3]. We reduce the series in eq. (5.2.27) to a single term by taking the inner product with functions $\vec{i}_z \times \vec{H}_{tk}$. We get:

$$a_k(0) < \vec{E}_{tk} \cdot \vec{i}_z \times \vec{H}_{tk} > = < \vec{E}_t \cdot \vec{i}_z \times \vec{H}_{tk} > \tag{5.2.29}$$

This gives the equation for $a_k(0)$:

$$a_k(0) = \frac{< \vec{E}_t \cdot \vec{i}_z \times \vec{H}_{tk} >}{< \vec{E}_{tk} \cdot \vec{i}_z \times \vec{H}_{tk} >} \tag{5.2.30}$$

In order to reduce the computation time, functions $\vec{E}_{tk}$, $\vec{H}_{tk}$ should be normalized as follows:

$$< \vec{E}_{tk} \cdot \vec{i}_z \times \vec{H}_{tk} > = 1 \tag{5.2.31}$$

Eq. (5.2.30) reduces to:

$$a_k(0) = < \vec{E}_t \cdot \vec{i}_z \times \vec{H}_{tk} > \tag{5.2.32}$$

This may be written in the form of an integral, as follows:

$$a_k(0) = \iint_S \vec{E}_t \cdot \vec{i}_z \times \vec{H}_{tk}^* ds \tag{5.2.33}$$

In the discrete domain, eq. (5.2.33) becomes:

$$\begin{aligned} a_k(0) &= \sum_{i_x} \sum_{i_y} \left[\Delta x e_x \left(i_x + \frac{1}{2}, i_y, i_{z0} \right) \cdot h_{yk}^* \left(i_x + \frac{1}{2}, i_y \right) \right. \\ &+ \left. \Delta y e_y \left(i_x, i_y + \frac{1}{2}, i_{z0} \right) \cdot h_{xk}^* \left(i_x, i_y + \frac{1}{2} \right) \right] \end{aligned} \tag{5.2.34}$$

where the fields are discretized in both methods in the same manner. If the eigenfunction expansion part of the hybrid algorithm is based on the solutions of 2D finite difference scheme, eq. (5.2.34) may be used directly as it is. Otherwise, the following expressions should be used for calculating of functions h_{xk} and h_{yk}:

$$h_{xk} \left(i_x, i_y + \frac{1}{2} \right) = \frac{1}{\Delta x \Delta y} \int_{-\frac{1}{2}}^{\frac{1}{2}} \int_0^1 H_{xk} \left(i_x + \alpha_x, i_y + \alpha_y \right) d\alpha_x d\alpha_y \tag{5.2.35}$$

$$h_{yk} \left(i_x + \frac{1}{2}, i_y \right) = \frac{1}{\Delta x \Delta y} \int_0^1 \int_{-\frac{1}{2}}^{\frac{1}{2}} H_{yk} \left(i_x + \alpha_x, i_y + \alpha_y \right) d\alpha_x d\alpha_y \tag{5.2.36}$$

An analogous derivation may be carried out if one assumes that the expansion functions are evaluated for $\beta_{zk}^2 = \text{const}$. In this case, matrix $\underline{\underline{Z}}^{\,2}$ in (5.2.11) becomes:

$$\underline{\underline{Z}}^{\,2} = \beta_{z0}^2 \underline{\underline{I}} \tag{5.2.37}$$

[3] See appendix B.

We use the orthogonality relations between flux density fields and normalize $\vec{D}_{tk}$, $\vec{B}_{tk}$ as follows:

$$< \vec{D}_{tk} \cdot \vec{i}_z \times \vec{B}_{tk} >= 1 \tag{5.2.38}$$

We calculate coefficients a_k at plane 0 in the following way:

$$a_k(0) =< \vec{D}_t \cdot \vec{i}_z \times \vec{B}_{tk} > \tag{5.2.39}$$

This defines the interface as follows:

$$\begin{aligned} a_k(0) &= \sum_{i_x} \sum_{i_y} \left[\Delta x d_x \left(i_x + \frac{1}{2}, i_y, i_{z0} \right) \cdot b^*_{yk} \left(i_x + \frac{1}{2}, i_y \right) \right. \\ &+ \left. \Delta y d_y \left(i_x, i_y + \frac{1}{2}, i_{z0} \right) \cdot b^*_{xk} \left(i_x, i_y + \frac{1}{2} \right) \right] \end{aligned} \tag{5.2.40}$$

where b_{xk}, b_{yk} are given by the following equations:

$$b_{xk} \left(i_x, i_y + \frac{1}{2} \right) = \frac{1}{\Delta x \Delta y} \int_{-\frac{1}{2}}^{\frac{1}{2}} \int_0^1 B_{xk} \left(i_x + \alpha_x, i_y + \alpha_y \right) d\alpha_x d\alpha_y \tag{5.2.41}$$

$$b_{yk} \left(i_x + \frac{1}{2}, i_y \right) = \frac{1}{\Delta x \Delta y} \int_0^1 \int_{-\frac{1}{2}}^{\frac{1}{2}} B_{yk} \left(i_x + \alpha_x, i_y + \alpha_y \right) d\alpha_x d\alpha_y \tag{5.2.42}$$

"eigenfunction expansion" to "finite difference" interface In order to define the interface from the eigenfunction expansion technique to the standard finite difference scheme, we match the tangential electric field at a different plane denoted by $i_z = 1$ in fig. 5.2.5:

$$\vec{E}_t = \sum_k a_k(1) \vec{E}_{tk} \tag{5.2.43}$$

This may be written in the discrete domain as follows:

$$e_x \left(i_x + \frac{1}{2}, i_y, i_{z0} \right) = \sum_k a_k(1) e_{xk} \left(i_x + \frac{1}{2}, i_y \right) \tag{5.2.44}$$

$$e_y \left(i_x, i_y + \frac{1}{2}, i_{z0} \right) = \sum_k a_k(1) e_{yk} \left(i_x, i_y + \frac{1}{2} \right) \tag{5.2.45}$$

Eqs. (5.2.44) and (5.2.45) define the interface.

5.3 General 3D subdomains

In this section, we present eigenfunction expansion technique with the space domain decomposition, which does not make any assumptions about the uniformity of subdomains. In the first step, we divide the domain into a set of subregions. A sample division is shown in fig. 5.3.1.

Unlike in the previous case, the eigenfunction expansion is carried out in 3D. To this end, every subregion is analyzed separately by closing it with the electric or magnetic walls at the boundaries of the division. Each boundary between two regions corresponds to two opposite walls, the electric on one side and the magnetic on the other. In order to satisfy the continuity (field matching) condition, the electric and magnetic surface currents are introduced. The electric surface current $\vec{J}_{ij}$ is defined at the electric wall

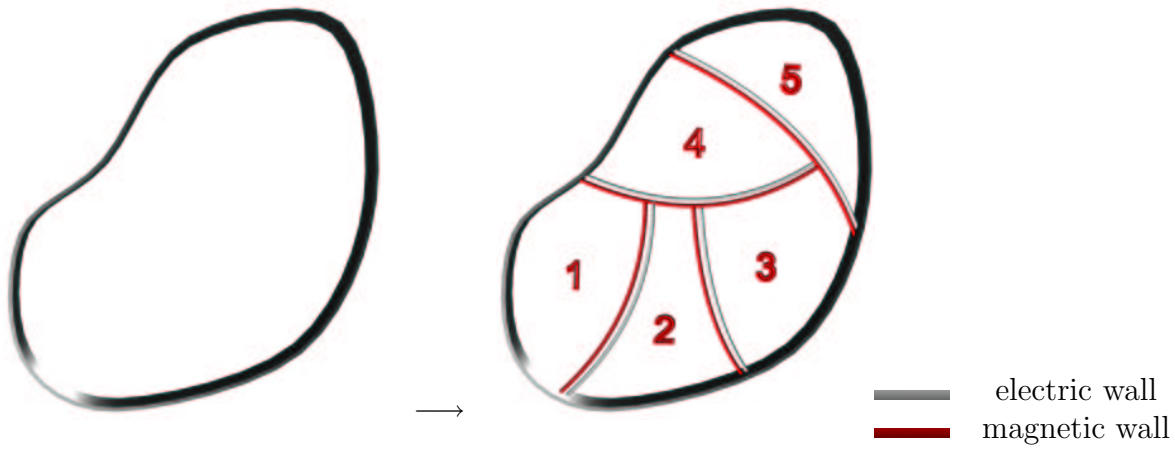

Figure 5.3.1: *Space domain decomposition in a general 3D approach.*

and the magnetic surface current $\vec{K}_{ij}$ at the magnetic wall. $\vec{J}_{ij}$, $\vec{K}_{ij}$ denote currents at the boundary in region i determined by the field in the neighboring region j. They are defined in terms of the tangential intensity field components in region j:

$$\vec{J}_{ij} = -\vec{n} \times \vec{H}_j \tag{5.3.1}$$
$$\vec{K}_{ij} = \vec{n} \times \vec{E}_j \tag{5.3.2}$$

In the following section, we derive the algorithm for modeling general 3D structures based on the presented space domain decomposition and on the eigenfunction expansion technique. The eigenfunctions taken into expansion are the modes of each subdomain being the solutions with the absence of coupling currents. In sec. 5.2.3, we introduce the interface between the new technique and the standard 3D finite difference schemes.

5.3.1 Formulation of the algorithm

Let us write Maxwell's equations for region i adjacent to region j:

$$\nabla \times \vec{H}_i = j\omega\vec{D}_i + \vec{J}_{ij} \tag{5.3.3}$$
$$\nabla \times \vec{E}_i = -j\omega\vec{B}_i - \vec{K}_{ij} \tag{5.3.4}$$

Putting (5.3.1), (5.3.2) into these equations, we get:

$$\nabla \times \vec{H}_i = j\omega\vec{D}_i - \vec{n} \times \vec{H}_j \tag{5.3.5}$$
$$\nabla \times \vec{E}_i = -j\omega\vec{B}_i - \vec{n} \times \vec{E}_j \tag{5.3.6}$$

Let us assume that we know the solution for region i totally enclosed by perfect electric and magnetic walls. These solutions are resonances occurring at ω_k with modal fields $\vec{E}_{ik}$ and $\vec{H}_{ik}$. The corresponding equations may be written as follows:

$$\nabla \times \vec{H}_{ik} = j\omega_{ik}\vec{D}_{ik} \tag{5.3.7}$$
$$\nabla \times \vec{E}_{ik} = -j\omega_{ik}\vec{B}_{ik} \tag{5.3.8}$$

Now, the fields in subregion i are expressed by the series of modes $\vec{E}_{ik}$, $\vec{H}_{ik}$:

$$\vec{E}_i = \sum_k a_{ik}\vec{E}_{ik} \tag{5.3.9}$$
$$\vec{H}_i = \sum_k b_{ik}\vec{H}_{ik} \tag{5.3.10}$$

with unknown coefficients a_{ik}, b_{ik}. Putting (5.3.9), (5.3.10) into (5.3.5), we get:

$$\sum_k b_{ik} \nabla \times \vec{H}_{ik} = j\omega \sum_k a_{ik} \vec{D}_{ik} - \vec{n} \times \vec{H}_j \tag{5.3.11}$$

Using eq. (5.3.7), this leads to the following equation:

$$j \sum_k (\omega a_{ik} - \omega_{ik} b_{ik}) \vec{D}_{ik} = \vec{n} \times \vec{H}_j \tag{5.3.12}$$

We take advantage of the orthogonality relations between flux density and intensity fields and apply a scalar product with a testing function $\vec{E}_{im}$, to both sides of (5.3.12). This reduces the series on the left hand side to a single term. We get:

$$j(\omega a_{im} - \omega_{im} b_{im}) < \vec{D}_{im}, \vec{E}_{im} > = < \vec{n} \times \vec{H}_j, \vec{E}_{im} > \tag{5.3.13}$$

It gives:

$$j\omega a_{im} - j\omega_{im} b_{im} = \frac{< \vec{n} \times \vec{H}_j, \vec{E}_{im} >}{< \vec{D}_{im}, \vec{E}_{im} >} \tag{5.3.14}$$

Now, we expand the magnetic field in the outer region j into a series of modes, analogously to eq. (5.3.10) written for region i:

$$\vec{H}_j = \sum_n b_{jn} \vec{H}_{jn} \tag{5.3.15}$$

We also assume that region i may have common boundary with several outer regions j. Eq. (5.3.14) becomes:

$$j\omega a_{im} - j\omega_{im} b_{im} = \sum_j \sum_n \frac{< \vec{n} \times \vec{H}_{jn}, \vec{E}_{im} >}{< \vec{D}_{im}, \vec{E}_{im} >} b_{jn} \tag{5.3.16}$$

Index j in the sum is swept over every neighboring region of subdomain i.

In a similar manner, starting from (5.3.6), we may develop the following equation:

$$j\omega b_{im} - j\omega_{im} a_{im} = -\sum_j \sum_n \frac{< \vec{n} \times \vec{E}_{jn}, \vec{H}_{im} >}{< \vec{B}_{im}, \vec{H}_{im} >} a_{jn} \tag{5.3.17}$$

Eqs. (5.3.16) and (5.3.17) may be written in a form of a matrix eigenproblem:

$$\omega \begin{bmatrix} \underline{a} \\ \underline{b} \end{bmatrix} = \begin{bmatrix} \underline{\underline{0}} & \underline{\underline{\Omega}} - \underline{\underline{A}} \\ \underline{\underline{\Omega}} - \underline{\underline{B}} & \underline{\underline{0}} \end{bmatrix} \begin{bmatrix} \underline{a} \\ \underline{b} \end{bmatrix} \tag{5.3.18}$$

where coefficients $A_{im,jn}$ and $B_{im,jn}$ are defined as follows; if $i \neq j$:

$$A_{im,jn} = j \frac{\left\langle \vec{n} \times \vec{H}_{jn}, \vec{E}_{im} \right\rangle}{\left\langle \vec{D}_{im}, \vec{E}_{im} \right\rangle} \tag{5.3.19}$$

$$B_{im,jn} = -j \frac{\left\langle \vec{n} \times \vec{E}_{jn}, \vec{H}_{im} \right\rangle}{\left\langle \vec{B}_{im}, \vec{H}_{im} \right\rangle} \tag{5.3.20}$$

and for $i = j$ coefficients $A_{im,jn}$ and $B_{im,jn}$ are equal 0. Note, that the scalar products in the numerators denote integrals over coupling surface S_{ij} and the scalar products in the

denominators are integrals over the entire volume V_i of region i. For instance, eq. (5.3.19) takes up the form:

$$A_{im,jn} = j\frac{\iint_{S_{ij}}(\vec{n}\times\vec{H}_{jn})\cdot\vec{E}_{im}\,ds}{\iiint_{V_i}\vec{D}_{im}\cdot\vec{E}_{im}\,dv} \tag{5.3.21}$$

Also note, that if the region is surrounded by electric and/or magnetic walls, then:

$$\left\langle\vec{D}_{im},\vec{E}_{im}\right\rangle = -\left\langle\vec{B}_{im},\vec{H}_{im}\right\rangle \tag{5.3.22}$$

We may construct two other eigenproblems by extracting vector $\underline{b}$ from eq. (5.3.18):

$$\omega^2\underline{a} = (\underline{\underline{\Omega}} - \underline{\underline{A}})(\underline{\underline{\Omega}} - \underline{\underline{B}})\underline{a} \tag{5.3.23}$$

or extracting vector $\underline{a}$:

$$\omega^2\underline{b} = (\underline{\underline{\Omega}} - \underline{\underline{B}})(\underline{\underline{\Omega}} - \underline{\underline{A}})\underline{b} \tag{5.3.24}$$

Explicit update scheme In order to derive the explicit update scheme from eq. (5.3.18), we rewrite it in the following form:

$$j\omega\begin{bmatrix}\underline{a}\\ \underline{c}\end{bmatrix} = \begin{bmatrix}\underline{\underline{0}} & \underline{\underline{\Omega}} - \underline{\underline{A}}\\ -\underline{\underline{\Omega}} + \underline{\underline{B}} & \underline{\underline{0}}\end{bmatrix}\begin{bmatrix}\underline{a}\\ \underline{c}\end{bmatrix} \tag{5.3.25}$$

where $\underline{c} = j\underline{b}$. Eq. (5.3.25) may be solved using the explicit update leap-frog procedure defined by the following equations:

$$\underline{c}^{\,i+0.5} = -\Delta t(\underline{\underline{\Omega}} - \underline{\underline{B}})\underline{a}^{\,i} + \underline{c}^{\,i-0.5} \tag{5.3.26}$$

$$\underline{a}^{\,i+1} = \Delta t(\underline{\underline{\Omega}} - \underline{\underline{A}})\underline{c}^{\,i+0.5} + \underline{a}^{\,i} \tag{5.3.27}$$

Another explicit update algorithm may be constructed from eigenproblem (5.3.23):

$$\underline{a}^{\,i+1} = [2\underline{\underline{I}} - \Delta t^2(\underline{\underline{\Omega}} - \underline{\underline{A}})(\underline{\underline{\Omega}} - \underline{\underline{B}})]\underline{a}^{\,i} - \underline{a}^{\,i-1} \tag{5.3.28}$$

and from eigenproblem (5.3.24):

$$\underline{b}^{\,i+0.5} = [2\underline{\underline{I}} - \Delta t^2(\underline{\underline{\Omega}} - \underline{\underline{B}})(\underline{\underline{\Omega}} - \underline{\underline{A}})]\underline{b}^{\,i-0.5} - \underline{b}^{\,i-1.5} \tag{5.3.29}$$

It is believed, that the algorithms defined by eqs. (5.3.26), (5.3.27), (5.3.28), and (5.3.29) are stable if the following condition is satisfied:

$$|\Delta t| \le \frac{1}{2\max_{i,k}\omega_{ik}} \tag{5.3.30}$$

5.3.2 Interface with Finite-Difference methods

In this section, we use the eigenfunction expansion algorithm presented in sec. 5.3.1 together with the finite difference techniques to create a new hybrid procedure. In the new approach, the eigenfunction expansion is applied for modeling of the subregions closed with the virtual electric and/or magnetic walls. The standard finite difference technique is used in the rest of the domain. Analogously to the technique presented in sec. 5.2.3, the interface is defined at two planes of Yee's grid. This is shown in fig. 5.3.2. "Finite difference" to "modal expansion" interface is defined at plane 0. The interface working in the other direction is defined at plane 1. Both partial interfaces are described below.

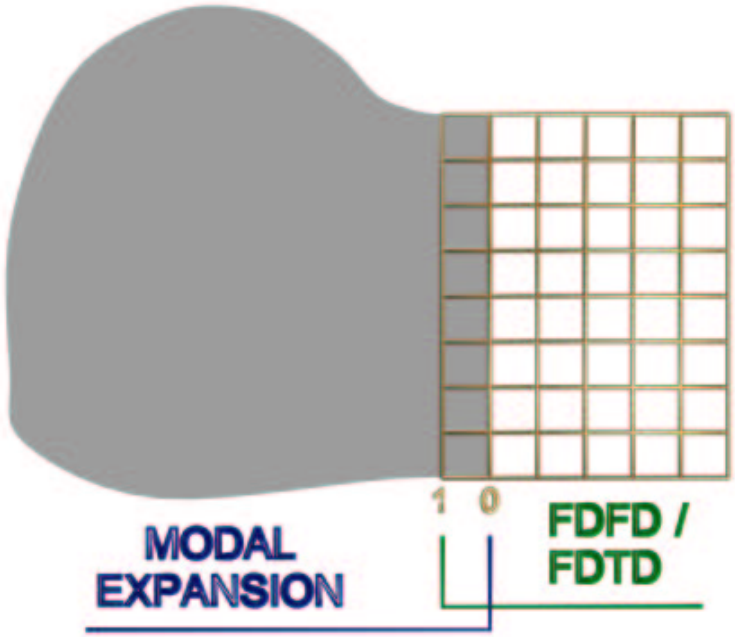

Figure 5.3.2: *Interface between the general 3D modal expansion algorithm and the standard finite difference technique.*

"finite difference" to "modal expansion" interface Eq. (5.3.18) including the interface, becomes:

$$\omega \begin{bmatrix} \underline{a} \\ \underline{b} \end{bmatrix} = \begin{bmatrix} \underline{\underline{0}} & \underline{\underline{\Omega}} - \underline{\underline{A}} \\ \underline{\underline{\Omega}} - \underline{\underline{B}} & \underline{\underline{0}} \end{bmatrix} \begin{bmatrix} \underline{a} \\ \underline{b} \end{bmatrix} + \begin{bmatrix} \underline{a}' \\ \underline{b}' \end{bmatrix} \tag{5.3.31}$$

where the additional primed vectors are associated with the interface. If we use the interface at a magnetic plane, coefficients b'_{ik} vanish, and coefficients a'_{ik} are given by the following equation:

$$a'_{ik} = -j \frac{\left\langle \vec{n} \times \vec{H}_{\mathrm{fd}}, \vec{E}_{ik} \right\rangle}{\left\langle \vec{E}_{ik}, \vec{D}_{ik} \right\rangle} \tag{5.3.32}$$

where $\vec{H}_{\mathrm{fd}}$ denote the intensity magnetic field at the boundary. This field is calculated using the finite difference procedure. Analogously, for the interface at an electric plane, we get:

$$b'_{ik} = j \frac{\left\langle \vec{n} \times \vec{E}_{\mathrm{fd}}, \vec{H}_{ik} \right\rangle}{\left\langle \vec{B}_{ik}, \vec{H}_{ik} \right\rangle} \tag{5.3.33}$$

and $\vec{E}_{\mathrm{fd}}$ is the intensity electric field at the boundary. Coefficients a'_{ik} vanish in this case.

"modal expansion" to "finite difference" interface If the interface is defined at the electric plane, we calculate the unknown electric field components at "finite difference part" based on eq. (5.3.9) in the following way:

$$\vec{E}_{\mathrm{fd}} = \sum_k a_{ik} \vec{E}_{ik} \tag{5.3.34}$$

Analogously, for the interface at the magnetic plane, we get:

$$\vec{H}_{\mathrm{fd}} = \sum_k b_{ik} \vec{H}_{ik} \tag{5.3.35}$$

Chapter 6

Eigenfunction expansion techniques for waveguides

6.1 Introduction

An important class of hybrid techniques discussed in chapter 5, involves the conversion of a 3D finite-difference problem into 1D. This can be achieved whenever the subspace to be analyzed is uniform in one direction and bounded in the other two. For such a case the field distribution in the transverse direction is expanded in the series of eigenfunctions and only one space coordinate needs to be discretized. This leads to the method which is called the partial eigenfunction expansion (PEE). When the cross-section is homogeneous, the eigenfunction expansion is straightforward both for time and frequency formulations. This is because the subspace treated with the PEE algorithm is in fact a section of a homogeneous waveguide and the eigenfunctions define the modal field distribution, which, in this type of guides, does not depend on frequency. Hence, the eigenfunctions can be calculated only once and then used as a basis both for frequency and time domain analysis. When the cross-section in loaded with an inhomogeneous material, the basis is more difficult to define. For inhomogeneous guides, the modal field distribution changes with frequency and this implies that the field has to be evaluated again for each frequency and it becomes unsuitable as a basis in time domain analysis. To overcome this one needs to derive eigenfunction formulations for waveguides in which the field at each frequency is well represented by the series involving functions that are independent of frequency. In [52] modal fields evaluated at cutoff were proposed to this end. A similar basis was also proposed by Rozzi et al. [66] in the context of fast evaluation of dispersion characteristics in fin lines. Indeed, since the PEE is applicable to the sections of waveguides one may develop formulations which are useful in the PEE by looking at the problem in more general context of finding the frequency dependent characteristics and modal fields using the expansion of fields into series of entire domain basis functions [57–59][1].

We start the presentation of the new algorithms from general operator investigations performed in sec. 6.2. We introduce eigenfunction expansion algorithms for bidirectional guides in sec. 6.3. In sec. 6.4, we give a note about practical aspects of calculation of the basis.

[1]The PEE method based on eq. (5.2.11) given *a priori* in chapter 5, and developed here in sec. 6.3.1 as one of the eigenfunction expansion algorithms.

6.2 General operator investigations

The problem of finding dispersion characteristics of a waveguide in a general form may be presented as the eigenproblem:

$$\mathbf{L}u = \lambda \mathbf{B}u \tag{6.2.1}$$

where $\mathbf{L}$, $\mathbf{B}$ are operators derived from Maxwell's equations. The solutions of this equation (λ_k, u_k) are the eigenpairs with physical interpretation depending on the operators. Usually (also in this thesis) λ_k is one of the variables β_{zk}^2, β_{zk}, ω_k^2, or ω_k, where β_{zk} is the propagation constant of the kth mode for a fixed value of frequency, and ω_k is the angular frequency of the kth mode for a fixed value of propagation constant[2]. Function u_k represents the field distribution of the kth mode. Operator $\mathbf{L}$ may be expressed as:

$$\mathbf{L} = \mathbf{M} + \gamma \mathbf{N} \tag{6.2.2}$$

where γ is a parameter. In practice, (λ_k, γ) represents one of the pairs: (β_{zk}^2, ω^2), (β_{zk}, ω), (ω_k^2, β_z^2), or (ω_k, β_z).

Substituting (6.2.2) into (6.2.1), we get the following eigenproblem, which typically has to be solved for a large number of values of γ:

$$(\mathbf{M} + \gamma \mathbf{N})u = \lambda \mathbf{B}u \tag{6.2.3}$$

As a result, one gets the dispersion characteristic of the waveguide in the form $\lambda(\gamma)$. Solving of eq. (6.2.3) using standard methods for a large number of values of parameter γ may be very time-consuming. We present new methods of solving these eigenproblems based on the knowledge of the solution at a few points $(\lambda_i, \gamma_i, u_i)$. General EE algorithms are presented in sec. 6.2.1. In sec. 6.2.2, we introduce special cases of these methods which take advantage of orthogonality relations between the fields. The latter class includes the formulations which may directly be applied in the PEE algorithms in time and frequency domain.

6.2.1 General form of eigenfunction expansion algorithms

Consider the eigenproblem of the form (6.2.3). We assume that we know the solution of this eigenproblem at K discrete points $\gamma_1, \gamma_2, ..., \gamma_K$:

$$(\mathbf{M} + \gamma_k \mathbf{N})u_k = \lambda_k \mathbf{B}u_k \tag{6.2.4}$$

To find the solution for $\gamma \neq \gamma_k$, we approximate function u by the series of known eigenfunctions u_k:

$$u = \sum_k a_k u_k \tag{6.2.5}$$

Substituting (6.2.5) into (6.2.3), we get:

$$\sum_k a_k (\mathbf{M} + \gamma \mathbf{N})u_k = \sum_k a_k \lambda \mathbf{B}u_k \tag{6.2.6}$$

Using (6.2.4), eq. (6.2.6) takes up the form:

$$\sum_k a_k (\gamma - \gamma_k)\mathbf{N}u_k = \sum_k a_k (\lambda - \lambda_k)\mathbf{B}u_k \tag{6.2.7}$$

[2]See sec. 3.5.3 for various formulations of eigenproblems in 2D electromagnetics.

It is important to note, that operator **M** has vanished at this step. In practice, this means significant simplification of the equation, since operator **M** is usually associated with a complicated differential operator, and the remaining operators **N** and **B** are simple scaling functions. Taking the inner product of both sides of (6.2.7) with testing functions p_l, we get:

$$\sum_k a_k(\gamma - \gamma_k) \langle \mathbf{N}u_k, p_l \rangle = \sum_k a_k(\lambda - \lambda_k) \langle \mathbf{B}u_k, p_l \rangle \tag{6.2.8}$$

This equation may be presented in the form of a generalized matrix eigenproblem:

$$\underline{\underline{T}}(\gamma \underline{\underline{I}} - \underline{\underline{\Gamma}})\underline{a} = \underline{\underline{V}}(\lambda \underline{\underline{I}} - \underline{\underline{\Lambda}})\underline{a} \tag{6.2.9}$$

with the elements of matrices $\underline{\underline{T}}$ and $\underline{\underline{V}}$ given by:

$$T_{lk} = \langle \mathbf{N}u_k, p_l \rangle \tag{6.2.10}$$

$$V_{lk} = \langle \mathbf{B}u_k, p_l \rangle \tag{6.2.11}$$

and $\underline{\underline{\Lambda}}$, $\underline{\underline{\Gamma}}$ being diagonal matrices:

$$\underline{\underline{\Lambda}} = \mathrm{diag}(\lambda_k) \tag{6.2.12}$$

$$\underline{\underline{\Gamma}} = \mathrm{diag}(\gamma_k) \tag{6.2.13}$$

Solving of (6.2.9) yields the characteristics $\lambda(\gamma)$ or $\gamma(\lambda)$ depending on which of two variables, γ or λ, is treated as a parameter. For the fixed value of γ, eq. (6.2.9) has the eigenpairs $(\lambda_m, \underline{a}_m)$, and for fixed λ, the eigenpairs are $(\gamma_m, \underline{a}_m)$. The elements of eigenvectors $\underline{a}_m$ are magnitudes of the eigenfunctions taken into expansion.

6.2.2 Eigenfunction expansion algorithms based on orthogonality relations

In the previous section we did not make any assumption about the testing functions p_l. Let us now assume, that they are the eigenfunctions w_{l*} of the eigenproblem transposed to (6.2.4):

$$(\mathbf{M}^H + \gamma_k \mathbf{N}^H) w_{k*} = \lambda_k^* \mathbf{B}^H w_{k*} \tag{6.2.14}$$

Taking into consideration the orthogonality between left and right eigenvectors of an operator (see discussion in app. B), we see that if $\gamma_k = \mathrm{const}(k)$ (i.e. $\gamma_1 = \gamma_2 = \ldots = \gamma_K$), matrix $\underline{\underline{V}}$ defined by eq. (6.2.11) is diagonal. For the same reason, matrix $\underline{\underline{T}}$ given by eq. (6.2.10) is diagonal, when $\lambda_k = \mathrm{const}(k)$. In both cases, the construction of eigenproblem may be simplified. Since these cases are dual to each other, we limit the discussion to a constant value of $\gamma_k = \gamma_0$. We may construct two eigenproblems for, respectively, λ and γ being a parameter:

$$(\lambda \underline{\underline{I}} - \underline{\underline{\Lambda}})^{-1} \underline{\underline{R}}\,\underline{a} = \frac{1}{\gamma - \gamma_0} \cdot \underline{a} \tag{6.2.15}$$

$$\left[(\gamma - \gamma_0)\underline{\underline{R}} + \underline{\underline{\Lambda}}\right] \underline{a} = \lambda \underline{a} \tag{6.2.16}$$

The first formulation gives eigenvalues $(\gamma - \gamma_0)^{-1}$ and leads to characteristics in form $\gamma(\lambda)$. In the second case, the eigenvalues are λ, giving characteristics $\lambda(\gamma)$. The elements of matrix $\underline{\underline{R}}$ are given by the equation:

$$R_{lk} = \frac{\langle \mathbf{N}u_k, w_{l*} \rangle}{\langle \mathbf{B}u_l, w_{l*} \rangle} \tag{6.2.17}$$

Alternative forms of the eigenproblem are also possible. Choosing functions $(\mathbf{BN}^{-1})^H w_{l*}$ as testing functions p_l yields diagonality of matrix $\underline{\underline{T}}$ in eq. (6.2.9). This gives the following eigenproblem with parameter λ:

$$\underline{\underline{\tilde{R}}}\,(\lambda\underline{\underline{I}} - \underline{\underline{\Lambda}})\underline{a} = (\gamma - \gamma_0)\underline{a} \tag{6.2.18}$$

The eigenvalues are $(\gamma - \gamma_0)$ and the elements of matrix $\underline{\underline{\tilde{R}}}$ are:

$$\tilde{R}_{lk} = \frac{\langle \mathbf{BN}^{-1}\mathbf{B}u_k, w_{l*}\rangle}{\langle \mathbf{B}u_l, w_{l*}\rangle} \tag{6.2.19}$$

6.3 Algorithms for bidirectional media

In the previous section, we introduced the EE algorithms in a general operator forms. Here, we will substitute the eigenproblems for bidirectional waveguides formulated in sec. 3.5.3 into those templates. We assume, that the waveguide is filled with nondispersive materials, and hence may be described by equation of the form (6.2.3), with operators $\mathbf{M}$ and $\mathbf{N}$ independent on λ and γ. In sec. 6.3.1, we derive a general form of the EE algorithms. In sec. 6.3.2, we present their special cases taking advantage of the orthogonality relations between the field components.

6.3.1 General form

In order to define a general eigenfunction expansion algorithm for bidirectional waveguides filled with non-dispersive materials, we start the analysis from wave equation (A.3.14). This equation may be presented in the form (6.2.3), where the symbols are defined as follows:

$$\mathbf{M} = \mathbf{Z_m G_{tm} M_{zz}^{-1} D_{tm} Z_e E_{tt}^{-1}} + \mathbf{Z_m M_{tt}^{-1} Z_e G_{te} E_{zz}^{-1} D_{te}} \tag{6.3.1}$$

$$\mathbf{N} = -\mathbf{Z_m M_{tt}^{-1} Z_e E_{tt}^{-1}} \tag{6.3.2}$$

$$\mathbf{B} = \mathbf{I} \tag{6.3.3}$$

$$\lambda = \omega^2 \tag{6.3.4}$$

$$\gamma = \beta_z^2 \tag{6.3.5}$$

$$u = d_t \tag{6.3.6}$$

Further on, we follow the procedure presented in sec. 6.2.1. Since we did not make any assumption regarding functions p_l, they may be arbitrary. Here, we choose functions $p_l = \mathbf{Z_m} b_{tl*}$ which are the left eigenfunctions of the operator[3]. As introduced in sec. 6.2.2, this approach enables one to take advantage of the orthogonality relations between the fields[4] if one of the variables ω_l^2 or β_{zl}^2 has a fixed value independent of l. These cases are discussed in sec. 6.3.2.

For the problem at hand, eq. (6.2.8) becomes:

$$\sum_k a_k(\omega^2 - \omega_k^2)\,\langle d_{tl}, \mathbf{Z_m} b_{tl*}\rangle = -\sum_k a_k(\beta_z^2 - \beta_{zk}^2)\left\langle \mathbf{Z_m M_{tt}^{-1} Z_e E_{tt}^{-1}} d_{tk}, \mathbf{Z_m} b_{tl*}\right\rangle \tag{6.3.7}$$

[3]Functions b_{tl*} represent transverse magnetic flux densities corresponding to the points $(\omega_l^*, \beta_{zl}^*)$ from the dispersion characteristics.

[4]See appendix B.

The right side may be simplified by rearranging the operators in the inner product. We get:

$$\sum_k a_k(\omega^2 - \omega_k^2)\,\langle d_{tl}, \mathbf{Z_m} b_{tl*}\rangle = \sum_k a_k(\beta_z^2 - \beta_{zk}^2)\,\langle e_{tk}, \mathbf{Z_m} h_{tl*}\rangle \tag{6.3.8}$$

From this equation, we derive a generalized eigenproblem, which gives the eigenvalues β_z^2 versus ω or ω^2 versus β_z. The eigenproblem is given by the following matrix equation (compare to eq. 6.2.9):

$$\underline{\underline{G}}\,(\omega^2\underline{\underline{I}} - \underline{\underline{\Omega}}^{\,2})\underline{a} = \underline{\underline{S}}\,(\beta_z^2\underline{\underline{I}} - \underline{\underline{Z}}^{\,2})\underline{a} \tag{6.3.9}$$

where: $\underline{\underline{\Omega}}^{\,2} = \mathrm{diag}(\omega_k^2)$, $\underline{\underline{Z}}^{\,2} = \mathrm{diag}(\beta_{zk}^2)$, and the elements of matrices $\underline{\underline{G}}$ and $\underline{\underline{S}}$ are given by the equations:

$$G_{lk} = \langle d_{tk}, \mathbf{Z_m} b_{tl*}\rangle \tag{6.3.10}$$

$$S_{lk} = \langle e_{tk}, \mathbf{Z_m} h_{tl*}\rangle \tag{6.3.11}$$

Analogous equation written for the magnetic fields has the form:

$$\underline{\underline{G}}^{\,H}(\omega^2\underline{\underline{I}} - \underline{\underline{\Omega}}^{\,2})\underline{b} = \underline{\underline{S}}^{\,H}(\beta_z^2\underline{\underline{I}} - \underline{\underline{Z}}^{\,2})\underline{b} \tag{6.3.12}$$

The elements of eigenvectors $\underline{a}$ are the magnitudes of electric flux density (or electric intensity) functions taken into expansion. The elements of eigenvectors $\underline{b}$ correspond to the magnetic fields.

Equation (6.3.9) and its transposed counterpart (6.3.12) involve terms proportional to ω^2 and β_z^2 and hence have the form which is suitable for the PEE algorithms. The detailed description of the application or the wave equations given in this form for the time and frequency analysis of uniform subdomains was given earlier in section 5.2.2 of this thesis.

6.3.2 Algorithms based on orthogonality relations

According to the discussion performed in sec. 6.2.2, the EE algorithms may be simplified if we fix one of the parameters λ or γ in the original eigenproblem (6.2.3). This is due to the orthogonality relations between the functions in the inner product. For the problem at hand, this simplification takes place if we fix one of the variables ω^2 or β_z^2 when calculating the basis. Both cases generate a set of eigenproblems which may be treated as separate EE algorithms. All these techniques are listed below.

Basis for $\beta_z = \beta_{z0} = \mathrm{const}$ In this case, we use orthogonality relation (B.2.10). Eqs. (6.2.15), (6.2.16) generate two pairs of eigenproblems:

$$(\omega^2\underline{\underline{I}} - \underline{\underline{\Omega}}^{\,2})^{-1}\underline{\underline{A}}\,\underline{a} = \frac{1}{\beta_z^2 - \beta_{z0}^2}\cdot\underline{a} \tag{6.3.13}$$

$$(\omega^2\underline{\underline{I}} - \underline{\underline{\Omega}}^{\,2})^{-1}\underline{\underline{A}}'\underline{b} = \frac{1}{\beta_z^2 - \beta_{z0}^2}\cdot\underline{b} \tag{6.3.14}$$

$$\left[(\beta_z^2 - \beta_{z0}^2)\underline{\underline{A}} + \underline{\underline{\Omega}}^{\,2}\right]\underline{a} = \omega^2\underline{a} \tag{6.3.15}$$

$$\left[(\beta_z^2 - \beta_{z0}^2)\underline{\underline{A}}' + \underline{\underline{\Omega}}^{\,2}\right]\underline{b} = \omega^2\underline{b} \tag{6.3.16}$$

where $\underline{\underline{\Omega}}^2 = \mathrm{diag}(\omega_k^2)$, and the elements of matrices $\underline{\underline{A}}$, $\underline{\underline{A}}'$ are given by the equations:

$$A_{lk} = \frac{\langle e_{tk}, \mathbf{Z_m} h_{tl*} \rangle}{\langle d_{tl}, \mathbf{Z_m} b_{tl*} \rangle} \tag{6.3.17}$$

$$A'_{lk} = \frac{\langle h_{tk}, \mathbf{Z_e} e_{tl*} \rangle}{\langle b_{tl}, \mathbf{Z_e} d_{tl*} \rangle} \tag{6.3.18}$$

Note, that matrices $\underline{\underline{\Omega}}^2$, $\underline{\underline{A}}$ and $\underline{\underline{A}}'$ do not depend on ω or β and hence do not have to be recalculated when sweeping the parameter. A similar situation takes place for the remaining algorithms.

Eq. (6.2.18) leads to the following eigenproblems:

$$\underline{\underline{\tilde{A}}}(\omega^2 \underline{\underline{I}} - \underline{\underline{\Omega}}^2)\underline{a} = (\beta_z^2 - \beta_{z0}^2)\underline{a} \tag{6.3.19}$$

$$\underline{\underline{\tilde{A}}}'(\omega^2 \underline{\underline{I}} - \underline{\underline{\Omega}}^2)\underline{b} = (\beta_z^2 - \beta_{z0}^2)\underline{b} \tag{6.3.20}$$

with $\underline{\underline{\Omega}}^2 = \mathrm{diag}(\omega_k^2)$, and $\underline{\underline{\tilde{A}}}$, $\underline{\underline{\tilde{A}}}'$ defined by:

$$\tilde{A}_{lk} = \frac{\langle \mathbf{M_{tt}} \mathbf{Z_e} d_{tk}, \mathbf{Z_e} \mathbf{E_{tt}} \mathbf{Z_m} b_{tl*} \rangle}{\langle d_{tl}, \mathbf{Z_m} b_{tl*} \rangle} \tag{6.3.21}$$

$$\tilde{A}'_{lk} = \frac{\langle \mathbf{E_{tt}} \mathbf{Z_m} b_{tk}, \mathbf{Z_m} \mathbf{M_{tt}} \mathbf{Z_e} d_{tl*} \rangle}{\langle b_{tl}, \mathbf{Z_e} d_{tl*} \rangle} \tag{6.3.22}$$

If the fields are normalized as follows:

$$\langle d_{tl}, \mathbf{Z_m} b_{tl*} \rangle = \xi \tag{6.3.23}$$

where $\xi \neq 0$ is a constant, pairs of matrices $\underline{\underline{A}}'$, $\underline{\underline{A}}$ and $\underline{\underline{\tilde{A}}}'$, $\underline{\underline{\tilde{A}}}$ are Hilbertian transpose of one another (i.e., $\underline{\underline{A}}' = \underline{\underline{A}}^H$ and $\underline{\underline{\tilde{A}}}' = \underline{\underline{\tilde{A}}}^H$).

Basis for $\omega = \omega_0 = \mathrm{const}$ Now, we consider the basis constructed from modes at frequency ω_0. The suitable orthogonality relation is given by eq. (B.2.12). From (6.2.15) and (6.2.16), we get the following equations:

$$(\beta_z^2 \underline{\underline{I}} - \underline{\underline{Z}}^2)^{-1} \underline{\underline{C}}\, \underline{a} = \frac{1}{\omega^2 - \omega_0^2} \cdot \underline{a} \tag{6.3.24}$$

$$(\beta_z^2 \underline{\underline{I}} - \underline{\underline{Z}}^2)^{-1} \underline{\underline{C}}'\, \underline{b} = \frac{1}{\omega^2 - \omega_0^2} \cdot \underline{b} \tag{6.3.25}$$

$$\left[(\omega^2 - \omega_0^2)\underline{\underline{C}} + \underline{\underline{Z}}^2\right] \underline{a} = \beta_z^2 \underline{a} \tag{6.3.26}$$

$$\left[(\omega^2 - \omega_0^2)\underline{\underline{C}}' + \underline{\underline{Z}}^2\right] \underline{b} = \beta_z^2 \underline{b} \tag{6.3.27}$$

where $\underline{\underline{Z}}^2 = \mathrm{diag}(\beta_{zk}^2)$, and $\underline{\underline{C}}$, $\underline{\underline{C}}'$ are defined as follows:

$$C_{lk} = \frac{\langle d_{tk}, \mathbf{Z_m} b_{tl*} \rangle}{\langle e_{tl}, \mathbf{Z_m} h_{tl*} \rangle} \tag{6.3.28}$$

$$C'_{lk} = \frac{\langle b_{tk}, \mathbf{Z_e} d_{tl*} \rangle}{\langle h_{tl}, \mathbf{Z_e} e_{tl*} \rangle} \tag{6.3.29}$$

The alternative algorithm (6.2.18) takes up the following form:

$$\underline{\underline{\tilde{C}}}(\beta_z^2 \underline{\underline{I}} - \underline{\underline{Z}}^2)\underline{a} = (\omega^2 - \omega_0^2)\underline{a} \tag{6.3.30}$$

$$\underline{\underline{\tilde{C}}}'(\beta_z^2 \underline{\underline{I}} - \underline{\underline{Z}}^2)\underline{b} = (\omega^2 - \omega_0^2)\underline{b} \tag{6.3.31}$$

where $\underline{\underline{Z}}^2 = \mathrm{diag}(\beta_{zk}^2)$, and $\underline{\underline{\tilde{C}}}$, $\underline{\underline{\tilde{C}}}'$ are given by equations:

$$\tilde{C}_{lk} = \frac{\left\langle \mathbf{M}_{\mathbf{tt}}^{-1}\mathbf{Z}_{\mathbf{e}}e_{tk}, \mathbf{Z}_{\mathbf{e}}\mathbf{E}_{\mathbf{tt}}^{-1}\mathbf{Z}_{\mathbf{m}}h_{tl*}\right\rangle}{\langle e_{tl}, \mathbf{Z}_{\mathbf{m}}h_{tl*}\rangle} \tag{6.3.32}$$

$$\tilde{C}'_{lk} = \frac{\left\langle \mathbf{E}_{\mathbf{tt}}^{-1}\mathbf{Z}_{\mathbf{m}}h_{tk}, \mathbf{Z}_{\mathbf{m}}\mathbf{M}_{\mathbf{tt}}^{-1}\mathbf{Z}_{\mathbf{e}}e_{tl*}\right\rangle}{\langle h_{tl}, \mathbf{Z}_{\mathbf{e}}e_{tl*}\rangle} \tag{6.3.33}$$

6.4 Methods for calculation of EE basis

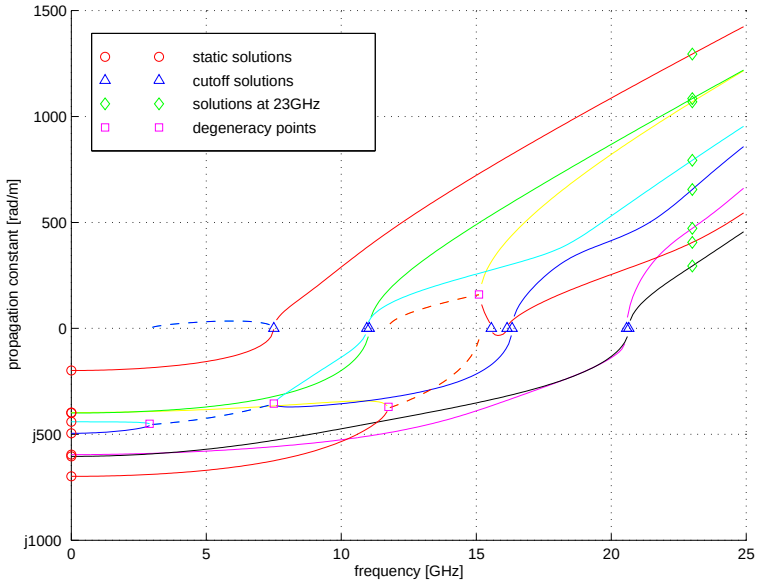

Figure 6.4.1: *Sample dispersion characteristics of a waveguide, various bases and degeneration points.*

In order to construct the EE eigenproblems presented in the previous sections, we have to calculate the basis. At the first step we should choose points at the dispersion characteristics of the analyzed waveguide at which the basis will be constructed. The choice of these points may have large influence on the final results. Fig. 6.4.1 presents sample dispersion characteristics and several possible bases[5] consisting of: static solutions (circles), cutoff solutions (triangles), and modes at 23GHz (diamonds). In all these cases we may take advantage of the orthogonality relations between the fields as described earlier. However, there are more possibilities for this choice. Let us look at the desired properties of the basis. The basis has to be minimal [38], i.e. none of its elements can be a linear combination of the others. Otherwise, one of the matrices $\underline{\underline{G}}$ or $\underline{\underline{S}}$ in eq. (6.3.9) will be singular. It is obvious, that the solutions for $\omega_k = \omega_0 = \text{const}$ or $\beta_{zk} = \beta_{z0} = \text{const}$ give a minimal basis, if they do not contain points of degeneracy at the dispersion characteristics[6]. Points of degeneracy are not present in the basis calculated for strictly imaginary ω_k or for strictly real β_{zk}. This includes a static case ($\omega_k = 0$) and cutoff ($\beta_{zk} = 0$).

[5] See also fig. 5.2.3.

[6] These are points at which two strictly real or strictly imaginary modes change their character giving a pair of two coupled complex modes.

Once the points for the basis have been chosen from the dispersion characteristics, we have to find distributions of the appropriate field components at these points. This requires solving one or a few eigenproblems developed in sec. 3.5.3 using a standard method. Both, the electric and magnetic field components have to be determined. However, there is no need to solve of a pair of eigenproblems, one for the electric and the other for the magnetic field. The electric field may be calculated from the magnetic one (and vice versa) using Maxwell's equations. Therefore, it is enough to solve only one eigenproblem corresponding to one field component and find the other from the relations between the fields. Such an approach is presented in sec. 6.4.1.

Further reduction of the computation effort during construction of the basis may be achieved if it is built from the static modes or the modes at cutoff. In both these cases, it is enough to solve two smaller scalar eigenproblems instead of a big one. This leads to the determination of the longitudinal field components e_z and h_z. The transverse fields are found based on Maxwell's relations. Procedures for determination of the transverse field components at cutoff and in the static case are presented in, respectively, secs. 6.4.2 and 6.4.3. It should be noted, that the eigenfunctions being solutions of the eigenproblems formulated in sec. 3.5.3 are basis functions, and such functions have to be determined. With appropriate scaling, these functions become the field distributions for the corresponding modes. In some cases the basis function exists but the corresponding field distribution vanishes. It means, that this function has zero amplitude. Such a situation takes place in the case of the static solutions and the modes at cutoff. For instance, modes E at cutoff have the longitudinal field component e_z (d_z) and the transverse field h_t (b_t). All the other fields vanish. In other words, basis function e_t has zero amplitude.

6.4.1 Basis constructed from an arbitrary set of modes

When constructing a basis in a general case, the electric transverse field components may be calculated from the magnetic ones and vice versa. In order to find such a relation, we may use the four field components formulations for bidirectional waveguides presented in tab. 3.5.7. Expressing e_t in terms of the magnetic field, we get:

$$e_t = -\frac{\omega}{\beta_z}\mathbf{Z_m}b_t + \frac{1}{\omega\beta_z}\mathbf{G_{te}}\mathbf{E_{zz}^{-1}}\mathbf{D_{te}}\mathbf{Z_m}h_t \tag{6.4.1}$$

An analogous equation for h_t in terms of the electric fields has the form:

$$h_t = \frac{\omega}{\beta_z}\mathbf{Z_e}d_t + \frac{1}{\omega\beta_z}\mathbf{G_{tm}}\mathbf{M_{zz}^{-1}}\mathbf{D_{tm}}\mathbf{Z_e}e_t \tag{6.4.2}$$

If basis functions are to be found instead of the actual field distribution, we may use these equations also for $\beta_z = 0$ disregarding factors $\frac{1}{\beta_z}$. Note, however, that some of the cutoff field components have zero amplitude in the real field distribution.

Eqs. (6.4.1), (6.4.2) have two dual counterparts, which may also be used as relations between electric and magnetic fields (compare with the formulations in tab. 3.5.8):

$$d_t = -\frac{\beta_z}{\omega}\mathbf{Z_m}h_t + \frac{1}{\beta_z\omega}\mathbf{Z_m}\mathbf{G_{tm}}\mathbf{M_{zz}^{-1}}\mathbf{D_{tm}}b_t \tag{6.4.3}$$

$$b_t = \frac{\beta_z}{\omega}\mathbf{Z_e}e_t - \frac{1}{\beta_z\omega}\mathbf{Z_e}\mathbf{G_{te}}\mathbf{E_{zz}^{-1}}\mathbf{D_{te}}d_t \tag{6.4.4}$$

These equations may also be used for building the basis in static case ($\omega = 0$), if one disregards factors $\frac{1}{\omega}$.

6.4.2 Basis consisting of modes at cutoff

For $\beta_{zk} = 0$, i.e. at cutoff, the modes are of type TM ($h_z = 0$) or TE ($e_z = 0$). In this case, formulations for the transverse field components presented in tab. 3.5.9 may be split into two scalar eigenproblems, for e_z and h_z field components (tab. 3.5.10):

$$\mathbf{E}_{\mathbf{zz}}^{-1}\mathbf{D}_{\mathbf{te}}\mathbf{Z}_{\mathbf{m}}\mathbf{M}_{\mathbf{tt}}^{-1}\mathbf{Z}_{\mathbf{e}}\mathbf{G}_{\mathbf{te}}e_{zj} = \omega_{ej}^2 e_{zj} \tag{6.4.5}$$

$$\mathbf{M}_{\mathbf{zz}}^{-1}\mathbf{D}_{\mathbf{tm}}\mathbf{Z}_{\mathbf{e}}\mathbf{E}_{\mathbf{tt}}^{-1}\mathbf{Z}_{\mathbf{m}}\mathbf{G}_{\mathbf{tm}}h_{zj} = \omega_{hj}^2 h_{zj} \tag{6.4.6}$$

Note, that the size of the problems is reduced by a factor of two.

The solutions of eqs. (6.4.5) and (6.4.6) are, respectively, eigenpairs (ω_{ej}, e_{zj}) and (ω_{hj}, h_{zj}), from which we calculate the transverse field components. The appropriate equations for modes TM have the form:

$$b_{tej} = \frac{1}{j\omega_{ej}}\mathbf{Z}_{\mathbf{e}}\mathbf{G}_{\mathbf{te}}e_{zj} \tag{6.4.7}$$

$$h_{tej} = \mathbf{M}_{\mathbf{tt}}^{-1}b_{tej} \tag{6.4.8}$$

$$e_{tej} \leftarrow -\omega_{ej}\mathbf{Z}_{\mathbf{m}}b_{tej} + \frac{1}{\omega_{ej}}\mathbf{G}_{\mathbf{te}}\mathbf{E}_{\mathbf{zz}}^{-1}\mathbf{D}_{\mathbf{te}}\mathbf{Z}_{\mathbf{m}}h_{tej} \tag{6.4.9}$$

$$d_{tej} = \mathbf{E}_{\mathbf{tt}}e_{tej} \tag{6.4.10}$$

For modes TE, we use the following equations:

$$d_{thj} = -\frac{1}{j\omega_{hj}}\mathbf{Z}_{\mathbf{m}}\mathbf{G}_{\mathbf{tm}}h_{zj} \tag{6.4.11}$$

$$e_{thj} = \mathbf{E}_{\mathbf{tt}}^{-1}d_{thj} \tag{6.4.12}$$

$$h_{thj} \leftarrow \omega_{hj}\mathbf{Z}_{\mathbf{e}}d_{thj} + \frac{1}{\omega_{hj}}\mathbf{G}_{\mathbf{tm}}\mathbf{M}_{\mathbf{zz}}^{-1}\mathbf{D}_{\mathbf{tm}}\mathbf{Z}_{\mathbf{e}}e_{thj} \tag{6.4.13}$$

$$b_{thj} = \mathbf{M}_{\mathbf{tt}}h_{thj} \tag{6.4.14}$$

Expressions for basis functions e_{tej} and h_{thj} ((6.4.9) and (6.4.13)) are, respectively, (6.4.1) and (6.4.2) with scaling factor $\frac{1}{\beta_z}$ omitted. These functions have zero amplitude in the actual field distribution.

6.4.3 Basis consisting of static modes

For $\omega_k = 0$, the modes are of the type E or H. The longitudinal field components corresponding to these modes are the solutions of the following two scalar eigenproblems (from tab. 3.5.10) related to, respectively, modes E and H:

$$\mathbf{E}_{\mathbf{zz}}^{-1}\mathbf{D}_{\mathbf{te}}\mathbf{E}_{\mathbf{tt}}\mathbf{G}_{\mathbf{te}}e_{zj} = \beta_{zej}^2 e_{zj} \tag{6.4.15}$$

$$\mathbf{M}_{\mathbf{zz}}^{-1}\mathbf{D}_{\mathbf{tm}}\mathbf{M}_{\mathbf{tt}}\mathbf{G}_{\mathbf{tm}}h_{zj} = \beta_{zhj}^2 h_{zj} \tag{6.4.16}$$

The transverse field components are calculated from the following equations. For modes E:

$$e_{tej} = -\frac{1}{j\beta_{zej}}\mathbf{G}_{\mathbf{te}}e_{zj} \tag{6.4.17}$$

$$d_{tej} = \mathbf{E}_{\mathbf{tt}}e_{tej} \tag{6.4.18}$$

$$b_{tej} \leftarrow \beta_{zej}\mathbf{Z}_{\mathbf{e}}e_{tej} - \frac{1}{\beta_{zej}}\mathbf{Z}_{\mathbf{e}}\mathbf{G}_{\mathbf{te}}\mathbf{E}_{\mathbf{zz}}^{-1}\mathbf{D}_{\mathbf{te}}d_{tej} \tag{6.4.19}$$

$$h_{tej} = \mathbf{M}_{\mathbf{tt}}^{-1}b_{tej} \tag{6.4.20}$$

and for modes H:

$$h_{thj} = -\frac{1}{j\beta_{zhj}}\mathbf{G_{tm}}h_{zj} \tag{6.4.21}$$

$$b_{thj} = \mathbf{M_{tt}}h_{thj} \tag{6.4.22}$$

$$d_{thj} \leftarrow -\beta_{zhj}\mathbf{Z_m}h_{thj} + \frac{1}{\beta_{zhj}}\mathbf{Z_m}\mathbf{G_{tm}}\mathbf{M_{zz}^{-1}}\mathbf{D_{tm}}b_{thj} \tag{6.4.23}$$

$$e_{thj} = \mathbf{E_{tt}^{-1}}d_{thj} \tag{6.4.24}$$

Formulae (6.4.19), (6.4.23) correspond to (6.4.4) and (6.4.3) respectively, with factor $\frac{1}{\omega}$ disregarded.

6.5 Fast analysis of waveguides

The algorithms developed in this chapter can all be used for fast analysis of the dispersive properties of waveguides. Finding dispersion characteristics of a waveguide is a very common problem in electromagnetics. In chapter 3, we presented methods of solving this problem based on a discretization of various formulations of dispersion equation with the finite difference method. In practice, such an approach requires construction and solving of a large and complicated boundary value problem for a large number of frequencies or propagation constants depending on the choice of a parameter being swept. Such an approach may be very inefficient as the numerical complexity associated with finding eigenvalues is identical at each point. The eigenfunction expansion algorithms developed in this chapter can radically reduce the computation effort. The standard finite difference procedure described in chapter 3 is used only at a few points chosen from the dispersion characteristics (eg. at cutoff, static, or any other arbitrary case). These solutions are used as a basis for the field expansion[7]. Using this basis and the method of moments the dispersion equation is converted into a matrix eigenproblem with a small dense matrix operator. The numerical complexity is dramatically reduced compared to the traditional approach.

In order to compare the time performance of the presented algorithms versus standard methods, we define the following variables:

N	—	number of frequency / propagation constant points
M	—	number of modes to be found
M_{ee}	—	number of modes used in EE
t_{std}	—	calculation time in one standard eigenproblem
t_{ee}	—	calculation time in one EE eigenproblem

The total time in the standard method is given by the equation:

$$T_{std} = N \cdot t_{std}(M) \tag{6.5.1}$$

The total time required by the EE procedure in its general form may be estimated from the following formulae:

$$T_{ee} = M_{ee} \cdot t_{std}(1) + N \cdot t_{ee}(M) \tag{6.5.2}$$

[7]In fact, the method used for calculation of the basis is not important in this method. We use the finite difference method here but any of the techniques, including FEM or SDA, can be used when deemed more appropriate for the problem at hand.

For the algorithms based on the orthogonality relations this takes up the form:

$$T_{ee} = t_{std}(M_{ee}) + N \cdot t_{ee}(M) \tag{6.5.3}$$

Note, that we do not take into account the time required to construct the matrices, which in practice is very small in comparison with the time of solving an eigenproblem. The speedup of EE method over the standard method is given for the first case:

$$S = \frac{N \cdot t_{std}(M)}{M_{ee} \cdot t_{std}(1) + N \cdot t_{ee}(M)} \tag{6.5.4}$$

and in the second case:

$$S = \frac{N \cdot t_{std}(M)}{t_{std}(M_{ee}) + N \cdot t_{ee}(M)} \tag{6.5.5}$$

For large value of frequency or propagation constant points, in both cases, the speedup reaches its limit value:

$$S \longrightarrow \frac{t_{std}(M)}{t_{ee}(M)} \tag{6.5.6}$$

Since the size of the EE eigenproblems are much smaller than in the case of the standard algorithms, the speedup may be significant.

Chapter 7

Numerical results

7.1 Introduction

In the previous chapters, we presented various methods improving the standard finite-difference methods for electromagnetic problems. All these new algorithms require verification. Therefore, a series of numerical tests have been performed. The results of these tests are presented further on, in this chapter. It should be noted, that the numerical tests presented later were chosen from much larger set of tests performed to validate the algorithms. The results of these and the other tests prove that the techniques presented in the previous chapters satisfy all the required conditions for the entire range of parameters.

7.2 Basic algorithms for 2D structures

In this section, we present the results of the tests for 2D structures. In sec. 7.2.1, we deal with a test reducing the numerical dispersion error. In the following sections, we test various waveguides successively adding new elements to them, in order to test all the local algorithms presented in chapter 4: modeling of metal walls (sec. 7.2.2), dielectric boundaries (sec. 7.2.3), and conductive wedges placed in homogeneous (sec. 7.2.4) and inhomogeneous domains (sec. 7.2.5). As a benchmark, we use the cutoff frequencies calculated using the finite-difference frequency-domain method by solving matrix eigenproblems derived from two first formulations from tab. 3.5.10. These frequencies are compared with reference values, which are the cutoff frequencies calculated analytically or via extrapolation of the results for various grid sizes. If the waveguide is homogeneous, there is no need to make any other tests, since the dispersion characteristics are strictly determined by the cutoff frequencies. In the case of inhomogeneous waveguides, we also perform the tests for the static case analyzing the attenuation constants. These tests involve solving matrix eigenproblems arising from the static formulations from tab. 3.5.10.

In all performed calculations, we assumed that the speed of light in the vacuum[1] is equal to $c = 3 \cdot 10^8 m \cdot s^{-1}$.

[1] More exact value of c is $2.997928 \cdot 10^8 m \cdot s^{-1}$

7.2.1 Numerical dispersion

As shown in sec. 2.3.1, results of finite-difference methods are affected by the numerical dispersion error. We presented a method for the estimation of this error deriving a correction factor minimizing this error. In this section, we present an example of the estimation and the minimization of the numerical dispersion error in the case of the numerical analysis of a rectangular waveguide.

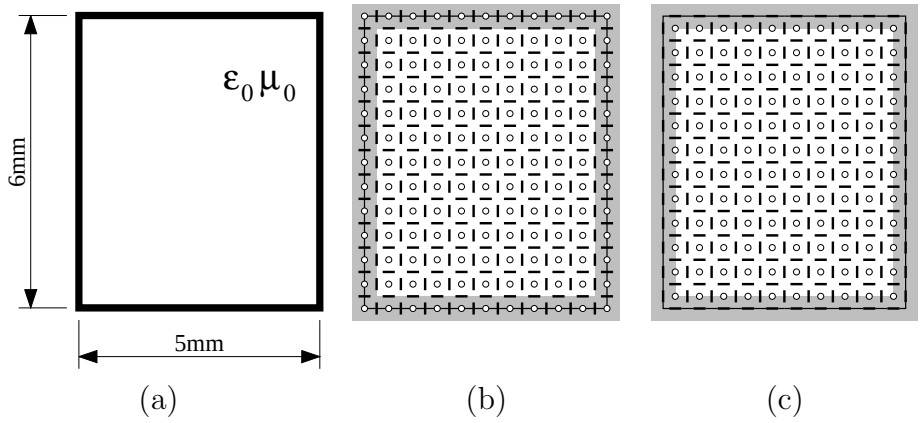

Figure 7.2.1: *Rectangular waveguide (a) and the same structure placed in Yee's grid: nodes E_z, H_x, H_y (b) H_z, E_x, E_y (c).*

The waveguide is shown in fig. 7.2.1(a). It has dimensions of 5mm×6mm and is filled with the vacuum. The structure is covered with Yee's mesh with the grid steps $\Delta x = \Delta y = 0.5$mm, i.e. 10×12 grid (see figs. 7.2.1(b,c)). The metal walls are placed on the appropriate nodes of the tangential electric field. This guarantees that the metal walls do not introduce any error into the results. The only source of errors, in this case, is the numerical dispersion. During the test, we calculate cutoff frequencies of the waveguide solving matrix eigenproblems arising from first two formulations given in tab. 3.5.10. The results are compared with the frequencies calculated analytically.

The results for the lowest order modes are presented in tab. 7.2.1. The table shows the analytical cutoff frequencies (f_{ref}) and the calculated frequencies together with the relative errors. The next two columns show the same quantities after correction. The actual error level after the correction is placed between $-\Delta/2$ and $\Delta/2$, where Δ is the estimated error level calculated from eq. (2.3.55). $\Delta/2$ is shown in the last column of the table.

For example, let us look at modes TM_{11}, TE_{11}. The cutoff frequency calculated analytically is about 39.05GHz. The solution of the finite-difference eigenproblem gives in this case the result about 38.91GHz which is 0.36% smaller than the exact value. The correction of this result leads to 39.11GHz with the relative error of 0.16%. It is clearly seen, that this error is in the range $-\Delta/2 \ldots \Delta/2$ ($\Delta/2$ in our case is 0.17%).

One may note that the actual error after correction in some cases (modes TE_{02}, TE_{20}, TE_{30}) slightly exceeds the estimated error range. In the worst case, for mode TE_{30}, this error is of order 0.72%, when the estimated level $\Delta/2$ is 0.61%. This is due to the fact, that the analysis of the numerical dispersion error performed in sec. 2.3.1.1 was based on approximation (2.3.13), and hence was not exact. Although this effect may grow up for higher order modes, it is not meaningful in the practical cases when the error level is small.

Table 7.2.1: *Cutoff frequencies of the rectangular waveguide calculated analytically and using the finite-difference algorithm before and after correction of the numerical dispersion error.*

			Before correction		After correction		
Mode		f_{ref}[GHz]	f[GHz]	err[%]	f[GHz]	err[%]	$\Delta/2$[%]
	TE_{01}	25.00	24.93	-0.29	24.98	-0.07	0.07
	TE_{10}	30.00	29.88	-0.41	29.97	-0.10	0.10
TM_{11}	TE_{11}	39.05	38.91	-0.36	39.11	0.16	0.17
	TE_{02}	50.00	49.43	-1.14	49.85	-0.30	0.28
TM_{12}	TE_{12}	58.31	57.76	-0.95	58.43	0.21	0.38
	TE_{20}	60.00	59.02	-1.64	59.74	-0.44	0.40
TM_{21}	TE_{21}	65.00	64.07	-1.44	64.99	-0.02	0.47
	TE_{03}	75.00	73.09	-2.55	74.46	-0.72	0.61
TM_{22}	TE_{22}	78.10	76.98	-1.43	78.60	0.63	0.68

Fig. 7.2.2 presents the error level $\Delta/2$ for homogeneous and inhomogeneous structures for cutoff modes versus the cutoff frequency (fig. 7.2.2(a)) and for static modes versus the static attenuation constant (fig. 7.2.2(b)). The homogeneous structures are filled with the vacuum and the inhomogeneous ones are filled with the vacuum and dielectric of parameters $\epsilon_r = 4$, $\mu_r = 1$. Note, that the data in fig. 7.2.2(a) corresponding to the homogeneous structures are valid in particular for the rectangular waveguide analyzed in this section, and hence match the values of $\Delta/2$ in tab. 7.2.1. The data from fig. 7.2.2 will serve as a reference for further tests.

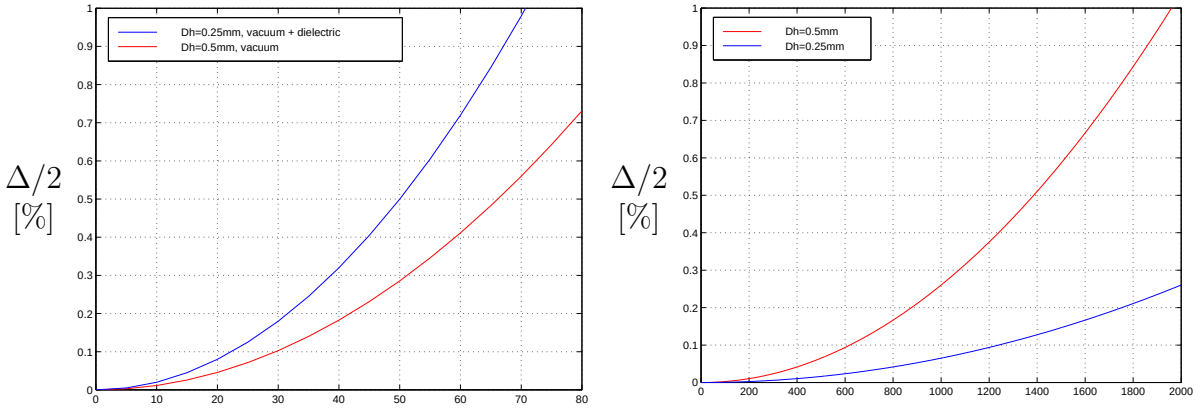

Figure 7.2.2: *Numerical dispersion error level for homogeneous and inhomogeneous structures for cutoff modes versus the cutoff frequency (a) and for static modes versus the static attenuation constant (b). The inhomogeneous structures are filled with the vacuum and dielectric of parameters* $\epsilon_r = 4$, $\mu_r = 1$.

7.2.2 Location of metal walls

In order to test the algorithm for modeling of metal planes, we analyze the same rectangular waveguide as in the previous section but shifting the structure with respect to Yee's grid by a normalized distance $-0.5 < x_t/\Delta x < 0.5$, $-0.5 < y_t/\Delta y < 0.5$. This covers every possible location with respect to the grid. Possible positions of the metal walls are shown in fig. 7.2.1(b,c) as a dark region. Note, that position (0,0) corresponds to the situation from the previous section, where the only source of errors is the numerical dispersion. The errors are calculated with respect to the analytical solution. The correction of the numerical dispersion is performed. Fig. 7.2.3 shows patterns of the relative errors in the calculated cutoff frequencies versus the normalized position of the structure for the lowest order TM and TE modes. For instance, the relative errors for mode TM_{11} take up the values from range $0.18\% \ldots 0.34\%$. The largest error is, hence, two times larger than the error level due to the numerical dispersion $\Delta/2$ which, for this frequency, is 0.17% (from tab. 7.2.1 or fig. 7.2.2(a)). The variation of the error, about 0.16%, is comparable with the numerical dispersion. One may note, that the error patterns for TM and TE modes with the same indices are the same (eg. modes TM_{11} and TE_{11} in the figure).

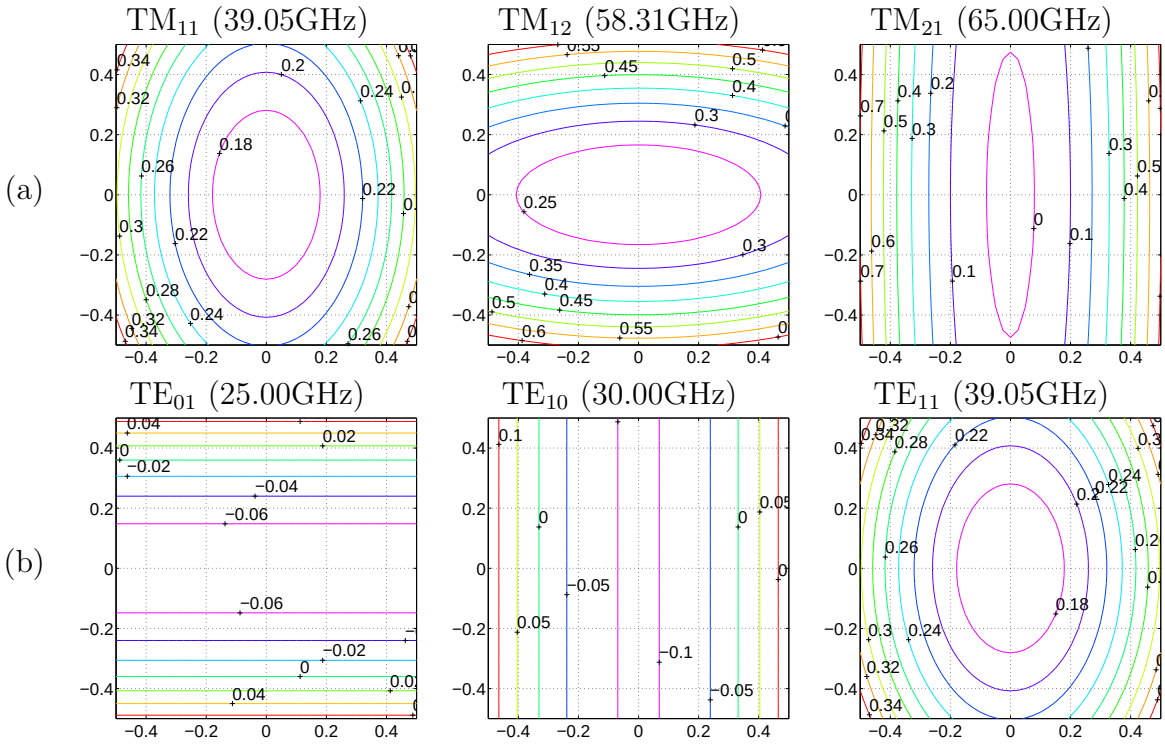

Figure 7.2.3: *Contours of relative error [%] of the cutoff frequencies of TM modes (a) and TE modes (b) versus normalized location of the rectangular waveguide with respect to Yee's cell.*

Rotation In the test described above, the metal walls were, in every case, parallel to one of the field components of Yee's grid. In order to test the algorithm for modeling of metal walls in a more general case, we rotate the structure with respect to its center. Fig. 7.2.4 shows three locations of the waveguide in the grid, at angles 0^o, 22.5^o and 45^o. Electric nodes are blue, magnetic nodes are red and removed nodes are green. The waveguide was rotated from 0^o to 45^o with step 1^o. The cutoff frequencies were calculated. Fig. 7.2.5 shows the relative error of the cutoff frequencies of TM and TE modes. Top charts correspond to the staircase approximation. The errors, in this case, are very large reaching level of about 5% for mode TE_{01} or even 9% for mode TM_{11}. Results corresponding to the new algorithm are shown in the bottom. We may see, that the error is highly reduced with the level comparable with the numerical dispersion (below 0.5%) for modes TE_{01} and TM_{11}.

It has to be underlined, that rotation does not change the norm maximum of the operator, so there is no need to change the time step in the FD-TD.

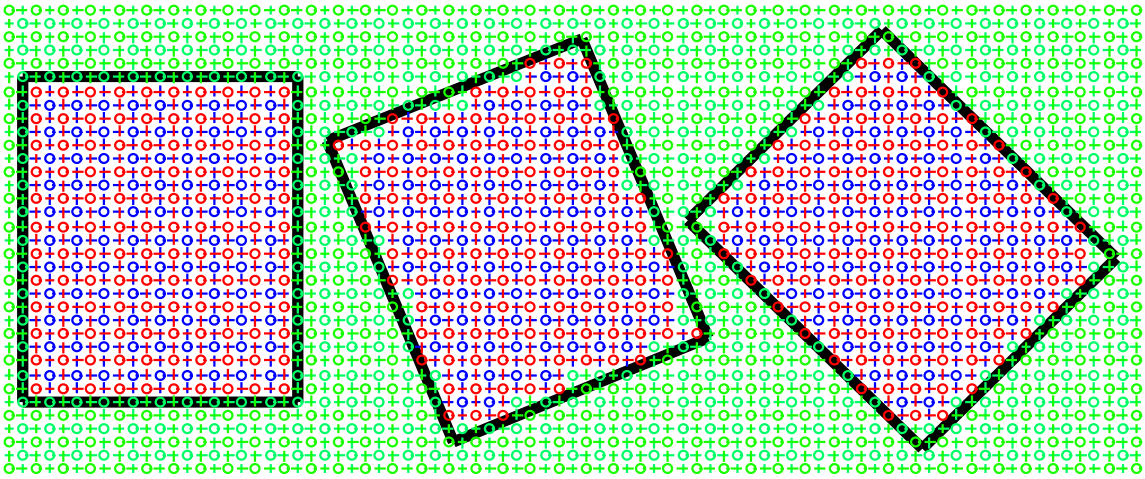

Figure 7.2.4: *Rotation of the rectangular waveguide in Yee's mesh.* 0^o, 22.5^o, 45^o.

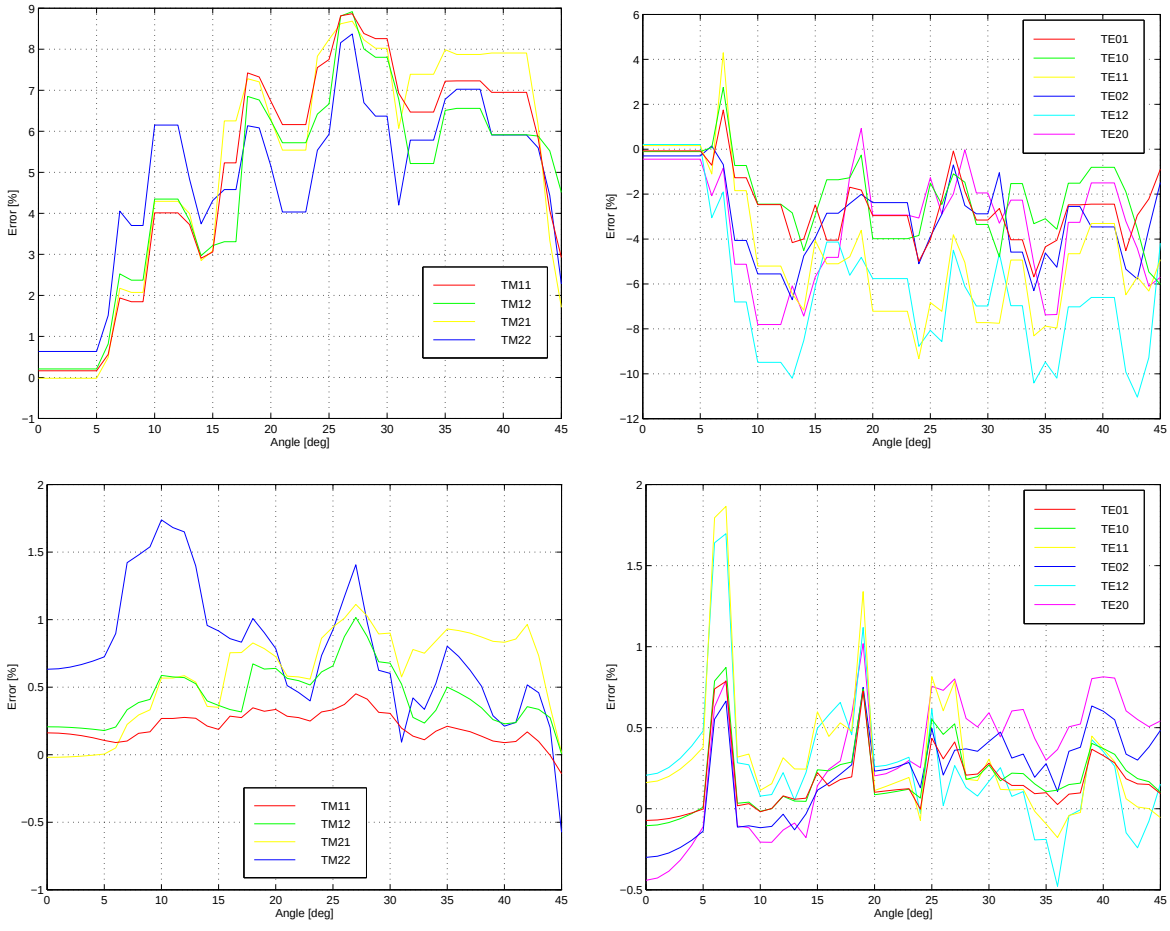

Figure 7.2.5: *Relative error [%] of the cutoff frequencies of TM (a) and TE modes (b) versus angle between the rectangular waveguide and Yee's grid: staircase approximation (top) and the new algorithm (bottom).*

7.2.3 Location of dielectric boundaries

In addition to the error caused by the location of metal walls an error may be introduced by location of boundaries between dielectrics. In order to test such a case, a structure from fig. 7.2.6 was analyzed using the finite-difference algorithm. This structure is a rectangular

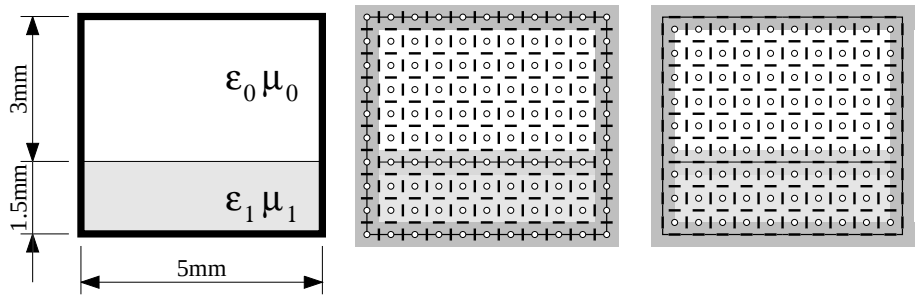

Figure 7.2.6: *Inhomogeneous rectangular waveguide (a) and the same structure placed in Yee's grid: nodes E_z, H_x, H_y (b) H_z, E_x, E_y (c).* $\epsilon_1 = 4\epsilon_0$. $\mu_1 = \mu_0$.

waveguide loaded inhomogenously, with two dielectrics of permittivity, respectively, ϵ_0 and $4\epsilon_0$. The waveguide supports modes of type LSE and LSM with respect to the vertical axis. The structure was shifted, taking every possible location with respect to 20×18 Yee's grid ($\Delta h = 0.25$mm). All possible locations of the boundaries are shown for 10×9 grid in figs. 7.2.6(b,c) as dark regions. Fig. 7.2.7 shows the contours of the relative errors in the calculated cutoff frequency with respect to the normalized position. The reference cutoff frequencies were calculated using the transverse resonance method [34, 57]. The same data was obtained by extrapolating the results of the finite-difference frequency-domain method with varying grid size. Since the structure is inhomogeneous, the static solutions are not in a simple relation to the cutoff solutions. Therefore, in addition to the cutoff case, we solved the matrix eigenproblems corresponding to the static formulations from tab. 3.5.10. This produced, for all locations of the structure, the contour plots given in fig. 7.2.8 showing the relative errors in the attenuation constant for the static modes. The errors for mode LSE_{11} are in the range $0\% \ldots 0.15\%$ at cutoff and $-0.04\% \ldots 0.10\%$ in the static case. The variation of these errors is comparable to the numerical dispersion error level, which is about 0.2% at cutoff (blue line in fig. 7.2.2(a)) and about 0.1% for the static solution (blue line in fig. 7.2.2(b)).

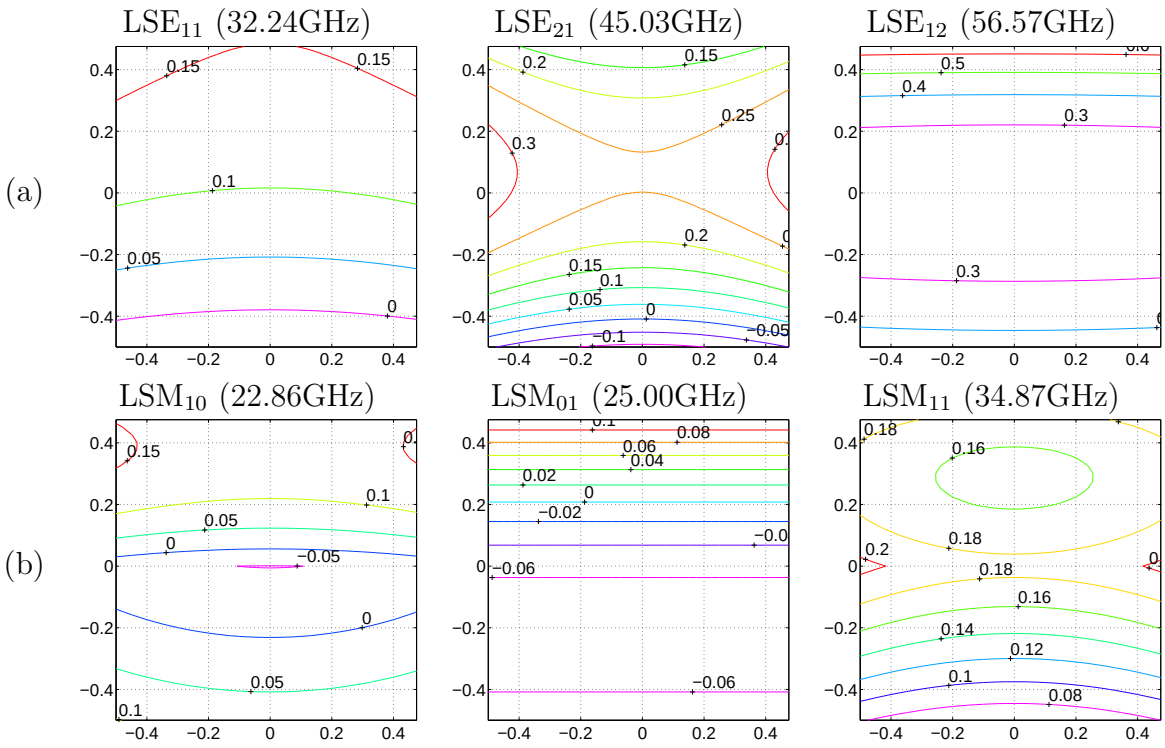

Figure 7.2.7: *Contours of relative error [%] of the cutoff frequencies of LSE modes (a) and LSM modes (b) versus normalized location of the inhomogeneous rectangular waveguide with respect to Yee's cell.*

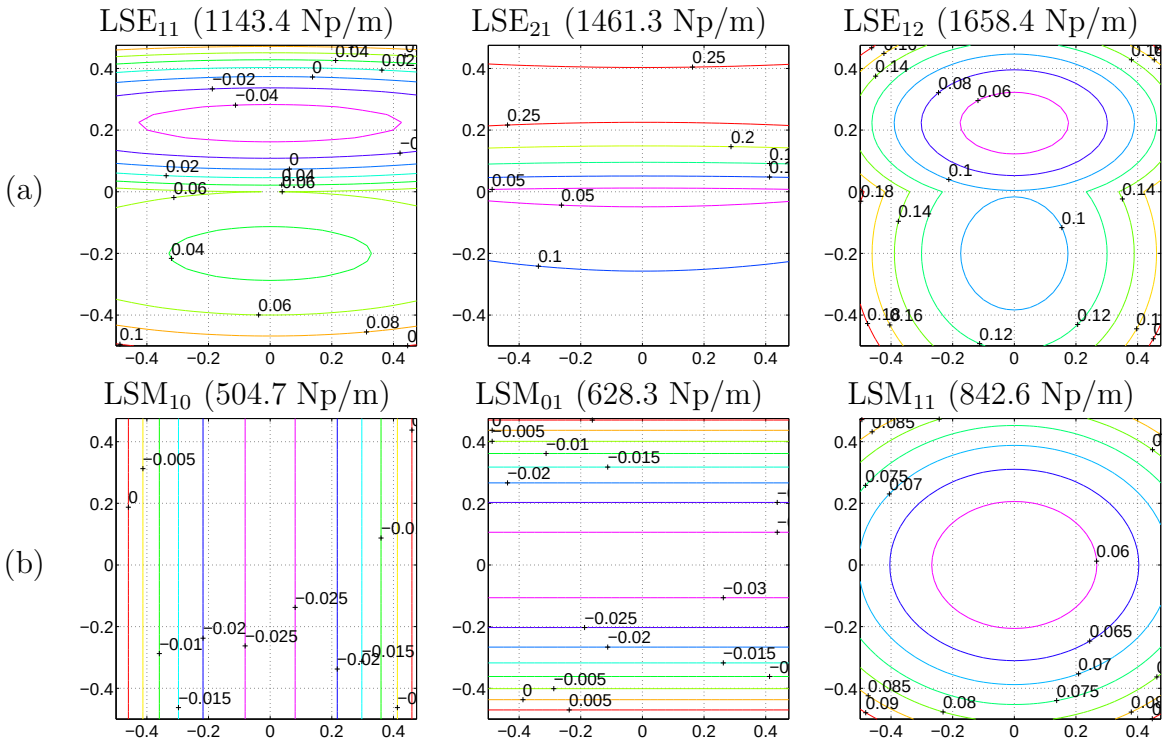

Figure 7.2.8: *Contours of relative error [%] of the static attenuation constants of LSE modes (a) and LSM modes (b) versus normalized location of the inhomogeneous rectangular waveguide with respect to Yee's cell.*

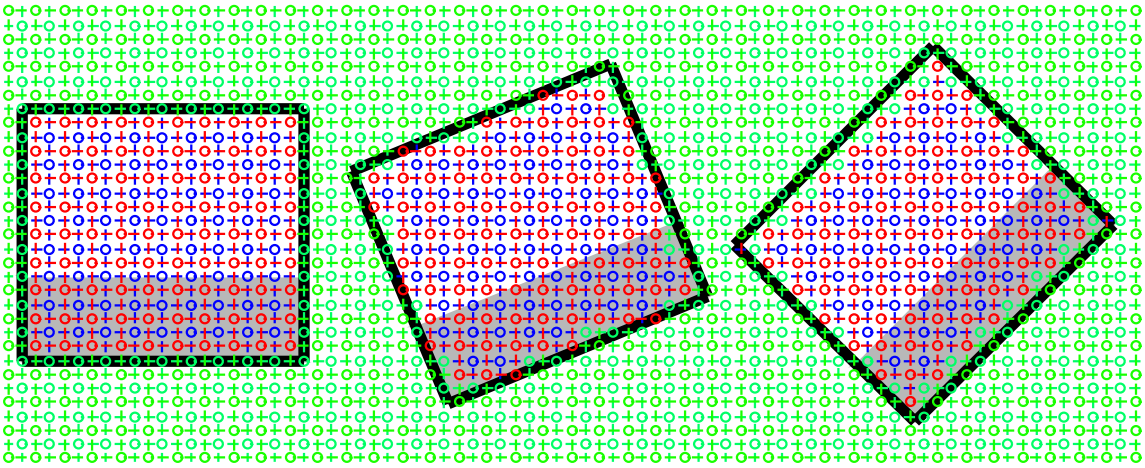

Figure 7.2.9: *Rotation of the inhomogeneous rectangular waveguide in Yee's mesh.* 0^o, 22.5^o, 45^o.

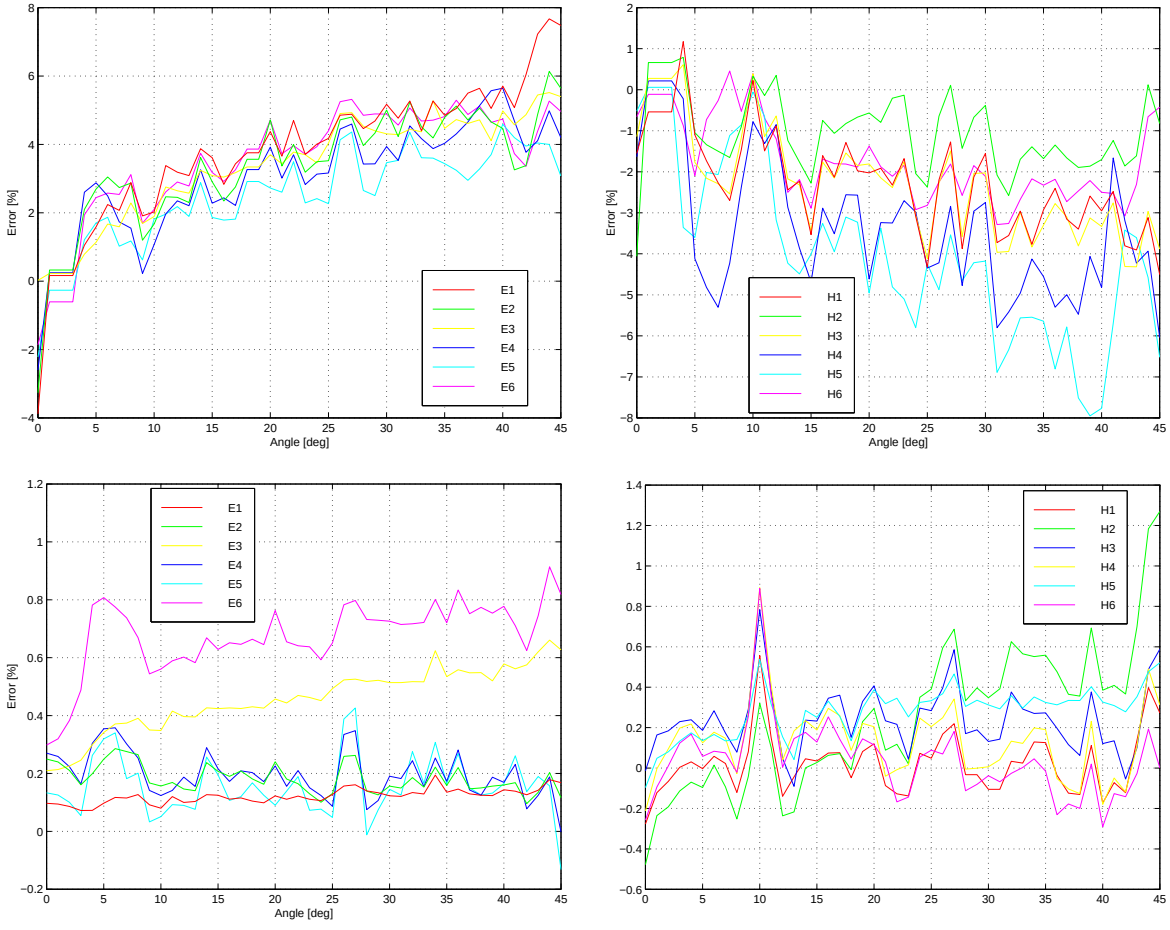

Figure 7.2.10: *Relative error [%] of the cutoff frequencies of LSE (a) and LSM modes (b) versus angle between the inhomogeneous rectangular waveguide and Yee's grid: staircase approximation (top) and the new algorithm (bottom).*

Rotation In order to test the algorithm in a more general case, we rotate the structure with respect to the grid versus the center of the waveguide. Three positions of the waveguide, at angle 0^o, 22.5^o and 45^o are presented in fig. 7.2.9. The results of calculating cutoff frequencies of the rotated waveguide are shown in fig. 7.2.10. The charts show the relative error in the calculated frequency for modes LSM and LSE. The results corresponding to the staircase approximation are given at the top. The staircase approximation here means no modeling of metal walls nor a dielectric boundary. The error levels are large. In the worst case for mode LSM_{10} we get about 4%, and for mode LSE_{11} we get about 8%. The error level is significantly reduced for the modified algorithm (bottom charts). Fig. 7.2.11 corresponds to solving of static equations. The figure shows the relative error of the static attenuation constants. Again, the top charts correspond to the staircase approximation and the bottom charts to the new algorithm. Also in this case, we observe large errors for the staircase algorithm and significant reduction of these errors for the new approach.

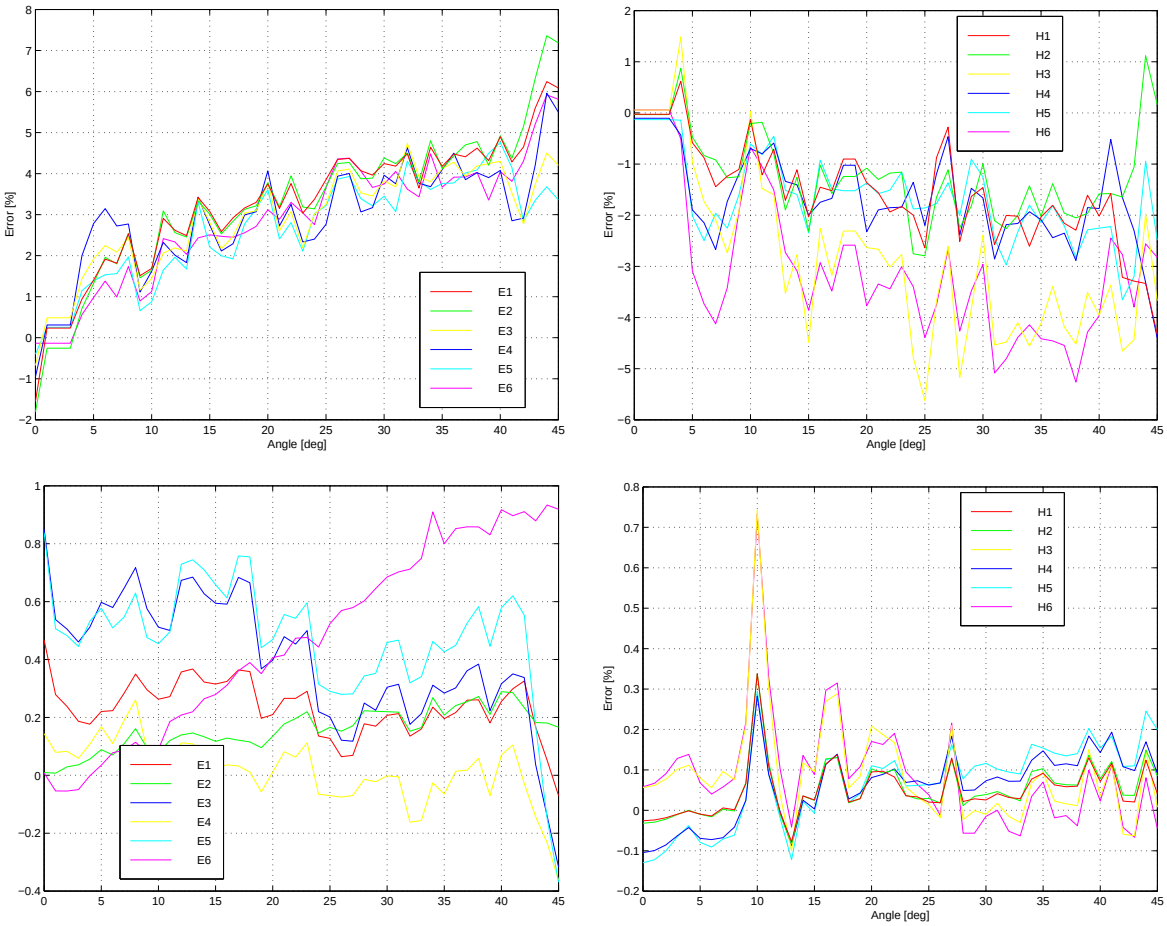

Figure 7.2.11: *Relative error [%] of the static attenuation constants of LSE (a) and LSM modes (b) versus angle between the inhomogeneous rectangular waveguide and Yee's grid: staircase approximation (top) and the new algorithm (bottom).*

7.2.4 Conductive wedges in homogeneous domains

In this and the next section, we deal with the structures containing conductive wedges. Here, we test a homogeneous waveguide with a single metal wedge placed in the symmetry plane. The structure is shown in fig. 7.2.12(a).

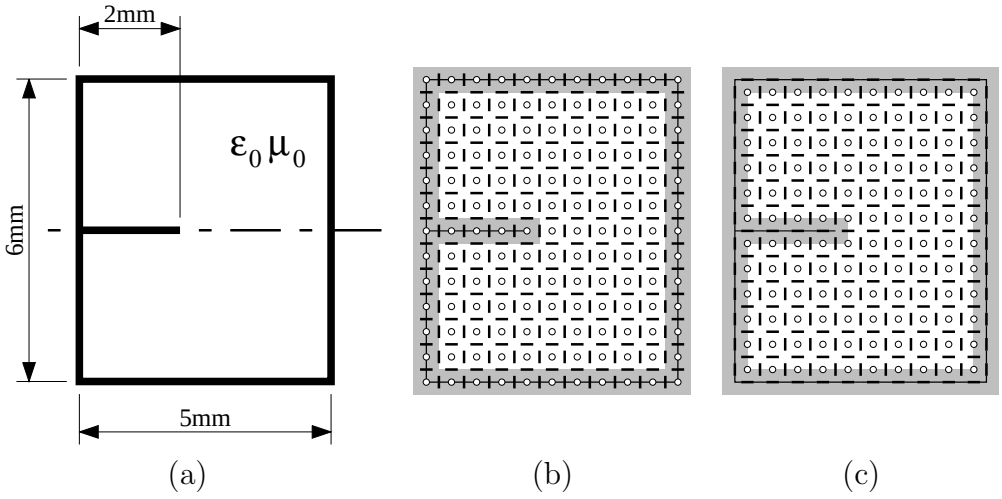

Figure 7.2.12: *Single-wedge line (a) and the same structure placed in Yee's grid: nodes E_z, H_x, H_y (b) H_z, E_x, E_y (c).*

As discussed in sec. 4.6, the metal wedge may lead to singularity of some of the field components and cause significant errors when using the standard finite-difference methods. Therefore, we developed a modification of the standard methods which should reduce the errors associated with singularities. In this section, we test the new algorithms. We also perform tests with the standard methods without modeling of the wedge in order to show how the new methods improve the accuracy.

The tests with the standard methods were performed for the grid sizes: 10×12, 20×24, 40×48, 80×96, 160×192. (The location of grid nodes for three field components and for 10×12 grid ($\Delta h = 0.5$mm) is presented in figs. 7.2.12(b,c) for TM and TE polarization respectively.) The structure is placed in Yee's mesh with the metal planes coinciding with the tangential electric field, so that the location of the walls does not introduce any error into the results. As in the previous sections, we calculate the cutoff frequencies of the waveguide. The results for various grid sizes are extrapolated and the extrapolated values are used as a reference. The frequencies and the relative errors are presented for modes TM and TE in, respectively, tabs. 7.2.2 and 7.2.3.

Since the test model has a plane of symmetry, we may expect the even and odd modes with respect to this plane. The odd modes (TM_o, TE_o) do not contain singularities and therefore we do not expect significant errors in this case. This is because the symmetry plane has the properties of the electric wall, which cancels the influence of the edge corner to the field. The largest errors may be expected for the even modes (TM_e, TE_e), where some of the field components may become singular at the edge (see fig. 7.2.13 showing the field distribution for the even modes). The tables show, as expected, that the errors for the odd modes are relatively small, and are caused only by the numerical dispersion. For instance, the cutoff frequencies of modes TM_{o1}, TE_{o1} calculated using the standard finite-difference algorithm with 10×12 Yee's grid are, respectively, 0.21% greater and 0.10%

Table 7.2.2: *Cutoff frequencies [GHz] of TM modes of the single-wedge line calculated with the standard finite difference algorithm.*

	10×12	20×24	40×48	80×96	160×192	Ext.
TM_{e1}	**48.01**	47.31	46.99	46.83	46.75	**46.6693**
	2.87%	1.38%	0.68%	0.34%	0.17%	
TM_{o1}	58.43	58.34	58.32	58.31	58.31	58.3095
	0.21%	0.05%	0.01%	0.00%	0.00%	
TM_{e2}	71.84	71.77	71.73	71.72	71.72	71.7135
	0.18%	0.08%	0.03%	0.01%	0.01%	
TM_{o2}	78.60	78.23	78.13	78.11	78.10	78.1025
	0.63%	0.16%	0.04%	0.01%	0.00%	

Table 7.2.3: *Cutoff frequencies [GHz] of TE modes of the single-wedge line calculated with the standard finite difference algorithm.*

	10×12	20×24	40×48	80×96	160×192	Ext.
TE_{e1}	**18.90**	19.29	19.48	19.57	19.62	**19.6686**
	-3.90%	-1.95%	-0.97%	-0.49%	-0.24%	
TE_{o1}	29.97	29.99	30.00	30.00	30.00	30.0000
	-0.10%	-0.03%	-0.01%	-0.00%	-0.00%	
TE_{e2}	35.55	35.60	35.63	35.64	35.65	35.6614
	-0.32%	-0.18%	-0.09%	-0.05%	-0.02%	
TE_{o2}	49.85	49.96	49.99	50.00	50.00	50.0000
	-0.30%	-0.07%	-0.02%	-0.00%	-0.00%	
TE_{e3}	55.75	56.05	56.20	56.26	56.30	56.3326
	-1.04%	-0.50%	-0.24%	-0.12%	-0.06%	
TE_{o3}	58.43	58.34	58.32	58.31	58.31	58.3095
	0.21%	0.05%	0.01%	0.00%	0.00%	
TE_{o4}	59.74	59.94	59.98	60.00	60.00	60.0000
	-0.44%	-0.10%	-0.03%	-0.01%	-0.00%	
TE_{e4}	64.73	64.93	65.02	65.06	65.08	65.1046
	-0.58%	-0.27%	-0.13%	-0.07%	-0.03%	
TE_{e5}	77.02	77.29	77.36	77.39	77.39	77.3994
	-0.49%	-0.14%	-0.05%	-0.02%	-0.01%	
TE_{o5}	78.60	78.23	78.13	78.11	78.10	78.1025
	0.63%	0.16%	0.04%	0.01%	0.00%	

Table 7.2.4: *Cutoff frequencies [GHz] of TM modes of the single-wedge line calculated with the finite difference algorithm with modeling of the wedge.*

	Ref.	10×12	20×24	40×48	80×96
TM_{e1}	**46.6693**	**46.76**	46.67	46.66	46.67
		0.19%	0.01%	-0.01%	-0.01%
TM_{o1}	58.3095	58.43	58.34	58.32	58.31
		0.21%	0.05%	0.01%	0.00%
TM_{e2}	71.7135	71.84	71.75	71.72	71.72
		0.18%	0.05%	0.01%	0.00%
TM_{o2}	78.1025	78.60	78.23	78.13	78.11
		0.63%	0.16%	0.04%	0.01%

Table 7.2.5: *Cutoff frequencies [GHz] of TE modes of the single-wedge line calculated with the finite difference algorithm with modeling of the wedge.*

	Ref.	10×12	20×24	40×48	80×96
TE_{e1}	**19.6686**	**19.67**	19.68	19.67	19.67
		0.02%	0.04%	0.03%	0.01%
TE_{o1}	30.0000	29.97	29.99	30.00	30.00
		-0.10%	-0.03%	-0.01%	-0.00%
TE_{e2}	35.6614	35.68	35.67	35.66	35.66
		0.04%	0.01%	0.01%	0.00%
TE_{o2}	50.0000	49.85	49.96	49.99	50.00
		-0.30%	-0.07%	-0.02%	-0.00%
TE_{e3}	56.3326	56.29	56.33	56.33	56.33
		-0.08%	-0.01%	0.00%	0.00%
TE_{o3}	58.3095	58.43	58.34	58.32	58.31
		0.21%	0.05%	0.01%	0.00%
TE_{o4}	60.0000	59.74	59.94	59.98	60.00
		-0.44%	-0.10%	-0.03%	-0.01%
TE_{e4}	65.1046	65.06	65.10	65.11	65.11
		-0.07%	-0.00%	0.00%	0.00%
TE_{e5}	77.3994	77.07	77.33	77.38	77.40
		-0.43%	-0.09%	-0.02%	-0.01%
TE_{o5}	78.1025	78.60	78.23	78.13	78.11
		0.63%	0.16%	0.04%	0.01%

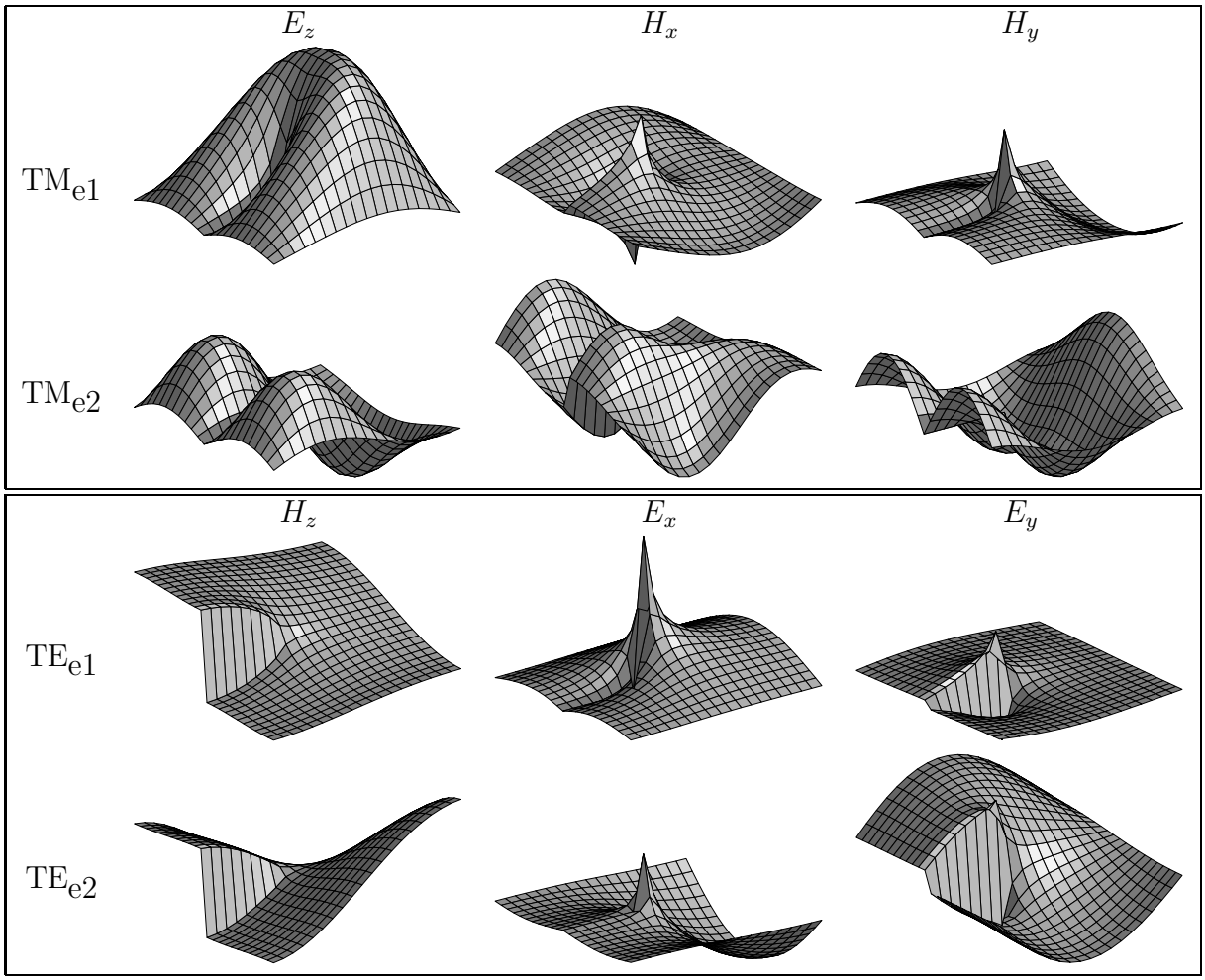

Figure 7.2.13: *Field distribution of the even modes of the single-wedge line*

smaller than the exact value. Note, that these errors are smaller than the numerical dispersion error which, as can be read from fig. 7.2.2(a), are: about 0.4% for TM_{o1} cutoff frequency (58.21GHz) and about 0.1% for TE_{o1} cutoff frequency (29.94GHz). For the even modes, however, the errors are significant. In the case of 10×12 grid the method produces 2.87% of the relative error for mode TM_{e1} and -3.90% for mode TE_{e1}, which is much more than might be expected if only the numerical dispersion errors were taken into account (from fig. 7.2.2(a), respectively, about 0.3% and 0.05%).

Tabs. 7.2.4 and 7.2.5 present the results for the modified finite-difference algorithm with modeling of the conductive edge described in sec. 4.6.2. The results show that the new algorithm has no influence on the odd modes. This is a desirable property of the algorithm, since, as noted, the odd modes have no singularity in the field. The entries corresponding to the odd modes are the same as in tabs. 7.2.2 and 7.2.3, and as before, the errors are caused only by the numerical dispersion. Significant improvement in accuracy of the calculations is observed in the case of the even modes. The errors caused by the edge corner are practically canceled. In the case of 10×12 grid the new method produces 0.19% of the relative error for mode TM_{e1} and 0.02% for mode TE_{e1}, which is comparable with the corresponding cases for the standard method with 160×192 grid (0.17% and -0.24% respectively).

In order to show the ability of the new algorithm to handle various locations of the

conductive edge with respect to the grid, the structure is shifted in $x - y$ plane as in the previous sections. (Dark regions in figs. 7.2.12(b,c) again indicate possible location of the boundaries.) Note, that the results for position (0,0) correspond to the frequencies from the tables discussed above.

Figs. 7.2.14 and 7.2.15 present the relative error contours versus the normalized position of the model for the cutoff frequencies of, respectively, modes TM and TE calculated using the standard (plots (a)) and modified (plots (b)) finite-difference algorithms with 10×12 grid. We may note large errors and large dependency of these errors on the position in the case of the even modes and the standard method. For mode $\mathrm{TM}_{\mathrm{e1}}$ we get the error range about $0\% \ldots 7\%$ and for mode $\mathrm{TE}_{\mathrm{e1}}$ the error range is about $-8\% \ldots 0\%$. In both cases the errors are significantly reduced when using the modified algorithm. For both modes, we get the error ranges, respectively, $0.2\% \ldots 0.8\%$ and $-0.2\% \ldots 0.6\%$. Although the error is significantly reduced, its variation is larger than the level of the numerical dispersion (respectively, about 0.3% and 0.05%). For the odd modes the errors are not significant in both the standard and the modified algorithms, and the ranges are comparable with the level of the numerical dispersion error.

Rotation Like in the previous sections, the second test concerns rotation of the structure with respect to the grid. Now, however, the waveguide is rotated versus the edge as shown in fig. 7.2.16. The relative error in the calculated cutoff frequency versus the angle is shown in fig. 7.2.17. The staircase approximation, as shown in the top charts, leads to large errors reaching about 8% in the case of mode $\mathrm{TE}_{\mathrm{e1}}$ and over 13% for mode $\mathrm{TM}_{\mathrm{e1}}$. The staircase approximation, in this case, means no modeling of metal walls and the edge. The bottom charts, corresponding to the new method, show significant reduction of the error.

Stability of the explicit update scheme For all the locations of the structure with respect to Yee's mesh, positiveness and the spectral radius of the operator were tested. The tests showed, that the algorithm for modeling of a conductive wedge has no influence on these properties. Therefore, the standard stability condition for the explicit update schemes, given for 2D by eq. (3.8.27), is not changed.

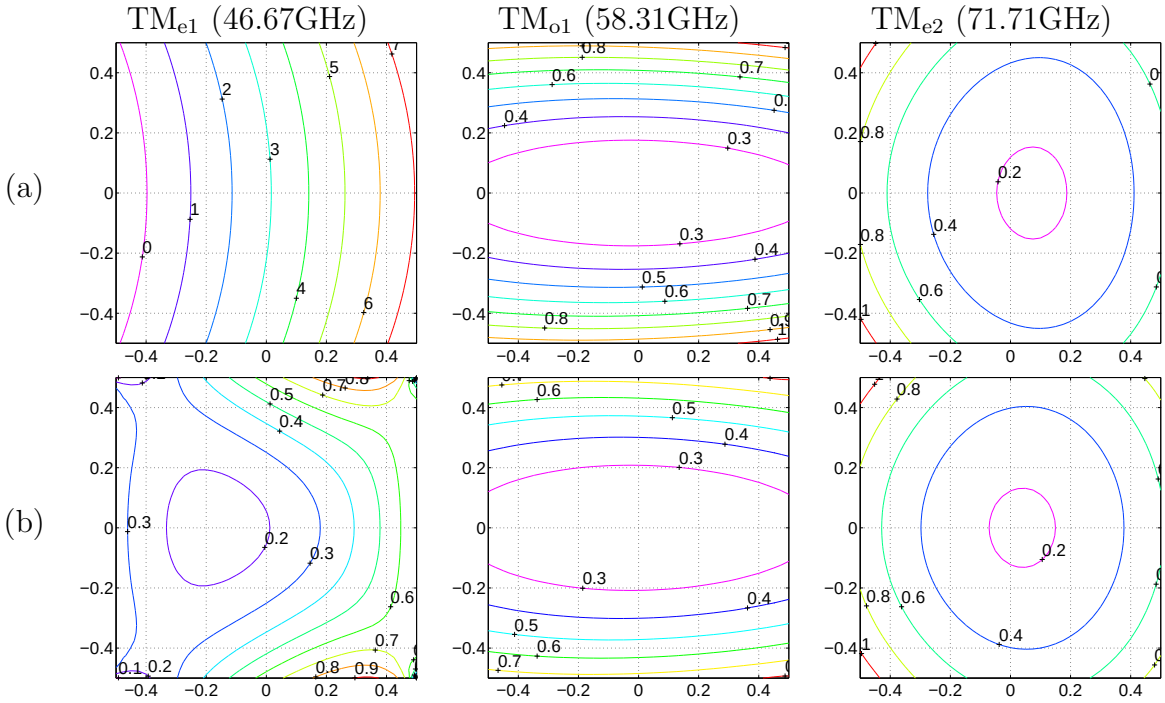

Figure 7.2.14: *Contours of relative error [%] of the cutoff frequencies of TM modes versus normalized location of the structure with respect to Yee's cell for the finite difference algorithm without (a) and with (b) correction.*

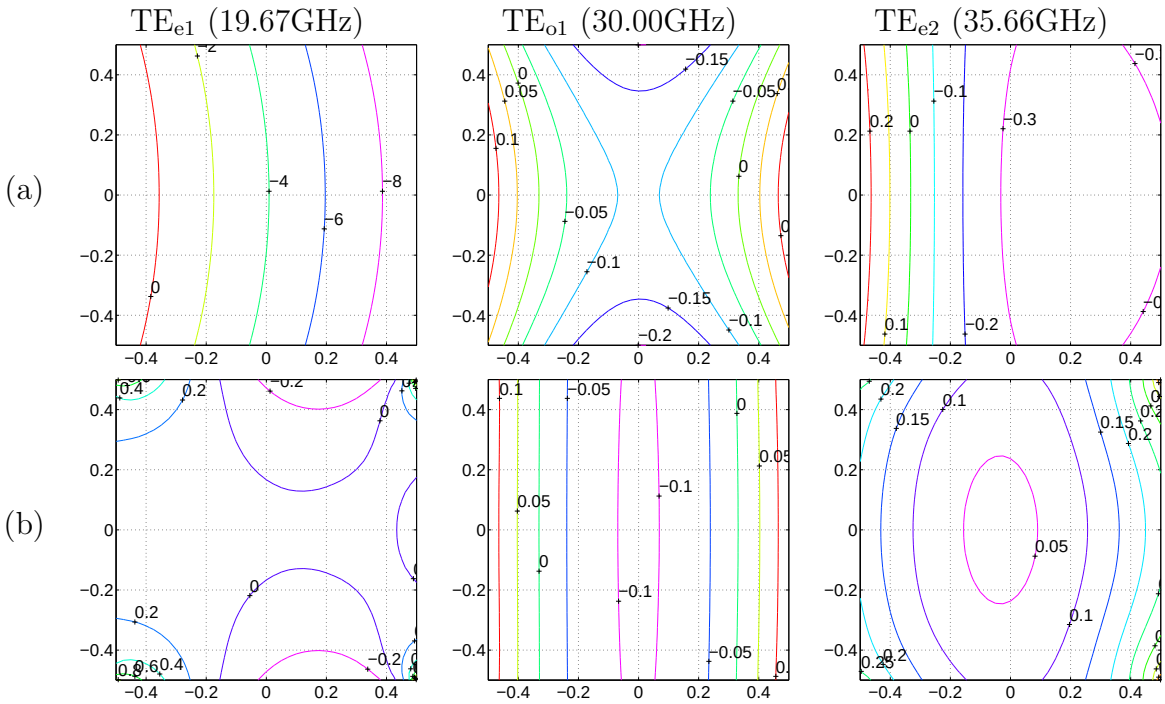

Figure 7.2.15: *Contours of relative error [%] of the cutoff frequencies of TE modes versus normalized location of the structure with respect to Yee's cell for the finite difference algorithm without (a) and with (b) correction.*

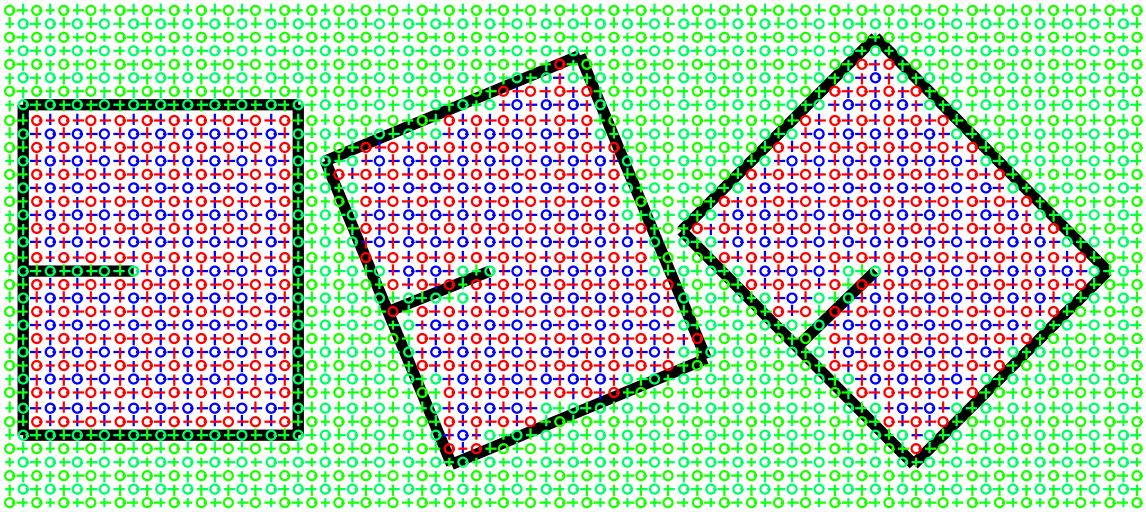

Figure 7.2.16: *Rotation of the single-wedge line in Yee's mesh.* 0^o, 22.5^o, 45^o.

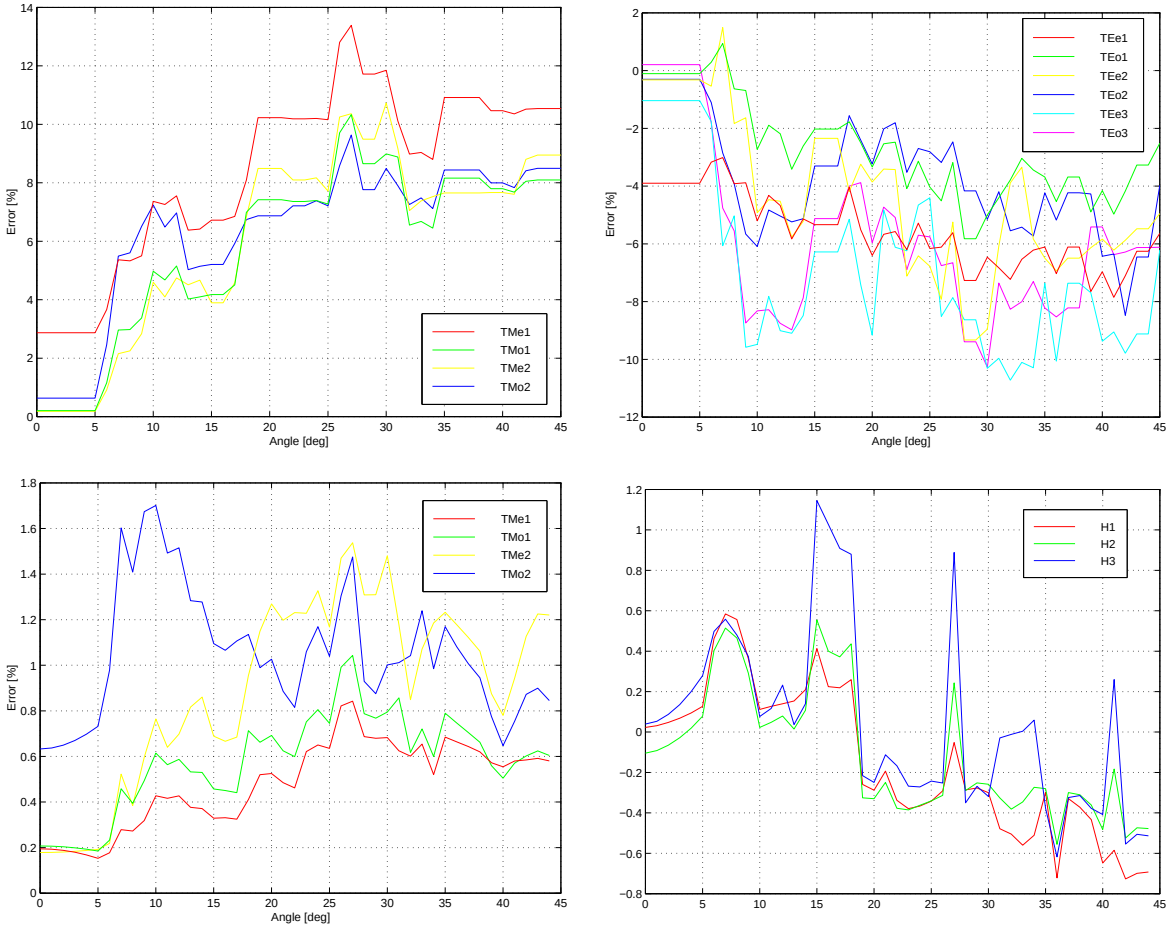

Figure 7.2.17: *Relative error [%] of the cutoff frequencies of TM (a) and TE modes (b) versus angle between the single-wedge line and Yee's grid: staircase approximation (top) and the new algorithm (bottom).*

7.2.5 Conductive wedges in inhomogeneous domains

The algorithm for modeling of conductive wedges presented in sec. 4.6.2 may also handle wedges placed in an inhomogeneous region. In order to test such a case, we numerically analyze the structure shown in fig. 7.2.18. This is a rectangular waveguide with a single

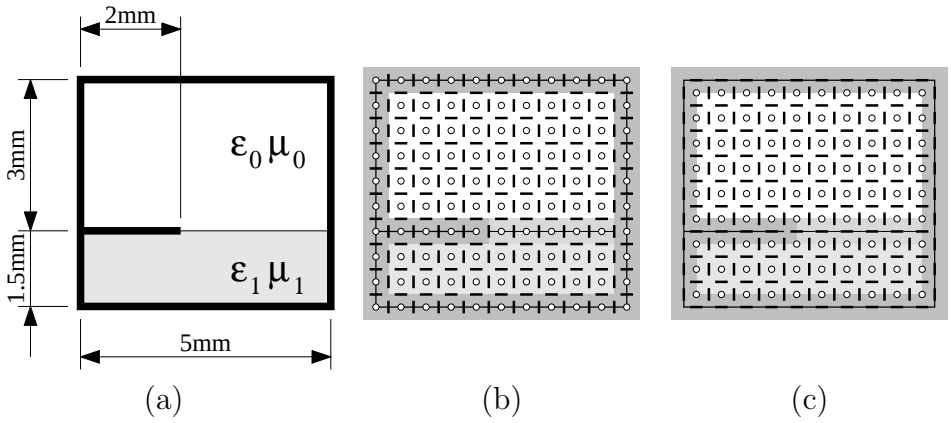

Figure 7.2.18: *Inhomogeneous single-wedge-line (a) and the same structure placed in Yee's grid: nodes E_z, H_x, H_y (b) H_z, E_x, E_y (c). $\epsilon_1 = 4\epsilon_0$. $\mu_1 = \mu_0$.*

conductive wedge placed on the boundary between two dielectrics. Analogously to the previous section, we present the cutoff frequencies of this structure and the corresponding relative errors calculated for various grid sizes with the standard and the modified finite-difference algorithms. The results for the standard method are shown for modes E and H in tabs. 7.2.6 and 7.2.7, respectively. The results of the modified method are given in tabs. 7.2.8, 7.2.9. One may observe significant reduction of error in the case of modes E_1 and H_1 for grid 20×18. In these cases, the standard method produces errors 1.36% and -3.23%. The use of the new approach reduces these errors to the levels 0.12% and 0.05% and this is less than the level of the numerical dispersion (respectively, about 0.3% and 0.05%).

Since the analyzed waveguide is inhomogeneous, the cutoff and static solutions are not simply related to each other. Therefore, we performed separate tests for the static case. The results are given in tabs. 7.2.10, 7.2.11 (the standard algorithm) and 7.2.12, 7.2.13 (the new technique). Also in this case, the errors are notably reduced (eg. from -2.52% to 0.04% (the level comparable with the numerical dispersion) in the case of mode H_1).

Analogously to the tests from the previous sections, we shifted the waveguide in the $x - y$ space testing the influence of the positioning of the structure relative to Yee's grid on the error level. The results for the standard and modified algorithms are shown for the case of the cutoff modes in the form of contour plots in fig. 7.2.19 for modes E and in fig. 7.2.20 for modes H. We may see, for instance, that the error for mode H_1 ranges from -8% to 0% in the case of the standard method and from -0.4% to 0.6% after the use of the modified algorithm. The reduction of the error is significant, but it is still at a larger level than the numerical dispersion. In the same manner, we present the results for the static case in figs. 7.2.19 and 7.2.20. All these plots show remarkable improvement in the error level for every position of the structure.

Table 7.2.6: *Cutoff frequencies [GHz] of E modes of the inhomogeneous single-wedge line calculated with the standard finite difference algorithm.*

	20×18	40×36	80×72	160×144	320×288	Ext.
E_1	**38.15**	37.88	37.76	37.70	37.67	**37.6387**
	1.36%	0.64%	0.31%	0.16%	0.08%	
E_2	53.89	53.76	53.68	53.64	53.61	53.5936
	0.54%	0.30%	0.16%	0.08%	0.04%	
E_3	57.44	57.19	57.11	57.08	57.07	57.0614
	0.66%	0.22%	0.08%	0.04%	0.02%	
E_4	62.67	62.56	62.53	62.52	62.51	62.5082
	0.25%	0.09%	0.04%	0.02%	0.01%	

Table 7.2.7: *Cutoff frequencies [GHz] of H modes of the inhomogeneous single-wedge line calculated with the standard finite difference algorithm.*

	20×18	40×36	80×72	160×144	320×288	Ext.
H_1	**13.95**	14.18	14.29	14.35	14.38	**14.4160**
	-3.23%	-1.66%	-0.85%	-0.43%	-0.22%	
H_2	23.41	23.51	23.54	23.56	23.56	23.5647
	-0.66%	-0.24%	-0.09%	-0.04%	-0.02%	
H_3	32.20	32.21	32.21	32.21	32.21	32.2106
	-0.03%	-0.00%	0.00%	0.00%	0.00%	
H_4	35.50	35.65	35.71	35.74	35.75	35.7648
	-0.75%	-0.33%	-0.15%	-0.07%	-0.03%	
H_5	47.96	48.16	48.24	48.27	48.28	48.2972
	-0.71%	-0.28%	-0.12%	-0.06%	-0.03%	
H_6	50.02	50.01	50.00	50.00	50.00	50.0000
	0.05%	0.02%	0.00%	0.00%	0.00%	
H_7	52.29	52.51	52.59	52.63	52.64	52.6600
	-0.69%	-0.29%	-0.13%	-0.06%	-0.03%	
H_8	57.31	57.30	57.31	57.31	57.32	57.3226
	-0.02%	-0.04%	-0.03%	-0.01%	-0.01%	
H_9	59.70	59.66	59.65	59.64	59.64	59.6454
	0.09%	0.02%	0.00%	-0.00%	-0.00%	
H_{10}	61.74	62.00	62.07	62.10	62.10	62.1098
	-0.59%	-0.18%	-0.06%	-0.02%	-0.01%	

Table 7.2.8: *Cutoff frequencies [GHz] of E modes of the inhomogeneous single-wedge line calculated with the finite difference algorithm with modeling of the wedge.*

	Ref.	20×18	40×36	80×72	160×144
E_1	**37.6387**	**37.68**	37.64	37.64	37.64
		0.12%	0.02%	-0.00%	-0.00%
E_2	53.5936	53.58	53.59	53.59	53.59
		-0.03%	-0.01%	-0.01%	-0.00%
E_3	57.0614	57.27	57.11	57.07	57.06
		0.37%	0.09%	0.02%	0.00%
E_4	62.5082	62.60	62.53	62.51	62.51
		0.15%	0.04%	0.01%	0.00%

Table 7.2.9: *Cutoff frequencies [GHz] of H modes of the inhomogeneous single-wedge line calculated with the finite difference algorithm with modeling of the wedge.*

	Ref.	20×18	40×36	80×72	160×144
H_1	**14.4160**	**14.42**	14.42	14.42	14.42
		0.05%	0.04%	0.02%	0.01%
H_2	23.5647	23.55	23.56	23.56	23.56
		-0.05%	-0.01%	-0.00%	-0.00%
H_3	32.2106	32.24	32.22	32.21	32.21
		0.09%	0.02%	0.01%	0.00%
H_4	35.7648	35.75	35.76	35.76	35.76
		-0.05%	-0.01%	-0.00%	-0.00%
H_5	48.2972	48.15	48.26	48.29	48.30
		-0.30%	-0.07%	-0.01%	-0.00%
H_6	50.0000	50.02	50.01	50.00	50.00
		0.05%	0.02%	0.00%	0.00%
H_7	52.6600	52.52	52.63	52.65	52.66
		-0.27%	-0.06%	-0.01%	-0.00%
H_8	57.3226	57.55	57.38	57.34	57.33
		0.39%	0.10%	0.03%	0.01%
H_9	59.6454	59.84	59.70	59.66	59.65
		0.33%	0.09%	0.02%	0.01%
H_{10}	62.1098	61.81	62.04	62.09	62.11
		-0.49%	-0.12%	-0.03%	-0.01%

Table 7.2.10: *Static attenuation constants [Np/m] of E modes of the inhomogeneous single-wedge line calculated with the standard finite difference algorithm.*

	20×18	40×36	80×72	160×144	320×288	Ext.
E_1	**1162.2**	1150.9	1146.6	1144.8	1144.0	**1143.346**
	1.65%	0.66%	0.28%	0.13%	0.06%	
E_2	1468.7	1464.5	1462.9	1462.1	1461.7	1461.333
	0.51%	0.22%	0.11%	0.06%	0.03%	
E_3	1670.3	1663.4	1660.7	1659.5	1659.0	1658.470
	0.71%	0.30%	0.13%	0.06%	0.03%	
E_4	2081.3	2068.5	2061.7	2058.2	2056.5	2054.764
	1.29%	0.67%	0.34%	0.17%	0.08%	

Table 7.2.11: *Static attenuation constants [Np/m] of H modes of the inhomogeneous single-wedge line calculated with the standard finite difference algorithm.*

	20×18	40×36	80×72	160×144	320×288	Ext.
H_1	**492.0**	498.3	501.5	503.1	503.9	**504.688**
	-2.52%	-1.26%	-0.63%	-0.31%	-0.16%	
H_2	628.2	628.3	628.3	628.3	628.3	628.319
	-0.03%	-0.01%	-0.00%	-0.00%	-0.00%	
H_3	841.9	842.2	842.4	842.5	842.6	842.632
	-0.09%	-0.05%	-0.02%	-0.01%	-0.01%	
H_4	1157.8	1159.6	1160.5	1160.9	1161.1	1161.311
	-0.30%	-0.15%	-0.07%	-0.04%	-0.02%	
H_5	1255.3	1256.3	1256.6	1256.6	1256.6	1256.637
	-0.10%	-0.03%	-0.01%	-0.00%	-0.00%	
H_6	1410.3	1412.2	1413.2	1413.7	1413.9	1414.159
	-0.28%	-0.14%	-0.07%	-0.03%	-0.02%	
H_7	1469.9	1470.1	1470.1	1470.1	1470.1	1470.152
	-0.02%	-0.00%	-0.00%	-0.00%	-0.00%	
H_8	1790.5	1792.4	1793.6	1794.4	1794.7	1795.149
	-0.26%	-0.15%	-0.08%	-0.04%	-0.02%	
H_9	1880.4	1883.9	1884.7	1884.9	1884.9	1884.956
	-0.24%	-0.06%	-0.01%	-0.00%	-0.00%	
H_{10}	1983.2	1985.7	1986.6	1987.0	1987.1	1987.295
	-0.21%	-0.08%	-0.04%	-0.02%	-0.01%	

Table 7.2.12: *Static attenuation constants [Np/m] of E modes of the inhomogeneous single-wedge line calculated with the finite difference algorithm with modeling of the wedge.*

	Ref.	20×18	40×36	80×72	160×144
E_1	**1143.346**	**1144.0**	1143.4	1143.4	1143.3
		0.05%	0.01%	0.00%	0.00%
E_2	1461.333	1462.2	1461.5	1461.3	1461.3
		0.06%	0.01%	-0.00%	-0.00%
E_3	1658.470	1660.9	1659.0	1658.6	1658.5
		0.15%	0.03%	0.01%	0.00%
E_4	2054.764	2056.1	2054.8	2054.7	2054.7
		0.06%	0.00%	-0.00%	-0.00%

Table 7.2.13: *Static attenuation constants [Np/m] of H modes of the inhomogeneous single-wedge line calculated with the finite difference algorithm with modeling of the wedge.*

	Ref.	20×18	40×36	80×72	160×144
H_1	**504.688**	**504.9**	504.8	504.8	504.7
		0.04%	0.03%	0.02%	0.01%
H_2	628.319	628.2	628.3	628.3	628.3
		-0.03%	-0.01%	-0.00%	-0.00%
H_3	842.632	842.7	842.7	842.6	842.6
		0.01%	0.00%	0.00%	0.00%
H_4	1161.311	1161.2	1161.3	1161.3	1161.3
		-0.01%	0.00%	0.00%	0.00%
H_5	1256.637	1255.3	1256.3	1256.6	1256.6
		-0.10%	-0.03%	-0.01%	-0.00%
H_6	1414.159	1414.0	1414.2	1414.2	1414.2
		-0.01%	0.00%	0.00%	0.00%
H_7	1470.152	1470.0	1470.1	1470.1	1470.1
		-0.01%	-0.00%	-0.00%	-0.00%
H_8	1795.149	1797.3	1795.8	1795.3	1795.2
		0.12%	0.03%	0.01%	0.00%
H_9	1884.956	1880.4	1883.9	1884.7	1884.9
		-0.24%	-0.06%	-0.01%	-0.00%
H_{10}	1987.295	1985.7	1987.0	1987.2	1987.3
		-0.08%	-0.02%	-0.00%	-0.00%

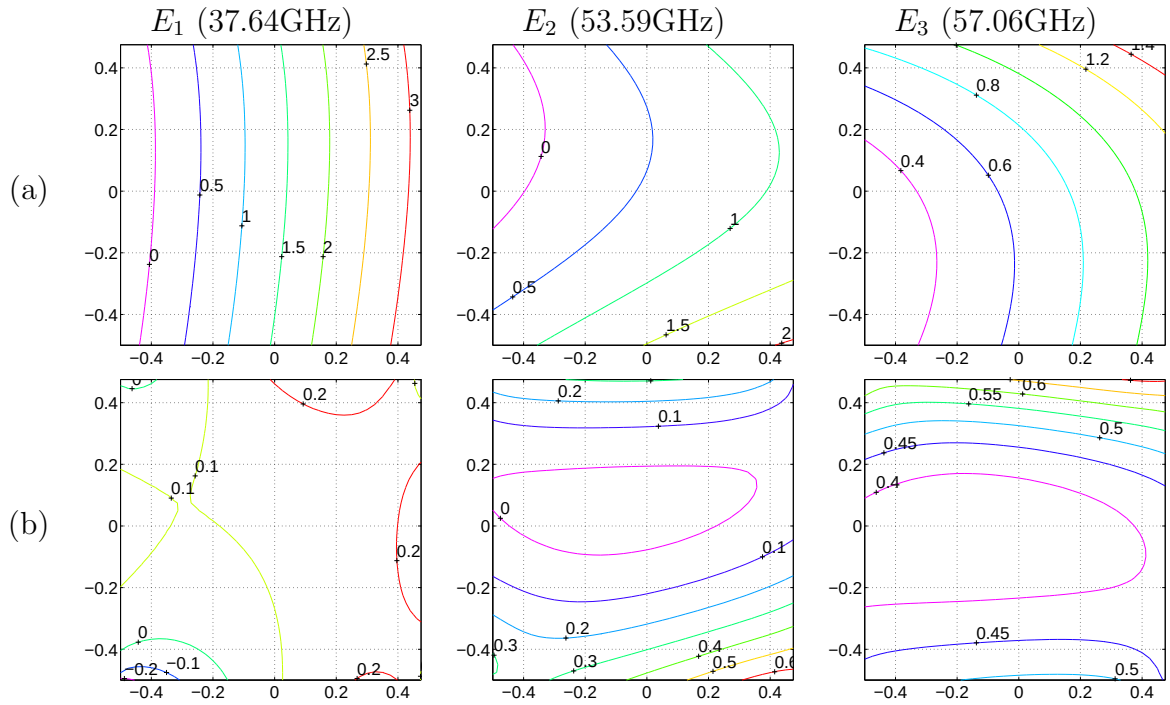

Figure 7.2.19: *Contours of relative error [%] of the cutoff frequencies of E modes versus normalized location of the structure with respect to Yee's cell for the finite difference algorithm without (a) and with (b) correction.*

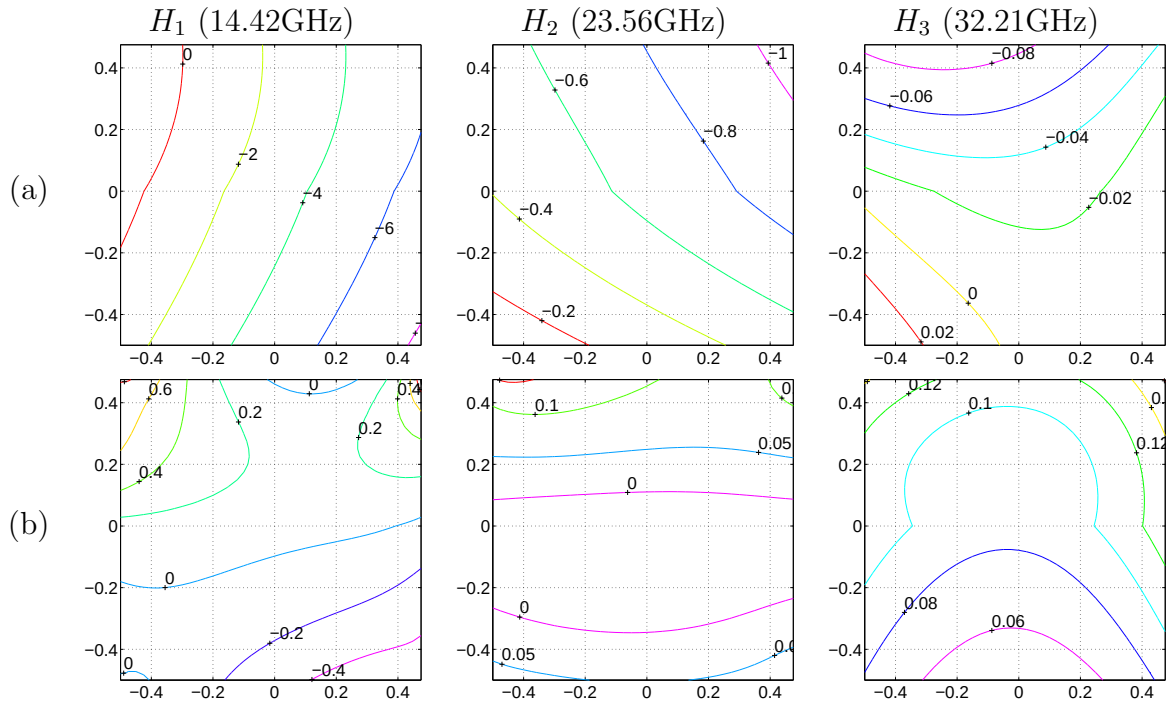

Figure 7.2.20: *Contours of relative error [%] of the cutoff frequencies of H modes versus normalized location of the structure with respect to Yee's cell for the finite difference algorithm without (a) and with (b) correction.*

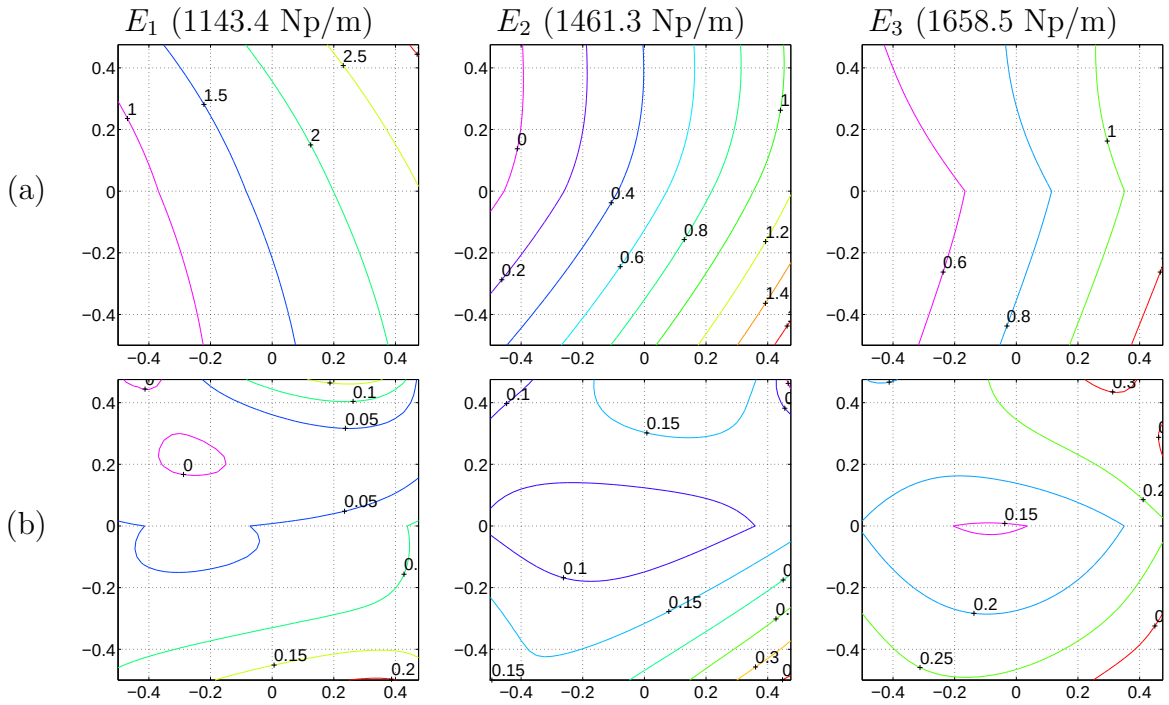

Figure 7.2.21: *Contours of relative error [%] of the static attenuation constant of E modes versus normalized location of the structure with respect to Yee's cell for the finite difference algorithm without (a) and with (b) correction.*

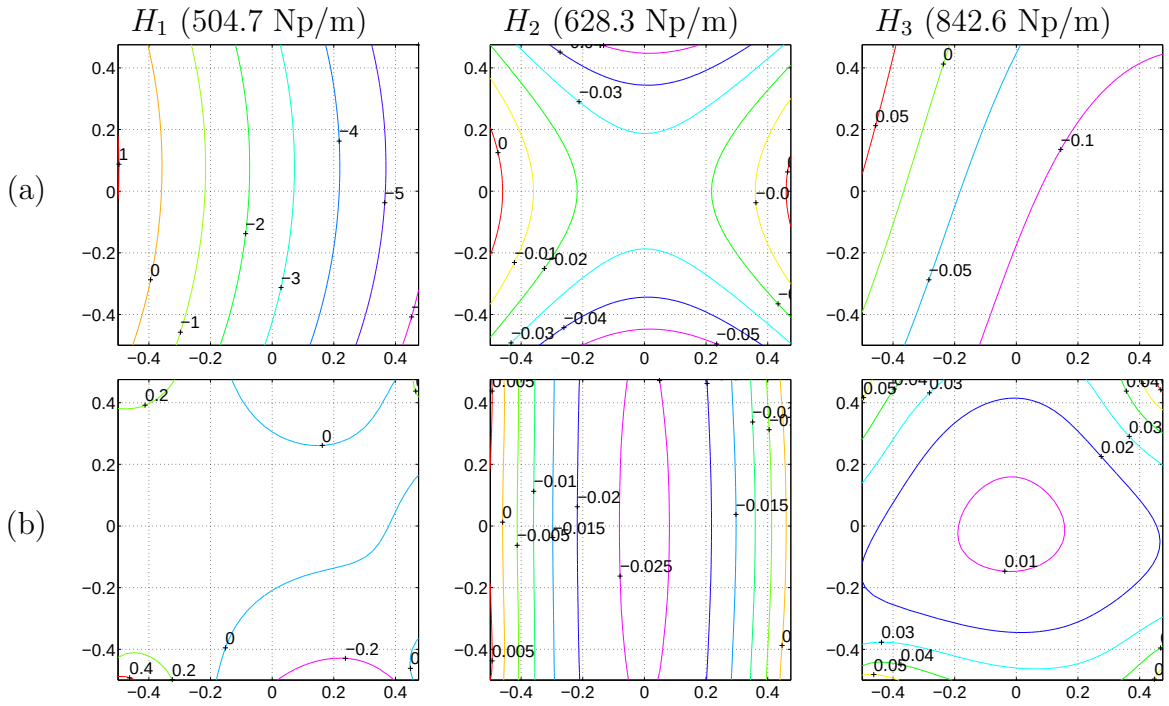

Figure 7.2.22: *Contours of relative error [%] of the static attenuation constant of H modes versus normalized location of the structure with respect to Yee's cell for the finite difference algorithm without (a) and with (b) correction.*

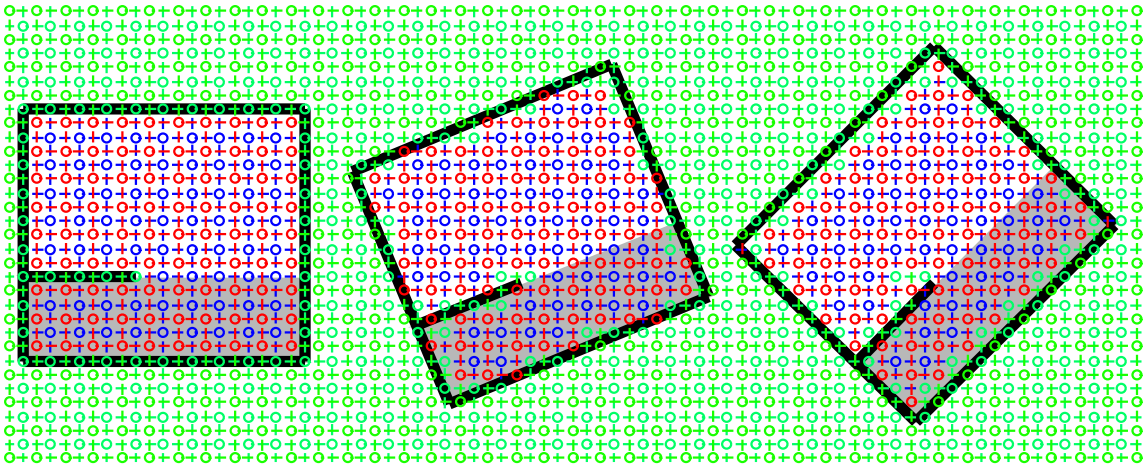

Figure 7.2.23: *Rotation of the inhomogeneous single-wedge line in Yee's mesh.* 0^o, 22.5^o, 45^o.

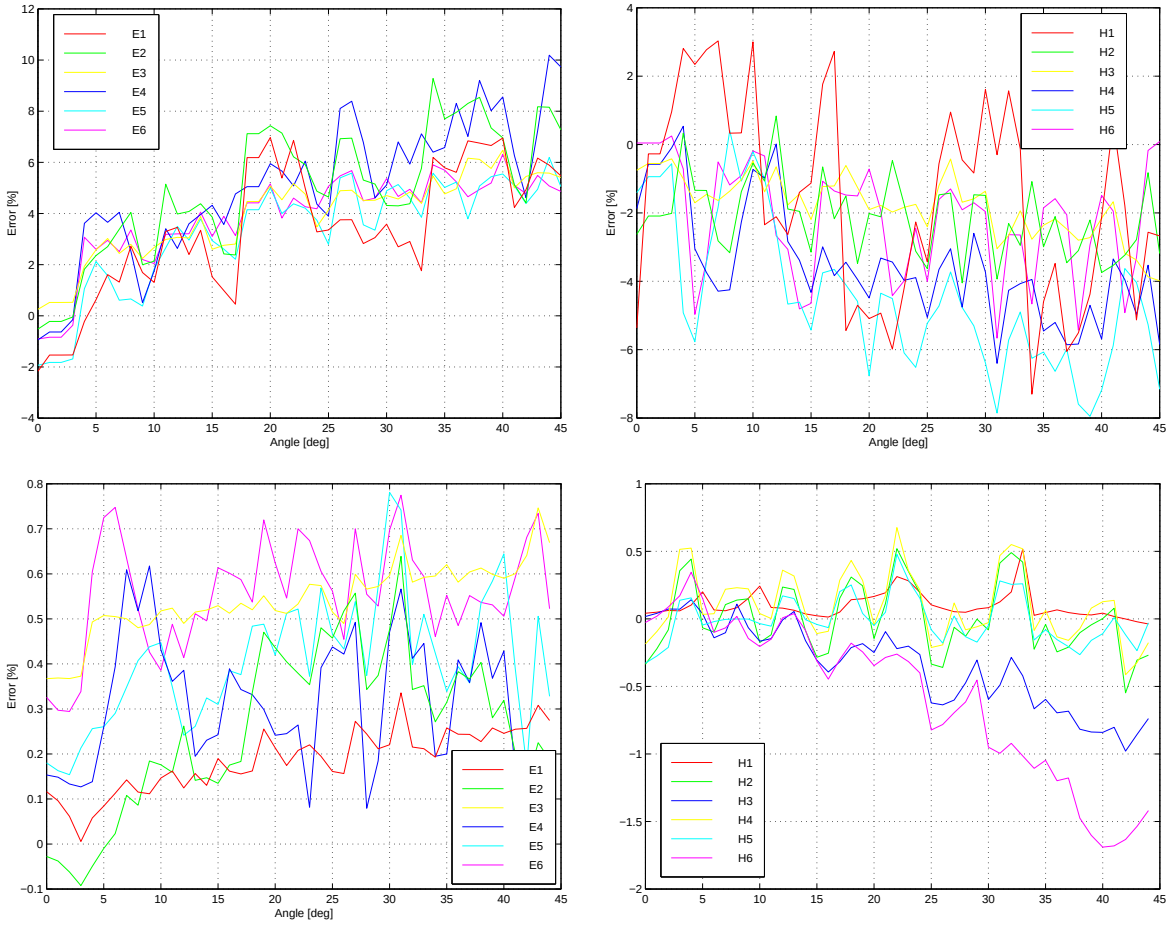

(a) (b)

Figure 7.2.24: *Relative error [%] of the cutoff frequencies of E (a) and H modes (b) versus angle between the inhomogeneous single-wedge line and Yee's grid: staircase approximation (top) and the new algorithm (bottom).*

Rotation In the next step, the waveguide is rotated versus the edge (see fig. 7.2.23). Two tests were performed, for calculating cutoff frequencies (fig. 7.2.24) and static attenuation constants (fig. 7.2.25). The staircase approximation with results at the top charts does not model metal walls, dielectric boundary, nor the edge. The errors are in this case large like in the previous tests. And again, we observe significant reduction of these errors for the modified algorithm.

Stability of the explicit update scheme Like in sec. 7.2.4, the tests with the inhomogeneous line, for various locations with respect to the grid, showed that the new algorithm has no influence on the positiveness and the spectral radius of the operator. This means that eq. (3.8.27) may still be used as a stablity condition for the explicit update schemes.

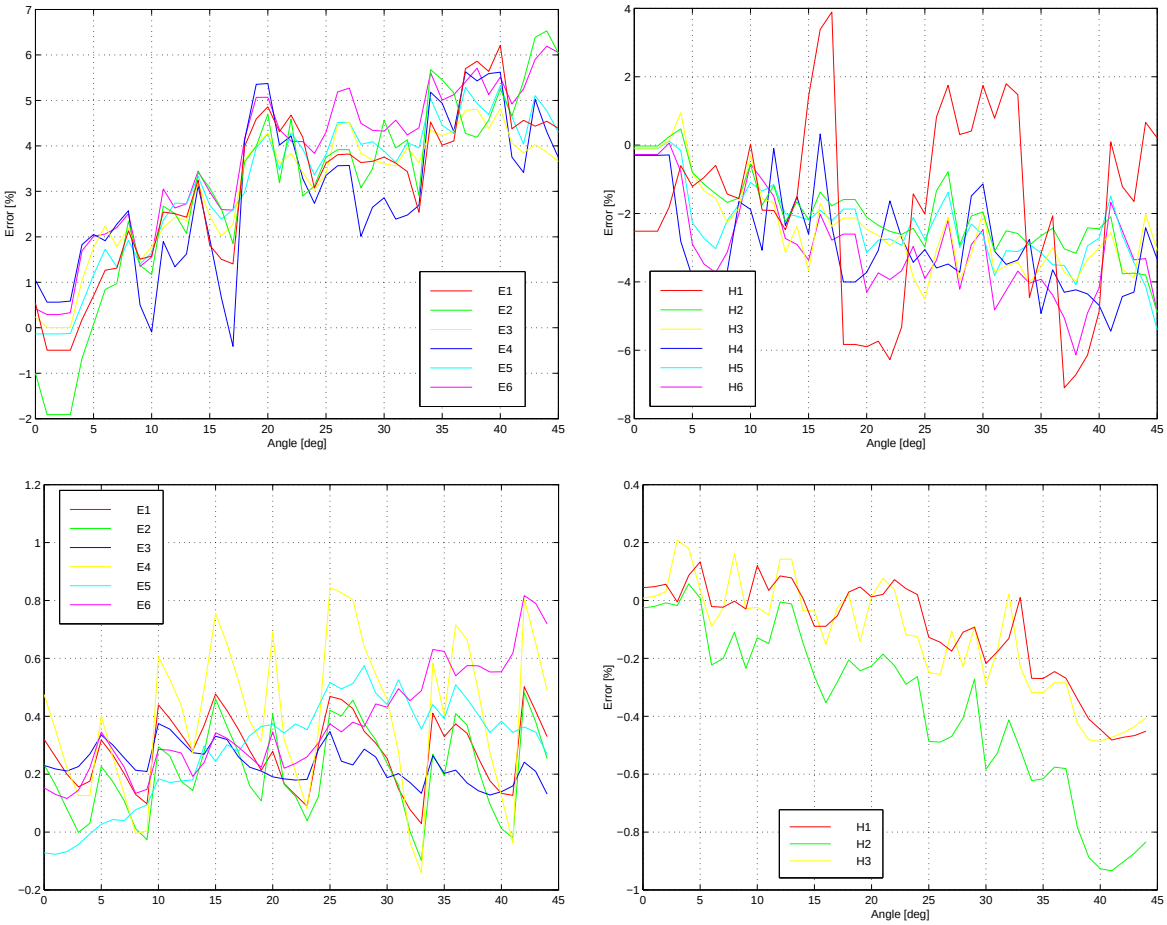

(a) (b)

Figure 7.2.25: *Relative error [%] of the static attenuation constants of E (a) and H modes (b) versus angle between the inhomogeneous single-wedge line and Yee's grid: staircase approximation (top) and the new algorithm (bottom).*

7.2.6 Circular waveguide

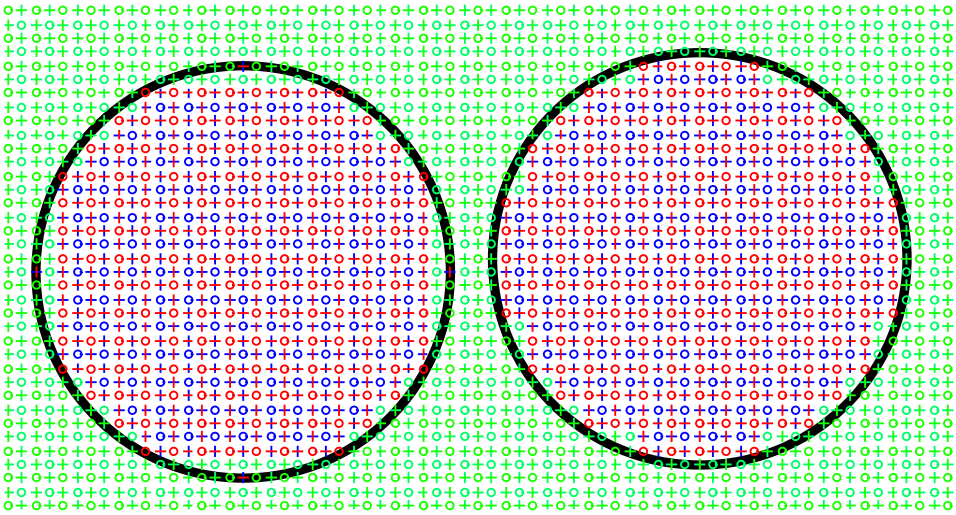

Figure 7.2.26: *Two positions of the circular waveguide in Yee's grid: node e_z in the center and node h_z in the center.*

In order to further test the algorithm for modeling of metal walls, we numerically analyze a circular waveguide of radius 3mm filled with the vacuum. We use the finite difference method with space step size $\Delta h = 0.4$mm. Fig. 7.2.26 shows two locations of the waveguide with respect to the grid: with nodes e_z (at the left side of the figure) and h_z (at the right) in the center. Tab. 7.2.14 presents the results of the tests. All the tests were performed for the two positions of the waveguide. Cutoff frequencies were calculated for metal walls modeled with the staircase approximation and with the new algorithm. The table shows relative errors of the cutoff frequencies with respect to the analytical solution.

The first index in the mode name denotes the order of Bessel function J (modes TM) or its derivative (modes TE). The second index denotes zeros of these functions. Note, that a pair of modes with the same indices exist for function orders greater than zero. These modes correspond to two sinusoidal variations in angular direction shifted in phase by 90^o with respect to each other. The results will be the same if the first index of the modes is odd. This corresponds to the same odd number of periods of the sinusoidal function in angular direction in the variation of the field. In this case, Yee's grid reveals a sort of symmetry, where directions x and y in the Cartesian coordinates have the same properties. This leads to the same result in the calculated cutoff frequency for odd modes. This property takes place for the staircase approximation and for the new algorithm for both locations of the waveguide with respect to the structure. However, an arbitrary location may spoil the symmetry and the results will differ. Even modes do not have such property.

One may note, that the error is very large for the staircase approximation. It may even reach about 9% in the case of mode TE_{41} for the location with node h_z in the center. The new algorithm strongly reduces this error pushing its magnitude down below 1% for the whole tested frequency range 0–110GHz. In the case of mode TE_{41} the error is reduced to about -0.3%.

Table 7.2.14: *Cutoff frequencies of the circular waveguide calculated by FD-FD and their relative errors with respect to the analytical solution. Electric walls modeled with staircase approximation and with the new algorithm. Results for two positions of the waveguide with respect to the grid.*

		e_z in the center				h_z in the center			
	Ref.	Staircase		New alg.		Staircase		New alg.	
	f [GHz]	f [GHz]	Err [%]	f [GHz]	Err [%]	f [GHz]	Err [%]	f [GHz]	Err [%]
TM_{01}	38.2740	39.89	4.23	38.23	-0.11	39.77	3.90	38.29	0.03
TM_{11}	60.9835	63.54	4.19	61.03	0.08	63.32	3.83	61.10	0.18
TM_{11}	60.9835	63.54	4.19	61.03	0.08	63.32	3.83	61.10	0.18
TM_{21}	81.7360	85.03	4.03	81.77	0.05	83.52	2.19	81.69	-0.05
TM_{21}	81.7360	85.19	4.23	82.15	0.50	86.06	5.30	82.37	0.77
TM_{02}	87.8548	91.43	4.07	88.19	0.39	91.14	3.74	88.21	0.41
TM_{31}	101.5434	105.61	4.01	102.00	0.45	104.86	3.27	102.04	0.49
TM_{31}	101.5434	105.61	4.01	102.00	0.45	104.86	3.27	102.04	0.49
TM_{12}	111.6565	116.03	3.91	112.38	0.65	116.02	3.91	112.39	0.65
TM_{12}	111.6565	116.03	3.91	112.38	0.65	116.02	3.91	112.39	0.65
TE_{11}	29.3033	29.31	0.01	29.34	0.13	28.77	-1.82	29.31	0.04
TE_{11}	29.3033	29.31	0.01	29.34	0.14	28.77	-1.82	29.31	0.04
TE_{21}	48.6097	46.67	-3.99	48.71	0.21	45.91	-5.55	48.62	0.02
TE_{21}	48.6097	49.52	1.87	48.74	0.26	48.16	-0.92	48.66	0.10
TE_{01}	60.9835	61.44	0.75	61.10	0.19	60.84	-0.24	61.01	0.05
TE_{31}	66.8640	65.11	-2.62	67.06	0.29	63.64	-4.82	66.89	0.04
TE_{31}	66.8640	65.11	-2.62	67.06	0.30	63.64	-4.82	66.89	0.04
TE_{41}	84.6315	77.19	-8.80	84.47	-0.19	77.09	-8.91	84.40	-0.27
TE_{41}	84.6315	87.91	3.87	85.35	0.85	81.99	-3.12	84.82	0.22
TE_{12}	84.8525	84.91	0.07	85.11	0.30	84.52	-0.39	84.91	0.07
TE_{12}	84.8525	84.91	0.07	85.11	0.30	84.52	-0.39	84.91	0.07
TE_{51}	102.1077	99.34	-2.71	102.42	0.30	94.36	-7.59	101.95	-0.16
TE_{51}	102.1077	99.34	-2.71	102.42	0.31	94.36	-7.59	101.95	-0.16
TE_{22}	106.7314	102.63	-3.84	107.02	0.27	103.74	-2.81	106.34	-0.36
TE_{22}	106.7314	105.90	-0.78	107.13	0.37	106.57	-0.15	107.19	0.43
TE_{02}	111.6565	111.92	0.24	112.14	0.43	111.22	-0.39	111.76	0.10

7.3 Eigenfunction expansion techniques

In this section, we present the numerical results of the tests carried out to verify the eigenfunction expansion techniques developed in chapter 6. We test the accuracy of the EE algorithms by analyzing the error functions defined in sec. 7.3.1. In sec. 7.3.2, we present the results for an image line analyzed by EE formulas based on the expansion functions calculated using the finite difference method.

7.3.1 Error functions

In the following equations, subscripts $_{\mathrm{ee}}$ denote quantities calculated using EE methods, and subscripts $_{\mathrm{ref}}$ denote reference quantities calculated using standard methods. We test the accuracy of the new EE algorithms by analyzing the following error functions related to the dispersion characteristics:

- the relative error of propagation constant:

$$\mathrm{err}_\beta = \frac{\beta_{z\mathrm{ee}} - \beta_{z\mathrm{ref}}}{\beta_{z\mathrm{ref}}} \cdot 100\% \tag{7.3.1}$$

- the relative error of frequency:

$$\mathrm{err}_f = \frac{f_{\mathrm{ee}} - f_{\mathrm{ref}}}{f_{\mathrm{ref}}} \cdot 100\% \tag{7.3.2}$$

We also need to define the error functions related to the field distribution. Since the eigenvectors are accurate up to the multiplicative constant we use the following definition:

- the relative transverse electric energy of error:

$$\mathrm{err}_E = \frac{\iint_S (\alpha_e \vec{E}_{t\mathrm{ee}} - \vec{E}_{t\mathrm{ref}}) \cdot (\alpha_e \vec{D}_{t\mathrm{ee}} - \vec{D}_{t\mathrm{ref}})^* ds}{\iint_S \vec{E}_{t\mathrm{ref}} \cdot \vec{D}^*_{t\mathrm{ref}} ds} \tag{7.3.3}$$

- the relative transverse magnetic energy of error:

$$\mathrm{err}_M = \frac{\iint_S (\alpha_m \vec{H}_{t\mathrm{ee}} - \vec{H}_{t\mathrm{ref}}) \cdot (\alpha_m \vec{B}_{t\mathrm{ee}} - \vec{B}_{t\mathrm{ref}})^* ds}{\iint_S \vec{H}_{t\mathrm{ref}} \cdot \vec{B}^*_{t\mathrm{ref}} ds} \tag{7.3.4}$$

where α_e, α_m are parameters, which minimize the errors. In app. C we calculate α_e (α_m) and derive the final form of functions err_E and err_M:

$$\mathrm{err}_E = 1 - \frac{|\iint_S \vec{E}_{t\mathrm{ee}} \cdot \vec{D}^*_{t\mathrm{ref}} ds|^2}{\iint_S \vec{E}_{t\mathrm{ee}} \cdot \vec{D}^*_{t\mathrm{ee}} ds \cdot \iint_S \vec{E}_{t\mathrm{ref}} \cdot \vec{D}^*_{t\mathrm{ref}} ds} \tag{7.3.5}$$

$$\mathrm{err}_M = 1 - \frac{|\iint_S \vec{H}_{t\mathrm{ee}} \cdot \vec{B}^*_{t\mathrm{ref}} ds|^2}{\iint_S \vec{H}_{t\mathrm{ee}} \cdot \vec{B}^*_{t\mathrm{ee}} ds \cdot \iint_S \vec{H}_{t\mathrm{ref}} \cdot \vec{B}^*_{t\mathrm{ref}} ds} \tag{7.3.6}$$

Further on, we express both errors in dB:

$$\mathrm{err}_{EdB} = 10 \log(\mathrm{err}_E) \tag{7.3.7}$$

$$\mathrm{err}_{MdB} = 10 \log(\mathrm{err}_M) \tag{7.3.8}$$

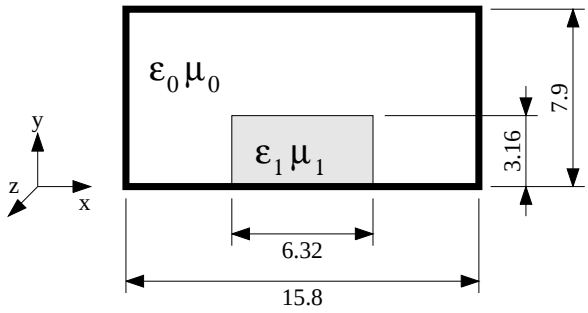

Figure 7.3.1: *Test model of an image guide. All dimensions are in* $[mm]$, $\epsilon_1 = 9\epsilon_0$, $\mu_1 = \mu_0$.

7.3.2 Numerical analysis of an image line

In order to test the new EE algorithms, we implemented these techniques in the form of a computer program and applied it to the image line shown in fig. 7.3.1. The basis for the EE method and the references were calculated using the finite-difference frequency-domain method with a square 40×20 grid. The metal walls of the structure coincide with the tangential electric field, and hence they do not introduce additional error into the results. The dispersion characteristics in the standard and inverse forms are shown in fig. 7.3.2. The standard characteristics give the propagation constants as functions of frequency and

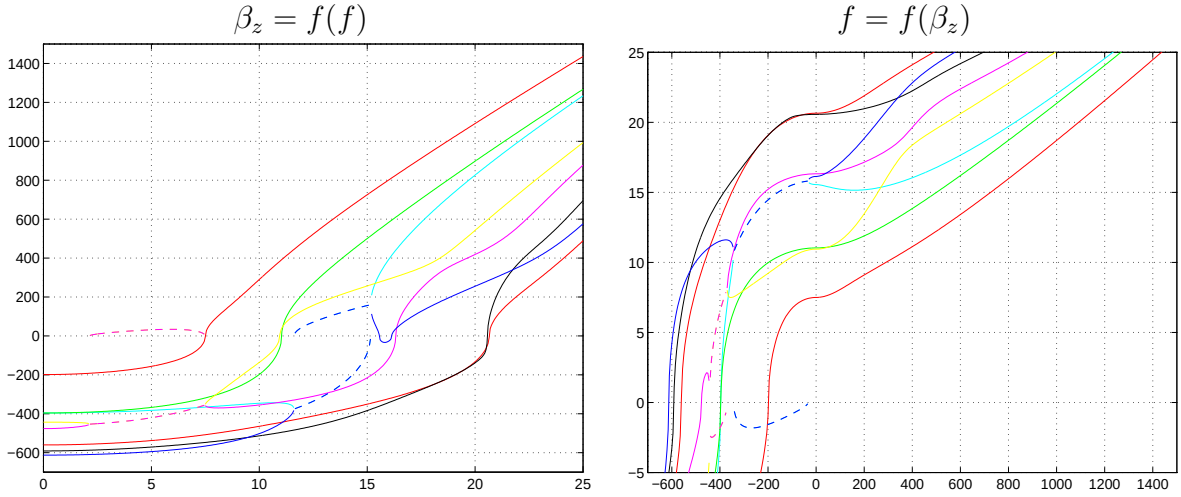

Figure 7.3.2: *Standard* $\beta_z = f(f)$ *and inverse* $f = f(\beta_z)$ *dispersion characteristics of the tested image line.*

are results of solving of eigenproblems arising from the discrete form of formulations from tab. 3.5.9 with parameter ω^2 and eigenvalues β_z^2. The inverse characteristics are frequencies versus propagation constants and correspond to the formulations with parameter β_z^2 and eigenvalues ω^2. One may observe complex modes which are denoted with the dashed line and appear in the frequency ranges $2.5 \ldots 7.5$GHz and $12 \ldots 15$GHz. One should also note the difference in the complex modes at the standard and the inverse characteristics. The standard characteristics are plotted for real frequencies, and the inverse characteristics are defined for strictly real or strictly imaginary propagation constant (i.e. for real β_z^2). The imaginary part of the propagation constant denotes attenuation in the longitudinal direction and the imaginary part of the frequency denotes attenuation in time.

At first, we present the results of the tests corresponding to the EE algorithms taking advantage of the orthogonality between the fields. Let us start from the algorithm defined by eqs. (6.3.13) and (6.3.14). This algorithm requires as a basis a set of modes corresponding to a fixed propagation constant β_{z0}. We chose a set of 20 lowest order cutoff modes ($\beta_{z0} = 0$). The algorithm provides the dispersion characteristics in the form $\beta_z(f)$. Relating these characteristics to the reference data, we get relative errors err_β in the propagation constants as functions of the frequency. Fig. 7.3.3 presents the real

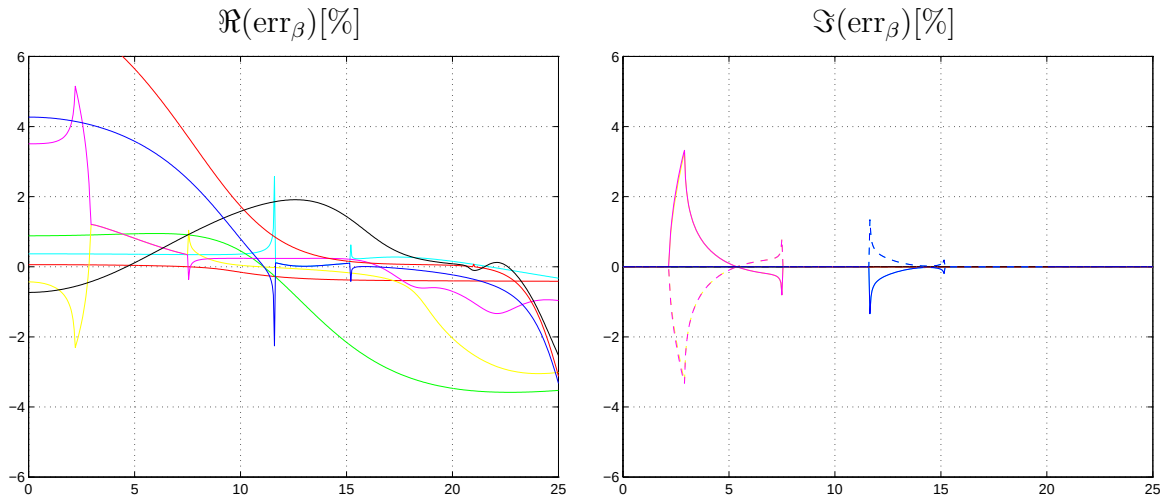

Figure 7.3.3: *Real and imaginary parts of relative error* $\mathrm{err}_\beta[\%]$ *in the propagation constant versus frequency [GHz] for the EE algorithm with* $\beta_{z0} = 0$ *and 20 modes used in the field expansion.*

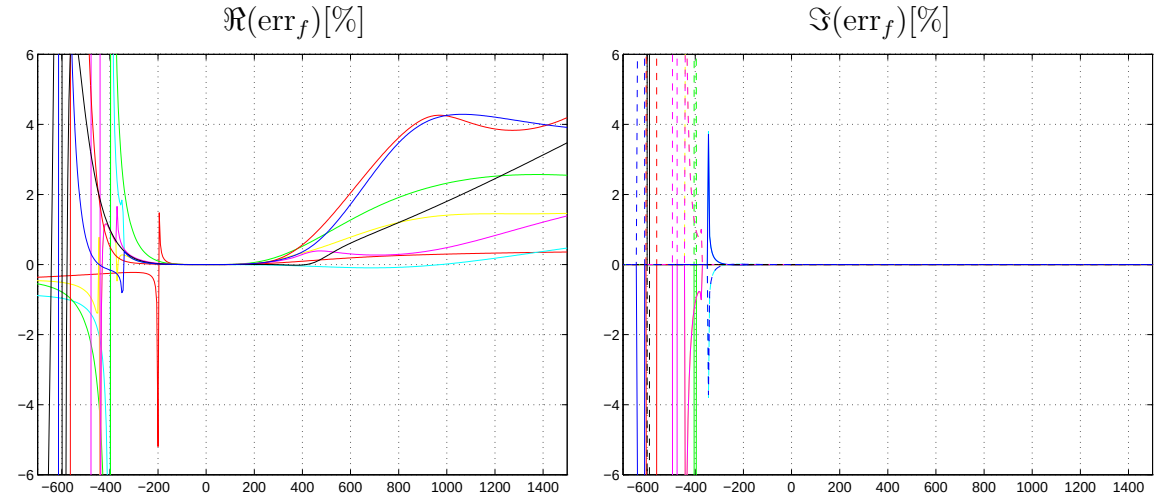

Figure 7.3.4: *Real and imaginary parts of relative error* $\mathrm{err}_f[\%]$ *in the frequency versus propagation constant [rad/m] for the EE algorithm with* $\beta_{z0} = 0$ *and 20 modes used in the field expansion.*

and the imaginary parts of this error in percents. The errors become zero at all points which form the basis of EE algorithm. For instance, error for the first mode becomes zero near 7.5GHz, which is its cutoff frequency. Imaginary part of the relative errors has nonzero value only for the parts of the characteristics corresponding to the complex

modes. Three out of eight calculated modes have the relative error lower than 1.5% in the whole investigated frequency range.

Fig. 7.3.4 presents analogous results for the algorithm with the same basis but derived from eqs. (6.3.15), (6.3.16). This algorithm gives the dispersion characteristics in the form $f(\beta_z)$. The figure shows the real and the imaginary parts of the relative error in frequency as a function of propagation constant. One may note that the error is zero for $\beta_z = 0$, i.e. at the basis, and grows up when the propagation constant goes away from zero. One may also observe peaks of the real and imaginary parts of error at the points corresponding to zero frequency. These peaks are associated with the relative nature of the error (the reference values are zero at these points) and they always appear when zero values of the functions are shifted with respect to the reference. They exist even if the shift is very small. Analogous peaks may be seen on the plots presented further on. We may read from the figure, that the maximum error for all calculated modes in the range of interest is about 4%.

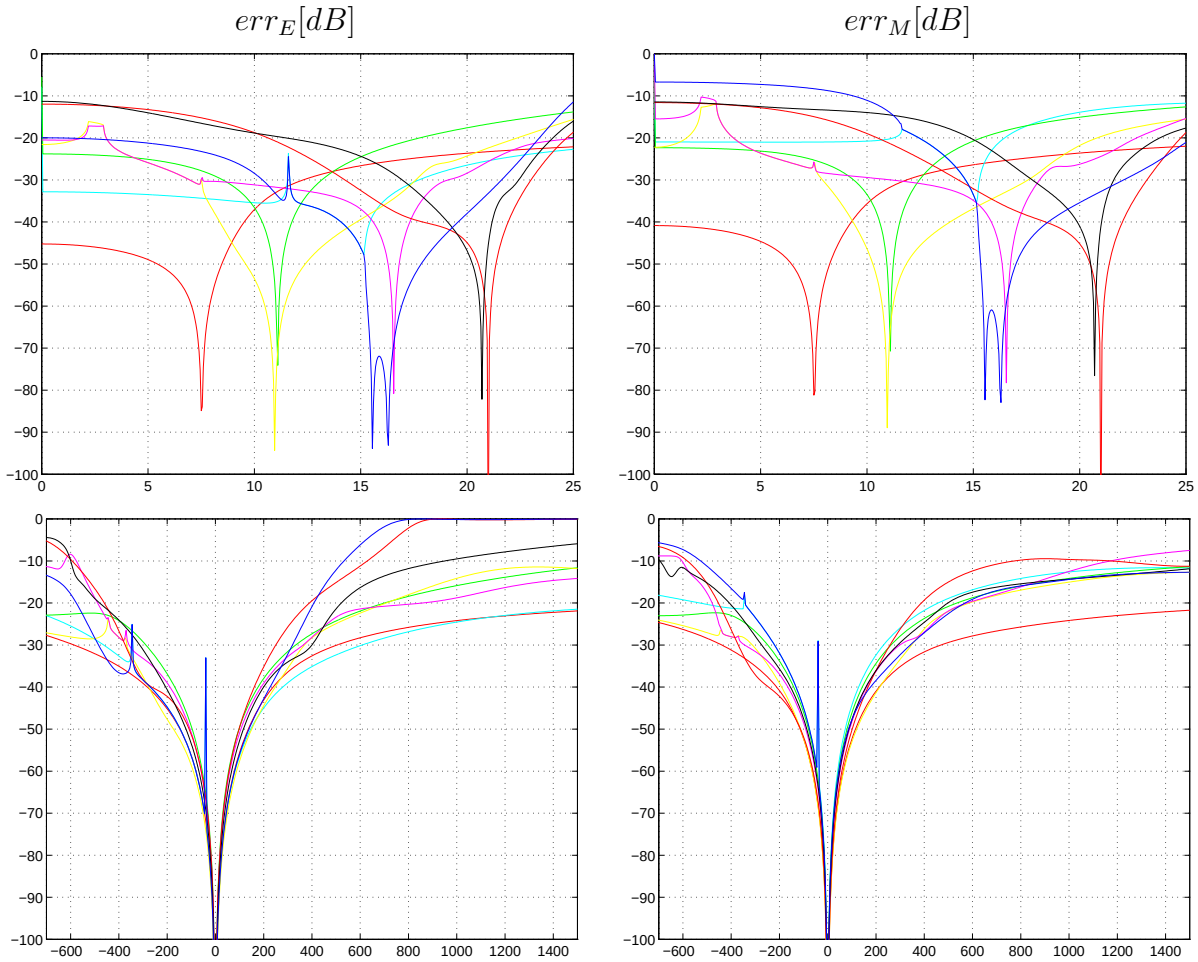

Figure 7.3.5: *Energy errors in the electric (err_E) and magnetic ($err_M[dB]$) fields [dB] versus frequency [GHz] and propagation constant [rad/m] for the EE algorithm with $\beta_{z0} = 0$ and 20 modes used in the field expansion.*

In fig. 7.3.5 we present energy errors for electric and magnetic fields for both algorithms presented above. The errors tend to zero at the points forming the basis. We can note that the error levels become smaller than -20dB in the regions where relative error of

eigenvalues is less than 1.5% (compare with figs. 7.3.3 and 7.3.4).

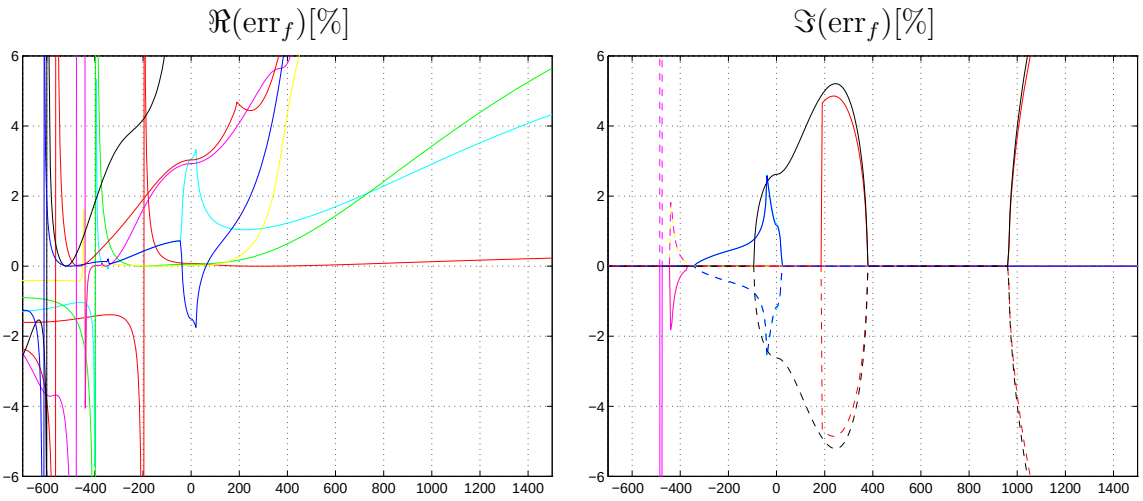

Figure 7.3.6: *Real and imaginary parts of relative error* $\mathrm{err}_f[\%]$ *in the frequency versus propagation constant [rad/m] for the EE algorithm with* $f_0 = 10GHz$ *and 20 modes used in the field expansion.*

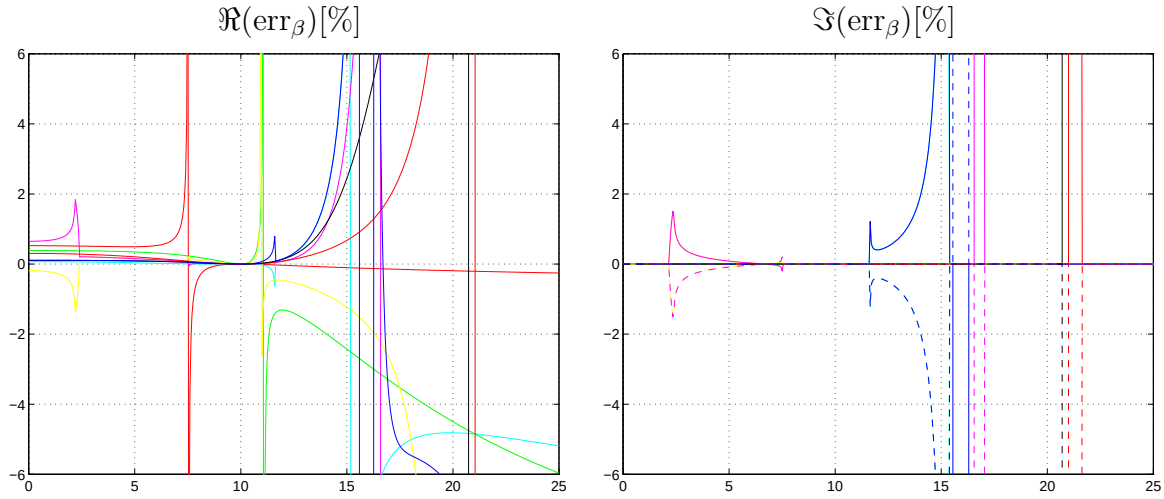

Figure 7.3.7: *Real and imaginary parts of relative error* $\mathrm{err}_\beta[\%]$ *in the propagation constant versus frequency [GHz] for the EE algorithm with* $f_0 = 10GHz$ *and 20 modes used in the field expansion.*

In the same manner, we present the results for the EE algorithms arising from eqs. (6.3.24) and (6.3.25). In this case, the basis must be formed out from the modes corresponding to a fixed frequency f_0. In our test, we chose frequency $f_0 = 10$GHz and 21 lowest order modes. The results in the form of the relative error in the frequency versus the propagation constant are shown in fig. 7.3.6. Comparing this figure with fig. 7.3.4, we see, that levels of errors in our test are in general much greater compared to the results presented earlier except for the regions where propagation constants correspond to frequency $f_0 = 10$GHz and minimal errors are observed.

The algorithm with the same basis but defined by eigenproblems (6.3.26) and (6.3.27) produces plots of errors in the propagation constants versus the frequency as shown in

fig. 7.3.7. As before, we may compare these results to the plots presented earlier in fig. 7.3.3. Comparing fig. 7.3.7 with fig. 7.3.3, we see, that now the levels of errors are much greater than in the previous case for frequencies above 15GHz. Naturally, minimum errors are observed for $f = 10$GHz. For frequencies below $f = 10$GHz errors are slightly lower than in the previous algorithm.

In general, the basis for EE algorithm may be formed from fields calculated for an arbitrary set of points from the dispersion characteristics. In this case, we do not take advantage of the orthogonality relations between the fields. The algorithm is defined by eqs. (6.3.9) and (6.3.12). Further on, we test the behavior of the fundamental mode calculated using the EE technique. The basis is constructed from fields of the lowest order mode calculated by means of the finite-difference frequency-domain method for a few (f, β_z) points. In our test, we chose two point basis consisting of modes computed at $f = 0$ and $\beta_z = 0$. The results are shown in fig. 7.3.8. We can see that even though only two points in the field expansion give dispersion characteristic error lower than 1.5% in the range of interest. Energy error is lower than -20dB for frequencies below 10GHz.

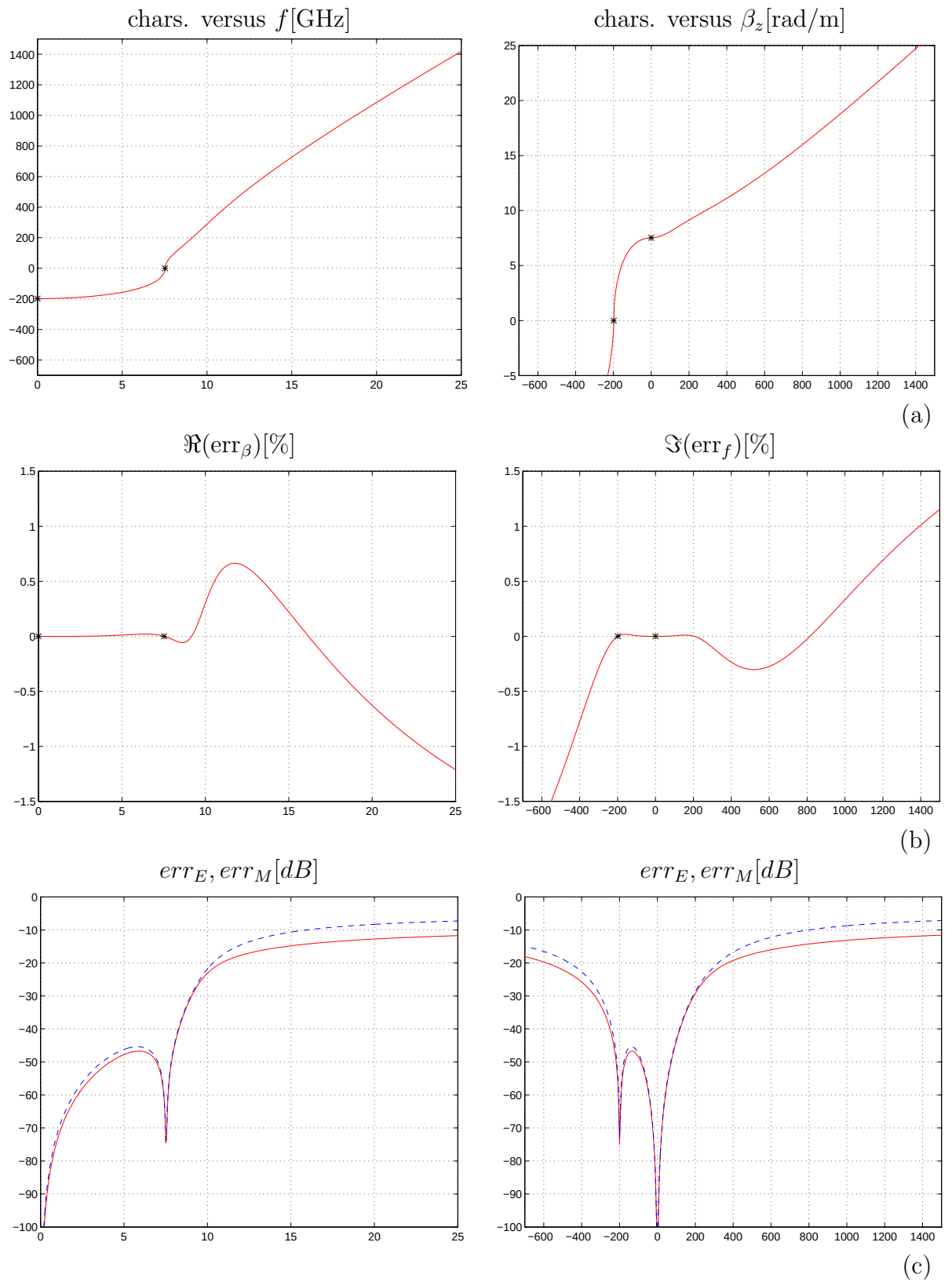

Figure 7.3.8: *Dispersion characteristics for the lowest order mode (a), the relative errors* [%] *(b) and energy error* $err_E[dB]$ *in the electric field (solid line) and* $err_M[dB]$ *in the magnetic field (dashed line) (c) for EE algorithms with basis consisting of 2 eigenfunctions calculated at points denoted by asterisk* [$*$].

Chapter 8

Conclusions

In this thesis, we presented a new approach to the finite-difference schemes and developed a series of new techniques speeding up the calculations and achieving higher accuracy of computations without increasing the numerical cost. The work may be summarized as follows:

- The finite-difference schemes in the domains of time and frequency are equivalent if the analyzed structure is lossless. It was shown, that the solution of one of these methods may be simply calculated from the other.

- The numerical dispersion error, which is strictly associated with the finite-difference schemes, may be reduced via centering which is equivalent to multiplication of the calculated frequency or propagation constant by a simple correction factor. This increases the accuracy of the computations without increasing the numerical cost. The correction factor depends on a number of variables and was derived for different finite-difference algorithms.

- Electromagnetic problems may be expressed in terms of a few basic operators. Discretization of these operators instead of the whole equations gives a common approach for every formulation. Discretized basic operators form basic matrices. They have a very simple form in the homogeneous parts of the domain. Using the concept of the basic operators, we classified a series of 2D and 3D electromagnetic problems. Written for a discrete space, they form matrix equations, which define various finite-difference algorithms.

- Modeling of metal walls, boundaries between dielectrics or conductive wedges may be performed via simple modification of the basic matrices corresponding to media properties. It was shown, that while sometimes local anisotropy is produced, the algorithms **do not change** the spectral radius of the global operator and the stability condition of the explicit-update schemes. Results of the numerical tests showed, that the new algorithms significantly improve the accuracy of the finite-difference methods.

- Significant reduction of the computation time may be achieved for some structures (eg. structures containing sections of waveguides), when some parts of the domain are analyzed using the method of moments. The field in these subdomains is expanded into a series of functions. These functions are a basis for the method of moments which is combined with the finite-difference algorithm, used in the other

subdomains, via a simple interface. Both methods form a new hybrid procedure, which may speed up the calculations for a large class of structures.

- If a waveguide has to be analyzed for many frequencies or propagation constants, the calculation time may be reduced by using the eigenfunction expansion technique. In this method, the standard, time-consuming methods need to be used only once to construct a basis of fields. This basis is then used by much faster method to get results for the entire range of parameters.

Appendix A

Formulation of eigenproblems

As discussed in sec. 3.5.3, a whole range of 2D eigenproblems may be derived from Maxwell's equations. In this appendix, we present these derivations using the operator formalism introduced in sec. 3.5. We also derive the transposed problems using properties of the basic operators derived in sec. 3.5.1.

A.1 General operator investigations

Let us consider a general eigenproblem of the form:

$$\mathbf{L}u_k = \lambda_k \mathbf{B}u_k \tag{A.1.1}$$

It may be converted to the standard eigenproblem by inverting operator $\mathbf{B}$:

$$\mathbf{B}^{-1}\mathbf{L}u_k = \lambda_k u_k \tag{A.1.2}$$

The transposed eigenproblem have the following form:

$$(\mathbf{B}^{-1}\mathbf{L})^H v_{k*} = \lambda_k^* v_{k*} \tag{A.1.3}$$

which is equivalent to:

$$\mathbf{L}^H \mathbf{B}^{-H} v_{k*} = \lambda_k^* v_{k*} \tag{A.1.4}$$

Additional subscript $_*$ in eigenvectors v_{k*} indicates, that the vector indices are associated with conjugate spectrum of operator $\mathbf{L}$. Eigenvectors v_{k*} are defined as follows:

$$v_{k*} = \mathbf{B}^H w_{k*} \tag{A.1.5}$$

where w_{k*} is the eigenvector of the following general eigenproblem:

$$\mathbf{L}^H w_{k*} = \lambda_k^* \mathbf{B}^H w_{k*} \tag{A.1.6}$$

v_{k*} is an eigenvector of the transposed eigenproblem (A.1.4) or so called a left eigenvector of (A.1.1).

A.2 Formulations for general anisotropic waveguides

In this section, we develop eigenproblems for general 2D case. We base the derivation on Maxwell's equations written in the forms (3.5.29), (3.5.30) or (3.5.31), (3.5.32).

A.2.1 6 field component ω and β_z formulations

Combining (3.5.29) and (3.5.30) into one matrix equation, we get:

$$\begin{bmatrix} -jm^*\beta_z\mathbf{Z_e} & -\mathbf{Z_e}\mathbf{G_{te}} & jn^*\omega\mathbf{M_{tt}} & jn^*\omega m^*\mathbf{M_{tz}} \\ -\mathbf{D_{tm}}\mathbf{Z_e} & 0 & jn^*\omega m\mathbf{M_{zt}} & jn^*\omega\mathbf{M_{zz}} \\ jn\omega m\mathbf{E_{tt}} & jn\omega\mathbf{E_{tz}} & jm\beta_z\mathbf{Z_m} & \mathbf{Z_m}\mathbf{G_{tm}} \\ jn\omega m^*\mathbf{E_{zt}} & jn\omega\mathbf{E_{zz}} & \mathbf{D_{te}}\mathbf{Z_m} & 0 \end{bmatrix} \begin{bmatrix} me_t \\ e_z \\ nh_t \\ mnh_z \end{bmatrix} = 0 \tag{A.2.1}$$

It is convenient to decompose the operator in eq. (A.2.1) into three parts:

$$\mathbf{L} = \mathbf{L_0} + (jn^*\omega)\mathbf{L}_\omega + (jm^*\beta_z)\mathbf{L}_\beta \tag{A.2.2}$$

where the partial operators are defined as follows:

$$\mathbf{L_0} = \begin{bmatrix} 0 & -\mathbf{Z_e}\mathbf{G_{te}} & 0 & 0 \\ -\mathbf{D_{tm}}\mathbf{Z_e} & 0 & 0 & 0 \\ 0 & 0 & 0 & \mathbf{Z_m}\mathbf{G_{tm}} \\ 0 & 0 & \mathbf{D_{te}}\mathbf{Z_m} & 0 \end{bmatrix} \tag{A.2.3}$$

$$\mathbf{L}_\omega = \begin{bmatrix} 0 & 0 & \mathbf{M_{tt}} & m^*\mathbf{M_{tz}} \\ 0 & 0 & m\mathbf{M_{zt}} & \mathbf{M_{zz}} \\ n^2\mathbf{E_{tt}} & n^2m\mathbf{E_{tz}} & 0 & 0 \\ n^2m^*\mathbf{E_{zt}} & n^2\mathbf{E_{zz}} & 0 & 0 \end{bmatrix} \tag{A.2.4}$$

$$\mathbf{L}_\beta = \begin{bmatrix} -\mathbf{Z_e} & 0 & 0 & 0 \\ 0 & 0 & 0 & 0 \\ 0 & 0 & m^2\mathbf{Z_m} & 0 \\ 0 & 0 & 0 & 0 \end{bmatrix} \tag{A.2.5}$$

Eq. (A.2.1) may be now written in the form:

$$[\mathbf{L_0} + (jn^*\omega)\mathbf{L}_\omega + (jm^*\beta_z)\mathbf{L}_\beta]\, u = 0 \tag{A.2.6}$$

According to (A.2.1) vectors u_k being the solutions of (A.2.6) for $\omega = \omega_k$, $\beta_z = \beta_{zk}$ have the form:

$$u_k = \begin{bmatrix} me_{tk} \\ e_{zk} \\ nh_{tk} \\ mnh_{zk} \end{bmatrix} \tag{A.2.7}$$

Transposed eigenproblem The transposed equation is given by:

$$\left[\mathbf{L_0}^H + (jn^*\omega)^*\mathbf{L}_\omega{}^H + (jm^*\beta_z)^*\mathbf{L}_\beta{}^H\right] w_* = 0 \tag{A.2.8}$$

with the following form of the transposed partial operators:

$$\mathbf{L_0}^H = \begin{bmatrix} 0 & -\mathbf{Z_m}\mathbf{G_{tm}} & 0 & 0 \\ -\mathbf{D_{te}}\mathbf{Z_m} & 0 & 0 & 0 \\ 0 & 0 & 0 & \mathbf{Z_e}\mathbf{G_{te}} \\ 0 & 0 & \mathbf{D_{tm}}\mathbf{Z_e} & 0 \end{bmatrix} \tag{A.2.9}$$

$$\mathbf{L}_\omega{}^H = \begin{bmatrix} 0 & 0 & n^2\mathbf{E_{tt}} & n^2 m\mathbf{E_{tz}} \\ 0 & 0 & n^2 m^*\mathbf{E_{zt}} & n^2\mathbf{E_{zz}} \\ \mathbf{M_{tt}} & m^*\mathbf{M_{tz}} & 0 & 0 \\ m\mathbf{M_{zt}} & \mathbf{M_{zz}} & 0 & 0 \end{bmatrix} \tag{A.2.10}$$

$$\mathbf{L}_\beta{}^H = m^2 \begin{bmatrix} m^2\mathbf{Z_m} & 0 & 0 & 0 \\ 0 & 0 & 0 & 0 \\ 0 & 0 & -\mathbf{Z_e} & 0 \\ 0 & 0 & 0 & 0 \end{bmatrix} \tag{A.2.11}$$

Comparing (A.2.8) with (A.2.1) we find vector w_{k*}:

$$w_{k*} = \begin{bmatrix} n^* h_{tk*} \\ mn^* h_{zk*} \\ me_{tk*} \\ e_{zk*} \end{bmatrix} \tag{A.2.12}$$

where fields h_{tk*}, h_{zk*}, e_{tk*}, e_{zk*} correspond to $\omega = \omega_k^*$ and $\beta_z = \beta_{zk}^*$.

Left eigenvectors For β_{zk} being the eigenvalue ($\omega = \text{const}$), we get the expression for v_{k*}:

$$v_{k*} = -\mathbf{L}_\beta{}^H w_{k*} = \begin{bmatrix} -\mathbf{Z_m} n^* h_{tk*} \\ 0 \\ \mathbf{Z_e} m^* e_{tk*} \\ 0 \end{bmatrix} \tag{A.2.13}$$

For ω_k being the eigenvalue ($\beta_z = \text{const}$) v_{k*} has the form:

$$v_{k*} = -\mathbf{L}_\omega{}^H w_{k*} = -n^2 \begin{bmatrix} md_{tk*} \\ d_{zk*} \\ nb_{tk*} \\ mnb_{zk*} \end{bmatrix} \tag{A.2.14}$$

A.2.2 4 field component ω formulation

From, respectively, (3.5.32) and (3.5.31), we get:

$$\begin{aligned} jn\omega md_t &= -jm\beta_z \mathbf{Z_m N_{tt}} nb_t - jm\beta_z \mathbf{Z_m} m^* \mathbf{N_{tz}} mnb_z \\ &- \mathbf{Z_m G_{tm}} m\mathbf{N_{zt}} nb_t - \mathbf{Z_m G_{tm} N_{zz}} mnb_z \end{aligned} \tag{A.2.15}$$

$$\begin{aligned} -jn^*\omega nb_t &= -jm^*\beta_z \mathbf{Z_e F_{tt}} md_t - jm^*\beta_z \mathbf{Z_e} m\mathbf{F_{tz}} d_z \\ &- \mathbf{Z_e G_{te}} m^* \mathbf{F_{zt}} md_t - \mathbf{Z_e G_{te} F_{zz}} d_z \end{aligned} \tag{A.2.16}$$

From (3.5.5), (3.5.6), we calculate the longitudinal field components:

$$d_z = \frac{1}{jm\beta_z} \mathbf{D_{te}} md_t \tag{A.2.17}$$

$$mnb_z = \frac{1}{jm^*\beta_z} \mathbf{D_{tm}} nb_t \tag{A.2.18}$$

Substituting (A.2.17) and (A.2.18) into (A.2.15) and (A.2.16), we get:

$$\begin{aligned}(jn^*\omega)md_t &= -(jm^*\beta_z)m^2n^2\mathbf{Z_m}\mathbf{N_{tt}}nb_t - m^2n^2\mathbf{Z_m}m^*\mathbf{N_{tz}}\mathbf{D_{tm}}nb_t \\ &- n^2\mathbf{Z_m}\mathbf{G_{tm}}m\mathbf{N_{zt}}nb_t - \frac{1}{jm^*\beta_z}n^2\mathbf{Z_m}\mathbf{G_{tm}}\mathbf{N_{zz}}\mathbf{D_{tm}}nb_t \qquad \text{(A.2.19)} \\ (jn^*\omega)nb_t &= (jm^*\beta_z)\mathbf{Z_e}\mathbf{F_{tt}}md_t + m^2\mathbf{Z_e}m\mathbf{F_{tz}}\mathbf{D_{te}}md_t \\ &+ \mathbf{Z_e}\mathbf{G_{te}}m^*\mathbf{F_{zt}}md_t + \frac{1}{jm^*\beta_z}m^2\mathbf{Z_e}\mathbf{G_{te}}\mathbf{F_{zz}}\mathbf{D_{te}}md_t \qquad \text{(A.2.20)}\end{aligned}$$

Combination of both equations into one matrix-operator equation results in the following eigenproblem:

$$\begin{bmatrix} 0 & \mathbf{L_{db1}}+\mathbf{L_{db2}}+\mathbf{L_{db3}}+\mathbf{L_{db4}} \\ \mathbf{L_{bd1}}+\mathbf{L_{bd2}}+\mathbf{L_{bd3}}+\mathbf{L_{bd4}} & 0 \end{bmatrix} \begin{bmatrix} md_t \\ nb_t \end{bmatrix} = jn^*\omega \begin{bmatrix} md_t \\ nb_t \end{bmatrix} \qquad \text{(A.2.21)}$$

where the sub-operators are given by the equations:

$$\begin{aligned}\mathbf{L_{db1}} &= -m^2n^2\mathbf{Z_m}m^*\mathbf{N_{tz}}\mathbf{D_{tm}} && \text{(A.2.22)} \\ \mathbf{L_{db2}} &= -n^2\mathbf{Z_m}\mathbf{G_{tm}}m\mathbf{N_{zt}} && \text{(A.2.23)} \\ \mathbf{L_{db3}} &= -\frac{1}{jm^*\beta_z}n^2\mathbf{Z_m}\mathbf{G_{tm}}\mathbf{N_{zz}}\mathbf{D_{tm}} && \text{(A.2.24)} \\ \mathbf{L_{db4}} &= -(jm^*\beta_z)m^2n^2\mathbf{Z_m}\mathbf{N_{tt}} && \text{(A.2.25)} \\ \mathbf{L_{bd1}} &= m^2\mathbf{Z_e}m\mathbf{F_{tz}}\mathbf{D_{te}} && \text{(A.2.26)} \\ \mathbf{L_{bd2}} &= \mathbf{Z_e}\mathbf{G_{te}}m^*\mathbf{F_{zt}} && \text{(A.2.27)} \\ \mathbf{L_{bd3}} &= \frac{1}{jm^*\beta_z}m^2\mathbf{Z_e}\mathbf{G_{te}}\mathbf{F_{zz}}\mathbf{D_{te}} && \text{(A.2.28)} \\ \mathbf{L_{bd4}} &= (jm^*\beta_z)\mathbf{Z_e}\mathbf{F_{tt}} && \text{(A.2.29)}\end{aligned}$$

Transposed eigenproblem The eigenproblem transposed to (A.2.21) may be written with the following operator:

$$\mathbf{L}^H = \begin{bmatrix} 0 & \mathbf{L}^H_{\mathbf{bd1}}+\mathbf{L}^H_{\mathbf{bd2}}+\mathbf{L}^H_{\mathbf{bd3}}+\mathbf{L}^H_{\mathbf{bd4}} \\ \mathbf{L}^H_{\mathbf{db1}}+\mathbf{L}^H_{\mathbf{db2}}+\mathbf{L}^H_{\mathbf{db3}}+\mathbf{L}^H_{\mathbf{db4}} & 0 \end{bmatrix} \qquad \text{(A.2.30)}$$

with the sub-operators given by the equations:

$$\begin{aligned}\mathbf{L}^H_{\mathbf{db1}} &= -m^2n^2\mathbf{G_{tm}}m\mathbf{N_{zt}}\mathbf{Z_e} = -m^2\mathbf{Z_e}\mathbf{L_{db2}}\mathbf{Z_e} && \text{(A.2.31)} \\ \mathbf{L}^H_{\mathbf{db2}} &= -n^2m^*\mathbf{N_{tz}}\mathbf{D_{tm}}\mathbf{Z_e} = -m^2\mathbf{Z_e}\mathbf{L_{db1}}\mathbf{Z_e} && \text{(A.2.32)} \\ \mathbf{L}^H_{\mathbf{db3}} &= -\frac{1}{jm\beta_z^*}n^2\mathbf{G_{tm}}\mathbf{N_{zz}}\mathbf{D_{tm}}\mathbf{Z_e} = -m^2\mathbf{Z_e}\mathbf{L_{db3*}}\mathbf{Z_e} && \text{(A.2.33)} \\ \mathbf{L}^H_{\mathbf{db4}} &= -(jm\beta_z^*)m^2n^2\mathbf{N_{tt}}\mathbf{Z_e} = -m^2\mathbf{Z_e}\mathbf{L_{db4*}}\mathbf{Z_e} && \text{(A.2.34)} \\ \mathbf{L}^H_{\mathbf{bd1}} &= m^2\mathbf{G_{te}}m^*\mathbf{F_{zt}}\mathbf{Z_m} = -m^2\mathbf{Z_m}\mathbf{L_{bd2}}\mathbf{Z_m} && \text{(A.2.35)} \\ \mathbf{L}^H_{\mathbf{bd2}} &= m\mathbf{F_{tz}}\mathbf{D_{te}}\mathbf{Z_m} = -m^2\mathbf{Z_m}\mathbf{L_{bd1}}\mathbf{Z_m} && \text{(A.2.36)} \\ \mathbf{L}^H_{\mathbf{bd3}} &= \frac{1}{jm\beta_z^*}m^2\mathbf{G_{te}}\mathbf{F_{zz}}\mathbf{D_{te}}\mathbf{Z_m} = -m^2\mathbf{Z_m}\mathbf{L_{bd3*}}\mathbf{Z_m} && \text{(A.2.37)} \\ \mathbf{L}^H_{\mathbf{bd4}} &= (jm^2\beta_z^*)\mathbf{F_{tt}}\mathbf{Z_m} = -m^2\mathbf{Z_m}\mathbf{L_{bd4*}}\mathbf{Z_m} && \text{(A.2.38)}\end{aligned}$$

From comparison of eq. (A.2.30) with (A.2.21) it follows, that eigenvectors of the transposed eigenproblem may be written in the form:

$$v_{k*} = \begin{bmatrix} \mathbf{Z_m} n^* b_{tk*} \\ -\mathbf{Z_e} m^* d_{tk*} \end{bmatrix} \tag{A.2.39}$$

A.2.3 4 field component β_z formulation

From (3.5.30) and (3.5.29), we get:

$$\begin{aligned} -(jm^*\beta_z)\mathbf{Z_e} me_t - \mathbf{Z_e G_{te}} e_z + (jn^*\omega)\mathbf{M_{tt}} h_t + (jn^*\omega)m^*\mathbf{M_{tz}} mnh_z &= 0 \quad \text{(A.2.40)} \\ -\mathbf{D_{tm}} \mathbf{Z_e} me_t + (jn^*\omega) m\mathbf{M_{zt}} nh_t + (jn^*\omega)\mathbf{M_{zz}} mnh_z &= 0 \quad \text{(A.2.41)} \\ -(jm\beta_z)\mathbf{Z_m} h_t - \mathbf{Z_m G_{tm}} mnh_z - (jn\omega)\mathbf{E_{tt}} me_t - (jn\omega) m\mathbf{E_{tz}} e_z &= 0 \quad \text{(A.2.42)} \\ -\mathbf{D_{te}} \mathbf{Z_m} nh_t - (jn\omega) m^*\mathbf{E_{zt}} ne_t - (jn\omega)\mathbf{E_{zz}} e_z &= 0 \quad \text{(A.2.43)} \end{aligned}$$

From (A.2.41) and (A.2.43), we calculate the longitudinal field components:

$$mnh_z = \frac{1}{jn^*\omega}\mathbf{M_{zz}^{-1} D_{tm} Z_e} me_t - \mathbf{M_{zz}^{-1}} m\mathbf{M_{zt}} nh_t \tag{A.2.44}$$

$$e_z = -\frac{1}{jn\omega}\mathbf{E_{zz}^{-1} D_{te} Z_m} nh_t - \mathbf{E_{zz}^{-1}} m^*\mathbf{E_{zt}} me_t \tag{A.2.45}$$

Inserting (A.2.44), (A.2.45) into (A.2.40), (A.2.42), we get:

$$\begin{aligned} 0 &= -(jm^*\beta_z)\mathbf{Z_e} me_t + \frac{1}{jn\omega}\mathbf{Z_e G_{te} E_{zz}^{-1} D_{te} Z_m} nh_t \\ &+ \mathbf{Z_e G_{te} E_{zz}^{-1}} m^*\mathbf{E_{zt}} me_t + (jn^*\omega)\mathbf{M_{tt}} nh_t \\ &+ m^*\mathbf{M_{tz} M_{zz}^{-1} D_{tm} Z_e} me_t - (jn^*\omega) m^*\mathbf{M_{tz} M_{zz}^{-1}} m\mathbf{M_{zt}} nh_t \quad \text{(A.2.46)} \\ 0 &= -(jm\beta_z)\mathbf{Z_m} nh_t - \frac{1}{jn^*\omega}\mathbf{Z_m G_{tm} M_{zz}^{-1} D_{tm} Z_e} me_t \\ &+ \mathbf{Z_m G_{tm} M_{zz}^{-1}} m\mathbf{M_{zt}} nh_t - (jn\omega)\mathbf{E_{tt}} me_t \\ &+ m\mathbf{E_{tz} E_{zz}^{-1} D_{te} Z_m} nh_t + (jn\omega) m\mathbf{E_{tz} E_{zz}^{-1}} m^*\mathbf{E_{zt}} me_t \quad \text{(A.2.47)} \end{aligned}$$

Applying, respectively, operator $-\mathbf{Z_m}$ and $-m^2\mathbf{Z_e}$ to both sides of these equations and rearranging the terms, we get:

$$\begin{aligned} (jm^*\beta_z) me_t &= \frac{1}{jn\omega}\mathbf{G_{te} E_{zz}^{-1} D_{te} Z_m} nh_t - (jn^*\omega)\mathbf{Z_m M_{tt}} nh_t \\ &+ (jn^*\omega)\mathbf{Z_m} m^*\mathbf{M_{tz} M_{zz}^{-1}} m\mathbf{M_{zt}} nh_t + \mathbf{G_{te} E_{zz}^{-1}} m^*\mathbf{E_{zt}} me_t \\ &- \mathbf{Z_m} m^*\mathbf{M_{tz} M_{zz}^{-1} D_{tm} Z_e} me_t \quad \text{(A.2.48)} \\ (jm^*\beta_z) h_t &= -\frac{1}{jn^*\omega} m^2\mathbf{G_{tm} M_{zz}^{-1} D_{tm} Z_e} me_t + (jn\omega) m^2\mathbf{Z_e E_{tt}} me_t \\ &- (jn\omega) m^2\mathbf{Z_e} m\mathbf{E_{tz} E_{zz}^{-1}} m^*\mathbf{E_{zt}} me_t + m^2\mathbf{G_{tm} M_{zz}^{-1}} m\mathbf{M_{zt}} nh_t \\ &- m^2\mathbf{Z_e} m\mathbf{E_{tz} E_{zz}^{-1} D_{te} Z_m} nh_t \quad \text{(A.2.49)} \end{aligned}$$

Combining (A.2.48) and (A.2.49) into one matrix-operator equation, we get the following eigenproblem:

$$\begin{bmatrix} \mathbf{L_{ee1}} + \mathbf{L_{ee2}} & \mathbf{L_{eh1}} + \mathbf{L_{eh2}} + \mathbf{L_{eh3}} \\ \mathbf{L_{he1}} + \mathbf{L_{he2}} + \mathbf{L_{he3}} & \mathbf{L_{hh1}} + \mathbf{L_{hh2}} \end{bmatrix} \begin{bmatrix} me_t \\ nh_t \end{bmatrix} = jm^*\beta_z \begin{bmatrix} me_t \\ nh_t \end{bmatrix} \tag{A.2.50}$$

with the following sub-operators:

$$\begin{aligned}
\mathbf{L_{ee1}} &= \mathbf{G_{te}}\mathbf{E_{zz}^{-1}}m^*\mathbf{E_{zt}} && \text{(A.2.51)}\\
\mathbf{L_{ee2}} &= -\mathbf{Z_m}m^*\mathbf{M_{tz}}\mathbf{M_{zz}^{-1}}\mathbf{D_{tm}}\mathbf{Z_e} && \text{(A.2.52)}\\
\mathbf{L_{eh1}} &= \frac{1}{jn\omega}\mathbf{G_{te}}\mathbf{E_{zz}^{-1}}\mathbf{D_{te}}\mathbf{Z_m} && \text{(A.2.53)}\\
\mathbf{L_{eh2}} &= -(jn^*\omega)\mathbf{Z_m}\mathbf{M_{tt}} && \text{(A.2.54)}\\
\mathbf{L_{eh3}} &= (jn^*\omega)\mathbf{Z_m}m^*\mathbf{M_{tz}}\mathbf{M_{zz}^{-1}}m\mathbf{M_{zt}} && \text{(A.2.55)}\\
\mathbf{L_{he1}} &= -\frac{1}{jn^*\omega}m^2\mathbf{G_{tm}}\mathbf{M_{zz}^{-1}}\mathbf{D_{tm}}\mathbf{Z_e} && \text{(A.2.56)}\\
\mathbf{L_{he2}} &= (jn\omega)m^2\mathbf{Z_e}\mathbf{E_{tt}} && \text{(A.2.57)}\\
\mathbf{L_{he3}} &= -(jn\omega)m^2\mathbf{Z_e}m\mathbf{E_{tz}}\mathbf{E_{zz}^{-1}}m^*\mathbf{E_{zt}} && \text{(A.2.58)}\\
\mathbf{L_{hh1}} &= m^2\mathbf{G_{tm}}\mathbf{M_{zz}^{-1}}m\mathbf{M_{zt}} && \text{(A.2.59)}\\
\mathbf{L_{hh2}} &= -m^2\mathbf{Z_e}m\mathbf{E_{tz}}\mathbf{E_{zz}^{-1}}\mathbf{D_{te}}\mathbf{Z_m} && \text{(A.2.60)}
\end{aligned}$$

Transposed eigenproblem The operator in the eigenproblem transposed to (A.2.50) takes up the form:

$$\mathbf{L}^H = \begin{bmatrix} \mathbf{L_{ee1}^H} + \mathbf{L_{ee2}^H} & \mathbf{L_{he1}^H} + \mathbf{L_{he2}^H} + \mathbf{L_{he3}^H} \\ \mathbf{L_{eh1}^H} + \mathbf{L_{eh2}^H} + \mathbf{L_{eh3}^H} & \mathbf{L_{hh1}^H} + \mathbf{L_{hh2}^H} \end{bmatrix} \qquad \text{(A.2.61)}$$

with the sub-operators defined as follows:

$$\begin{aligned}
\mathbf{L_{ee1}^H} &= -m\mathbf{E_{tz}}\mathbf{E_{zz}^{-1}}\mathbf{D_{te}} = m^2\mathbf{Z_m}\mathbf{L_{hh2}}\mathbf{Z_e} && \text{(A.2.62)}\\
\mathbf{L_{ee2}^H} &= \mathbf{Z_m}\mathbf{G_{tm}}\mathbf{M_{zz}^{-1}}m\mathbf{M_{zt}}\mathbf{Z_e} = m^2\mathbf{Z_m}\mathbf{L_{hh1}}\mathbf{Z_e} && \text{(A.2.63)}\\
\mathbf{L_{eh1}^H} &= \frac{1}{jn^*\omega^*}\mathbf{Z_e}\mathbf{G_{te}}\mathbf{E_{zz}^{-1}}\mathbf{D_{te}} = -n^2\mathbf{Z_e}\mathbf{L_{eh1*}}\mathbf{Z_e} && \text{(A.2.64)}\\
\mathbf{L_{eh2}^H} &= -(jn\omega^*)\mathbf{M_{tt}}\mathbf{Z_e} = -n^2\mathbf{Z_e}\mathbf{L_{eh2*}}\mathbf{Z_e} && \text{(A.2.65)}\\
\mathbf{L_{eh3}^H} &= (jn\omega^*)m^*\mathbf{M_{tz}}\mathbf{M_{zz}^{-1}}m\mathbf{M_{zt}}\mathbf{Z_e} = -n^2\mathbf{Z_e}\mathbf{L_{eh3*}}\mathbf{Z_m} && \text{(A.2.66)}\\
\mathbf{L_{he1}^H} &= -\frac{1}{jn\omega^*}m^2\mathbf{Z_m}\mathbf{G_{tm}}\mathbf{M_{zz}^{-1}}\mathbf{D_{tm}} = -n^2\mathbf{Z_m}\mathbf{L_{he1*}}\mathbf{Z_m} && \text{(A.2.67)}\\
\mathbf{L_{he2}^H} &= (jn^*\omega^*)m^2\mathbf{E_{tt}}\mathbf{Z_m} = -n^2\mathbf{Z_m}\mathbf{L_{he2*}}\mathbf{Z_m} && \text{(A.2.68)}\\
\mathbf{L_{he3}^H} &= -(jn^*\omega^*)m^2m\mathbf{E_{tz}}\mathbf{E_{zz}^{-1}}m^*\mathbf{E_{zt}}\mathbf{Z_m} = -n^2\mathbf{Z_m}\mathbf{L_{he3*}}\mathbf{Z_m} && \text{(A.2.69)}\\
\mathbf{L_{hh1}^H} &= -m^2m^*\mathbf{M_{tz}}\mathbf{M_{zz}^{-1}}\mathbf{D_{tm}} = m^2\mathbf{Z_e}\mathbf{L_{ee2}}\mathbf{Z_m} && \text{(A.2.70)}\\
\mathbf{L_{hh2}^H} &= m^2\mathbf{Z_e}\mathbf{G_{te}}\mathbf{E_{zz}^{-1}}\mathbf{E_{zt}}\mathbf{Z_m} = m^2\mathbf{Z_e}\mathbf{L_{ee1}}\mathbf{Z_m} && \text{(A.2.71)}
\end{aligned}$$

Comparison of the transposed eigenproblem with the previous equations leads to the following form of the eigenvectors:

$$v_{k*} = \begin{bmatrix} \mathbf{Z_m}n^*h_{tk*} \\ -\mathbf{Z_e}m^*e_{tk*} \end{bmatrix} \qquad \text{(A.2.72)}$$

A.2.4 3 field component ω^2 formulation

Elimination of magnetic or electric fields from Maxwell's equations leads to the following eigenproblems[1]:

$$\mathbf{FR_mNR_e}\begin{bmatrix} me_t \\ e_z \end{bmatrix} = \omega^2 \begin{bmatrix} me_t \\ e_z \end{bmatrix} \tag{A.2.73}$$

$$\mathbf{NR_eFR_m}\begin{bmatrix} h_t \\ mh_z \end{bmatrix} = \omega^2 \begin{bmatrix} h_t \\ mh_z \end{bmatrix} \tag{A.2.74}$$

$$\mathbf{R_mNR_eF}\begin{bmatrix} md_t \\ d_z \end{bmatrix} = \omega^2 \begin{bmatrix} md_t \\ d_z \end{bmatrix} \tag{A.2.75}$$

$$\mathbf{R_eFR_mN}\begin{bmatrix} b_t \\ mb_z \end{bmatrix} = \omega^2 \begin{bmatrix} b_t \\ mb_z \end{bmatrix} \tag{A.2.76}$$

where operators $\mathbf{R_m}$, $\mathbf{R_e}$, $\mathbf{F}$, $\mathbf{N}$ are defined as follows:

$$\mathbf{R_m} = \begin{bmatrix} -jm\beta_z\mathbf{Z_m} & -\mathbf{Z_mG_{tm}} \\ -\mathbf{D_{te}Z_m} & 0 \end{bmatrix} \tag{A.2.77}$$

$$\mathbf{R_e} = \begin{bmatrix} -jm^*\beta_z\mathbf{Z_e} & -\mathbf{Z_eG_{te}} \\ -\mathbf{D_{tm}Z_e} & 0 \end{bmatrix} \tag{A.2.78}$$

$$\mathbf{F} = \begin{bmatrix} \mathbf{F_{tt}} & \mathbf{F_{tz}} \\ \mathbf{F_{zt}} & \mathbf{F_{zz}} \end{bmatrix} \tag{A.2.79}$$

$$\mathbf{N} = \begin{bmatrix} \mathbf{N_{tt}} & \mathbf{N_{tz}} \\ \mathbf{N_{zt}} & \mathbf{N_{zz}} \end{bmatrix} \tag{A.2.80}$$

Note, that eigenproblem (A.2.73) is transposed to (A.2.75) and (A.2.74) is transposed to (A.2.76).

A.2.5 2 field component ω^2 formulation

We may eliminate the transverse magnetic or electric field components from (A.2.21) and get the following two field component formulations:

$$-n^2\mathbf{L_{db}} - n^2\mathbf{L_{bd}}d_t = \omega^2 d_t \tag{A.2.81}$$

$$\mathbf{L_{bd}L_{db}}b_t = \omega^2 b_t \tag{A.2.82}$$

where $\mathbf{L_{db}}$, $\mathbf{L_{bd}}$ are defined as follows:

$$\mathbf{L_{db}} = \mathbf{L_{db1}} + \mathbf{L_{db2}} + \mathbf{L_{db3}} + \mathbf{L_{db4}} \tag{A.2.83}$$

$$\mathbf{L_{bd}} = \mathbf{L_{bd1}} + \mathbf{L_{bd2}} + \mathbf{L_{bd3}} + \mathbf{L_{bd4}} \tag{A.2.84}$$

A.3 Formulations for bidirectional waveguides

In this section, we assume that the structure is strictly bidirectional, i.e. operators $\mathbf{E_{tz}}$, $\mathbf{E_{zt}}$, and $\mathbf{M_{tz}}$, $\mathbf{M_{zt}}$ vanish. This implies that $\mathbf{F_{tz}}$, $\mathbf{F_{zt}}$, and $\mathbf{N_{tz}}$, $\mathbf{N_{zt}}$ also vanish and $\mathbf{F_{tt}} = \mathbf{E_{tt}^{-1}}$, $\mathbf{F_{zz}} = \mathbf{E_{zz}^{-1}}$, $\mathbf{N_{tt}} = \mathbf{M_{tt}^{-1}}$, $\mathbf{N_{zz}} = \mathbf{M_{zz}^{-1}}$.

[1] Compare with 3D 3 component formulations in sec. 3.4.2.

A.3.1 Duality relations

In bidirectional waveguides, Maxwell's equations (3.5.29) and (3.5.30) take up the following form:

$$\begin{bmatrix} -jm\beta_z\mathbf{Z_m} & -\mathbf{Z_m}\mathbf{G_{tm}} \\ -\mathbf{D_{te}}\mathbf{Z_m} & 0 \end{bmatrix} \begin{bmatrix} nh_t \\ mnh_z \end{bmatrix} = jn\omega \begin{bmatrix} \mathbf{E_{tt}} & 0 \\ 0 & \mathbf{E_{zz}} \end{bmatrix} \begin{bmatrix} me_t \\ e_z \end{bmatrix} \tag{A.3.1}$$

$$\begin{bmatrix} -jm^*\beta_z\mathbf{Z_e} & -\mathbf{Z_e}\mathbf{G_{te}} \\ -\mathbf{D_{tm}}\mathbf{Z_e} & 0 \end{bmatrix} \begin{bmatrix} me_t \\ e_z \end{bmatrix} = -jn^*\omega \begin{bmatrix} \mathbf{M_{tt}} & 0 \\ 0 & \mathbf{M_{zz}} \end{bmatrix} \begin{bmatrix} nh_t \\ mnh_z \end{bmatrix} \tag{A.3.2}$$

It is easy to verify, that these equations may be written in the following form:

$$\begin{bmatrix} -jn\omega\mathbf{Z_m} & -\mathbf{Z_m}\mathbf{G_{tm}} \\ -\mathbf{D_{te}}\mathbf{Z_m} & 0 \end{bmatrix} \begin{bmatrix} -\mathbf{Z_e}md_t \\ mnh_z \end{bmatrix} = jm\beta_z \begin{bmatrix} -\mathbf{Z_m}\mathbf{M_{tt}^{-1}}\mathbf{Z_e} & 0 \\ 0 & -\mathbf{E_{zz}} \end{bmatrix} \begin{bmatrix} \mathbf{Z_m}nb_t \\ e_z \end{bmatrix} \tag{A.3.3}$$

$$\begin{bmatrix} -jn^*\omega\mathbf{Z_e} & -\mathbf{Z_e}\mathbf{G_{te}} \\ -\mathbf{D_{tm}}\mathbf{Z_e} & 0 \end{bmatrix} \begin{bmatrix} \mathbf{Z_m}nb_t \\ e_z \end{bmatrix} = -jm^*\beta_z \begin{bmatrix} \mathbf{Z_e}\mathbf{E_{tt}^{-1}}\mathbf{Z_m} & 0 \\ 0 & -\mathbf{M_{zz}} \end{bmatrix} \begin{bmatrix} -\mathbf{Z_e}md_t \\ mnh_z \end{bmatrix} \tag{A.3.4}$$

It is clearly seen, that two pairs of equations presented above are dual to each other with the duality relations of the physical quantities pointed out in tab. A.3.1. This means, that every formulation for bidirectional waveguides with respect to ω has its dual counterpart formulated with respect to β_z. The appropriate equations may be derived based on tab. A.3.1. Analogous duality relations may be written for general anisotropic waveguides. However, this case requires taking bianisotropy into account.

Table A.3.1: *Duality relations between physical quantities in bidirectional waveguides.*

ω	$\longleftrightarrow$	β_z
β_z	$\longleftrightarrow$	ω
e_t	$\longleftrightarrow$	$\mathbf{Z_m}b_t$
e_z	$\longleftrightarrow$	e_z
h_t	$\longleftrightarrow$	$-\mathbf{Z_e}d_t$
h_z	$\longleftrightarrow$	h_z
d_t	$\longleftrightarrow$	$\mathbf{Z_m}h_t$
d_z	$\longleftrightarrow$	$-d_z$
b_t	$\longleftrightarrow$	$-\mathbf{Z_e}e_t$
b_z	$\longleftrightarrow$	$-b_z$
$\mathbf{E_{tt}}$	$\longleftrightarrow$	$-\mathbf{Z_m}\mathbf{M_{tt}^{-1}}\mathbf{Z_e}$
$\mathbf{E_{zz}}$	$\longleftrightarrow$	$-\mathbf{E_{zz}}$
$\mathbf{M_{tt}}$	$\longleftrightarrow$	$-\mathbf{Z_e}\mathbf{E_{tt}^{-1}}\mathbf{Z_m}$
$\mathbf{M_{zz}}$	$\longleftrightarrow$	$-\mathbf{M_{zz}}$
m	$\longleftrightarrow$	n
n	$\longleftrightarrow$	m

A.3.2 4 field component $\omega\beta_z$ and ω^2 formulations

Eigenproblem (A.2.50) in the case of bidirectional structures may be written in the following way:

$$(\omega^2\mathbf{L_{\omega^2}} + \mathbf{L_0}) \begin{bmatrix} me_t \\ nh_t \end{bmatrix} = m^*n^*\omega\beta_z \begin{bmatrix} me_t \\ nh_t \end{bmatrix} \tag{A.3.5}$$

where operators $\mathbf{L}_{\omega^2}$, $\mathbf{L_0}$ are defined as follows:

$$\mathbf{L}_{\omega^2} = \begin{bmatrix} 0 & -n^2\mathbf{Z_m}\mathbf{M_{tt}} \\ m^2\mathbf{Z_e}\mathbf{E_{tt}} & 0 \end{bmatrix} \tag{A.3.6}$$

$$\mathbf{L_0} = \begin{bmatrix} 0 & -n^2\mathbf{G_{te}}\mathbf{E_{zz}^{-1}}\mathbf{D_{te}}\mathbf{Z_m} \\ m^2\mathbf{G_{tm}}\mathbf{M_{zz}^{-1}}\mathbf{D_{tm}}\mathbf{Z_e} & 0 \end{bmatrix} \tag{A.3.7}$$

If ω^2 is treated as a parameter and $(m^*n^*\omega\beta_z)$ is an eigenvalue, left eigenvectors $v_{k*} = w_{k*}$ are the same as in the case of (A.2.61), i.e. are given by eq. (A.2.72). If $(m^*n^*\omega\beta_z)$ is a parameter (ω^2 is an eigenvalue), the left eigenvectors are given by the following equation:

$$v_{k*} = -\mathbf{L}_{\omega^2}^H w_{k*} = \begin{bmatrix} md_t \\ nb_t \end{bmatrix} \tag{A.3.8}$$

A.3.3 4 field component $\omega\beta_z$ and β_z^2 formulations

From the discussion performed in sec. A.3.1 it follows, that eq. (A.3.5) has its dual counterpart. We may write it in the following form:

$$(\beta_z^2\mathbf{L}_{\beta^2} + \mathbf{L_0}) \begin{bmatrix} md_t \\ nb_t \end{bmatrix} = m^*n^*\omega\beta_z \begin{bmatrix} md_t \\ nb_t \end{bmatrix} \tag{A.3.9}$$

with operators $\mathbf{L}_{\beta^2}$, $\mathbf{L_0}$ defined in the following way:

$$\mathbf{L}_{\beta^2} = \begin{bmatrix} 0 & -n^2\mathbf{Z_m}\mathbf{M_{tt}^{-1}} \\ m^2\mathbf{Z_e}\mathbf{E_{tt}^{-1}} & 0 \end{bmatrix} \tag{A.3.10}$$

$$\mathbf{L_0} = \begin{bmatrix} 0 & n^2\mathbf{Z_m}\mathbf{G_{tm}}\mathbf{M_{zz}^{-1}}\mathbf{D_{tm}} \\ -m^2\mathbf{Z_e}\mathbf{G_{te}}\mathbf{E_{zz}^{-1}}\mathbf{D_{te}} & 0 \end{bmatrix} \tag{A.3.11}$$

If β_z^2 is a parameter and $(m^*n^*\omega\beta_z)$ is an eigenvalue, left eigenvectors $v_{k*} = w_{k*}$ are given by eq. (A.2.39). If $(m^*n^*\omega\beta_z)$ is a parameter (ω^2 is an eigenvalue), the left eigenvectors have the form:

$$v_{k*} = -\mathbf{L}_{\beta^2}^H w_{k*} = \begin{bmatrix} me_t \\ nh_t \end{bmatrix} \tag{A.3.12}$$

A.3.4 2 field component ω^2 formulation

Extracting the term $\omega^2 d_t$ from wave equation (3.5.4), we get:

$$\begin{aligned} \omega^2 d_t &= -\beta_z\mathbf{Z_m}\mathbf{M_{tt}^{-1}}\mathbf{Z_e}\mathbf{E_{tt}^{-1}}d_t + \mathbf{Z_m}\mathbf{G_{tm}}\mathbf{M_{zz}^{-1}}\mathbf{D_{tm}}\mathbf{Z_e}\mathbf{E_{tt}^{-1}}d_t \\ &+ j\beta_z\mathbf{Z_m}\mathbf{M_{tt}^{-1}}\mathbf{Z_e}\mathbf{G_{te}}\mathbf{E_{zz}^{-1}}d_z \end{aligned} \tag{A.3.13}$$

Substituting (3.5.5) into (A.3.13), we obtain an eigenproblem with ω_k^2 and d_{tk} being eigenpairs for a fixed value of β_z:

$$\begin{aligned} \omega^2 d_t &= -\beta_z^2\mathbf{Z_m}\mathbf{M_{tt}^{-1}}\mathbf{Z_e}\mathbf{E_{tt}^{-1}}d_t + \mathbf{Z_m}\mathbf{G_{tm}}\mathbf{M_{zz}^{-1}}\mathbf{D_{tm}}\mathbf{Z_e}\mathbf{E_{tt}^{-1}}d_t \\ &+ \mathbf{Z_m}\mathbf{M_{tt}^{-1}}\mathbf{Z_e}\mathbf{G_{te}}\mathbf{E_{zz}^{-1}}\mathbf{D_{te}}d_t \end{aligned} \tag{A.3.14}$$

An analogous approach may be applied to the magnetic flux density, giving the following equation:

$$\begin{aligned} \omega^2 b_t &= -\beta_z^2\mathbf{Z_e}\mathbf{E_{tt}^{-1}}\mathbf{Z_m}\mathbf{M_{tt}^{-1}}b_t + \mathbf{Z_e}\mathbf{G_{te}}\mathbf{E_{zz}^{-1}}\mathbf{D_{te}}\mathbf{Z_m}\mathbf{M_{tt}^{-1}}b_t \\ &+ \mathbf{Z_e}\mathbf{E_{tt}^{-1}}\mathbf{Z_m}\mathbf{G_{tm}}\mathbf{M_{zz}^{-1}}\mathbf{D_{tm}}b_t \end{aligned} \tag{A.3.15}$$

A.3.5 2 field component β_z^2 formulation

Eqs. (A.3.13), (A.3.14) have two dual counterparts:

$$\begin{aligned}\beta_z^2 e_t &= -\omega^2 \mathbf{Z_m M_{tt} Z_e E_{tt}} e_t - \mathbf{Z_m M_{tt} G_{tm} M_{zz}^{-1} D_{tm} Z_e} e_t \\ &+ \mathbf{G_{te} E_{zz}^{-1} D_{te} E_{tt}} e_t \qquad \text{(A.3.16)} \\ \beta_z^2 h_t &= -\omega^2 \mathbf{Z_e E_{tt} Z_m M_{tt}} h_t - \mathbf{Z_e E_{tt} G_{te} E_{zz}^{-1} D_{te} Z_m} h_t \\ &+ \mathbf{G_{tm} M_{zz}^{-1} D_{tm} M_{tt}} h_t \qquad \text{(A.3.17)}\end{aligned}$$

A.3.6 Scalar formulations

In two cases the analysis may be reduced to solving scalar eigenproblems. This may be done at cutoff and in the static case. The analysis is then split into modes E and H.

E modes at cutoff From (3.5.1), we get:

$$-\mathbf{D_{te} Z_m} h_t = j\omega \mathbf{E_{zz}} e_z \qquad \text{(A.3.18)}$$

From (3.5.2), for $\beta_z = 0$:

$$-\mathbf{Z_e G_{te}} e_z = -j\omega \mathbf{M_{tt}} h_t \qquad \text{(A.3.19)}$$

This gives:

$$h_t = \frac{1}{j\omega} \mathbf{M_{tt}^{-1} Z_e G_{te}} e_z \qquad \text{(A.3.20)}$$

We put (A.3.20) into (A.3.18) and multiply both sides of this equation by $-j\omega \mathbf{E_{zz}^{-1}}$. This gives the following eigenproblem:

$$\mathbf{E_{zz}^{-1} D_{te} Z_m M_{tt}^{-1} Z_e G_{te}} e_z = \omega^2 e_z \qquad \text{(A.3.21)}$$

The transposed eigenproblem has the form:

$$\mathbf{D_{te} Z_m M_{tt}^{-1} Z_e G_{te} E_{zz}^{-1}} d_z = \omega^2 d_z \qquad \text{(A.3.22)}$$

H modes at cutoff In a similar manner we may get the eigenproblem with scalar eigenfunctions h_z:

$$\mathbf{M_{zz}^{-1} D_{tm} Z_e E_{tt}^{-1} Z_m G_{tm}} h_z = \omega^2 h_z \qquad \text{(A.3.23)}$$

and its transpose with the eigenfunctions b_z:

$$\mathbf{D_{tm} Z_e E_{tt}^{-1} Z_m G_{tm} M_{zz}^{-1}} b_z = \omega^2 b_z \qquad \text{(A.3.24)}$$

E static modes From the duality relations given in sec. A.3.1, we get the eigenproblem dual to (A.3.21):

$$\mathbf{E_{zz}^{-1} D_{te} E_{tt} G_{te}} e_z = \beta_z^2 e_z \qquad \text{(A.3.25)}$$

The transposed eigenproblem with eigenfunctions d_z may be written as follows:

$$\mathbf{D_{te} E_{tt} G_{te} E_{zz}^{-1}} d_z = \beta_z^2 d_z \qquad \text{(A.3.26)}$$

H static modes The same procedure produces the eigenproblem with scalar eigenfunctions h_z:

$$\mathbf{M_{zz}^{-1} D_{tm} M_{tt} G_{tm}} h_z = \beta_z^2 h_z \qquad \text{(A.3.27)}$$

and its transpose with the eigenfunctions B_z:

$$\mathbf{D_{tm} M_{tt} G_{tm} M_{zz}^{-1}} b_z = \beta_z^2 b_z \qquad \text{(A.3.28)}$$

Appendix B

Orthogonality relations

One of the most fundamental properties of modes are the orthogonality relations. This appendix contains derivations of these relations for the problems derived in app. A.

B.1 General operator investigations

It is easy to verify, that vectors defined in sec. A.1 satisfy the following orthogonality relations:

$$\begin{aligned} 0 &= < \mathbf{L}u_k, w_{l*} > - < u_k, \mathbf{L}^H w_{l*} > \\ &= < \lambda_k \mathbf{B}u_k, w_{l*} > - < u_k, \lambda_l^* \mathbf{B}^H w_{l*} > \\ &= (\lambda_k - \lambda_l) < u_k, \mathbf{B}^H w_{l*} > \\ &= (\lambda_k - \lambda_l) < u_k, v_{l*} > \end{aligned} \tag{B.1.1}$$

This means, that if $\lambda_k \neq \lambda_l$, vectors u_k and v_{l*} are orthogonal:

$$< u_k, v_{l*} >= 0 \tag{B.1.2}$$

In many cases in electromagnetics, the eigenproblems may be written in the following form:

$$\mathbf{L}u_k = \gamma_k \mathbf{A}u_k + \lambda_k \mathbf{B}u_k \tag{B.1.3}$$

where γ and λ are independent parameters. A set of solutions (γ, λ) gives the dispersion characteristics. Let us now consider the transpose eigenproblem:

$$\mathbf{L}^H w_{l*} = \gamma_l^* \mathbf{A}^H w_{l*} + \lambda_l^* \mathbf{B}^H w_{l*} \tag{B.1.4}$$

Applying the inner product $\langle ., w_{l*} \rangle$ to both sides of eq. (B.1.3) and the inner product $\langle u_k, . \rangle$ to eq. (B.1.4), we get:

$$\langle \mathbf{L}u_k, w_{l*} \rangle = \langle \gamma_k \mathbf{A}u_k, w_{l*} \rangle + \langle \lambda_k \mathbf{B}u_k, w_{l*} \rangle \tag{B.1.5}$$

$$\left\langle u_k, \mathbf{L}^H w_{l*} \right\rangle = \left\langle u_k, \gamma_l^* \mathbf{A}^H w_{l*} \right\rangle + \left\langle u_k, \lambda_l^* \mathbf{B}^H w_{l*} \right\rangle \tag{B.1.6}$$

Subtracting (B.1.6) from (B.1.5) we get more general orthogonality relations:

$$(\gamma_k - \gamma_l) \langle \mathbf{A}u_k, w_{l*} \rangle + (\lambda_k - \lambda_l) \langle \mathbf{B}u_k, w_{l*} \rangle = 0 \tag{B.1.7}$$

B.2 Electromagnetic field in lossless waveguides

Based on the general investigations from the previous section and different formulations of electromagnetic eigenproblems derived in app. A, we may now present different orthogonality relations for 2D problems. Note, that the relations are independent on the choice of parameters m, n.

Modes in general anisotropic waveguides General relations (from eigenproblem in app. A.2.1):

$$\begin{aligned} 0 &= (\beta_{zk} - \beta_{zl}) \left(\langle e_{tk}, \mathbf{Z_m} h_{tl*} \rangle - \langle h_{tk}, \mathbf{Z_e} e_{tl*} \rangle \right) \\ &+ (\omega_k - \omega_l) \left(\langle e_k, d_{l*} \rangle + \langle h_k, b_{l*} \rangle \right) \end{aligned} \tag{B.2.1}$$

for $\beta_z = \text{const}$ (eigenproblems in apps. A.2.1, A.2.2, A.2.5):

$$(\omega_k - \omega_l) \left(\langle e_k, d_{l*} \rangle + \langle h_k, b_{l*} \rangle \right) = 0 \tag{B.2.2}$$

$$(\omega_k - \omega_l) \left(\langle d_{tk}, \mathbf{Z_m} b_{tl*} \rangle - \langle b_{tk}, \mathbf{Z_e} d_{tl*} \rangle \right) = 0 \tag{B.2.3}$$

$$(\omega_k^2 - \omega_l^2) \langle d_{tk}, \mathbf{Z_m} b_{tl*} \rangle = 0 \tag{B.2.4}$$

for $\omega = \text{const}$ (see app. A.2.1):

$$(\beta_{zk} - \beta_{zl}) \left(\langle e_{tk}, \mathbf{Z_m} h_{tl*} \rangle - \langle h_{tk}, \mathbf{Z_e} e_{tl*} \rangle \right) = 0 \tag{B.2.5}$$

Modes in bidirectional waveguides General relations (apps. A.3.2, A.3.3, A.3.4):

$$\begin{aligned} 0 &= (\beta_{zk}\omega_k - \beta_{zl}\omega_l) \left(\langle e_{tk}, \mathbf{Z_m} h_{tl*} \rangle - \langle h_{tk}, \mathbf{Z_e} e_{tl*} \rangle \right) \\ &+ (\omega_k^2 - \omega_l^2) \left(\langle e_{tk}, d_{tl*} \rangle + \langle h_{tk}, b_{tl*} \rangle \right) \end{aligned} \tag{B.2.6}$$

$$\begin{aligned} 0 &= (\beta_{zk}\omega_k - \beta_{zl}\omega_l) \left(\langle d_{tk}, \mathbf{Z_m} b_{tl*} \rangle - \langle b_{tk}, \mathbf{Z_e} d_{tl*} \rangle \right) \\ &+ (\beta_{zk}^2 - \beta_{zl}^2) \left(\langle d_{tk}, e_{tl*} \rangle + \langle b_{tk}, h_{tl*} \rangle \right) \end{aligned} \tag{B.2.7}$$

$$\begin{aligned} 0 &= (\beta_{zk}^2 - \beta_{zl}^2) \langle e_{tk}, \mathbf{Z_m} h_{tl*} \rangle \\ &- (\omega_k^2 - \omega_l^2) \langle d_{tk}, \mathbf{Z_m} b_{tl*} \rangle \end{aligned} \tag{B.2.8}$$

for $\beta_z^2 = \text{const}$ (apps. A.3.2, A.3.4):

$$(\beta_{zk}\omega_k - \beta_{zl}\omega_l) \left(\langle d_{tk}, \mathbf{Z_m} b_{tl*} \rangle - \langle b_{tk}, \mathbf{Z_e} d_{tl*} \rangle \right) = 0 \tag{B.2.9}$$

$$(\omega_k^2 - \omega_l^2) \langle d_{tk}, \mathbf{Z_m} b_{tl*} \rangle = 0 \tag{B.2.10}$$

for $\omega^2 = \text{const}$ (apps. A.3.3, A.3.5):

$$(\beta_{zk}\omega_k - \beta_{zl}\omega_l) \left(\langle e_{tk}, \mathbf{Z_m} h_{tl*} \rangle - \langle h_{tk}, \mathbf{Z_e} e_{tl*} \rangle \right) = 0 \tag{B.2.11}$$

$$(\beta_{zk}^2 - \beta_{zl}^2) \langle e_{tk}, \mathbf{Z_m} h_{tl*} \rangle = 0 \tag{B.2.12}$$

for $\beta_z\omega = \text{const}$ (apps. A.3.2, A.3.3):

$$(\omega_k^2 - \omega_l^2) \left(\langle d_{tk}, e_{tl*} \rangle + \langle b_{tk}, h_{tl*} \rangle \right) = 0 \tag{B.2.13}$$

$$(\beta_{zk}^2 - \beta_{zl}^2) \left(\langle e_{tk}, d_{tl*} \rangle + \langle h_{tk}, b_{tl*} \rangle \right) = 0 \tag{B.2.14}$$

Cutoff modes in bidirectional waveguides (from app. A.3.6 and eq. (B.2.2))

$$(\omega_k^2 - \omega_l^2)\,\langle e_{zk}, d_{zl*}\rangle = 0 \tag{B.2.15}$$

$$(\omega_k^2 - \omega_l^2)\,\langle e_{tk}, d_{tl*}\rangle = 0 \tag{B.2.16}$$

$$(\omega_k^2 - \omega_l^2)\,\langle h_{zk}, b_{zl*}\rangle = 0 \tag{B.2.17}$$

$$(\omega_k^2 - \omega_l^2)\,\langle h_{tk}, b_{tl*}\rangle = 0 \tag{B.2.18}$$

Static modes in bidirectional waveguides (app. A.3.6, eq. (B.2.2))

$$(\beta_{zk}^2 - \beta_{zl}^2)\,\langle e_{zk}, d_{zl*}\rangle = 0 \tag{B.2.19}$$

$$(\beta_{zk}^2 - \beta_{zl}^2)\,\langle e_{tk}, d_{tl*}\rangle = 0 \tag{B.2.20}$$

$$(\beta_{zk}^2 - \beta_{zl}^2)\,\langle h_{zk}, b_{zl*}\rangle = 0 \tag{B.2.21}$$

$$(\beta_{zk}^2 - \beta_{zl}^2)\,\langle h_{tk}, b_{tl*}\rangle = 0 \tag{B.2.22}$$

B.3 Electromagnetic field in lossless 3D resonators

In the same manner, we derive the orthogonality relations in the case of 3D problems.

$$(\omega_k - \omega_l)\,(\langle e_k, d_{l*}\rangle + \langle h_k, b_{l*}\rangle) = 0 \tag{B.3.1}$$

$$(\omega_k^2 - \omega_l^2)\,\langle e_k, d_{l*}\rangle = 0 \tag{B.3.2}$$

$$(\omega_k^2 - \omega_l^2)\,\langle h_k, b_{l*}\rangle = 0 \tag{B.3.3}$$

Appendix C

Field error functions

We derive the error functions related to the field distribution defined by equations (7.3.3) and (7.3.4) repeated below for completeness.

- the relative transverse electric energy of error:

$$\mathrm{err}_E = \frac{\iint_S (\alpha_e \vec{E}_{\mathrm{tee}} - \vec{E}_{\mathrm{tref}}) \cdot (\alpha_e \vec{D}_{\mathrm{tee}} - \vec{D}_{\mathrm{tref}})^* ds}{\iint_S \vec{E}_{\mathrm{tref}} \cdot \vec{D}^*_{\mathrm{tref}} ds} \tag{C.0.1}$$

- the relative transverse magnetic energy of error:

$$\mathrm{err}_M = \frac{\iint_S (\alpha_m \vec{H}_{\mathrm{tee}} - \vec{H}_{\mathrm{tref}}) \cdot (\alpha_m \vec{B}_{\mathrm{tee}} - \vec{B}_{\mathrm{tref}})^* ds}{\iint_S \vec{H}_{\mathrm{tref}} \cdot \vec{B}^*_{\mathrm{tref}} ds} \tag{C.0.2}$$

α_e, α_m are parameters, which minimize the errors. Further, we assume, that the materials are lossless, which implies, that err_E and err_M are real. In order to find α_e, we need to find zero of the derivative of err_E with respect to α_e. We decompose the terms in (C.0.1) into:

$$\mathrm{err}_E = |\alpha_e|^2 \frac{\iint_S \vec{E}_{\mathrm{tee}} \cdot \vec{D}^*_{\mathrm{tee}} ds}{\iint_S \vec{E}_{\mathrm{tref}} \cdot \vec{D}^*_{\mathrm{tref}} ds} - \alpha_e \frac{\iint_S \vec{E}_{\mathrm{tee}} \cdot \vec{D}^*_{\mathrm{tref}} ds}{\iint_S \vec{E}_{\mathrm{tref}} \cdot \vec{D}^*_{\mathrm{tref}} ds} - \alpha_e^* \frac{\iint_S \vec{E}_{\mathrm{tref}} \cdot \vec{D}^*_{\mathrm{tee}} ds}{\iint_S \vec{E}_{\mathrm{tref}} \cdot \vec{D}^*_{\mathrm{tref}} ds} + 1 \tag{C.0.3}$$

By decomposing α_e into real (α_{er}) and imaginary (α_{ei}) parts (i.e., $\alpha_e = \alpha_{er} + j\alpha_{ei}$), we get:

$$\mathrm{err}_E = (\alpha_{er}^2 + \alpha_{ei}^2) \frac{\iint_S \vec{E}_{\mathrm{tee}} \cdot \vec{D}^*_{\mathrm{tee}} ds}{\iint_S \vec{E}_{\mathrm{tref}} \cdot \vec{D}^*_{\mathrm{tref}} ds} - 2\alpha_{er} \frac{\Re(\iint_S \vec{E}_{\mathrm{tee}} \cdot \vec{D}^*_{\mathrm{tref}} ds)}{\iint_S \vec{E}_{\mathrm{tref}} \cdot \vec{D}^*_{\mathrm{tref}} ds} + 2\alpha_{ei} \frac{\Im(\iint_S \vec{E}_{\mathrm{tee}} \cdot \vec{D}^*_{\mathrm{tref}} ds)}{\iint_S \vec{E}_{\mathrm{tref}} \cdot \vec{D}^*_{\mathrm{tref}} ds} + 1 \tag{C.0.4}$$

Taking the derivatives of eq. (C.0.4) with respect to α_{er} and α_{ei}, we get:

$$\frac{\partial}{\partial \alpha_{er}} \mathrm{err}_E = 2\alpha_{er} \frac{\iint_S \vec{E}_{\mathrm{tee}} \cdot \vec{D}^*_{\mathrm{tee}} ds}{\iint_S \vec{E}_{\mathrm{tref}} \cdot \vec{D}^*_{\mathrm{tref}} ds} - 2 \frac{\Re(\iint_S \vec{E}_{\mathrm{tee}} \cdot \vec{D}^*_{\mathrm{tref}} ds)}{\iint_S \vec{E}_{\mathrm{tref}} \cdot \vec{D}^*_{\mathrm{tref}} ds} \tag{C.0.5}$$

$$\frac{\partial}{\partial \alpha_{ei}} \mathrm{err}_E = 2\alpha_{ei} \frac{\iint_S \vec{E}_{\mathrm{tee}} \cdot \vec{D}^*_{\mathrm{tee}} ds}{\iint_S \vec{E}_{\mathrm{tref}} \cdot \vec{D}^*_{\mathrm{tref}} ds} + 2 \frac{\Im(\iint_S \vec{E}_{\mathrm{tee}} \cdot \vec{D}^*_{\mathrm{tref}} ds)}{\iint_S \vec{E}_{\mathrm{tref}} \cdot \vec{D}^*_{\mathrm{tref}} ds} \tag{C.0.6}$$

Equating (C.0.5), (C.0.6) to zero, we calculate α_{er}, α_{ei}:

$$\alpha_{er} = \frac{\Re(\iint_S \vec{E}_{\mathrm{tee}} \cdot \vec{D}^*_{\mathrm{tref}} ds)}{\iint_S \vec{E}_{\mathrm{tee}} \cdot \vec{D}^*_{\mathrm{tee}} ds} \tag{C.0.7}$$

$$\alpha_{ei} = -\frac{\Im(\iint_S \vec{E}_{\mathrm{tee}} \cdot \vec{D}^*_{\mathrm{tref}} ds)}{\iint_S \vec{E}_{\mathrm{tee}} \cdot \vec{D}^*_{\mathrm{tee}} ds} \tag{C.0.8}$$

Finally, by putting (C.0.7) (C.0.8) into (C.0.4), function err_E takes up the form:

$$\mathrm{err}_E = 1 - \frac{|\iint_S \vec{E}_{\mathrm{tee}} \cdot \vec{D}^*_{\mathrm{tref}} ds|^2}{\iint_S \vec{E}_{\mathrm{tee}} \cdot \vec{D}^*_{\mathrm{tee}} ds \cdot \iint_S \vec{E}_{\mathrm{tref}} \cdot \vec{D}^*_{\mathrm{tref}} ds} \tag{C.0.9}$$

An analogous approach for function err_M leads to the following equation:

$$\mathrm{err}_M = 1 - \frac{|\iint_S \vec{H}_{\mathrm{tee}} \cdot \vec{B}^*_{\mathrm{tref}} ds|^2}{\iint_S \vec{H}_{\mathrm{tee}} \cdot \vec{B}^*_{\mathrm{tee}} ds \cdot \iint_S \vec{H}_{\mathrm{tref}} \cdot \vec{B}^*_{\mathrm{tref}} ds} \tag{C.0.10}$$

Acknowledgments

I would like to express my deep gratitude to my supervisor, Prof. Michał Mrozowski, for the scientific education, constant help, inspirations, and support in many ideas that lead this work to the successful end.

I wish to thank the State Committee of Scientific Research (KBN), which has sponsored this work with two grants, under the contract numbers 8 T11F 016 10 and 8 T11D 030 15.

I thank the Computer Center of the Tricity Academic Computer Network (CI TASK) for making its computers available for simulations performed under this work.

I also want to express my thanks to my colleagues, I have shared a single office with – to Patryk Dębicki, Piotr Jędrzejewski and Jacek Mielewski, for the time spent together and for all interesting discussions.

Last but not least, words of my appreciation and gratitude to my family, in particular to my wife, my parents, my grandmother and my sister, for their constant support, help and patience during my work on this thesis.

Copyright note

Bibliography

[1] M. M. Afande, K. Wu, M. Giroux, and R. G. Bosisio. A finite-difference frequency-domain method that introduces condensed nodes and image principle. *IEEE Trans. Microwave Theory Tech.*, 43:838–846, Apr. 1995.

[2] F. Alimenti, P. Mezzanotte, L. Roselli, and R. Sorrentino. Efficient analysis of waveguide components by FDTD combined with time domain modal expansion. *IEEE Microwave and Guided Wave Letters*, 5:351–353, Oct. 1995.

[3] W.F. Ames. *Numerical Methods for Partial Differential Equations*. Academic Press, 3rd edition, San Diego, USA, 1992.

[4] W. E. Arnoldi. The principle of minimized iterations in the solution of the matrix eigenvalue problem. *Quarterly of Applied Mathematics*, 9:17–29, 1951.

[5] D. M. Barry, W. McKenzie, C. M. Snowden, and H. J. Howes. Computer aided electromagnetic analysis and design of mic and mmic structures. *IEE Colloquium on Computer Aided Design of Microwave Circuits. Digest*, 99:4/1–6, Nov. 1985.

[6] K. Beilenhoff and W. Heinrich. Treatment of field singularities in the finite-Difference approximation. *IEEE MTT-S Digest*, 2:979–982, 1993.

[7] K. Beilenhoff, W. Heinrich, and H. L. Hartnagel. Improved finite-difference formulation in frequency domain for three-dimensional scattering problems. *IEEE Trans. Microwave Theory Tech.*, 40:540–546, Mar. 1992.

[8] K. Bierwirth, N. Schulz, and F. Arndt. Finite-difference analysis of rectangular dielectric waveguide structures. *IEEE Trans. Microwave Theory Tech.*, 34:1104–1113, Nov. 1986.

[9] M. Celuch-Marcysiak and W. Gwarek. Higher order modeling of media interfaces for enhanced FDTD analysis of microwave circuits. In *Proc. 24th European Microwave Conference*, pages 1530–1535, Cannes, France, 1994.

[10] M. Celuch-Marcysiak and W. K. Gwarek. Higher order modelling of media interfaces for enhanced FDTD analysis of microwave circuits. In *24th European Microwave Conf.*, pages 1530–1535, Cannes, France, September 1994.

[11] M. Celuch-Marcysiak and W.K. Gwarek. Implicit incorporation of nonlinear elements for unconditionally stable FDTD analysis at coarse time-steps. *MTT-S International Microwave Symposium Digest*, 96.3:1381–1384, Mar. 1996.

[12] Z. Chen, M.M. Ney, and W.J.R. Hoefer. A new Finite-Difference Time-Domain formulation and its equivalence with the TLM symmetrical condensed node. *Transactions on Microwave Theory and Techniques*, 39.12:2160–2169, Dec. 1991.

[13] W.C. Chew. *Waves and Fields in Inhomogeneous Media*. Van Nostrand Reinhold, New York, 1990.

[14] D.H. Choi and W.J.R. Hoefer. The Finite-Difference – Time-Domain method and its application to eigenvalue problems. *Transactions on Microwave Theory and Techniques*, MTT-34(12):1464–1470, Dec. 1986.

[15] D.H. Choi and W.J.R. Hoefer. A time domain finite difference method and its application. *MTT-S International Microwave Symposium Digest*, 86(1):793–796, Dec. 1986.

[16] M. Clemens, S. Drobny, H. Krüger, P. Pinder, O. Podebrad, B. Schillinger, B. Trapp, M. Wilke, T. Weiland, U. Becker, M. Bartsch, and M. Zhang. The electromagnetic simulation software package MAFIA 4. *Proc. of the ICCEA '99, Conferenz*, pages 565–568, Nov. 1–4 1999.

[17] M. Clemens, R. Schuhmann, and T. Weiland. Algebraic properties and conservation laws in the discrete electromagnetism. *Frequenz*, 53(11–12):219–225, Nov., Dec. 1999.

[18] D. G. Corr and J. B. Davies. Computer analysis of the fundamental and higher order modes in single and coupled microstrip. *IEEE Trans. Microwave Theory Tech.*, 20:669–678, Oct. 1972.

[19] I.J. Craddock and C.J. Railton. A new technique for the stable incorporation of static field solutions in the FDTD method for the analysis of thin wires and narrow strips. *Transactions on Microwave Theory and Techniques*, 46.8:1091–1096, Aug. 1998.

[20] M. P. Dębicki, P. Jędrzejewski, J. Mielewski, P. Przybyszewski, and M. Mrozowski. Application of the Arnoldi method to the solution of electromagnetic eigenproblems on the multiprocessor power challenge architecture. Technical report, Technical University of Gdańsk, Dept. ETI, Gdańsk, Poland, 1995.

[21] M. P. Dębicki, P. Jędrzejewski, J. Mielewski, P. Przybyszewski, and M. Mrozowski. Solution of electromagnetic eigenproblems on multiprocessor superscalar computers. *Proceedings of ACES'1996 Conference*, pages 214–220, Mar. 1996.

[22] P. Debicki, P. Jedrzejewski, A. Kreczkowski, J. Mielewski, M. Mrozowski, K. Nyka, P. Przybyszewski, M. Rewienski, and T. Rutkowski. Coping with numerical complexity in computational electromagnetics. In *Proc. 12th International Conference on Microwaves and Radar. MIKON-98*, volume 4, pages 175–197, Krakow, Poland, 1998.

[23] K. P. Esselle, M. Okoniewski, and M. A. Stuchly. Accurate modeling of field singularities at metal edges diagonal to the FD-TD grid. *IEEE Antennas and Propagation Society International Symposium 1997. Digest*, 4:2176–9, 1997.

[24] A. T. Galick, T. Kerkhoven, and U. Ravaioli. Iterative solution of the eigenvalue problem for a dielectric waveguide. *IEEE Trans. Microwave Theory Tech.*, 40:699–705, Apr. 1992.

[25] O.P. Gandhi, B.Q. Gao, and J.Y. Chen. A frequency-dependent Finite-Difference Time-Domain formulation for general dispersive media. *Transactions on Microwave Theory and Techniques*, 41.4:658–665, Apr. 1993.

[26] P. M. Goorjian, A. Taflove, R. M. Joseph, and S. C. Hagness. Computational modeling of femtosecond optical solitons from Maxwell's equations. *IEEE Journal of Quantum Electronics*, 28(10):2416–2422, 1992.

[27] W. Gwarek. *Analisis of Microwave Circuits with Two Dimensional Wave Propagation (in Polish).* Prace Naukowe, Politechnika Warszawska, Warsaw, 1988.

[28] W. K. Gwarek. Analysis of an arbitrarily-shaped planar circuit—A time-domain approach. *IEEE Transactions on Microwave Theory and Techniques*, 33(10):1067–1072, October 1985.

[29] W. K. Gwarek. Analysis of arbitrarily shaped two-dimensional microwave circuits by finite-difference time-domain method. *IEEE Transactions on Microwave Theory and Techniques*, 36(4):738–744, April 1988.

[30] W. K. Gwarek. Computer aided analysis of arbitrarily-shaped coaxial discontinuities. *IEEE Transactions on Microwave Theory and Techniques*, 36(2):337–342, February 1988.

[31] J. Van Hese and D. De Zutter. Modeling of discontinuities in general coaxial waveguide structures by the FDTD-method. *IEEE Trans. Microwave Theory Tech.*, MTT-40:547–556, Mar. 1992.

[32] J. S. Hornsby and A. Gopinath. Numerical analysis of a dielectric-loaded waveguide with a microstrip line – finite-difference methods. *IEEE Trans. Microwave Theory Tech.*, 17:684–690, Sep. 1969.

[33] N. H. Huynh and W. Heinrich. FDTD accuracy improvement by incorporation of 3D edge singularities. *IEEE MTT-S International Microwave Symposium Digest*, 4:1573–6, Jun. 1999.

[34] T. Itoh, editor. *Numerical Techniques for Microwave and Millimeter-Wave Passive Structures.* A Wiley–Interscience Publication, John Wiley & Sons, New York, 1989.

[35] T. Itoh and Bijan Houshmand, editors. *Time-Domain Methods for Microwave Structures: Analysis and Design.* IEEE Press, Piscataway, NJ, 1998.

[36] J. Jin. *The Finite Element Method in Electromagnetics.* John Wiley & Sons, New York, 1993.

[37] C.C. Johnson. *Field and Wave Electrodynamics.* McGraw–Hill, New York, 1965.

[38] D.S. Jones. *Methods in Electromagnetic Wave Propagation, vol.1: Theory and Guided Waves.* Clarendon Press, Oxford, 1987.

[39] R. M. Joseph and A. Taflove. Spatial soliton deflection mechanism indicated by FD-TD Maxwell's equations modeling. *IEEE Photonics Technology Letters*, 6(10):1251–1254, 1994.

[40] R. M. Joseph and A. Taflove. FDTD Maxwell's equations models for nonlinear electrodynamics and optics. *IEEE Transactions on Antennas and Propagation*, 45(3):364–374, March 1997.

[41] T. G. Jurgens, A. Taflove, K. Umashankar, and T. G. Moore. Finite-difference time-domain modeling of curved surfaces. *IEEE Transactions on Antennas and Propagation*, 40(4):357–366, April 1992.

[42] N. Kaneda, B. Houshmand, and T. Itoh. FDTD analysis of dielectric resonators with curved surfaces. *IEEE Trans. Microwave Theory Tech.*, 45:1645–1649, Sep. 1997.

[43] A. Kreczkowski, T. Rutkowski, and M. Mrozowski. Fast modal ABC's in the hybrid PEE–FDTD analysis of waveguide discontinuities. *IEEE Microwave and Guided Wave Letters,*, 9(5):186–188, May 1999.

[44] M. Krumpholz and L. P. B. Katehi. MRTD: New time-domain schemes based on multiresolution analysis. *IEEE Transactions on Microwave Theory and Techniques*, 44(4):555–571, April 1996.

[45] K. S. Kunz and R. J. Luebbers. *The Finite Difference Time Domain Method for Electromagnetics*. CRC Press, Boca Raton, FL, 1993.

[46] K. K. Mei and A. C. Cangellaris. Applications of field singularities at wedges and corners to time domain finite difference or finite element methods of field computations. *Radio Science*, 22(7):1239–46, Dec. 1987.

[47] J. Meixner. The behavior of electromagnetic fields at edges. *IEEE Trans. Antennas Propagat.*, AP-20:442–446, Jul. 1972.

[48] A. R. Mitchell and D. F. Griffiths. *The Finite Difference Methods in Partial Differential Equations*. John Wiley & Sons, Chichester, 1980.

[49] C. Mroczkowski, W.K. Gwarek, T. Morawski, and J. Modelski. Analysis of circular horn antennas using the FD-TD method. *MTT-S International Microwave Symposium Digest*, 92.1:421–424, Jan. 1992.

[50] M. Mrozowski. *Eigenfunction expansion techniques in the numerical analysis of inhomogeneously loaded waveguides and resonators*. Zeszyty Naukowe Politechniki Gdańskiej, Gdańsk, 1994.

[51] M. Mrozowski. A hybrid PEE-FDTD algorithm for accelerated time domain analysis of electromagnetic waves. *IEEE Microwave and Guided Wave Letters*, 4(10):323–325, Oct 1994.

[52] M. Mrozowski. New fast full wave eigenfunction expansion algorithms for time and frequency domain modeling of electromagnetic performance of MMIC's, transmission lines, discontinuities and package effects in high speed electronics circuits. Technical report, Technical University of Gdańsk, Dept. ETI, Gdańsk, Poland, 1995.

[53] M. Mrozowski. *Guided Electromagnetic Waves - Properties and Analysis*. Research Studies Press, Taunton, Somerset, England, 1997.

[54] G. Mur. Absorbing boundary conditions for the finite-difference approximation of the time-domain electromagnetic field equations. *IEEE Trans. Electromagnetic Compatibility*, 23:377–382, Nov. 1981.

[55] G. Mur. The modelling of singularities in the Finite-Difference approximation of the Time-Domain electromagnetic-field equations. *IEEE Trans. Microwave Theory Tech.*, MTT-29:1073–1077, Oct. 1981.

[56] P. Przybyszewski. A finite-difference algorithm for modeling of conductive wedges in 2D. *Proceedings of ACES'2000 Conference*, pages 951–958, Mar. 2000.

[57] P. Przybyszewski, J. Mielewski, and M. Mrozowski. Efficient eigenfuction expansion algorithms for analysis of waveguides. Technical report, Technical University of Gdańsk, Dept. ETI, Gdańsk, Poland, Dec. 1996.

[58] P. Przybyszewski, J. Mielewski, and M. Mrozowski. A fast technique for analysis of waveguides. *IEEE Microwave and Guided Wave Letters*, 8:109–111, Mar. 1998.

[59] P. Przybyszewski, J. Mielewski, and M. Mrozowski. A new class of eigenfunction expansion methods for fast frequency domain analysis of waveguides. *IEEE Trans. Microwave Theory Tech.*, 2001 (accepted for publication).

[60] P. Przybyszewski and M. Mrozowski. Modelling of the edge singularities in the Finite-Difference Time-Domain method. In *XI Microwave International Conference (MIKON'96)*, pages 198–202, May 1996.

[61] P. Przybyszewski and M. Mrozowski. A conductive wedge in Yee's mesh. *IEEE Microwave and Guided Wave Letters*, pages 66–68, Feb. 1998.

[62] C. J. Railton. An algorithm for the treatment of curved metallic laminas in the finite difference time domain method. *IEEE Trans. Microwave Theory Tech.*, MTT-41:1429–1438, Aug. 1993.

[63] C. J. Railton, I. J. Craddock, and J. B. Schneider. The analysis of general two-dimensional PEC structures using a modified CPFDTD algorithm. *IEEE Transactions on Microwave Theory and Techniques*, 44(10):1728–1733, October 1996.

[64] C. J. Railton and J. P. McGeehan. Analysis of microstrip discontinuities using the Finite-Difference Time-Domain technique. *IEEE MTT-S Digest*, pages 1009–1012, 1989.

[65] C. J. Railton and J. B. Schneider. An analytical and numerical analysis of several locally conformal FDTD schemes. *IEEE Transactions on Microwave Theory and Techniques*, 47(1):56–66, January 1999.

[66] T. Rozzi, L. Pierantoni, and M. Farina. Eigenvalue approach to the efficient determination of the hybrid and complex spectrum of inhomogeneous, closed waveguide. *IEEE Trans. Microwave Theory Tech.*, 45:345–353, Mar. 1997.

[67] Y. Saad. *Numerical methods for large eigenvalue problems*. Halsted Press-John Wiley & Sons Inc., New York, 1992.

[68] M. N. O. Sadiku. *Numerical Techniques in Electromagnetics*. CRC Press, Boca Raton, 1992.

[69] A.A. Samarskiy. *Theory of Finite Difference Schemes*. Nauka, Moscow, 1977. In Russian.

[70] N. Schulz, K. Bierwirth, and F. Arndt. Finite-difference method without spurious solutions for the hybrid-mode analysis of diffused channel waveguides. *IEEE Trans. Microwave Theory Tech.*, 38:722–729, Jun. 1990.

[71] E. Schweig and W. B. Bridges. Computer analysis of dielectric waveguides: a finite-difference method. *IEEE Trans. Microwave Theory Tech.*, 32:531–541, May 1984.

[72] T. Shibata and T. Itoh. A modification of FDTD formulas at conductor edge singularities. *Trans. of the Institute of Electronics, Information & Communication Engineers C-II*, 5:176–7, May 1997.

[73] D. B. Shorthouse and C. J. Railton. Incorporation of static singularities into the finite difference time domain technique with application to microstrip structures. In *Proc. 20th European Microwave Conference 90*, pages 531–6, Tunbridge Wells, UK, 1990. Microwave Exhibitions and Publishers.

[74] D. B. Shorthouse and C. J. Railton. The incorporation of static field solutions into the finite difference time domain algorithm. *IEEE Trans. Microwave Theory Tech.*, MTT-40:986–994, May 1992.

[75] R. Siushansian and J. LoVetri. A comparison of numerical techniques for modeling electromagnetic dispersive media. *Microwave and Guided Wave Letters*, 5.12:426–428, Dec. 1995.

[76] D. C. Sorensen. Implicitly restarted Arnoldi/Lanczos methods for large scale eigenvalue calculations. In *Proc. ICASE/LaRC Workshop on Parallel Numerical Algorithms*, Kluwer, Norfolk, Va, May 23-25 1994.

[77] D. M. Sullivan. *Electromagnetic Simulation Using the FDTD Method*. IEEE Press, New York, 2000.

[78] A. Taflove. Application of the finite-difference time-domain method to sinusoidal steady-state electromagnetic-penetration problems. *IEEE Transactions on Electromagnetic Compatibility*, EMC-22(3):191–202, August 1980.

[79] A. Taflove. *Computational Electrodynamics: The Finite-Difference Time-Domain Method*. Artech House, Boston, MA, 1995.

[80] A. Taflove, editor. *Advances in Computational Electrodynamics: The Finite-Difference Time-Domain Method*. Artech House, Boston, MA, 1998.

[81] A. Taflove and M. E. Brodwin. Computation of the electromagnetic fields and induced temperatures within a model of the microwave irradiated human eye. *IEEE Transactions on Microwave Theory and Techniques*, MTT-23(11):888–896, November 1975.

[82] A. Taflove and M. E. Brodwin. Numerical solution of steady-state electromagnetic scattering problems using the time-dependent Maxwell's equations. *IEEE Transactions on Microwave Theory and Techniques*, MTT-23(8):623–630, 1975.

[83] A. Taflove and S. Hagness. *Computational Electrodynamics: The Finite-Difference Time-Domain Method, 2 ed.* Artech House, Boston, MA, 2000.

[84] A. Taflove and K. Umashankar. Radar cross section of general three-dimensional scatterers. *IEEE Transactions on Electromagnetic Compatibility*, EMC-25(4):433–440, November 1983.

[85] P. Thoma and T. Weiland. Numerical stability of finite difference time domain methods. *IEEE Transactions on Magnetics*, 34:2740–3, Sep. 1998.

[86] V. Vemuri and W. J. Karplus. *Digital Computer Treatment of Partial Differential Equations*. Prentice-Hall Series in Computational Mathematics. Prentice-Hall, Englewood Cliffs, New Jersey, 1981.

[87] S. Watanabe and M. Taki. An improved FDTD model for the feeding gap of a thin-wire antenna. *Microwave and Guided Wave Letters*, 8.4:152–154, Apr. 1998.

[88] T. Weiland. Eine Methode zur Lösung der Maxwellschen Gleichungen für sechskomponentige Felder auf diskreter Basis. *AEÜ*, 31:116–120, Mar. 1977.

[89] T. Weiland. Eine numerische Methode zur Lösung des Eigenwellenproblems längshomogener Wellenleiter. *AEÜ*, 31:308–314, Jul./Aug. 1977.

[90] K. S. Yee. Numerical solution of initial boundary value problems involving maxwell's equations in isotropic media. *IEEE Trans. Antennas Propagat.*, AP-14:302–307, May 1996.

[91] R. W. Ziolkowski and J. B. Judkins. Full-wave vector Maxwell equation modeling of the self-focusing of ultrashort optical pulses in a nonlinear Kerr medium exhibiting a finite response time. *Journal of the Optical Society of America, B Opt. Phys.*, 10(2):186–198, February 1993.